Aerosol Hygroscopic Growth in Marine and Continental Air

A thesis presented to
The National University of Ireland Galway
For the Degree of Doctor of Philosophy

By Jakub Białek

March 2013

Supervisor: Professor Colin O'Dowd

School of Physics

National University of Ireland Galway

Abstract

Aerosol particulate matter contributes significantly to the global climate directly, through scattering and absorption of solar radiation, and indirectly, through changing cloud reflectance and cloud cover persistence. This thesis presents the results of several studies on the hygroscopicity of marine aerosol and of anthropogenic aerosol.

Analysis of a two-year long aerosol hygroscopicity dataset from the Mace Head atmospheric research station located near Carna, Co. Galway show that hygroscopic growth-factors (HGFs) were found to be associated with size distribution clusters, characteristic of five aerosol source categories: *low sea-salt marine, high sea-salt marine*, *coastal-nucleation*, *open-ocean nucleation*, and *continental*. Chemical composition of atmospheric aerosol particles under clean marine air conditions was found to contain the following constituents: 46% (30-54%) of partially-modified ammonium-sulphate particles, 23% (11-40%) of partially-modified sea-salt and the remaining 31% (25-35%) being attributed to two distinct aerosol organic species. On average, 30% of marine aerosol was found to be predominantly of organic origin and in the case of anthropogenically polluted aerosol, 60% of total aerosol mass was organic.

Observation and analysis of open ocean new particle formation events revealed that, amongst potential gaseous precursors, nitrogenated compounds in the form of amines can stabilize clusters from evaporating, which effectively increases particle nucleation and growth, thus promoting open ocean new particle production. This work suggests that amides and organic nitrate may also play a key role in aerosol nucleation processes. Primary-produced sea-spray aerosol comprising sea salt when enriched with organic matter, may suppress light-scattering enhancement as a function of increasing relative humidity. Sea spray aerosol exhibits a dichotomous behaviour manifested in a low hygroscopic growth factor but with high cloud condensation nuclei (CCN) activation efficiency. Aerosol dominated by organics possesses a HGF value of 1.25 or less, while aerosol dominated by sulphate led to a HGF ~1.65. Sea salt dominated particles showed the highest values of HGF of more than 1.8. CCN activation was dependent on aerosol chemical composition, but did not follow a typical hygroscopicity dependence pattern – that is, particles with the lowest HGF were more readily activated than particles with the highest HGF values.

This work also investigated properties and diurnal patterns of anthropogenically produced aerosol in one of the most polluted regions in Europe – river Po Valley in Italy. Large diurnal variations in the chemical composition were observed with massive peaks in nitrates, albeit without an increase in HGF, but also consistent with an increase in the hydrocarbon-like family (measured by the HR-Tof-AMS), suggesting a hydrophilic coating around the inorganic nitrate, thus suppressing water uptake.

An unique opportunity of observing the Eyjafjallajökull volcano ash plume over Mace Head revealed a bimodal size distribution and an increased CCN activation efficiency which yielded information on ash cloud dispersion, as well as information on the impact of long range transport on volcanic ash physicochemical properties.

These studies represents one of the first synergistic combinations of aerosol mass spectrometer chemical composition information with HGF information resulting in improved quantification of marine and urban aerosol influences on the direct aerosol radiative effect.

Thesis outline

Page

ABSTRACT **1**

THESIS OUTLINE **3**

TABLE OF ABBREVIATIONS AND SYMBOLS **9**

1. INTRODUCTION **11**

1.1 Aims **11**

1.2 Atmospheric Aerosols **12**

1.2.1 General Properties 12

1.2.2 The direct and semi-direct effect of aerosol on climate 13

1.2.3 The indirect effect of aerosol on climate 14

1.3 Formation, growth and sources of atmospheric aerosol **16**

1.3.1 Aerosol formation in marine air 17

1.3.2 Biomass burning 22

1.3.3 Urban aerosol 22

1.4 Climate aerosol interactions, marine aerosol and the CLAW Hypothesis **23**

2. PREVIOUS STUDIES OF HYGROSCOPICITY **29**

3. INSTRUMENTATION **35**

3.1 Hygroscopic Tandem Differential Mobility Analyser (HTDMA). **35**

3.1.1 The HTDMA setup 36

3.1.2 The principle of HTDMA data inversion. 37

3.1.3 HTDMA Calibration 39

3.1.4 Choosing proper inversion resolution for the dataset. 41

3.1.5 Error estimation 44

3.2 Aerosol mass spectrometer (AMS) 44

3.2.1 Aerosol Mass Spectrometer 44

4. SUMMARY OF PAPERS 47

ON THE CONTRIBUTION OF ORGANICS TO THE NORTH EAST ATLANTIC AEROSOL NUMBER CONCENTRATION 53

Abstract 53

1. Introduction 54

2. Experimental details 55

3. Data analysis 55

4. Results and discussion 57

5. Conclusion 61

Acknowledgments 62

References 62

Appendix A1. Aerosol size distributions k-means clustering 64

Appendix A2. Aerosol size distributions k-means clustering log normal fitting 69

HYGROSCOPIC AND CHEMICAL CHARACTERISATION OF PO VALLEY AEROSOL 71

Abstract 71

1. Introduction 73

2. Methods and Instrumentation 74

3. Measurements Location 76

4. Meteorological Overview 77

4.1 Meteorological overview for the chosen cases 77

4.1.1 Case 1: 07.07.2009 12:00 to 09.07.2009 12:00 77

4.1.2 Case 2: 09.07.2009 12:00 to 11.07.2009 12:00 77

5 Results & Discussion 78

5.1 Diurnal Variability – Case Studies. 79

5.1.1 Case 1, period D: 07.07.2009 12:00 to 09.07.2009 12:00 (Figure 3) 79

5.1.2 Case 2, period E: 09.07.2009 12:00 to 11.07.2009 12:00 (Figure 5) 82

6 Conclusions 86

References. 87

Appendix B1. Supplementary data supporting the organonitrate-driven suppression of HGF from the ATOFMS. 92

PRIMARY MARINE ORGANIC AEROSOL: A DICHOTOMY OF LOW HYGROSCOPICITY AND HIGH CCN ACTIVITY 93

Abstract 93

1. Introduction 93

2. Experiment 94

3. Results 94

4. Discussion 97

5. Conclusions **99**

References **99**

THE EYJAFJALLAJÖKULL ASH PLUME - PART I: PHYSICAL, CHEMICAL AND OPTICAL CHARACTERISTICS **103**

1. Introduction **104**

2. Experimental **104**

3. Results **108**

3.1. Case 1: 19th-20th April 2010 108

3.2. Case 2: 2nd-5th May 2010 110

3.3 Case 3: May 17th-18th 113

3.4 Off-line chemical analysis 116

3.5 Scanning electron microscopy analysis 116

3.6 Ozone depletion in the ash plume 117

4. Discussion **118**

5. Conclusions **120**

Acknowledgements **120**

References **120**

ON THE EFFECT OF WIND SPEED ON SUBMICRON SEA SALT MASS CONCENTRATIONS AND SOURCE FLUXES **123**

1. Introduction **123**

2. Experimental Setup for Ambient Air Measurements **124**

3. Experimental Setup for Laboratory and Sea Salt calibration 126

4. Comparison of Online and Off-Line Sea Salt Concentrations 129

5. Sea Salt Mass Dependency on Wind Speed 130

6. Conclusions 136

Acknowledgments. 137

References 137

NITROGENATED AND ALIPHATIC ORGANIC VAPOURS AS POSSIBLE DRIVERS FOR MARINE SECONDARY ORGANIC AEROSOL GROWTH 143

Abstract 144

1. Introduction 144

2. Methods 146

2.1 Location 146

2.2 Instrumentation 146

2.2.1 Real-time physical instrumentation 146

2.2.2 Real-time chemical instrumentation 147

2.3 Quantum Chemistry Simulations 147

3. Results 148

3.1 Detection of open ocean nucleation events 148

3.2 Aerosol chemical characterisation during open ocean formation and growth events 149

3.3 Aerosol hygroscopicity and CCN properties during open ocean formation and growth events 152

4. Discussion and conclusion 153

Acknowledgements **154**

References **154**

5 CONCLUSIONS AND FUTURE OUTLOOK **159**

ACKNOWLEDGMENTS **165**

REFERENCES **167**

LIST OF ALL PUBLICATIONS **179**

Table of abbreviations and symbols

APM	radiation absorbing particulate matter
CCN	cloud condensation nuclei
CCNc	cloud condensation nuclei counter
$c(g, D)$	see GF-PDF
CPC	condensation particle counter
DMA	differential mobility analyser
DMS	dimethyl sulphide
D	particle diameter
D_0	electrical mobility diameter set at DMA1 (dry diameter selected by DMA1)
D_{aero}	vacuum aerodynamic diameter
D_i	mobility diameter of a particle carrying i charges with electrical mobility diameter D_0: $D_i = u_i(D_0)$
D_{set}	electrical mobility diameter set at DMA2: $D_{\text{set}} = g_{\text{set}} D_0$
EC	elemental carbon
FWHM_D	full width at half maximum of DMA's transfer function in the diameter space
$f_{z,i}(D)$	function calculating the electrical mobility of a particle with dry diameter D
GAW	Global Aerosol Watch
g_{mean}	mean HGF of the GF-PDF as defined in Eq. (C.4)
g_{set}	HGF set at DMA2: $g_{\text{set}} = D_{\text{set}}/D_0$
$\hat{g}$	true HGF of the particles (in terms of mobility diameter ratio)
GF-PDF	growth factor probability density function, $c(g, D_0)$, for particles with dry diameter $D = D_0$ to exhibit a HGF = g. The total probability of exhibiting a certain GF is unity.
HTDMA	hygroscopic tandem differential mobility analyser
HGF, g	diameter growth factor: $g = D/D_0$
HR-ToF-AMS	high resolution, time of flight aerosol mass spectrometer
$JO(^1D)$	photolysis frequency
$K_{TDMA}^{g,i}(g_{\text{set}}, \hat{g}, D_0)$	TDMA kernel as a function of g_{set} and D_0 for particles carrying i charges and having a true HGF = $\hat{g}$
k_{inlet}	factor to adjust the measurement uncertainty level due to variations of the particle concentration at the TDMA inlet
K_{kernel}	factor to adjust the measurement uncertainty level due deviations of the true kernel function from the kernel function used in the inversion algorithm
Kn	the Knudsen number $2\lambda/D$
λ	mean free path of particle

MDF	measurement distribution function $m_{TDMA}^{g,total}(g_{\text{set}}, D_0)$. This is the particle concentration measured at the outlet of the TDMA as a function of HGF, g_{set}, set at DMA2 for a defined dry size (D_0) selected with DMA1
MSA	methane sulfonic acid
n	number of counts in a single data point of the MDF
n_{max}	maximum number of counts in any data point of the MDF
n_{total}	total number of counts recorded in the whole MDF
Δn_{poiss}	uncertainty of the number of counts to account for Poisson counting statistics
Δn_{inlet}	uncertainty of the number of counts to account for variations of the particle concentration at the TDMA inlet
Δn_{kernel}	uncertainty of the number of counts introduced to account for deviations of the true kernel function from the kernel function used in the inversion algorithm
$\Delta n_{\text{overall}}$	overall uncertainty of the number of counts in a data point of the MDF obtained by combination of Δn_{poiss}, Δn_{inlet} and Δn_{kernel}
N_{inlet}^{i}	normalisation factor for the TDMA kernel function for particles carrying i charges: $N_{\text{inlet}} = p_i(D_i)\frac{dN_{poly}}{d\ ln\ D(D_i)}$
$\frac{dN_{poly}}{d\ ln\ D(D_i)}$	number size distribution of dried, polydisperse aerosol at TDMA inlet
OC	organic carbon
PAH	polycyclic aromatic hydrocarbons
PARFORCE	New Particle Formation and Fate in the Coastal Environment
$p_i(D)$	number fraction of particles in the polydisperse aerosol with diameter D carrying i charges
Q_{sh}	sheath air flow rate in the DMA
Q_{ex}	excess air flow rate in the DMA
Q_{ae}	polydisperse sample flow rate at DMA inlet
Q_{sa}	monodisperse sample flow rate at DMA outlet
R-MDF	reconstituted MDF. This is the calculated MDF obtained by sending the inverted GF-PDF back through the TDMA's forward function
RH	relative humidity, ratio between the water vapour content and total possible water vapour content at a given temperature and pressure expressed in percentage
SMPS	scanning mobility particle sizer
SOA	secondary organic aerosol
TDMA	tandem differential mobility analyser
TSC	thermodynamically stable clusters
VOC	volatile organic compounds
Z(D)	electrical mobility of particle as a function of its diameter

1. Introduction

1.1 Aims

This work tackles perhaps the most uncertain geophysical question relating to the future climate of planet Earth: how does the global climate depend on aerosol emissions to the atmosphere and what might be their effect on the global radiation budget. To understand this global problem, one has to understand the role of submicron particulate matter in global climate forcing and how it might oppose the very well-known and described "greenhouse effect" – or how cleaner air could potentially accelerate global warming.

Aerosol particles present in the atmosphere can influence the climate in a direct way (i.e. light scattering) and in an indirect way, acting as cloud condensation nuclei (CCN) which can be *activated* in supersaturated water vapour conditions to form cloud droplets (Kohler, 1936). The activation process involves saturation of the surrounding air in relative humidity exceeding 100% (usually a fraction of per cent above 100%) which enables a liquid particle (previously in dynamic equilibrium with water vapour) to spontaneously grow to super micron sizes. The indirect effect of aerosols on the climate is not well understood yet and includes changes in cloud albedo (smaller sized droplets give rise to higher scattering and reflectance of solar radiation) and changes in cloud microphysical properties (the number of droplets per volume in a cloud strongly depends on the particle size distribution and supersaturation ratio) thus influencing cloud lifetime and the hydrological cycle (Kohler, 1936; Rosenfeld, 2006; Twomey, 1977b; Twomey, 1974) . The latter has much stronger effect on the albedo than the former i.e. the increase in the droplet concentration increases albedo much faster than reduction in the droplet size.

The ability of solid particles to become liquid droplets, and for liquid particles to uptake water vapour, and subsequently grow through the process of water vapour diffusion , is known as hygroscopicity and describes its affinity to water vapour (how easily particles can uptake water vapour from the surrounding air). If one compares the initial size of a dry particle to the size of the particle exposed to high relative humidity (*RH*), one can calculate its hygroscopic growth factor:

$$\boldsymbol{HGF = \frac{D}{D_0}} \qquad \textbf{(1)}$$

Such studies can lead, not only to direct quantification of water uptake properties, and thus their haze and cloud forming capabilities, but also, hygroscopic properties can indirectly elucidate the chemical composition of atmospheric aerosols.

This work focuses on a study of aerosol hygroscopicity under different clean and polluted environments, and thus under different aerosol composition regimes. The scientific goals of this work are:

- To investigate hygroscopic properties of aerosol during long term measurements (over 2 years of continuous data) in the marine environment of western Ireland at the Mace Head Atmospheric Research Station.
- To investigate the influence of the organic fraction on secondary marine aerosol (so called *open ocean nucleation events* during algae bloom periods – gas to particle conversion).
- To investigate the influence of the organic fraction on primary marine aerosol (that is the organic fraction of aerosol mass associated with sea spray production, also influenced by algae bloom periods).
- To compare hygroscopic properties of aerosol from clean and polluted sector air mass advections.
- To focus on particular case studies during several intensive measurement field campaigns.

1.2 Atmospheric Aerosols

The general definition of aerosols is described as a collection of particulate matter (dry particles or droplets of solutes) suspended in a gaseous medium, usually air (Hinds, 1999). This implies that the word "aerosol" should never be used as a definition of particles only but should also refer to the dynamic interactions of gas-to-particle-to-gas processes (i.e. equilibrium between the evaporation and condensation of vapours on the particle or droplet).

1.2.1 General Properties

Aerosol particles in the atmosphere originate from anthropogenic activities, such as combustion of fossil fuels and industrial emissions, and from natural sources, such as sea spray, soil dust, and volcanoes. Aerosols can be emitted directly as particulate

matter (primary aerosol) or formed in the atmosphere by gas-to-particle conversion processes (secondary aerosol). Atmospheric aerosol particles size can range from a few nanometres (stable clusters, nucleation mode) to tens of microns (coarse mode) (Seinfeld & Pandis, 2006). Once emitted, particles will grow or shrink and change the composition by condensation of vapour species or by evaporation, by coagulating with other particles, by chemical reaction, or by activation in the presence of water supersaturation to become fog and cloud droplets. Particles smaller than 1 μm diameter generally have atmospheric number concentrations in the range from around 100-200 per cm^3 in marine environment (O'Dowd et al., 2001) to 1000's, typically in the range of 10^4per cm^3 in polluted urban environments (Jones & Walker, 1994; Li et al., 1993). Super-micron particles are usually found at concentrations less than 1 cm^{-3} but can dominate the mass.

The fate, or lifetime, of aerosol particles in the atmosphere depends on their size, chemical composition as well as the height at which they are emitted. Their lifetime in the atmosphere ranges from several seconds up to more than a year. Large particles (over 100 microns) become too heavy to be considered suspended and they gradually sediment gravitationally to the ground/ocean surface. Particles small enough to reach the stratosphere by, e.g., volcanic eruptions (or emitted close to it as in the case of jet engines) can stay there for very long time until mixed again into the troposphere and scavenged via precipitation, or degrade chemically (photolysis) and slowly evaporate.

1.2.2 The direct and semi-direct effect of aerosol on climate

Atmospheric aerosols can influence the climate in many different ways. There are two major types of aerosol impact: *direct* and *indirect* radiative effects. The *direct effect* occurs when aerosol particles scatter solar radiation. If the particles are considered as uniformly spherical, light propagation through aerosol layers can be described by Maxwell's equations and the scattering effect of those particles is known as "Mie scattering" and was described for the first time by Mie (1907).

The larger part of the energy that reaches Earth's surface comes in the band of visible spectrum (400-700nm). The backscattering of incoming radiation is most effective when the particle diameter is of the same order as the wavelength of radiation. Since the majority of aerosol particles are roughly of the same dimensions as solar

radiation wavelengths, scattering and backscattering is more effective for the visible spectrum. This creates a negative disproportionality in the energy budget as more heat is radiated back into space that it is provided over the visible spectrum reaching the surface, thus cooling the atmosphere.

Some aerosol particles have properties which make them good energy absorbing material. This category comprises soot particles or particles with soot, which can be categorised as elemental carbon (EC) or black carbon (BC), depending on their method of measurement. Those particles have high energy absorption efficiency and add to heating of the atmosphere. But, apart from this effect, absorbing particulate matter (APM) also has other impacts on the climate: It can influence stability of cloud layers by: (1) warming up clouds which leads to more evaporation and ultimately dissipation of clouds (i.e. cloud "burn out" effect, (Hansen et al., 1997)), (2) creating more convection from below the cloud base and increasing their vertical height, thus increasing precipitation, (3) reducing cloud height, precipitation and reflectance by reducing convection if APM accumulates over the cloud layer. When APM accumulates on snow cover, it can accelerate its melting and if this happens over a large area, the global albedo of the planet can be affected (Flanner et al., 2007). Those effects of APM are commonly called a *semi-direct effect*. It has not been yet clear whether or not it has positive or negative impact on global climate forcing (i.e the difference between radiative energy received from the Sun and the amount of energy radiated back into space (Koch & Del Genio, 2010)) but, overall, a cooling direct aerosol effect is estimated at -0.5 W/m^2 (Solomon et al., 2007).

1.2.3 The indirect effect of aerosol on climate

Another way for aerosol to affect global climate is to act as cloud condensation nuclei - CCN (Twomey, 1977a). Each aerosol particle in ambient sub saturated humidity conditions contains a certain amount of water vapour which is in dynamic equilibrium with the surroundings. Usually this means that a particle or droplet grows only to a certain size, which depends on its initial size and chemical composition (Dusek et al., 2006). However, when exposed to super-saturated conditions, with the relative humidity (RH) exceeding 100%, a particle can depart from equilibrium and grow rapidly to super-micron sizes. In such cases, it is said that a particle *activates* into a cloud droplet. Growth of activated particles is limited only by water vapour availability

(supersaturation) in the immediate surroundings of a droplet, thus a greater population of particles competing for water vapour means that, ultimately, their growth is limited to

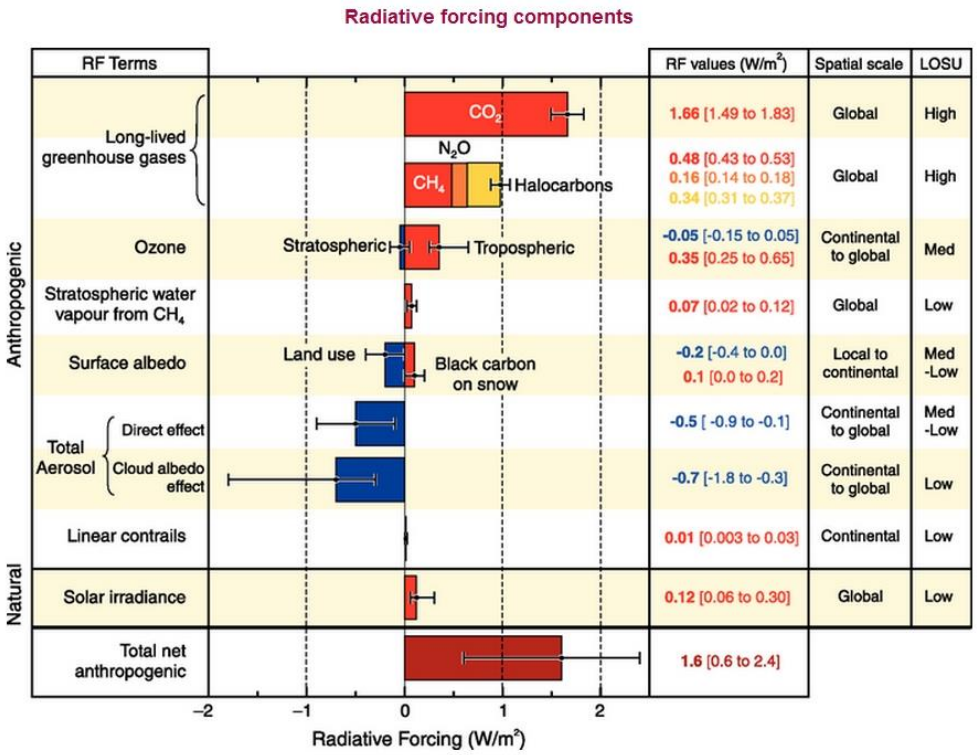

Figure 1. Global average radiative forcing (RF) in 2005 (best estimates and 5 to 95% uncertainty ranges) with respect to 1750 for CO_2, CH_4, N_2O and other important agents and mechanisms, together with the typical geographical extent (spatial scale) of the forcing and the assessed level of scientific understanding (LOSU). Aerosols from explosive volcanic eruptions contribute an additional episodic cooling term for a few years following an eruption. The range for linear contrails does not include other possible effects of aviation on cloudiness. Reproduced from (Solomon et al., 2007).

smaller sizes. Particles exceeding a certain size will precipitate from cloud in the form of rain or drizzle. A higher number concentration of smaller particles can lead to higher reflectance of a cloud and less precipitation (Lohmann & Feichter, 2005). The former is known as the *primary indirect aerosol effect* and the latter as the *secondary indirect aerosol effect*. The primary indirect effect resulting in cooling for low and medium level clouds means a cooling effect due to aerosol particles reflecting the solar radiation back into space. However, for high altitude clouds (cirrus, jet contrails) this effect can lead to increased long wave radiation backscatter due to the injected black carbon and changes in the ice water content, which can result in warming of the atmosphere (Lohmann & Feichter, 2005).

Together, the primary and secondary indirect effect is believed to contribute to cooling of the global climate and is estimated at -0.7 W/m^2 (Solomon et al., 2007). However, incomplete knowledge and a large uncertainty about the role of particulate matter in climate forcing may lead to large estimation errors. This results in a large uncertainty in radiative forcing due to anthropogenic aerosols, varying from 0.6 to 2.4 Wm^{-2}, as shown in Figure 1. At the highest confidence levels (at maximum whiskers range), the cooling effect of aerosol can reach a total over 3 W/m^2. This implies that, if emissions of PM were to be fully stopped, this could lead to effective warming corresponding to a doubling of the present concentration of atmospheric CO_2.

1.3 Formation, growth and sources of atmospheric aerosol

Depending on the formation mechanisms, aerosol particles can be generically segregated into two groups: *primary* and *secondary* aerosol. The source of primary aerosol particles can be either mechanical (erosion, sea spray, road dust etc.) or biogenic (bacteria, viruses, algae, pollen, spores etc.). Particles associated with incomplete combustion processes can also be considered as primary.

Secondary aerosol particles are formed by gas-to-particle conversion. This process is often referred to as *nucleation*, condensation growth or a multiphase chemical process. Supersaturated vapours condense readily on an available surface, rather than form new particles. Therefore, nucleation tends to be more frequent when the condensable surface of the aerosol is small. Factors such as photochemistry, volatile organic compounds (VOC) concentrations and meteorological influences (such as relative humidity) also seem to play important roles for nucleation e.g. (Kulmala & Kerminen, 2008).

Freshly nucleated particles are commonly defined as stable clusters of molecules larger than 3 nm (e.g.(Kulmala et al., 2004)). This threshold can be smaller when ion induced nucleation is considered (Kulmala et al., 2000). Clusters of 1-2 nm ions can grow to Aitken mode when condensable vapours are available (Aitken, 1897). Once nucleated, particles coagulate with each other and with larger particles. The process of growth is dominated by condensation of VOC vapours and growth rates can be as fast as 20nm/hr. However, the bigger they get, the slower the process of growing by condensation becomes due to limited concentration of VOCs. If the air consists of relatively low

VOCs and of other particles, nucleation stops at around 20-30 nm, e.g. coastal nucleation in the marine air (O'Dowd et al., 1999). However, if a relatively high VOC concentration is available particles can grow further in size and become potential CCN. Once activated, uptake of SO_2 (can oxidize to sulphuric acid), H_2SO_4, HNO_3 and NH_3 is enhanced due to the larger surface area. This process is known as cloud processing and can lead to production of inorganic salts such as ammonium sulphate, bisulphate and nitrate. When the droplet dries out, salts remain on the particles which now grow to a size of around 100 nm. Mechanisms of particle formation and growth along with a simple size distribution of each mode are presented in Figure 2.

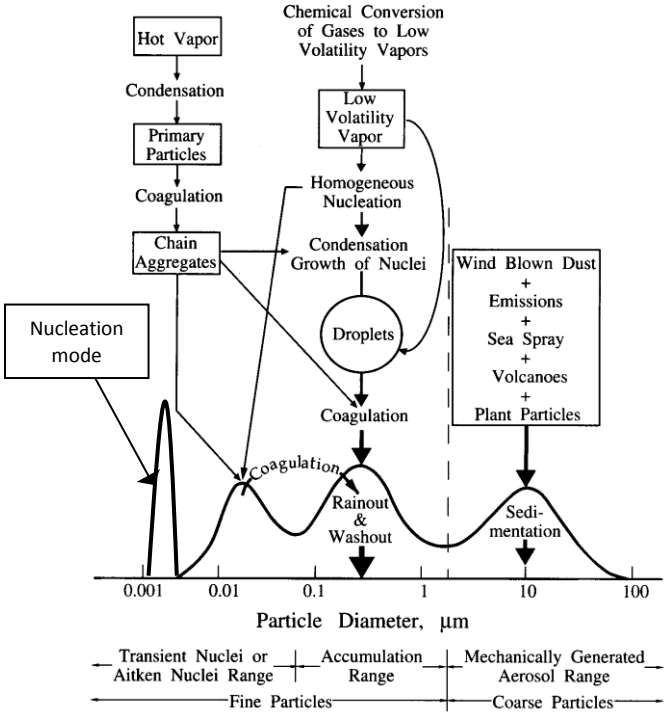

Figure 2. Distribution of surface area of an atmospheric aerosol – a simplified schematic. Main sources, modes, particle formation and removal mechanisms are shown. Modified reproduction from (Seinfeld & Pandis, 1998).

1.3.1 Aerosol formation in marine air

The primary marine aerosol production is driven by the interaction of wind pressure at the ocean surface and leads to the mechanical production of sea-spray aerosol (sea spray is considered as a combination of inorganic sea salt and organic matter). Sea spray production occurs due to the bubble-bursting process resulting from foam (whitecap) generation, producing film and jet drops. Resulting sea-spray consist of particles in the range of tens of nanometres up to several micrometres. Based on visual estimation it is suggested that whitecap formation can occur at wind speeds greater or equal to about 4

m/s. At higher wind speeds, the direct shearing of wave tops can result in spume droplet formation at sizes from tens to hundreds of micrometres (O'Dowd & de Leeuw, 2007).

New particle formation in the marine boundary layer is believed to occur by two main mechanisms: 1, binary nucleation of sulphuric acid and water or 2, ternary nucleation involving three molecules. For the first time, production rates of tropospheric ultrafine particles (with detectable size of order of 3 nm diameter) were measured by Weber et al. (1996) and were shown to be orders of magnitude greater than nucleation rates predicted by the binary theory of homogeneous nucleation for sulphuric acid and water. The most likely third species is ammonia, which being abundant in the troposphere, has been shown to enhance nucleation rates of sulphuric acid. For ternary nucleation to occur, high concentration of sulphuric acid is required (Weber et al., 1998). This, however, is not a frequent phenomenon at the Mace Head station and occurs only with flow from the tropical sector (SW-WSW). In such cases, high concentration of MSA (methane sulfonic acid) is observed. Aerosol growth models predict that there is insufficient concentration of sulphuric acid for it to be a major factor in new particles formation events, and therefore aerosol growth cannot occur solely by its condensation (O'Dowd et al., 2002d). On particular days however, distinct relation between H_2SO_4 and ultra-fine particles (3nm~10nm) concentration was sporadically observed leading to the conclusion that H_2SO_4 may play an important role in the new particle formation, but not growth to a detectable size (Figure 3). Concentrations ratios of MSA/sulphuric acid and differences between the measured OH profiles and ozone photolysis frequency did not agree with the simple photochemical box model calculation (Berresheim et al., 2002). Differences were most prominent during particle nucleation events taking place on sunny days at low tide.

These results suggest that the oxidation capacity and the particle formation capacity in the coastal boundary layer were considerably affected by influence of other compounds present in the coastal marine environment (Berresheim et al., 2002).

Figure 3 shows an example of a typical coastal nucleation event at the Mace Head station. The highest concentration of newly nucleated particles coincide with low tide and increasing photolysis frequency - $JO(^1D)$. Low tide is believed to trigger an oxidative stress in algae species *Laminaria digitata*, which compensate this by release

of large quantities of molecular iodine (Ashu-Ayem et al., 2012), which in turn can later take part in the nucleation process. Photolysis frequency is a function of particle's radiation absorption ability, probability of decomposition and actinic flux in the UV-A range (Trebs et al., 2009). An initial decrease in H_2SO_4 concentration during the peak concentration of nucleation mode particles is clearly seen which points to the fact that, at least in the initial phase of nucleation, sulphuric acid plays a significant role in new particles formation but can later be coated with another chemical compound (e.g. organic or inorganic acids, iodine compounds).

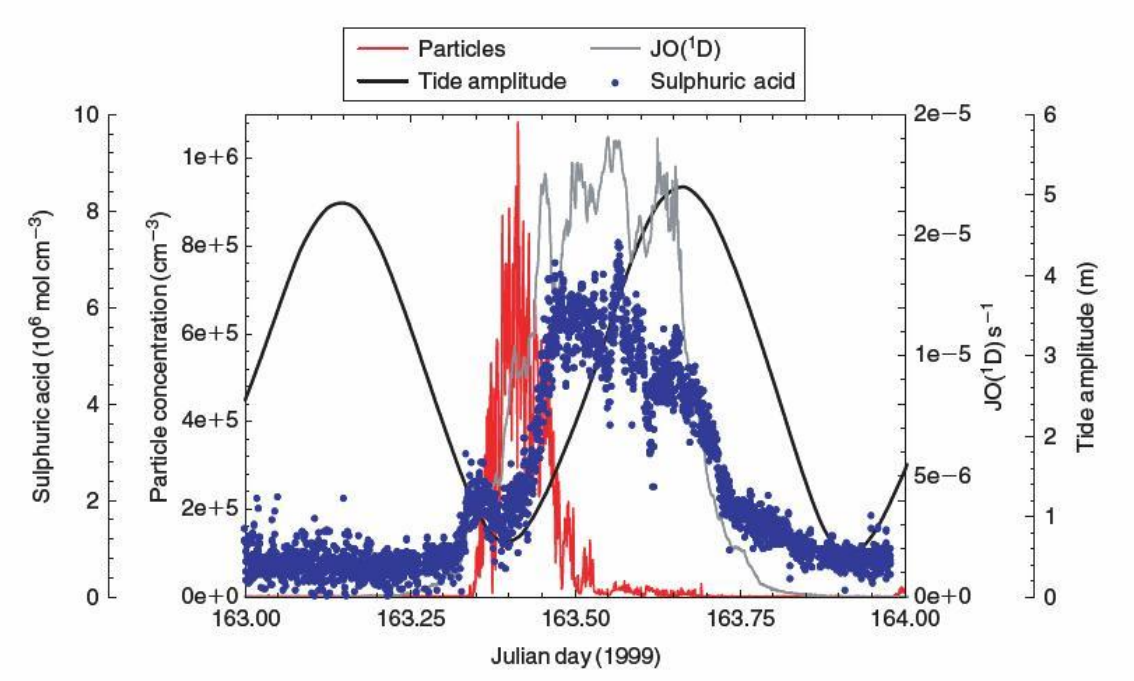

Figure 3. An example of a coastal nucleation event at Mace Head. Also shown are the tidal cycle, photolysis range JO (^{1}D) and sulphuric acid concentrations. Reproduced from (O'Dowd et al., 2002c).

Another compound which is periodically in abundance at Mace Head is iodine. It is well known that molecular iodine as well as its oxides is released by algae Laminaria digitata (Cainey et al., 2007a; Cainey et al., 2007b; Chance et al., 2009; Kupper et al., 2008; McFiggans et al., 2004; Palmer et al., 2005). The iodine is released in a short burst and might be triggered by production of H_2O_2 – a source of the OH radical. The key (aqueous phase) reactions in this system are suggested to be (Küpper et al., 1998):

$$H_2O_2 + I^- \leftrightarrow HOI + OH^-$$

$$HOI + I^- + H^+ \leftrightarrow I_2 + H_2O$$

For nucleation to occur, stable nuclei are required for a vapour to condense on. The newly formed particles with sizes greater than the critical cluster (about 1 nm) but still smaller than 3 nm, are called thermodynamically stable clusters (TSC). TSC can grow to detectable size (i.e. greater than 3nm) in two possible ways. First, the concentration of pre-existing aerosols is low (e.g. due to precipitation or clean sector flow conditions), and the growth to 3 nm size by self-coagulation only takes around one hour. Second, if there is a high concentration of available condensable vapours (such as organics, inorganic acids and ammonia in polluted sector flow) growth through condensation to detectable sizes and even to Aitken mode size occurs over a timescale of about 1-2 hours (Kulmala et al., 2000).

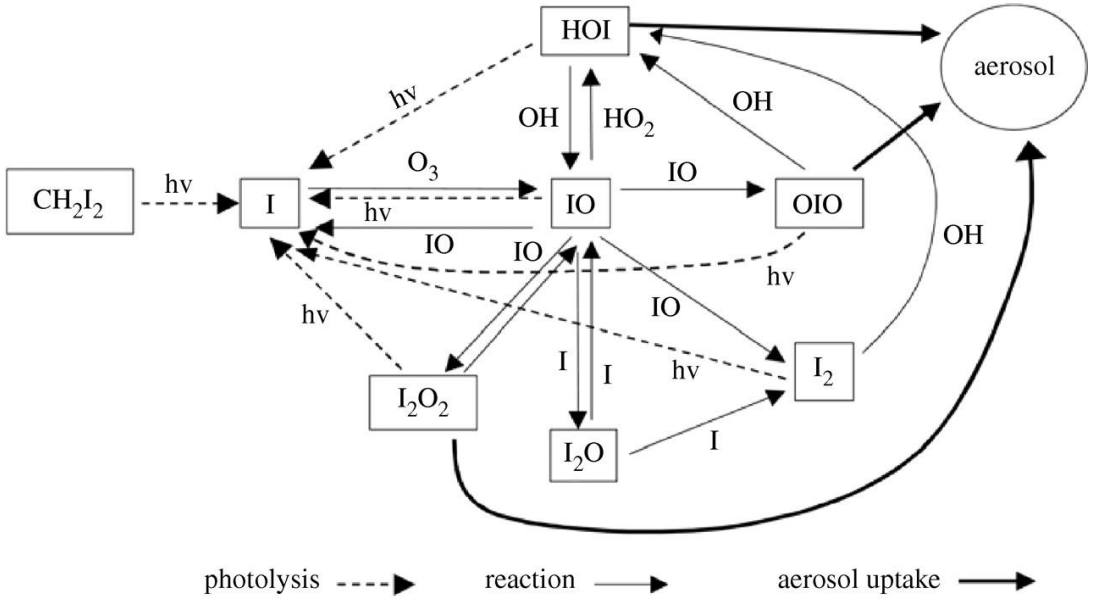

Figure 4. Iodine cycle schematic involving photolysis of biogenically released iodine compounds. Reproduced from (O'Dowd et al., 2002c).

The molecular iodine emitted into the atmosphere by algae during the oxidative stress undergoes photolysis and is a source of the majority of available iodine atoms. Free iodine reacts with atmospheric ozone forming the iodine monoxide (Figure 4). By the self-reaction of iodine monoxide the higher oxides are formed. If the concentration of such oxides is high enough, further polymerisation to clusters growing by further condensation can occur. In a few hours, the polymerisation can lead to the formation of iodine containing particles (Burkholder et al., 2003). Vakeva et al. (2002a) reported in their studies of two New Particle Formation and Fate in the Coastal Environment (PARFORCE) field campaigns that HGF of freshly nucleated fine particles (8 – 10nm) was low, which suggested the presence of a low solubility compound while clean

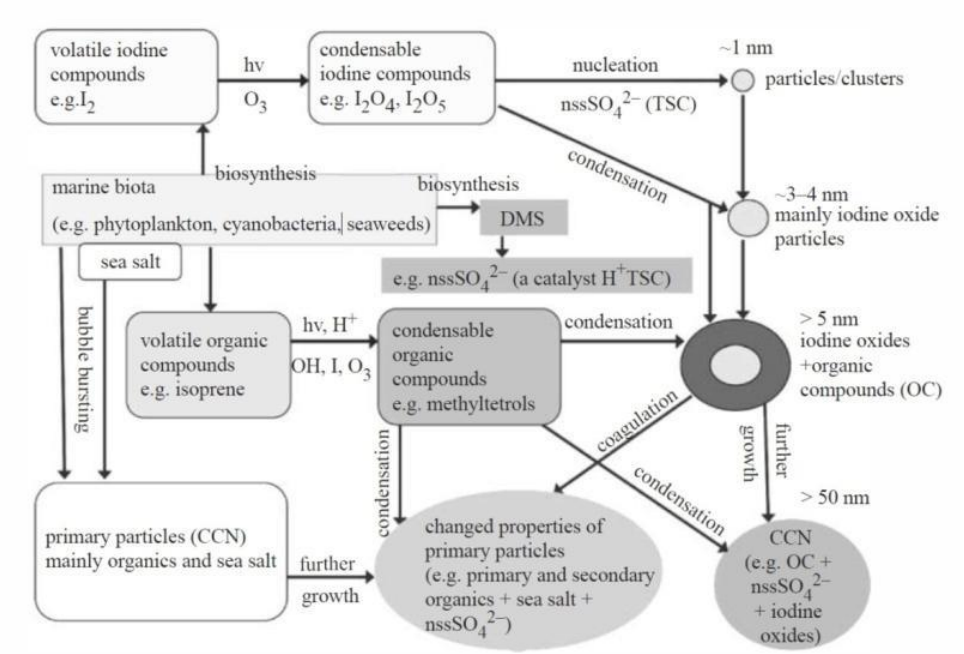

Figure 5. Secondary aerosol production in the marine air involving nucleation of iodine and sulphuric compounds. Reproduced from (Vaattovaara et al., 2006).

background growth factors resembled those of $(NH_4)_2SO_4$. Those results showed that HGF of new particles was comparable to I_2O_4. O'Dowd et al. (2012) have investigated a subset of this mechanism (the clustering of OIO only) in their study of the photolysis of CH_3I and CH_2I_2 and found that published IO and OIO concentrations are unable to explain the observed fine particle concentration bursts. As the sea salt and sulphate aerosol is always present in the coastal marine environment, it can act as a condensation sink for the precursor iodine oxides. It has been proven that heterogeneous nucleation is thermodynamically preferential to homogenous nucleation due to the lowered energy barrier by pre-existing insoluble or soluble nuclei. Therefore, despite the fact that the homogenous process cannot be favoured in competition for the iodine oxide vapours over the pre-existing aerosol, it can lead to a very efficient process of stabilisation of background TSCs (O'Dowd et al., 1999). Particles containing iodine may thus influence climate forcing in two ways: iodine species may stabilise the TSCs, or particles formed solely from iodine may directly enhance the CCN formation. (McFiggans et al., 2004). The latter seems to be contradicted in the recent study of McFiggans et al. (2010), in which they investigated iodine involvement in new particle formation. They concluded that iodine TSCs in fact were the nuclei for the volatile organic compounds to condense on and promote the growth to Aitken mode size particles. Studies involving application of the M7 microphysical model (in this model particles are represented by 7 groups (or

modes, hence M7 (Vignati et al., 2004)) showed that nucleation involving iodine oxide activation by sulphuric acid with additional concentration of low volatility condensable vapour, yielded over 600% increase in the aerosol concentration, comparing to background levels (Monahan et al., 2010). This confirms the fact that iodine alone may be unable to yield high concentration of Aitken mode aerosol, and thus cannot lead to an increase in CCN concentration.

1.3.2 Biomass burning

This type of aerosol emission includes periodic fields and pastures burn-outs as well as emissions caused by heating, waste burning and other non-industrial emissions. Effects of biomass burning have been so far poorly described but recent studies lead to the conclusion that biomass burning can have very significant impact on global climate.

Experiments performed by Hennigan et al. (2012) in an environmental chamber led to characterization of the effects of photo-chemical aging on biomass burning emissions resulting in climatologically important conclusions. Photo-oxidation of diluted exhaust fumes from incineration of twelve different types of fuels was investigated and resulted in substantial new particle formation that caused an increase in particle number concentration by a factor of four. The influence of generated secondary organic aerosol on new particle growth rates and strong enhancement in cloud condensation nuclei (CCN) concentrations was described. The resulting data were used in global model simulations and led to conclusion that nucleation in photo-chemically aging fire plumes produces evidently higher CCN concentrations over large areas. The resulting annual indirect forcing from CCN caused by nucleation and growth in biomass burning plumes was estimated at -0.2 W m^{-2}. These results show that biomass burning has a significant impact on climate that has not been previously considered.

1.3.3 Urban aerosol

The complexity of anthropogenic pollution is a major problem in fully understanding its impact on the climate. Emissions of very complex organic and inorganic compounds (produced mainly by industry, transportation and agriculture) make it very difficult to study. Main sources of the primary particles (directly emitted from combustion sources) include heavy and light duty diesel engine vehicles, wood burning, cooking, heavy and light industries and many others. Once emitted, they undergo modification in the

presence of several atmospheric oxidants (NO_x, OH radicals), leading to production of secondary particles with markedly different physical and chemical properties compared to their precursor primarily generated particles. Typical urban air is polluted with low-volatility gas-phase precursors, including long chain n-alkanes, PAHs and large olefins, which are potentially a large source of secondary organic aerosol (SOA), (Dall'Osto & Harrison, 2011). Polycyclic Aromatic Hydrocarbons (PAH's) have been found to be a major component of diesel engines and wood burning emissions (Schauer et al., 1999; Schauer et al., 2001). The photo-oxidation process involving these compounds yield high molecular weight oxygenated compounds which can undergo transition into the particle phase and lead to intensive SOA formation (Mihele et al., 2002). The current atmospheric models normally do not include SOA production from gas-phase reactions of polycyclic aromatic hydrocarbons (PAHs). Anthropogenic pollution intrusions at the Global Aerosol Watch station (GAW) Mace Head site were studied in this work.

1.4 Climate aerosol interactions, marine aerosol and the CLAW Hypothesis

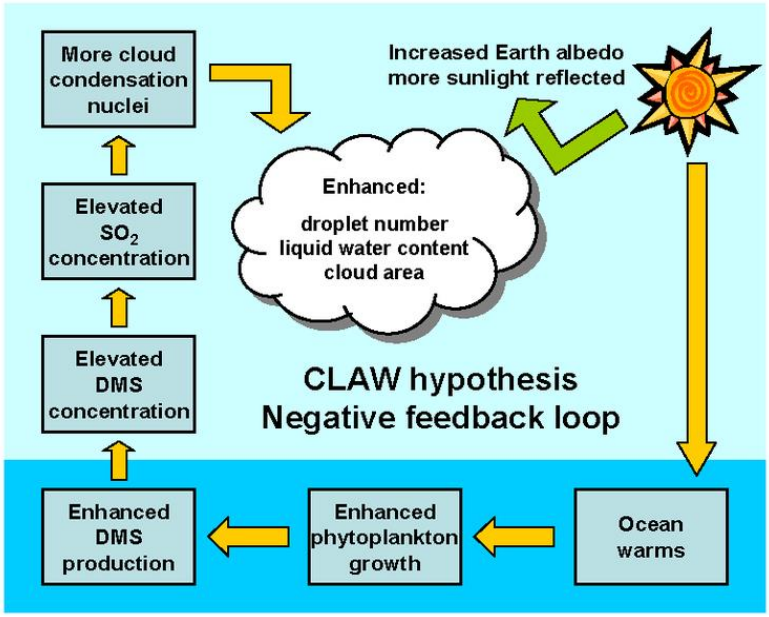

Figure 6. The CLAW hypothesis describes interactions between solar radiation energy and DMS production in ocean water and its impact on CCN production (Charlson et al., 1987).

"CLAW" derives from first letters of the surnames of the authors: Robert Charlson, James Lovelock, Meinrat Andreae and Stephen Warren (Charlson et al., 1987). The CLAW hypothesis was introduced as an idea of a feedback loop linking the ocean ecosystems with the Earth's climate (Charlson et al., 1987). The idea was proposed that

that dimethyl sulphide (DMS) producing phytoplankton might respond to variations in the ocean's surface temperature driven by climate forcing, and that this response was part of a negative feedback loop that stabilized the temperature of the atmosphere (Figure 6).

The hypothesis is an example of planetary self-regulating homeostasis (Lovelock, 1979) whose main component is based on the feedback loop that starts with an increase in the sun's energy reaching the ocean surface. This increase can accelerate the growth of certain species of phytoplankton by an increased photosynthesis rate. Phytoplankton species such as coccolithophorids, synthesize dimethylsulfoniopropionate (DMSP) as an end-product of their metabolism. Increase in the production of this waste leads to enhancement in concentration of its breakdown product, dimethyl sulphide (DMS). Emitted to the atmosphere by bubble bursting, DMS can be oxidized in the atmosphere to SO_2, and further to H_2SO_4 and other sulphate aerosols. Being moderately hygroscopic (HGF 1.6-1.7), these aerosols can grow in sub-saturated conditions to sizes allowing their activation into cloud condensation nuclei in super-saturated layers of air, thus increasing cloud droplet number. Less energy then reaches the ocean surface and thus the photosynthesis rate is slowed down and negative feedback loop is created. This process is a good example of the indirect aerosol effect (see chapter 1.2.3). Figure 6 shows schematic diagram describing the CLAW hypothesis. Note that the feedback loop can operate in the reverse direction, such that a decline in solar energy leads to reduced cloud cover and thus to an increase in the amount of solar energy reaching the ocean surface. Some laboratory and field studies of the CLAW hypothesis reported that there may be an evidence supporting its mechanism, (Andreae et al., 1995; Ayers & Gras, 1991; Cropp et al., 2005), although Vallina et al. (2007) have found evidence that opposes the CLAW theory by claiming that there exists strong positive correlation between energy reaching surface layer of the ocean and DMS concentrations irrespective of latitude, temperature or phytoplankton concentration. Others have suggested that a mechanism similar to the CLAW hypothesis may operate in the Earth's sulphur cycle without the requirement of a biological component (Shaw et al., 1998).

At the time the CLAW hypothesis was proposed little was known about organics' contribution to global climate forcing. Recent studies describing significant influence of biogenically produced aerosols contradict main fundamentals of CLAW theory

(O'Dowd et al., 2010; O'Dowd et al., 2002b; O'Dowd et al., 2004; O'Dowd et al., 2002e; O'Dowd et al., 2008; Ovadnevaite et al., 2011a; Ovadnevaite et al., 2011b). It has been shown that the marine aerosol contributes significantly to the global aerosol load and, consequently, has an important impact on both the Earth's albedo and climate. The physical and chemical characteristics of submicron marine aerosol over the North Atlantic Ocean during plankton blooms progressing from spring through to autumn (Figure 7) changes so that the organic fraction dominates and contributes about 63% to the submicron aerosol mass in summer (about 45% is water-insoluble and about 18% water-soluble (O'Dowd et al., 2004)). In winter, when biological activity is at its lowest, the organic fraction decreases to 15% (O'Dowd et al., 2004). Model simulations indicate that organic matter can enhance the cloud droplet concentration by 15% to more than 100% and is therefore an important component of the aerosol–cloud–climate feedback system involving marine biota. The results indicate that an important source of organic matter from the ocean was omitted from current climate-modelling predictions and should be taken into account (O'Dowd et al., 2004).

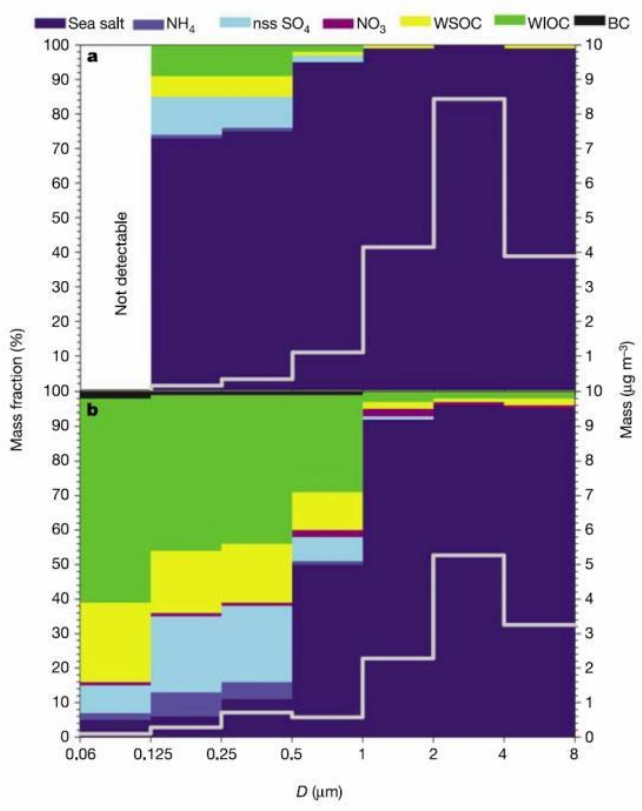

Figure 7. Chemical composition of marine aerosols - average size-segregated chemical compositions and absolute mass concentrations for North Atlantic marine aerosols sampled for low biogenic activity (a) and high biogenic activity (b) periods. The concentrations of water-soluble organic carbon (WSOC), water-insoluble organic carbon (WIOC) and black carbon (BC) are reported as mass of organic matter (O'Dowd et al., 2004).

Laboratory and field experiments performed over the past ten years have proven that, not only sulphuric compounds can act as sources of CCN to the remote marine boundary layer but also more intricate, organic-inorganic complexes can act as efficient cloud condensation nuclei sources. Murphy et al. (1998) obtained empirical evidence that major numbers of CCN-size particles containing sea salt are enriched with organics in the remote marine boundary layer (MBL). Bigg (2007) proved the existence of an organic alternative to DMS as a source of CCN. Sellegri et al. (2006) and later Bigg and Leck (2008) concluded that bubble bursting at the ocean surface is a major source of not only mass but also aerosol number to the boundary layer and that organic surfactants have a major impact on the number concentration of CCN. This mechanism facilitates the transfer of inorganic and organic compounds of sea water to the atmosphere. Inorganic components are composed of sea salt and sulphates whereas the organic compounds originate from phytoplankton waste and other organic matter in the ocean surface. In this light, the concentration of CCN is an outcome of emissions of organically enriched sea salt spray reliant on biological activity and wind speed (Quinn & Bates, 2011). This updated view of the multiple sources of CCN to the MBL is depicted in Figure 8.

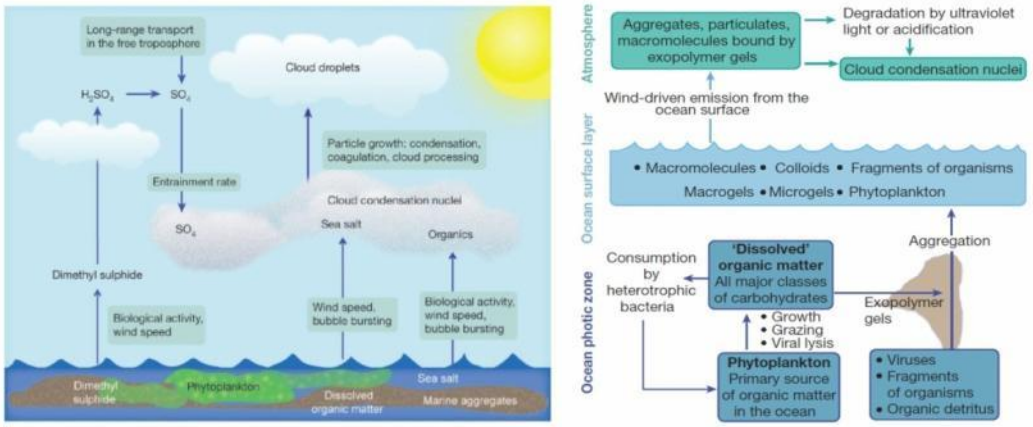

Figure 8. Major sources and production mechanisms for CCN in the remote MBL. DMS contributes to the MBL CCN population primarily via particle nucleation in the free troposphere in cloud outflow regions with subsequent subsidence. Sea salt and organics are emitted as a result of wind-driven bubble bursting. Phytoplankton is the primary source of organic matter in the ocean. The large pool of dissolved organic matter composed of all major classes of carbohydrates resides within the ocean photic zone and is derived from phytoplankton growth, grazing by predators and viral lysis. Also residing within the photic zone are small particulates composed of other algae, bacteria, viruses, fragments of larger organisms and organic detritus. This organic matter becomes bound together by exopolymer gels secreted by marine organisms. The resulting aggregates are injected into the atmosphere through bubble bursting and contribute to the MBL CCN population either directly or after degradation by ultraviolet light or acidification. Figure reproduced from (Quinn & Bates, 2011).

2. Previous Studies of Hygroscopicity

Field studies into aerosol hygroscopicity have been performed in the last fifteen years or so over extensive areas of the marine environment, both over open oceans (on ships) and in coastal areas (such as Mace Head). Covering the majority of oceans, these comprehensive studies elucidated not only the origins and state of mixing of newly formed particles (Vakeva et al., 2002a; Vakeva et al., 2002b) but also identified major hygroscopic groups and major aerosol constituents (Berg et al., 1998; Massling et al., 2006; Massling et al., 2003; Swietlicki et al., 2000; Tomlinson et al., 2007; Zhou et al., 2001a).

Generally, researchers reported a group of moderately hygroscopic particles (with HGF (see equation 1 on page 11) ranging from 1.6 to 1.9) as the predominant hygroscopicity group in most remote marine environments. The most common definition of the HGF describes it as a difference between the dry particle's size – D_0 (usually at RH<10%) and particle size after the specific for the instrument treatment (here high relative humidity set at 90%). The dependence of hygroscopicity on air mass origin was the most evident influencing factor, particularly when the air was sampled close to anthropogenically-polluted areas. HGFs of moderately-hygroscopic, internally mixed aerosol particles in the marine air were reported to be higher than aerosol originating from anthropogenically influenced areas (Berg et al., 1998) and sometimes even higher that HGF of pure neutralized sulphates (such as ammonium sulphate). In the remote marine air it was often the only hygroscopic group observed. This led to the conclusion that, at least part of the marine aerosol emitted by oceanic organisms, consisted of non-neutralized sulphate (concentration of ammonia needed for the full neutralization of dimethyl sulphide-derived sulphuric compounds was usually too low in the marine environment (Quinn et al., 1988)).

The primary sea salt aerosol particle concentration was reported to correlate well with wind speed in most of the studies. This type of aerosol was represented by the Sea Salt group of aerosol hygroscopicity, with HGF above 1.9 (sometimes exceeding 2.2 in value). Berg et al. (1998) reported that the externally mixed sea salt particles were sometimes observed even in the size range of 35nm. This was later confirmed by the laboratory studies of Mårtensson et al. (2003) who found that the majority of freshly

generated sea salt – like aerosol was found to dominate sizes of around 100nm in number size distribution, but with the considerable contribution of particles from the lower size range.

The primary sea salt aerosol production starts when wind speeds exceed 4 m/s (Lewis & Schwartz, 2004). Although the majority of mass of the primary aerosol is carried by super micron particles associated with forced breaking of sea water bubbles (Sellegri et al., 2006), the highest number concentration occurs in the submicron size range. This property of the primary aerosol is very important in estimating the radiative climate forcing, as the most effective scattering of solar radiation occurs in the aerosol size regime close to the wavelength of the radiation making the hygroscopicity measurements highly relevant.

The HGF of the more hygroscopic aerosol group exhibited lower values than the pure reference ammonium sulphate in most of the studies (Asmi et al., 2010; Crahan et al., 2006; Fuentes et al., 2011; Kreidenweis et al., 2005; Mochida et al., 2011; Ovadnevaite et al., 2011a; Topping et al., 2005). This suggests that the volume fraction of ammonium sulphate was less than 1.0 and, subsequently, points towards organic compounds as being the additional volume fraction of the more hygroscopic particles group (O'Dowd et al., 2004; Quinn & Bates, 2005). Kaku et al. (2006) estimated that c.a. 8% of the aerosol sampled over the North-eastern Pacific Ocean was composed of insoluble organic compounds. Furthermore, it has been suggested that the organic mono layer created over the aerosol droplets may significantly alter both sub- and supersaturated aerosol behaviour, suppressing its activation and cloud droplet formation efficiency. Studies performed by Ovadnevaite et al. (2011b) using an aerosol mass spectrometer revealed an even higher organic contribution to the primary generated marine aerosol. It was estimated that up to at least 37% of marine organic mass peaking at 3.8 $\mu g/m^3$ can be associated with the primary generated sea spray.

Another mechanism influencing the HGF of the primary marine aerosol was described by Svenningsson et al. (2007). It involves H_2SO_4 uptake by the sea salt aerosol particles and subsequent conversion of part of NaCl into Na_2SO_4, which exhibits HGF value of around 1.66. This conversion results in a HGF drop of the sea-spray aerosol particles whose HGF resembles that of ammonium bisulphate. Observations of excess non-sea salt sulphate in the marine air by Andreae et al. (1986) seem to support

this phenomenon, adding another mechanism lowering the HGF, as described by Ovadnevaite et al. (2011b).

A recent study by O'Dowd et al. (2010) reports occurrence a large scale occurrence of the marine air open ocean nucleation events. During these new particles production periods, particles as small as 15 nm were observed to grow to sizes of over 50 nm in a time frame of 48 hours. During these plumes, particles at the lower measurement size range of the HTDMA exhibited HGF values of around 1.4, similar to highly oxidized organic compounds. A growth rate of 0.8 nm/h points to a source region particles located c.a. 700 km from the shore. Taking into account the duration of growth events, it can be concluded that the nucleation occurs over the large spatial scales. This supports the statement that the marine secondary aerosol contributes significantly to the overall marine aerosol population.

Studies performed over the Arctic pack ice revealed that particles of the nearly hydrophobic group are more ubiquitous there than over the warm water oceans during the summer (Zhou et al., 2001b). Orellana et al. (2011) suggest that, while composed primarily of insoluble organic polymers, the microgel particles can be formed in the process of bubble bursting and can undergo a phase transition when exposed to changes in pH, subsequently growing and acting as efficient CCN. Moreover, UV radiation can easily break colloidal gels to a particle size range from around 40 nm down to a few nanometres which, in turn, can influence new particle formation and increase the CCN number concentration.

Studies performed in the rural and urban environment generally revealed existence of a bimodal HGF spectrum in areas situated closer to the large urban centres, while the more remote rural sites were under influence of a more aged, cloud processed, hygroscopic monomodal aerosol particles (Busch et al., 2002; Ehn et al., 2007; Gasparini et al., 2004; Gasparini et al., 2006; Hämeri et al., 2001; Petäjä et al., 2005; Svenningsson et al., 1994; Svenningsson et al., 1992; Van Dingenen et al., 2005; Weingartner et al., 2002). The classification of the HGF modes in such regions was changed, comparing to the marine environment, to better reflect overall lower values of hygroscopic growth factor. The nearly hydrophobic group was described as particles exhibiting HGF of 1.0-1.1, the less hygroscopic group exhibited HGF values from 1.25 to 1.35 and the more hygroscopic group HGF values from 1.4 to 1.6.

The rural environment is often influenced by biomass burning events, during which the nearly hydrophobic (HGF 1-1.12) and the less hygroscopic (HGF 1.125 – 1.3) particle groups are dominant. Due to an incomplete and low temperature burning (Mircea et al., 2005), emitted aerosol contains organic compounds of limited hygroscopicity. Aitken mode particles represent better the primary chemical composition in this environment, as their growth is usually driven by the condensation of available gaseous compounds and by coagulation. An accumulation mode particle usually composes of the transformed Aitken mode particles which undergo cloud processing. While primarily less hygroscopic, more hydrophilic material is added and particles return from cloud outflow larger and more hygroscopic. These processes usually occur in urban environments and close to rural environments which leads to observation of an externally mixed aerosol. Less hygroscopic aerosol are generally observed in nearly all the forests sites, while the nearly hydrophobic aerosol is observed usually at sites influenced by combustion, transport and agricultural activities such as occur in the Po Valley or central Germany.

The boreal forests are found to be sites of efficient new particle production events despite lack of anthropogenic emissions. It was found that the main precursors for particle formation were monoterpenes emitted by the needle trees (Tunved et al., 2006a; Tunved et al., 2006b). This was later confirmed by O'Dowd et al. (2002a) and Cavalli et al. (2006) who concluded that, in order to be able to explain the mass increase during the nucleation events, the gaseous monoterpenes oxidation products have to be accounted for as the precursors to particle formation. The chamber experiments performed by Virkkula et al. (1999) showed that the HGF of particles generated by a mixture of monoterpenes such as alpha-pinene and oxidants ranges between 1.07 and 1.12. In a field study, Hameri et al. (2001) showed that the nucleation mode composed of the internally mixed, less hygroscopic aerosol exhibiting HGF of 1.1 – 1.15. This indicated the important role of condensing organic vapours in the new particle formation events. Emissions of monoterpenes by needle forests are correlated well with the temperature. This link points to the important dependency between the global temperature changes and the intensity of new particle formation, thus influencing the direct and indirect aerosol climate effect.

The urban environment is mostly affected by transportation and heavy industry emissions. There are relatively few extensive studies of hygroscopicity of diesel and petrol engines exhaust. Weingartner et al. (1997) showed that HGF values of diesel generated soot particles ranged between 1.01 and 1.02. Furthermore, the spark generated soot particles tend to collapse when exposed to high humidity, thus exhibiting HGF values less than 1. Grose et al. (2006) reported that freshly nucleated diesel exhaust particles consisted mainly of sulphates, which led to the conclusion that sulphuric acid produced from high sulphur content fuel takes part in new particle formation as a stable cluster's precursor. It is possible that the nearly hydrophobic aerosol group undergoes ageing and oxidation processes and, ultimately, enters the domain of a less hygroscopic aerosol group. The majority of the more hygroscopic aerosol measured by a HTDMA in urban environments exhibits HGF values similar to those measured in rural sites and is usually associated with regional background emissions entering the city via advecting air masses. This results in the urban aerosol being almost always externally mixed with nearly hydrophobic particles, created by transportation and industry, with a more hygroscopic group arriving from the outskirts of urban centres. On the other hand, efficient combustion of biofuels and wood burning pollution can contribute to the more hygroscopic group of aerosol, as these processes generate aerosol rich in alkaline salts but very lean in organic compounds and soot (Rissler et al., 2005).

In general, present HTDMA data are unable to reveal the exact chemical composition of the more hygroscopic aerosol groups and the HTDMA is more of an indirect technique to chemically characterize the aerosol. Complementary chemical aerosol measurement instruments (such as the AMS), used in parallel with hygroscopicity studies, bring added value with more detailed chemical information along with the HTDMA state of mixing (i.e. hygroscopic separation of the particles groups with different affinity to the water).

3. Instrumentation

3.1 Hygroscopic Tandem Differential Mobility Analyser (HTDMA).

A tandem differential mobility analyser (TDMA) principle of operation is based on an electric field created by application of a high voltage (in kV) to the central electrode. This enables classification and analysis of charged aerosol particles, whose size can range from several nanometres to about 1µm in a gaseous medium. A typical setup usually consists of:

(1), a *particle charger*, which allows the aerosol particles to acquire a specific electrical charge distribution (a function of particle size). In a dipolar diffusion particle charger the gas is ionized by a radiation from the radioactive source (e.g. ^{85}Kr). Gas ions of both negative and positive polarity diffuse to the aerosol particles and charge equilibrium is attained

(2), a *classifier*, which selects a narrow (quasi-monodisperse) aerosol size distribution (also known as DMA1)

(3), a particle conditioner, depending on the type of setup, can be an oven for volatilization of organic components, an alcohol vapour infuser, or a humidifier for exposure of particles to water vapour

(4), *differential mobility analyser (DMA2)*, which separates particles with different electrical mobility after conditioning. The path of the particles inside of the DMA2 is shaped by the electric field with the direction perpendicular to the laminar sheath flow. The voltage between the central rod and the outer, grounded, shell is controlled and adjusted accordingly to the electrical mobility of a chosen particle size bin. This mode of DMA operation is also called continuous voltage scanning and it is a working principle of the scanning mobility particle sizer (SMPS).

(5), an *aerosol particle detector,* using e.g. a TSI condensation particle counter (CPC).

Figure 9 shows a cross section through a typical DMA. F_1 is a sheath flow, F_2 is the polydisperse aerosol sample, F_3 is the quasi-monodisperse (classified) aerosol exiting the DMA and the F_4 is an excess air.

The electrical mobility, Z, is a function of particle diameter, D, and the number p of elementary charges, i:

$$Z(D) = \frac{p \cdot i}{3\pi\eta D}\left\{1 + Kn\left[A + Bi^{-\frac{C}{Kn}}\right]\right\} \quad (2)$$

where, Kn is the Knudsen number $2\lambda/D$ (λ being the mean free path of gas molecule), η stands for dynamic fluid viscosity. A, B and C are empirical constants: A=1.142, B=0.558 and C=0.999 (Allen & Raabe, 1985).

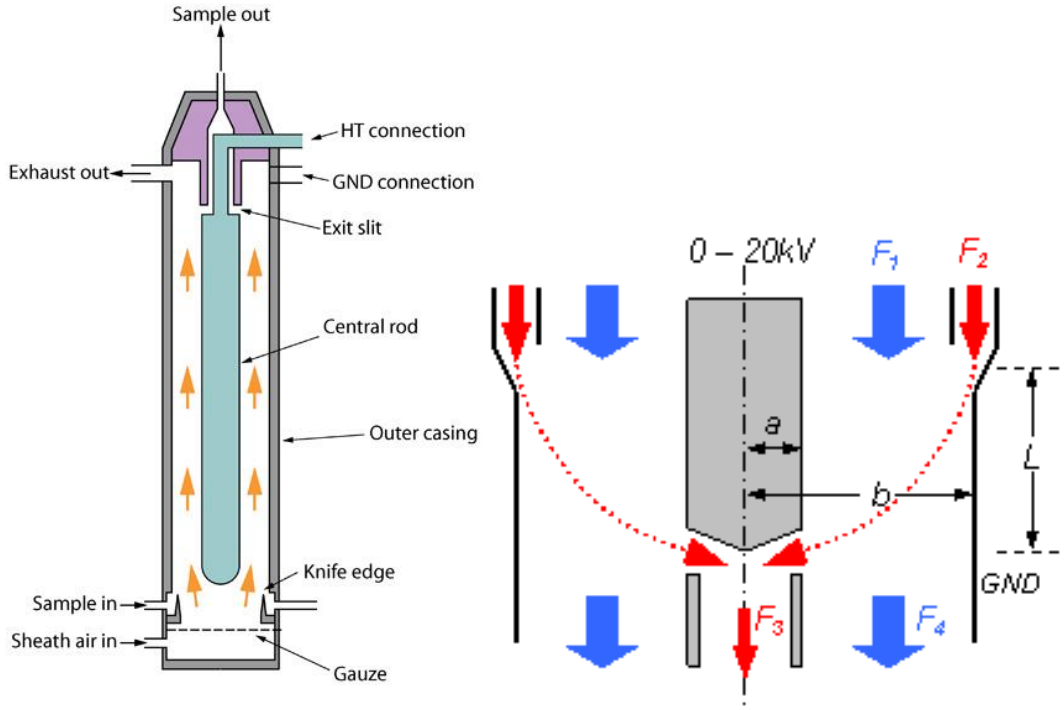

Figure 9. Example of a typical DMA assembly and cross section through the cylinder and central rod.

3.1.1 The HTDMA setup

The HTDMA setup deployed at the Mace Head station follows recommendations described by (Duplissy et al., 2009). Figure 10 shows a schematic diagram of the HTDMA used in this study. The HTDMA setup deployed at the Mace Head atmospheric research station consists of Nafion dryer at the inlet of a first DMA (DMA1), with a Gore-Tex humidifier regulating the relative humidity in a second DMA (DMA2) by humidifying the aerosol and the sheath flow. A CPC is used to count the aerosol number concentration after DMA2. The Peltier-controlled temperature box contains the second DMA and sheath flow coil for temperature equalization. PC running

the control software and data acquisition tools is placed outside the system to minimise the interferences with the relative humidity (RH) probes.

Acquired data were checked for temperature stability, RH stability in DMA2 and recalculated to 90% RH when applicable. Inversion bins (see chapter 3.1.4) were set depending on the period of measurement: 0.05 for short term studies and 0.1 for long term observations. In this work, a piecewise linear fit of retrieval was used in order to calculate the growth factor probability density function (GF-PDF, see chapter 3.1.2).

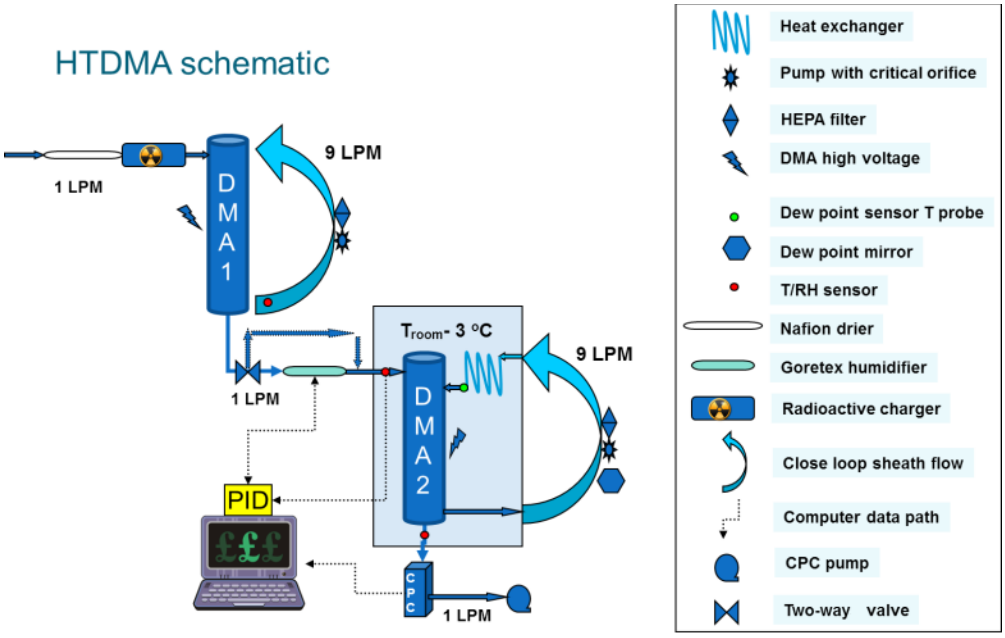

Figure 10. HTDMA setup used in this work, currently deployed at the GAW Mace Head site.

3.1.2 The principle of HTDMA data inversion.

The measured distribution function (MDF) is represented by an integral of the particle's true growth factor probability density function - GF-PDF.

Probability density function describes how likely it is for the variable (here HGF) to assume a certain value. The integral of the variable density over the region gives the probability of said variable to fall within a given region. The probability density function is non-negative everywhere, and its integral over the entire space is unity. It is a result of the transfer functions of the DMAs being of finite width (instead of being just a single value) and the TDMA's transfer probability (i.e. probability of a particle of a

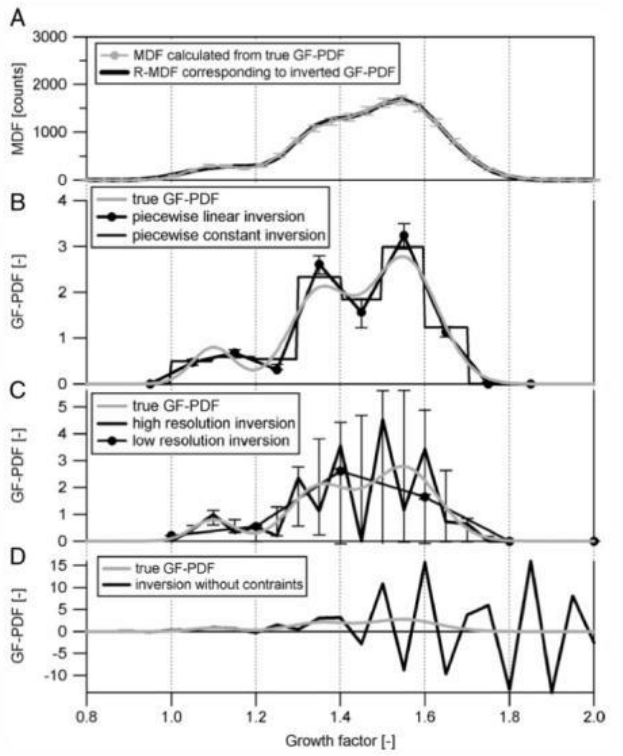

Figure 11. Principle of TDMAinv (reproduced from (Gysel et al., 2009)).

given electrical mobility passing through the DMA's electrical field into the sampling slit) being dependent on the HGF of the sample. Therefore, to account for these uncertainties, a suitable data inversion is needed (Gysel et al., 2009). This approach represents the inverted GF-PDF as a piecewise linear function instead of an overlapping Gaussian distribution as used in the TDMAfit algorithm (Stolzenburg & McMurry, 1988). HTDMA data included in this thesis and in all of the publications have been inverted and analysed using the TDMAinv-toolkit which allows for automatic data inversion and analysis (http://people.web.psi.ch/gysel/).

At the centre of all TDMA inversion approaches is a technique which allows finding an inverted GF-PDF such that a minimum residual is obtained between the measured MDF and the fitted (or reconstructed) MDF (R-MDF). The R-MDF is usually calculated from the inverted GF-PDF using the TDMA's mathematical model (Cubison et al., 2005). In the inversion approach used in this work, the inverted GF-PDF is represented by the piecewise linear function as shown in **Figure 11**. Panel A shows the measured distribution function (MDF), whereas panels B, C, and D shows simulated true GF-PDF's. The MDF inversion was done using a piecewise linear (thick, bold line in panel

B) and piecewise constant function (thin, bold lines in panel B). The bold line in panel A represents the reconstructed MDF (R-MDF) – the result of sending the piecewise linear inversion back through the forward function. The forward function is a mathematical model of the TDMA response for a particles exhibiting true GF, and can be described by:

$$m_{\mathrm{TDMA}}^{g,\mathrm{total}}(g_{\mathrm{set}}, D_0) = \sum_{i=1,2,\ldots} N_{\mathrm{inlet}}^{i}(D_i) \int_0^{\infty} c(\hat{g}, D_i) K_{\mathrm{TDMA}}^{g,i}(g_{\mathrm{set}}, \hat{g}, D_0)\, \mathrm{d}\hat{g} \qquad \textbf{(3)}$$

Detailed description of TDMA forward function can be found in (Gysel et al., 2009).

Panel C shows the effect of an incorrect resolution set in the inversion algorithm (thick and thin bold lines). Panel D shows the oscillations that can occur without fit constraints (Gysel et al., 2009).

3.1.3 HTDMA Calibration

As the kernel function is a key element of the data inversion and analysis, it has to be properly calibrated. The kernel function can be described as the normalised particles concentration carrying *n* charges with dry diameter $D_n = u_n(D_0)$, which is measured at the outlet of the TDMA. Conditions are that the DMA1 is set to diameter D_0, the DMA2 is set to diameter $D_{set} = g_{set}D_0$ and all particles of diameter D_n exhibit a true HGF.

Figure 12 shows a theoretical kernel for a HTDMA with a flow ratio of 1:10 (aerosol/sheath) in both first and second DMAs and for particles with a dry diameter D_0 = 100 nm. It is not possible to calibrate the HTDMA response for particles with HGF other than a true growth factor of 1 (dashed line in Figure 12) because there is no treatment that can make all particles grow by an exactly known HGF. To calibrate the TDMA for HGF = 1.0 (i.e. offset calibration), it is necessary to bypass the humidifier, and thus not change the particle size between both DMAs. The mean HGF of MDF measured during the calibration is usually several percents different from 1. Calibration of measured distribution function (MDF) is done by dividing the HGFs of all data points by the value of the offset. This guarantees that a HGF = 1.0 is obtained for particles exhibiting a true HGF of 1.0. RH uncertainties, which are larger than the HGF accuracy

achieved by a correctly operated HTDMA (i.e. the air flow rates in the DMAs are maintained at constant level and correct particles sizing of both DMAs has been tested with certified monodisperse PSL spheres), make accurate calibration with salts of known HGF very difficult to attain.

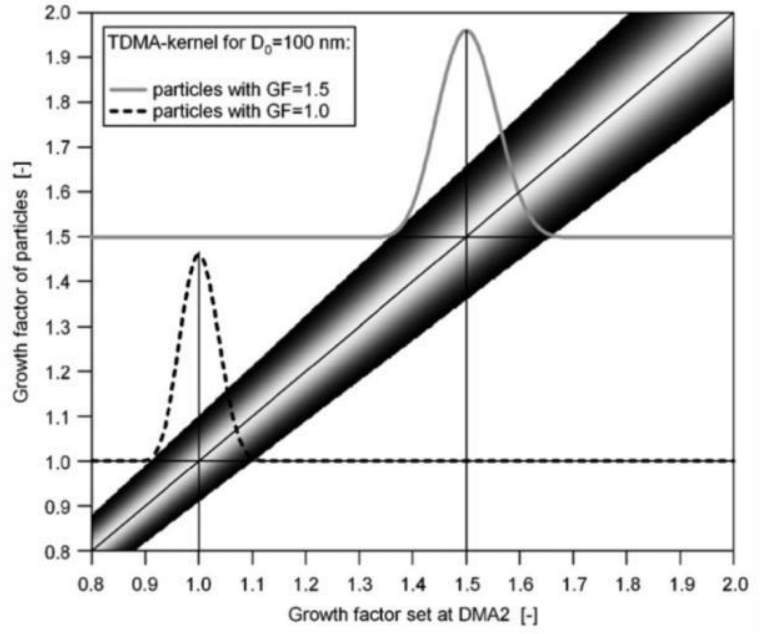

Figure 12. Image of theoretical TDMA kernel function for an aerosol to sheath flow ratio of 1:10 in both DMAs and for particles carrying a single charge with dry diameter D_0 = 100 nm. The dashed and grey lines illustrate the TDMA response on particles exhibiting a HGF of 1.0 and 1.5, respectively.

The MDF measured for the offset calibration is also utilized in estimation of the HTDMA kernel width, i.e. determination of the actual width of the TDMA transfer function. This determination (or calibration) is done by changing the full width at half maximum ($FWHM_D$) of the DMA transfer functions until the corresponding HGF matches the measured distribution function of the offset calibration. Figure 13 shows an example, where the DMA's $FWHM_D$ was found to be around 1.536 times wider than estimated by theory, constantly across a range of different D_0. The broadening occurring in DMA1 and DMA2 is considered to be the same as it is virtually impossible to find differences in broadening factors between both DMAs.

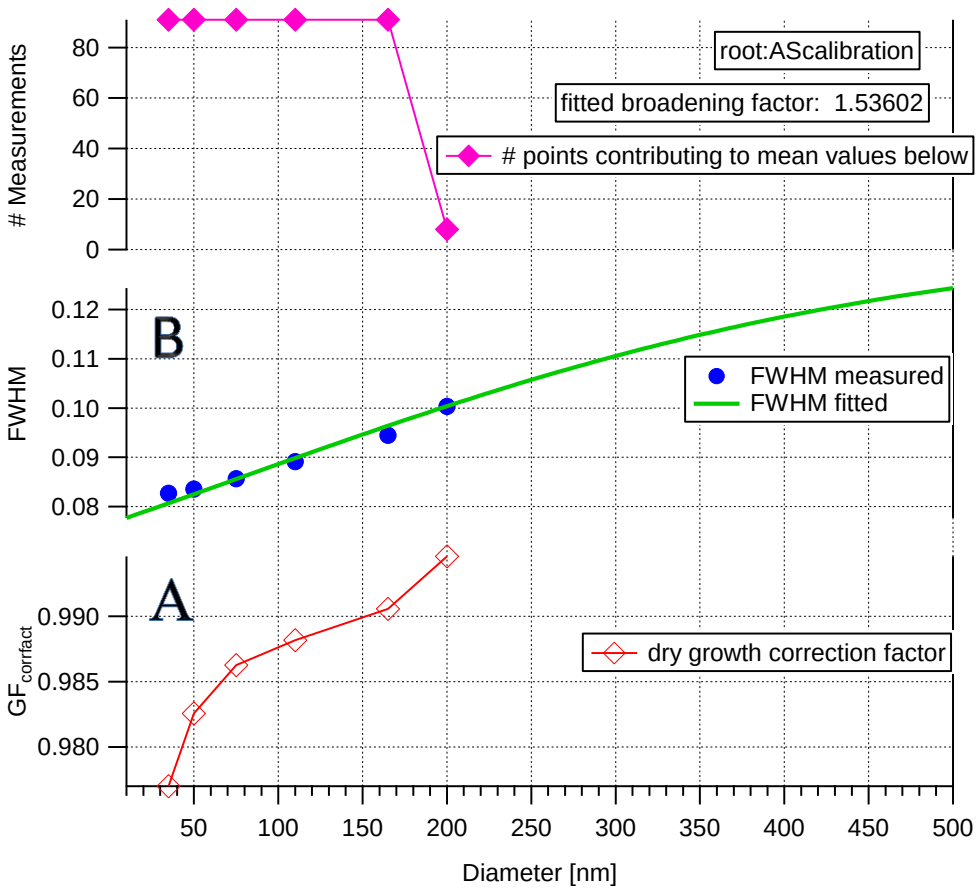

Figure 13. Offset calibration of TDMA. (A) HGF offset correction factor. (B) Measured relative $FWHM_D/D_0$ of DMAs**.**

3.1.4 Choosing proper inversion resolution for the dataset.

A proper resolution of the inversion (i.e. retrieval size bins separation) is of main concern in HTDMA data analysis. Too low a retrieval bin size setting will lead to unreasonable high amount of peaks, not justified by the physico-chemical properties of the sample. On the other hand, choosing too large a bin size will lead to smearing and loss of information about the intricate shape of the true HGF distribution. The synthetic example of choosing too high or too low a bin resolution is illustrated in Chapter 3.1.2, **Figure 11**, panel C as thin and thick black lines, (Gysel et al., 2009). Excessive oscillations can be seen as unreasonable high numbers of peaks. While the integral of such a retrieval will still yield proper particles concentration fractions, the mixing state of an aerosol sample however, will be shown incorrectly. To avoid such interpretation, one has to carefully check the influence of the given resolution on the analysed dataset. In order to do this, a HTDMA transfer function width for a few key HGFs has to be found. It can be done using the kernel function calculated for the HTDMA based on

ammonium sulphate dry calibration data (see Chapter 3.1.3). The key HGF can be chosen by specifying main aerosol chemical compounds (e.g. ammonium sulphate, sea salts) for the given measured samples (i.e. given dataset), extracting one-dimensional slices through the TDMA kernel function, corresponding to their known HGFs and fitting the obtained distributions with a log normal function until minimal residuals are obtained.

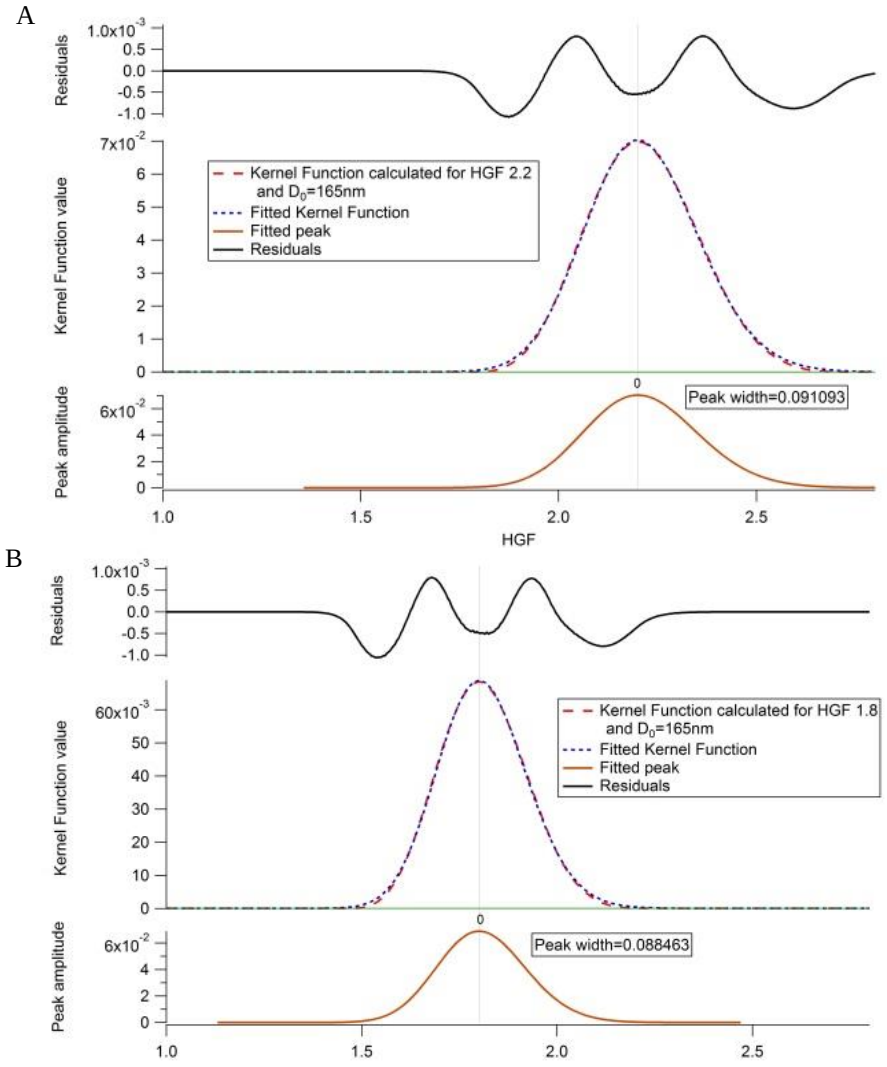

Figure 14. An example of TDMA transfer functions obtained by a fitting one-dimensional slice through the TDMA kernel functions with a log normal function. In this case, two main aerosol compounds were identified and their typical HGF values of 2.2 (Sea Salts – panel A) and 1.8 (Ammonium Sulfate – panel B) were selected from the TDMA Kernel Function.

The resulting peaks can be used for fitting the ambient data. Depending on the chosen retrieval resolution, precision of the fit will vary when using fixed peak width values

obtained from the Kernel function fitting (Figure 14). Changing the retrieval bin size (i.e. resolution), one can obtain the fit that matches the best chosen key compounds. In such case, the resolution of the inversion is chosen properly and will represent well the entire dataset. An example of a good retrieval resolution is shown in Figure 15 during the high sea salt event.

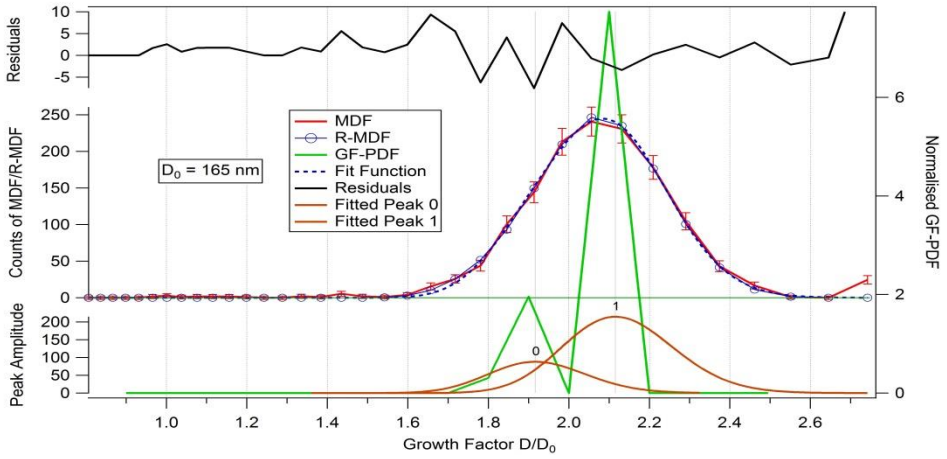

Figure 15. An example of retrieval resolution matching well measured ambient data during a high sea salt event at Mace Head station.

The green line represent retrieved GF-PDF for one scan for D_0=165nm. The measured distribution function (MDF) is fitted with the reconstructed MDF (R-MDF) calculated from the inverted HGF-PDF using the TDMA forward model described by (Cubison et al., 2005). If the residuals cannot be decreased further, the algorithm assumes that the fit is the best possible. However, in the case of an inadequate retrieval resolution, the fit can include several peaks, not justified by the chemistry and physics of the aerosol sample. In this example, the fitted piece-wise linear function corresponds well with two log-normal peaks fitted using an external fitting tool constrained with the peak width acquired from the calculated kernel function. The peaks represent two key components found during the high sea salt events: internally mixed ammonium sulphate with the HGF around 1.8 and sea salt exhibiting an electrical mobility HGF of 2.2. This proves that, in the case of high sea salt events, the chosen resolution of the retrieval will be adequate and will yield a reasonably inverted HGF-PDF. In order to be able to properly asses the best inversion resolution for the given sample, one has to perform such a test for different cases of aerosol distribution and mixing states. Only then one can be certain that the chosen resolution will allow proper retrieval for the whole dataset.

3.1.5 Error estimation

The number of counts in a data point of the MDF is affected by uncertainties. The uncertainty of the number of counts to resulting from Poisson counting statistics can be described as $\Delta n = \sqrt{n}$. Changes in the aerosol concentration in the HTDMA inlet, Δn_{inlet}, can be estimated as 5% for ambient concentrations and 5-10% for the nebulizer. Uncertainty in Δn_{kernel} arising from kernel calculation errors is estimated to be around 1%. Overall estimation uncertainty can be calculated from the expression:

$$\Delta n_{total} = \sqrt{n^2 + n_{inlet}^2 + n_{kernel}^2} \quad (4)$$

Good estimation of the counting uncertainty, Δn_{total}, allows appropriate weighting of each measured point of the MDF while inverting. Quantitative interpretation of the residuals of the inversion results can also be attained. The systematic uncertainties are taken into account outside of the inversion process (Gysel et al., 2009).

3.2 Aerosol mass spectrometer (AMS)

The Aerodyne high resolution time of flight aerosol mass spectrometer was used in this thesis to study the aerosol particle chemical composition.

3.2.1 Aerosol Mass Spectrometer

The ARI (AERODYNE RESEARCH, Inc.) Aerosol Mass Spectrometer provides real-time size resolved chemical composition analysis of volatile and semi-volatile particulate matter. The combination of size and chemical analysis of sub-micron aerosol mass loading with fast time resolution makes the ARI AMS unique. It provides compositional information on ensembles of particles, with limited single-particle information. The instrument combines standard vacuum and mass spectrometric techniques with aerosol sampling techniques (excerpt from ARI Tof HR-AMS manual). Figure 16 shows block diagram of AMS principle of operation.

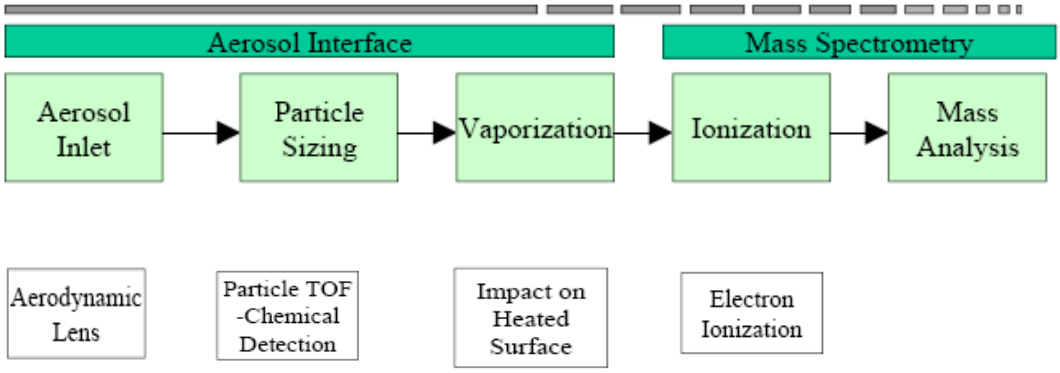

Figure 16. Principle of operation of the ARI HR-TOF-AMS deployed at the GAW Mace Head site.

Aerosols enter the AMS through a particle-sampling inlet that restricts the flow with a 100 μm (or similar diameter) critical orifice (Figure 17). They proceed through a lens that focuses the aerosols into a tight beam of approximately one millimetre in diameter, using 6 apertures. Gases are removed later by differential pumping. Upon exiting the lens, particles undergo acceleration due to the supersonic expansion triggered by the pressure difference between the aerosol sampling chamber and the aerodynamic particle sizing chambers. This expansion differentiates aerosol particles' speed accordingly to their size. After passing through the lens, the particles enter the particle sizing chamber. A rotating chopper wheel, with two radial slits located 180^{o} apart, intercepts the focused particle beam. The chopper can be placed in any one of three positions: a) blocking the beam entirely so that particles cannot pass through (beam closed); b) in the retracted position so that all aerosol particles can pass through (beam open) and c) – slicing (or chopping) position that allows particles to pass through the radial slits only (beam chopped).

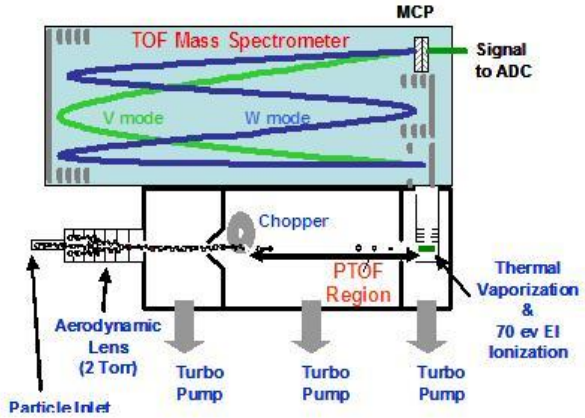

Figure 17. Simplified schematic of the ARI HR-TOF-AMS.

The particle time of flight between the chopper and the detector is the measurement of a particle's velocity. From this measurement the particle's vacuum aerodynamic diameter (D_{aero}) can be inferred. After passing the flight chamber, particles are focused onto a heater surface. Upon collision with a resistively heated "oven", non-refractory particles vaporize rapidly in the high-vacuum environment. This so called flash-vaporization process takes place inside of the electron impact ionizer where the vaporized compounds are converted to positive ions. Ions are directed to the High Resolution Time of Flight Mass Spectrometer (HR-ToF-AMS) where they are detected as impulses of light. The electron impact ionization process is a universal process; therefore, any species in the gas phase will be detectable. The AMS does not efficiently detect low-volatility materials such as black carbon, crustal oxides and certain metals. However, lower volatility species adsorbed on such material can be detected. Detailed descriptions of the AMS and its operation are given by (Jayne et al., 2000b; Jimenez et al., 2003) and (Jimenez et al., 2006).

4. Summary of papers

This thesis consists of 6 papers published or submitted to peer-reviewed journals; two publications as lead author, three with major roles, and one with moderate contribution.

Paper 1: Lead author

On the Contribution of Organics to North East Atlantic Aerosol Number Concentration

Bialek, J., Dall'Osto, M., Monahan, C., Beddows, D., O'Dowd, C. 2012. On the contribution of organics to the North East Atlantic aerosol number concentration. *Environmental Research Letters*, **7**(4), 044013.

This paper investigates a two-year long seasonality study in HTDMA and SMPS data. To provide similarity analysis, a k-mean statistical clustering method was used with the SMPS data. Five unique aerosol categories for hygroscopic growth-factor (HGFs) were found to be associated with size distribution clusters: *low sea-salt marine*, *high sea-salt marine*, *coastal-nucleation*, *open-ocean nucleation*, and *continental* scenarios. In clean marine air conditions, contributions from different species comprised 46% (30-54%) partially-modified ammonium-sulphate particles, 23% (11-40%) partially-modified sea-salt and the remaining 31% (25-35%) contribution being attributed to two distinct organic species. On average, 30% of marine aerosol was found to be predominantly of organic origin and in the case of anthropogenically polluted aerosol, 60% of the total mass was organic. Four GF-PDF integration bins were designated as follows: 1-1.2 for Nearly Hydrophobic (NH), 1.3-1.5 for Less Hygroscopic (LH), 1.6-1.8 for More Hygroscopic (MH) and 2-2.2 for Sea-Salt (SS). In all but the continental case and high sea-salt case, the MH mode dominated number concentration (52-54%) and a general trend of increasing HGFs was observed for increasing sizes associated with this mode. In the high sea-salt case, sea-salt dominated the number concentration with a 40% contribution. Two predominantly-organic HGF modes were observed with HGFs of 1.19 for the NH mode and between 1.42 and 1.52 for the LH mode. The NH mode contributed between 9% and 19% to total number concentration, the highest occurring for the coastal case, while the LH mode contributed 12% to 45% with the highest occurring for the continental case. **The author was responsible for HTDMA data acquisition, quality assurance, processing and analysis as well as maintaining constant, high quality, long-term measurements at the Mace Head station.** ***The author provided data and expertise necessary to combine HTDMA deliverables with SMPS data processing outcomes and wrote ~70% of the paper and provided 100% of the data for analysis.***

Paper 2: Lead author

Hygroscopic and Chemical Characterization of Po Valley Aerosol

Bialek, J., Dall'Osto, M., Vaattovaara, P., Ovadnevaite, J., Decesari, S., Laaksonen, A., O'Dowd, C. Hygroscopic and chemical characterisation of Po Valley aerosol. *Atmos. Chem. Phys. Discuss*, **13**, 3247-3278.

This paper investigates outcomes of a two-week EUSAAR intensive campaign in San Pietro Capofiume in the Po Valley. HTDMA data were combined with data from state-of-art instruments such as a HR-ToF-AMS, a O-TDMA, radiometers and basic meteorological components. This study shows the overall campaign HGF time series, diurnal variation of four hygroscopic groups, size resolved HGF and means HGF for the whole duration of the campaign, size resolved diurnal variability of HGF for the whole campaign. The study also provided diurnal patterns for HGF, OGF, AMS mass fractions, PMF factors, temperature and solar radiation for two contrasting case studies based on different air mass back trajectories. The campaign-average minima in HGFs occurred just before and during sunrise from 03:00-06:00, but more generally, the whole night shows very low hygroscopicity, particularly in the smaller particle sizes. The average HGFs increased from 1.18 for the smallest sized particles (35 nm) to 1.38 for the largest sizes (165 nm) for the lowest HGF period while during the day, the HGF gradually increased to achieve maximum values in the early afternoon hours from 12:00-15:00, reaching 1.32 for 35 nm particles and 1.46 for 165 nm particles.

Organic TDMA versus HTDMA and AMS organic load for both periods in common for both TDMAs sizes of 50 nm was shown to underline organic load variation in Aitken mode aerosol. The highest OGFs (around 1.15) are found during increased concentrations of oxygenated organic aerosol while the lowest OGF (around 1.05) values were recorded during increased concentration of sulphate aerosol for the 50nm size. ***The author supervised HTDMA deployment during the campaign, provided HTDMA, AMS and meteorological data analysis and wrote the major part of paper (~80%). The paper is centred on the author's HTDMA data.***

Paper 3: Contributing author role - major

Primary marine organic aerosol: A dichotomy of low hygroscopicity and high CCN activity.

Ovadnevaite, J., Ceburnis, D., Martucci, G., Bialek, J., Monahan, C., Rinaldi, M., Facchini, M.C., Berresheim, H., Worsnop, D.R., O'Dowd, C. 2011. Primary marine organic aerosol: A dichotomy of low hygroscopicity and high CCN activity. *Geophysical Research Letters*, **38**(21), L21806

This paper describes dichotomous behaviour of marine aerosol in water uptake in both sub and supersaturated conditions. Two distinct periods were chosen: late summer-autumn primary matter-enriched sea spray production episodes and spring-summer open ocean secondary aerosol production episodes. The dichotomous behaviour of primary organic aerosol was manifested in low hygroscopic growth factor (HGF) but high cloud condensation nuclei (CCN) activation efficiency. Aerosol dominated by organics possessed a low HGF of 1.25 or less, while sulphate dominance led to a HGF∼1.65. The sea salt dominated particles exhibited the highest values of HGF of more than 1.8. CCN activation was dependent on aerosol chemical composition, but did not follow a typical hygroscopicity dependence pattern – that is, particles with the lowest HGF were more readily activated than particles with the highest HGF. It's been proven that such behaviour is not only influenced by particle size but also by it chemical composition. Organic matter, transferred from surface of the ocean, comprises compounds such as polysaccharides, proteins, nucleic acids, lipids and so called exopolymer substances. Those compounds can effectively lower surface tension and influence the Kelvin term from modified Köhler equation, thus changing the activation efficiency of CCN. Using the SMPS size distribution data, an innovative approach was taken to achieve closure between laboratory studies and observations at Mace Head by combining the weighted mean size from the SMPS with aerosol chemical composition using the aerosol mass spectrometer (AMS), to provide estimated sea spray nuclei and sulphate nuclei. ***The author was responsible for HTDMA and CCN data acquisition and processing, and provided expertise in interpretation of results and contributed to writing parts of the paper and contributed 50% of the Figures. The authors data were fundamental and of primary importance to the paper.***

Paper 4: Contributing author role: major

The Eyjafjallajökull ash plume - Part I: Physical, chemical and optical characteristics.

O'Dowd, C., Ceburnis, D., Ovadnevaite, J., Martucci, G., Bialek, J., Monahan, C., Berresheim, H., Vaishya, A., Grigas, T., Jennings, S.G. 2012. The Eyjafjallajökull ash plume–Part I: Physical, chemical and optical characteristics. *Atmospheric Environment*, **48**, 129-142

The paper describes observation of Eyjafjallajökull volcano ash cloud over Mace Head station between April 19th and 18th May 2010. The scanning electron microscopy (SEM) and Energy-dispersive X-ray spectroscopy (EDX) results revealed different physical and chemical properties of ash sampled at the beginning and at the end of the eruption. Additionally, the wide range of instrumentation deployed during the plume helped to better understand chemical processes occurring in the ash cloud and estimate potential impact on air quality in areas situated far from volcanic eruptions. It has been revealed that CCN concentrations at all supersaturations less than 0.75% were equal and the CCN/CN ratio was 1. This indicated that the volcanic aerosol particles were all very soluble and quite large in size such that no Kelvin effect could be detected. The higher CCN/CN ratio in the case presented appears to be due to the presence of an ultrafine aerosol typically associated with coastal particle production events. This ultrafine mode leads to elevated particle number concentrations at sizes of less than 30 - 50 nm. The aerosol growth factor spanned from 1.58 for 75 nm sizes to 1.7 for 165 nm sizes, pointing to a strong sulphate growth factor signature. Optical backscatter of ash cloud was clearly enhanced; and the use of a Jenoptic Ceilometer allowed observation of ash plume evolution over time. SMPS and APS data analysis shows that the ash size distribution was bimodal with a super-micron mode of 2.5 μm in diameter while the submicron mode varied between 185 nm to 395nm during the low and high explosive phases respectively. ***The author contributed to this paper by performing SEM and EDX analysis as well as providing HTDMA hygroscopicity data and expertise. He wrote 15% of the large collaborative effort and contributed ~20% of the scientific input.***

Paper 5: Contributing author role – major.

New Findings on the Effect of Wind Speed on Submicron Sea Salt Mass Concentrations and Source Fluxes

Ovadnevaite, J., Ceburnis, D., Canagaratna, M., Berresheim, H., Bialek, J., Martucci, G., Worsnop, D.R., O'Dowd, C. 2012. On the effect of wind speed on submicron sea salt mass concentrations and source fluxes. *Journal of Geophysical Research*, **117**(D16), D16201

This paper evaluated the ability of a HR-ToF-AMS to quantify submicron sea salt mass concentrations. This included both laboratory and long-time ambient measurements. The use of a HTDMA allowed identification of high-sea salt content marine aerosol production episodes. Aerosol particle hygroscopic growth factor (HGF) at 90% relative humidity was determined for dry size particles of 35, 50, 75, 110 and 165 nm. The use of HTDMA in the laboratory experiments was a novel approach. The setup consisted of a bubbler with artificial sea salt solution (which generated aerosol particles resembling primary aerosol produced by bubble bursts in the white caps), with a HTDMA and an AMS connected to its output. A Nafion dryer was installed between the HTDMA outlet and the AMS inlet to prevent flooding of the AMS with condensed water and thus bring the aerosol to a lower RH, resembling more of a marine environment. Such a setup enabled us to select only those aerosol particles which exhibited HGF values closest to that of natural sea salt (around 2.2) and to determine the dependence of AMS sea salt detection efficiency on particle phase (or water content) by sampling the highest purity sea salt possible. This calibration enabled the quantification of sea salt mass as a function of increasing and decreasing wind speed. ***The author provided long term HTDMA measurements with data analysis and interpretation He assisted the calibration with setting up of a HTDMA-AMS hybrid. He contributed to approximately 10% of the writing and 30% of the scientific input.***

Paper 6: Contributing author role – moderate

Nitrogenated and aliphatic organic vapours as possible drivers for Marine Secondary Organic Aerosol growth

Dall'Osto, M., Ceburnis, D., Monahan, C., Worsnop, D.R., Bialek, J., Kulmala, M., Kurtén, T., Ehn, M., Wenger, J., Sodeau, J. 2012. Nitrogenated and aliphatic organic vapors as possible drivers for marine secondary organic aerosol growth. *Journal of Geophysical Research*, **117**(D12), D12311

This paper investigates nitrogenated compounds like amines, amides and organic nitrates as plausible candidates in open ocean nucleation events. The events were

detected in air advecting over North East (NE) Atlantic waters during the EUCAARI Intensive Observation Period in June 2008 at Mace Head. SMPS measurements showed a slow increase in size (in the matter of a few days). Simultaneous to this growth, changes in chemical compositions were also detected. A HR-Tof-AMS was used to determine chemical composition of the aerosol. A HTDMA and DMT CCNC were deployed to investigate hygroscopic and CCN activation properties of the plumes. Microphysical and chemical characterisation of open ocean nucleation aerosol plumes was carried out and analyses showed that changes observed in the growing accumulation mode particles results from condensation since all modes are growing simultaneously, and further, the condensing species is likely to be the same across all modes. The results indicate that N-containing organic species appear to be a key component in the formation and/or growth of open ocean secondary marine aerosol particles. Despite an increase in the particle number concentration, the initial effect is to suppress hygroscopicity and CCN activity. Those open ocean nucleation events originated in the clean marine sector, and therefore it is likely that the organic compounds responsible for particle formation and growth are mainly of biogenic origin. ***All CCN and HTDMA data analysis was provided by the author, comprising ~40% of the scientific input and 20% of the writing.***

On the contribution of organics to the North East Atlantic aerosol number concentration

Jakub Bialek[1], Manuel Dall'Osto[1,2], Ciaran Monahan[1], David Beddows[3] and Colin O'Dowd[1]

[1]*School of Physics and Centre for Climate and Air Pollution Studies, Ryan Institute, National University of Ireland Galway, University Road, Galway, Ireland*

[2]*Institute for Environmental Assessment and Water Research (IDAEA-CSIC), Barcelona, Spain*

[3]*National Centre for Atmospheric Science, Division of Environmental Health and Risk Management, School of Geography, Earth and Environmental Sciences, University of Birmingham, Edgbaston, Birmingham B15 2TT, UK*

Abstract

k-means statistical-cluster analysis of submicron aerosol size distributions is combined with coincident humidity tandem differential mobility analyser data, leading to five unique aerosol categories for hygroscopic growth factors (HGFs): low sea-salt background marine, high sea-salt background marine, coastal nucleation, open ocean nucleation and anthropogenically influenced scenarios. When considering only marine conditions, and generic aerosol species associated with this environment (e.g. non-sea-salt sulphate, sea-salt, partly soluble organic matter and water insoluble organic matter), the two-year annual average contribution to aerosol number concentration from the different generic species was made up as follows: 46% (30–54%) of partially modified ammonium sulphate particles; 23% (11–40%) of partially modified sea-salt; and the remaining 31% (25–35%) contribution attributed to two distinct organic species as evidenced by different, but low, HGFs. The analysis reveals that on annual timescales, ~30% of the submicron marine aerosol number concentration is sourced from predominantly organic aerosol while 60% of the anthropogenic aerosol number is predominantly organic. Coastal nucleation events show the highest contribution of the lowest HGF mode (1.19), although this contribution is more likely to be influenced by inorganic iodine oxides. While organic mass internally mixed with inorganic salts will lower the activation potential of these mixed aerosol types, thereby potentially reducing the concentration of cloud condensation nuclei (CCN), pure organic water soluble particles are still likely to be activated into cloud droplets, thereby increasing the concentration of CCN. A combination of dynamics and aerosol concentrations will determine which effect will prevail under given conditions.

1. Introduction

The hygroscopic growth behaviour of aerosol particles is one of the important parameters controlling the direct and indirect climate effects because, due to water uptake, aerosol particles change their size and their optical properties (Tang 1996) with scattering efficiency typically increasing with increasing particle size. The major proportion of hygroscopic particle growth is usually related to inorganic species such as ammonium nitrate, ammonium sulphate and sodium chloride—common species whose hygroscopic growth behaviour is known relatively accurately (Tang and Munkelwitz 1994). For example, the hygroscopic growth factor (HGF, defined here as the ratio the particle diameter exposed to 90% relative humidity to that at 40% relative humidity) for pure sea-salt is 2.2 while that for pure ammonium sulphate is 1.8 for accumulation mode sizes (specifically, 165 nm diameter). In contrast, hydrocarbon-like organic species possess a HGF close to 1, while oxygenated organic species possess a HGF of the order of 1.2–1.4 (Liu and Wang 2010). Organics often contribute substantially to fine aerosol mass and potentially impact on hygroscopicity (Kanakidou *et al* 2005,O'Dowd *et al* 2004); however, their contribution to the number population and distribution is not often quantified, particularly through measurements. HGF analysis, in addition to elucidation of aerosol hygroscopicity, can also elucidate both the state of mixing of the aerosol population (i.e. whether the aerosol is internally mixed or externally mixed), and the contribution of generic aerosol types to the number concentration. Number concentration is important particularly in terms of influencing cloud droplet number concentration and the indirect radiative effect of aerosols on cloud microphysics specifically, all else being equal, an increase/decrease in the number of CCN results in a concomitant increase/decrease in droplet concentration, a decrease/increase in effective radius, and ultimately, an increase/decrease in cloud albedo (Twomey 1974). At a given saturation, the CCN concentration is determined by the number concentration of particles of a given hygroscopicity and state of mixing. Chemical composition drives hygroscopicity and therefore, the concentration of particles possessing a particular hygroscopic grouping can elucidate the contribution of particular aerosol chemical type to the aerosol and CCN population. Given that even the organic aerosol in clean marine air with low hygroscopicity can be efficient CCN (in contrast to polluted air) (Ovadnevaite *et al* 2011a), hygroscopic growth factor measurements provide a useful approach towards quantification of the relative contribution of different aerosol species, or types, to the CCN population.

This study deployed a humidity tandem differential mobility analyser (H-TDMA) to quantify the relative contribution of predominantly organic and predominantly inorganic aerosol in marine and continental air over the North East Atlantic. Previous studies, using bulk chemical analysis, have demonstrated a strong seasonal cycle in organic enrichment in clean marine aerosol, with peak enrichment occurring during summer (O'Dowd *et al* 2004). The fractional organic mass increased with decreasing particle size. More elaborate on-line mass spectrometry used for chemical characterization of primary organic plumes point to primary organic sea-spray number concentrations exceeding $300 cm^{-3}$ (Ovadnevaite *et al* 2011b) under certain conditions. In the latter study, the primary organic spray was characterized by HGFs of the order of 1.2 or less (Ovadnevaite *et al* 2011a).

Prior to the aforementioned study, typical HGFs reported for marine aerosols were more characteristic of predominantly inorganic (sulfate and sea-salt) aerosol species (for example, over the western North Pacific (Maßling *et al* 2007)); over the eastern North Pacific (Berg *et al* 1998); along with other oceanic regions Swietlicki *et al* 2000, Zhou *et al* 2001, Maßling *et al* 2003, Tomlinson*et al* 2007, Good *et al* 2010). These studies were campaign based which, consequently, may have missed periods of high biological activity if present. In contrast, analysis of continental aerosol sampled at the same location (Mace Head) revealed multiple HGF modes including low hygroscopicity modes at 1.1 and 1.2 and were also associated with high organic mass fractions (Dall'Osto *et al* 2010). The longest time series for HGF in marine air exists for Mace Head where measurements started in June 2008. Two years of HGF data, covering 2009–10, are analysed in the present work.

2. Experimental details

The Mace Head Atmospheric Research Station is located in Connemara, County Galway on the Atlantic Ocean coastline of Ireland at 53°19'36" N, 9° 54'14" W and offers a clean sector from 190° through to 300°. Meteorological records show that, on average, over 60% of the air masses arriving at the station are from the clean sector (Jennings *et al* 2003, O'Connor *et al* 2008). Air is sampled at 10 m height from a main air inlet positioned at 80–120 m from coastline depending on tide height (available at:www.macehead.org). Size distributions were sampled using a Thermo Systems Inc. scanning mobility particle sizer (SMPS) operating 10 min size distribution scans between 20 and 500 nm (Wang and Flagan 1990) and a nano-SMPS covering sizes 3–20 nm.

Hygroscopic properties of aerosol were measured using a H-TDMA, as described in Nilsson *et al* (2009), and Rader and McMurry (1986). A higher HGF indicates more hygroscopic particles resulting from a higher affinity for water. The Mace Head H-TDMA incorporates a dry DMA (RH<40% dried with Nafion™ dyer), Gore-Tex™ humidifier and a second DMA placed in a temperature controlled box for stabilization of the relative humidity. In the humidifier, the aerosol sample is humidified to 90% relative humidity. Particle diameter is given as a mobility diameter—for volume equivalent diameter one should apply a correction factor of 1.08 to the generally cubic sea salt mode. HGFs are determined for dry size particles of 35, 50, 75, 110 and 165 nm. An inversion algorithm is used to retrieve the HGF probability distribution function (PDF), corrected for multiple charges, inherent broadening of measured distribution and for humidity variations in the second DMA, following Gysel *et al* (2009). The standard deviation (σ) of the HGF–PDF is sensitive to small values of total particle concentration (n_{total}) with an accuracy of ±80%, ±50%, ±10% and ±5% forn_{total} 10, 50, 1000 and 5000, respectively. In the marine environment, such noise occurs sometimes during 'clean sector' advection with relatively low wind speed (below 5 m s^{-1}). Additionally, the sensitivity of σ to small n_{total} decreases with increasing breadth of the HGF–PDF, which, in the marine environment, is often broad due to the external mixing of sea-salt, organic compounds and inorganic salts. Overall, the mean HGF σ, due to counting statistics is between 5 and 10% of the HGF in the marine environment.

3. Data analysis

Following the study of Dall'Osto *et al* (2011), one-hour average SMPS size distributions were analysed by using *k*-means cluster analysis (Beddows *et al* 2009). The size distributions were normalized by their vector length and cluster analysed. The use of cluster analysis was justified in this work using a cluster tendency test, providing a calculated Hopkins index of 0.20, implying the presence of cluster structures in the dataset. The *k*-means method minimizes the sum of the squared distances between all points and the cluster centre and identifies homogeneous groups by minimizing the clustering error (defined as the sum of the squared-Euclidean distances between each dataset point and the corresponding cluster centre). The clustering reduces the complexity of the dataset and this simplification allows easier characterization according to temporal and spatial trends. In order to choose the optimum number of clusters the Dunn-index (DI) was used, which aims to identify dense and well-separated clusters. The DI is defined as the ratio between the minimal inter-cluster distance to maximal intra-cluster distance. Since the method's internal criteria seeks clusters with high intra-cluster similarity and low inter-cluster similarity, algorithms that produce clusters with high DI are more desirable. In other words, for Dunn's index, it was required to find clustering which maximizes this index. The Dunn-index for the results of the *k*-mean cluster analysis for different cluster numbers showed a clear maximum for 15 clusters for the 2009 dataset and 11 clusters for the 2010 dataset, which were further grouped into five generic categories. There was 72% data coverage for the year 2009 and 81% for 2010 amounting to more than 10 000 h over coincident H-TDMA and SMPS measurements. Following Dall'Osto *et al* (2011), the 15 (for 2009) and 11 (for 2010) clusters were further grouped into five more generic aerosol types found in the region. This final re-grouping was fundamentally based on size distribution similarities, as per the primary clustering techniques outlined above and in more detail in the supplementary information section (available atstacks.iop.org/ERL/7/044013/mmedia) , and also on similarities in air mass categorization and meteorological parameters. The combined set of parameters allowed the distinction between two typical background marine distributions, one with low sea-salt concentrations and the other with high sea-salt concentrations; another marine background distribution type but occurring under open ocean new particle production and growth events (O'Dowd *et al* 2010); another with size distribution and associated aerosol properties typical of anthropogenically influenced aerosol; and finally, an aerosol type characterized by the presence of a strong nucleation mode resulting from coastal new particle production events. As outlined in Dall'Osto *et al* (2011), the background clean marine clusters occur predominantly in maritime tropical, polar and Arctic air masses; anthropogenic air masses are predominantly polar continental or polar continental marine; open ocean new particle production events are also predominantly in maritime tropical, polar and Arctic air masses as typically are coastal nucleation events.

4. Results and discussion

The clustering procedure identified the following five categories: (1) high sea-salt background marine (occurring for 9% of the data coverage period over the two years) typical of background clean marine size distributions with secondary mode visible in the larger accumulation mode sizes (300–400 nm diameter) during winter months; (2) low sea-salt background marine (occurring for 25% of the data coverage period) with a clear bimodality in the submicron size range; (3) open ocean nucleation (occurring for 23% of the period), characterized by a dominant Aitken mode between 15 and 50 nm with a spring seasonality peaking in May and corresponding to the North East Atlantic high biological activity period (O'Dowd *et al* 2010, Dall'Osto *et al* 2012); (4) anthropogenically influenced (occurring for 28% of the period), characterized by size distributions generally monomodal in submicron sizes; (5) coastal nucleation (occurring for 15% of the period), with a clear and dominant nucleation mode at sizes less than 10 nm.

The total particle number concentrations (average±1σ) for diameters $D > 10$ nm (N_{10}) and $D>3$ nm (N_3) for high sea-salt background marine were 353 ± 159 cm^{-3} and 993 ± 248 cm^{-3}; for low sea-salt background marine were 680 ± 306 cm^{-3} and 2100 ± 525 cm^{-3}; for anthropogenically modified were 1443 ± 505 cm^{-3} and 2076 ± 519 cm^{-3}; for open ocean nucleation were 2039 ± 714 cm^{-3} and 8068 ± 2017 cm^{-3}; and for coastal nucleation cases were 5852 ± 2048 cm^{-3} and 19195 ± 4800 cm^{-3}, respectively. Given that the nucleation mode can overwhelm number concentrations, and that particles less than 35 nm in size are unlikely to be activated as cloud condensation nuclei, the contribution of different aerosol species, as derived from the H-TDMA analysis, is presented in terms of contribution of HGF modes at sizes larger than 35 nm, while accepting there is an interpolation uncertainty over the five H-TDMA sizes, from 35 to 165 nm. Consequently, the concentration of particles larger than 35 nm (N_{35}) diameter is also reported for the five clusters and the relative concentration of different HGF modes to total number concentration, discussed later, refers to N_{35}. Specifically, for high sea-salt background marine $N_{35}= 374 \pm 112$ cm^{-3}, for low sea-salt background marine $N_{35}=352 \pm 106$ cm^{-3}, for open ocean nucleation $N_{35}=665 \pm 200$ cm^{-3}, coastal nucleation $N_{35}=701 \pm 210$ cm^{-3} and for anthropogenically influenced $N_{35}=1650 \pm 555$ cm^{-3}.

Associated with the size distribution clusters, there were distinct HGF–PDFs which can be characterized by different combinations of HGF categories. Specifically, four HGF modes were found, although with slightly different HGF bins compared to those reported by Swietlicki *et al* (2000): 1–1.2 for nearly hydrophobic (NH), 1.3–1.5 for low hygroscopicity (LH), 1.6–1.8 for mainly hygroscopic (MH) and 2–2.2 for sea-salt (SS). The relative contributions of each mode to the HGF–PDF vary strongly with the origin of the air masses (i.e. aerosol category).

The five size distribution categories and associated HGF–PDFs are shown in figure 1. For the high sea-salt background marine category, typical of the cleanest marine winter conditions, the two main modes correspond to MH and SS for sizes 75 nm and larger while the contributions from NH and LH modes become more important for 35 and 50 nm sizes. Examination of the interpolated HGF contour plot reveals a three-mode external mixture with HGF-1.2 dominating at lower sizes, 2.0–2.1

dominating at larger sizes and the most dominant HGF mode increasing from 1.4 for smaller sizes to 1.7 at larger sizes. The SS mode is still seen for particles down to 35 nm, while the NH mode is also persistent for 165 nm sizes. It should be noted that pure ammonium sulfate or sea-salt HGFs are not seen in this case, or any case for that matter, suggesting that these predominantly inorganic aerosols are always influenced to some degree by organics. For the low sea-salt background marine case, a similar pattern is seen as in the high sea-salt case, except the SS mode is much diminished. The gradual increase in HGF with increasing particle size is seen for the dominant HGF mode.

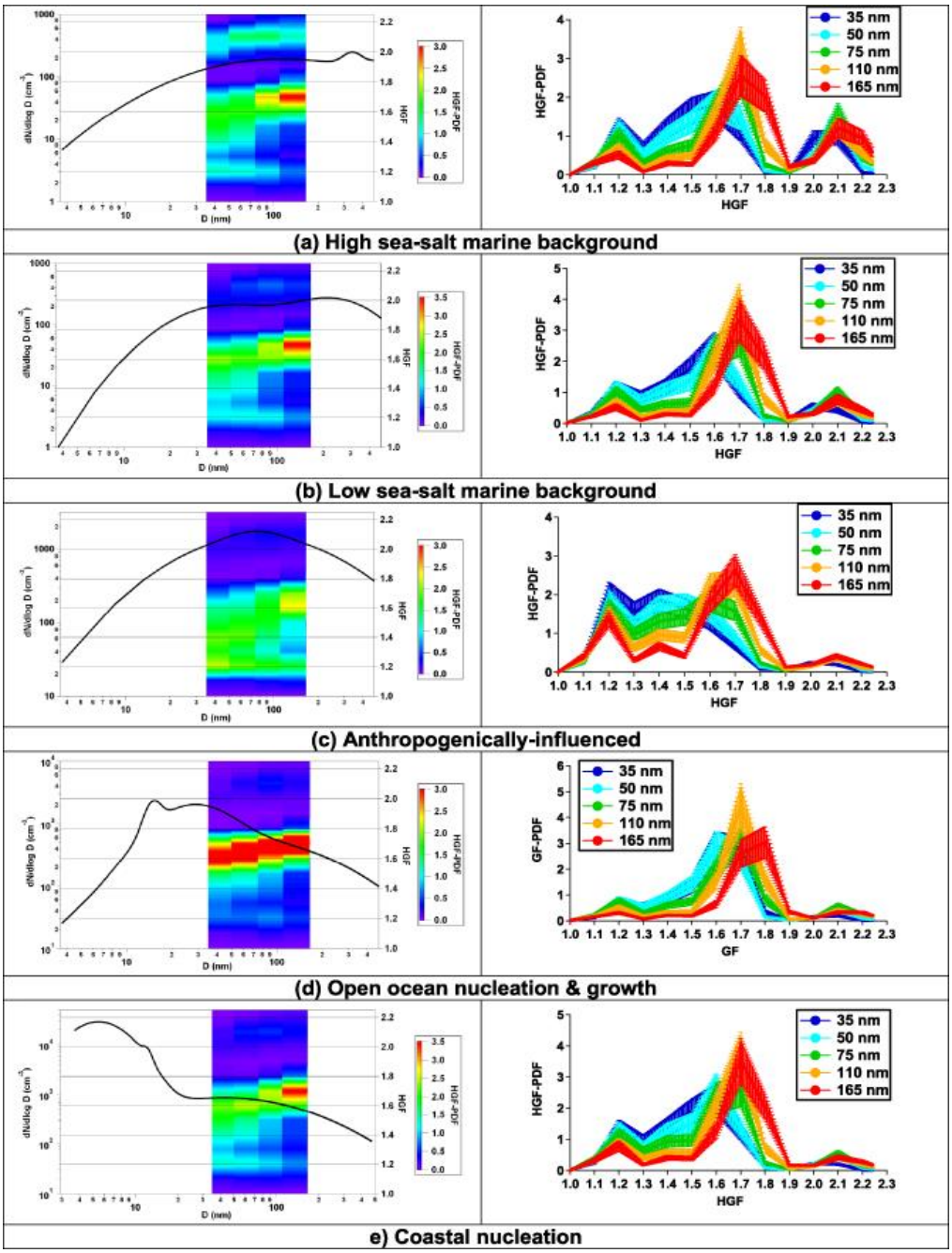

Figure 1. Left panel: clustered size distributions (±1 standard deviation) and coincident H-TDMA derived and interpolated contour map of HGF–PDF. Right panel: size-selected HGF–PDF as a function of size for clustered categories.

For the anthropogenically influenced category, the SS mode is the least pronounced and a much broader distribution of HGFs is evident. The larger, 110 and 165 nm, particles PDF is characterized by a bimodal distribution with peaks below 1.2 and between 1.6 and 1.7, whereas the smallest sized particles, 35 and 50 nm, possess a PDF with a peak at 1.2 and a broad peak between 1.35 and 1.6. Overall, there is a systematic lowering in PDF towards low HGFs in comparison to marine conditions. For the open ocean nucleation category, the interpolated contour plot reveals one dominant MH mode, although increasing in HGF from 1.6 for 35 nm particles to 1.8 for 165 nm particles; however, two less pronounced modes are also seen at 1.2 and 2.1 HGFs. For the coastal nucleation category, there is again a dominant MH mode ranging from HGF 1.5 to 1.7, increasing with particle size, and notable NH and LH modes. Next to the continental case, the coastal category has the lowest HGF distribution, although this is thought to be more likely due to condensation of iodine oxides rather than organics (Väkevä *et al* 2002).

HGF–PDFs were averaged over the five different aerosol sizes and the resultant PDFs are illustrated in figure 2 for the five cluster categories. The distinction between the high sea-salt background marine and low sea-salt background marine category is evident. Again, no pure sea-salt or pure sulfate modes are evident, suggesting a degree of internal mixing between organics and the inorganic salts, and two clear, predominantly organic, modes are evident at 1.2 and 1.4. The HGF–PDFs were fitted with log-normal distributions (see figure SI 4 available at stacks.iop.org/ERL/7/044013/mmedia) to calculate the relative contribution of each of the four dominant modes to the total (normalized) number concentration and the results are presented in table 1.

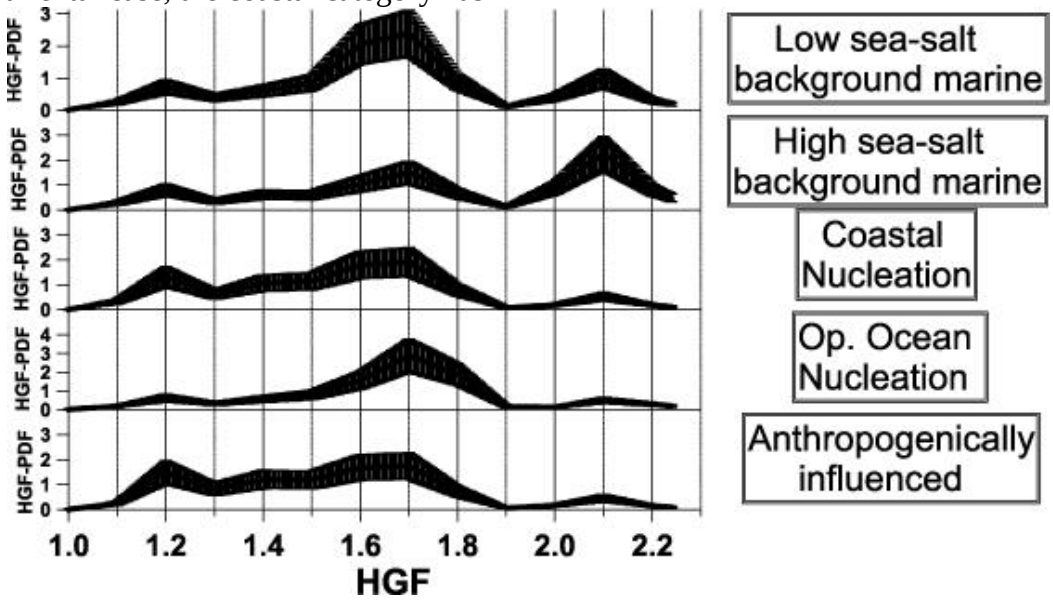

Figure 2. HGF–PDFs for clustered categories averaged over the five H-TDMA sizes of 35, 50, 75, 110 and 165 nm.

Table 1. Relative contributions of different HGF modes to total number concentrations of analysed sizes. Nearly hydrophobic (NH), low hygroscopicity (LH), mainly hygroscopic (MH) and sea-salt (SS)—see figure SI 4 available atstacks.iop.org/ERL/7/044013/mmedia.

	Hygroscopic growth factor mode			
Cluster category	NH mode	LH mode	MH mode	SS mode
High sea-salt background marine	1.18 ± 0.14(13%)	1.48 ± 0.5(12%)	1.69 ± 0.17(35%)	2.10 ± 0.18(40%)
Low sea-salt background marine	1.19 ± 0.18(11%)	1.42 ± 0.25(19%)	1.69 ± 0.23(52%)	2.10 ± 0.18(17%)
Anthropogenic	1.19 ± 0.13(15%)	1.42 ± 0.24(45%)	1.66 ± 0.24(30%)	2.10 ± 0.17(10%)
Coastal nucleation	1.19 ± 0.15(19%)	1.42 ± 0.20(20%)	1.65 ± 0.24(50%)	2.10 ± 0.17(10%)
Open ocean nucleation	1.19 ± 0.19(9%)	1.52 ± 0.31(26%)	1.71 ± 0.21(54%)	2.10 ± 0.18(11%)

For the high sea-salt background marine case, 40% of the number concentrations is contributed by predominantly-sea-salt particles (HGF=2.1), 35% by predominantly sulfate particles (HGF=1.69) and the remaining 25% by predominantly organic particles with hygroscopicity ranging from 1.19 to 1.42. For the low sea-salt background marine case, the sea-salt contribution decreases to 17%, the sulfate contribution increases to 52% while the organic contribution increases to 30%. The open ocean nucleation case is dominated also by sulfate aerosol (54%), with the next most important contribution (26%) coming from a HGF mode of 1.52. The coastal nucleation case is again dominated by sulfates (50%), with 39% from the two lowest HGF modes. Finally, for the continental case, the largest contribution of 45% comes from the 1.43 HGF mode, with 15% coming from the 1.19 HGF mode and 30% and 10% from sulfate and sea-salt, respectively. These results point to an important role for organics in terms of their contribution. In particular, while organic mass internally mixed with inorganic salts will lower the activation potential of these mixed aerosol types, thereby potentially reducing the concentration of CCN, pure organic water soluble particles are still likely to be activated into cloud droplets, thereby increasing the concentration of CCN. Which effect will dominate will depend on an interplay between the overall CCN concentration and dynamics.

5. Conclusion

Two years of aerosol size distributions are analysed and characterized in terms of *k*-mean cluster analysis leading to five generic classifications. These five categories were labelled high sea-salt background marine, low sea-salt marine, open ocean nucleation, coastal nucleation and, anthropogenically influenced and for each one, the average HGF–PDFs were obtained. Over the five categories, four broad modes of HGFs were encountered to different degrees: 1.19 (NH), 1.42–1.52 (LH), 1.65–1.7 (MH) and 2.1 (SS). In all but the anthropogenically influenced case and high sea-salt background marine case, the MH mode dominated number concentration (52–54%) and a general trend of increasing HGFs was observed for increasing sizes associated with this mode. In the high sea-salt background marine case, sea-salt dominated the number concentration with a 40% contribution. Two predominantly organic HGF modes were observed with HGFs of 1.19 for the LH mode and between 1.42 and 1.52 for the LH mode. The NH mode contributed between 9% and 19% to total number concentration, the highest occurring for the coastal case, while the LH mode contributed 12% to 45% with the highest occurring from the anthropogenically influenced case. Combining both organic HGF modes, predominantly organic particles contribute between 25 and 30% to general background marine number concentration, 35% for open ocean nucleation cases, and 60% for anthropogenically influenced cases. For the coastal nucleation case, where low HGFs are thought to be significantly influenced by iodine oxidize rather than organics, the contribution of the two lower HGF modes was 49%. In summary, over yearly timescales, aerosol particles of predominantly organic composition contribute ~30% to total submicron marine number concentration population and ~60% to the continental number concentration population. While organic mass internally mixed with inorganic salts will lower the activation potential of these mixed aerosol types, thereby potentially reducing the concentration of CCN, pure organic water soluble particles are still likely to be activated into cloud droplets, thereby increasing the concentration of CCN.

Acknowledgments

This work was supported by the HEA-PRTLI4 Environment and Climate Change: Impact and Responses programme, European Commission FP7 EUCAARI, and EPA Ireland.

References

Beddows D C S, Dall'Osto M and HarrisonR M 2009 Cluster analysis of rural, urban and curbside atmospheric particle size data Environ. Sci. Technol. 43 4694–700

Berg O H, Swietlicki E and Krejci R 1998 Hygroscopic growth of aerosol particles in the marine boundary layer over the pacific and southern oceans during the first aerosol characterization experiment (ACE 1) J. Geophys. Res.—Atmos. 103 16535–45

Dall'Osto M, Monahan C, Greaney R, Beddows D C S, Harrison R M, Ceburnis D and O'Dowd C D 2011 A statistical analysis of North East Atlantic (submicron) aerosol size distributions Atmos. Chem. Phys. 11 12567–78

Dall'Osto M et al 2010 Aerosol properties associated with air masses arriving into the North East Atlantic during the 2008 Mace Head EUCAARI intensive observing period: an overview Atmos. Chem. Phys. 10 8413–35

Dall'Osto M et al 2012 Nitrogenated and aliphatic organic vapors as possible drivers for marine secondary organic aerosol growth J. Geophys. Res. 117 D12311

Good N, Topping D O, Allan J D, Flynn M, Fuentes E, Irwin M, Williams P I, Coe H and McFiggans G 2010 Consistency between parameterisations of aerosol hygroscopicity and CCN activity during the RHaMBLe discovery cruise Atmos. Chem. Phys. 10 3189–203

Gysel M, McFiggans G B and Coe H 2009 Inversion of tandem differential mobility analyzer (TDMA) measurements J. Aerosol Sci. 40 134–51

Jennings S G, Kleefeld C, O'Dowd C D, Junker C, Spain T G, O'Brien P, Roddy A F and O'Connor T C 2003 Mace Head Atmospheric Research Station—characterization of aerosol radiative parameters Boreal Env. Res. 8 303–14

Kanakidou M et al 2005 Organic aerosol and global climate modelling: a review Atmos. Chem. Phys. 5 1053–123

Liu X and Wang J 2010 How important is organic aerosol hygroscopicity to aerosol indirect forcing? Environ. Res. Lett. 5 044010 IOPscience

Maßling A, Leinert S, Wiedensohler A and Covert D 2007 Hygroscopic growth of sub-micrometer and one micrometer aerosol particles measured during ACE-Asia Atmos. Chem. Phys. 7 3249–59

Maßling A, Wiedensohler A, Busch B, Neusüß C, Quinn P, Bates T and Covert D 2003 Hygroscopic properties of different aerosol types over the Atlantic and Indian oceans Atmos. Chem. Phys. 3 1377–97

Nilsson E, Swietlicki E, Sjogren S, Löndahl J, Nyman M and Svenningsson B 2009 Development of an H-TDMA for long term unattended measurement of hygroscopic properties of atmospheric aerosol particles Atmos. Meas. Tech. 2 313–8

O'Connor T C, Jennings S G and O'Dowd C 2008 Highlights from 50 years of aerosol measurements at Mace Head Atmos. Res. 90 338–55

O'Dowd C D, Facchini M C, Cavalli F, Ceburnis D, Mircea M, Decesari S, Fuzzi S, Yoon Y, J and Putaud J P 2004 Biogenically-driven organic contribution to marine aerosol Nature 431 676–80

O'Dowd C D, Monahan C and Dall'Osto M 2010 On the occurrence of open ocean particle production events Geophys. Res. Lett. 37 L19805

Ovadnevaite J, Ceburnis D, Martucci G, Bialek J, Monahan C, Rinaldi M, Facchini M C, Berresheim H, Worsnop D R and O'Dowd C 2011a Primary marine organic aerosol: a dichotomy of low hygroscopicity and high CCN activity Geophys. Res. Lett. 38 L21806

Ovadnevaite J, O'Dowd C, Dall'Osto M, Ceburnis D, Worsnop D R and Berresheim H 2011b Detecting high contributions of primary organic matter to marine aerosol: a case study Geophys. Res. Lett. 38 L02807

Rader D J and McMurry P H 1986 Application of the tandem differential mobility analyzer to studies of droplet growth or evaporation J. Aerosol Sci. 17 771–87

Tang I N 1996 Chemical and size effects of hygroscopic aerosols on light scatterring coeffcients J. Geophys. Res. 101 19245–50

Tang I N and Munkelwitz H R 1994 Water activities, densities and refractive indices of aqueous sulfates and soldium nitrate droplets of atmospheric importance J. Geophys. Res. 99 18801–8

Tomlinson J M, Li R and Collins D R 2007 Physical and chemical properties of the aerosol within the southeastern Pacific marine boundary layer J. Geophys. Res. 112 D12211

Twomey S 1974 Pollution and the planetary albedo Atmos. Environ. 8 1251–6

Swietlicki E et al 2000 Hygroscopic properties of aerosol particles in the north-eastern Atlantic during ACE-2 Tellus B 52 201–27

Väkevä M, Hämeri K and Aalto P P 2002 Hygroscopic properties of nucleation mode and Aitken mode particles during nucleation bursts and in background air on the west coast of Ireland J. Geophys. Res. 107 8104

Wang S C and Flagan R C 1990 Scanning electrical mobility spectrometer Aerosol. Sci. Technol. 13 230–40

Zhou J C et al 2001 Hygroscopic properties of aerosol particles over the central Arctic Ocean during summer J. Geophys. Res.—Atmos. 106 32111–23

Appendix A1. Aerosol size distributions k-means clustering

The procedure for clustering SMPS data from the Mace Head research station has been reported in depth by Dall'Osto et al. [2011], where a one year dataset (year 2008) was analysed. The current study uses the SMPS data from the years 2009 and 2010. As an illustrative example of the clustering analysis technique, we show the procedure for the 2010 SMPS dataset. Additional background mathematical information on the K-mean clustering approach is reported in Beddows et al. [2009]. Following the study of Dall'Osto et al. [2011], one-hour average SMPS size distributions were generated and analyzed. A two-step process was used to overcome the computation limitation set by the maximum size of the data matrix that could be held, and practically processed, within Cran R operated on a 32 bit Windows PC using 3.5 GB RAM (Windows XP Pro limitation). For the datasets collected in 2010, a random selection of 5000 spectra was taken from the data set and analysed using k-means cluster analysis. The results of this analysis were then used to train a Support Vector Machine which was used to classify the remaining 1000-2000 spectra into the clustered groups [Beddows et al., 2009].

The results for the cluster validity values obtained by applying K-means methods were validated by the Dunn index and the Silhouette width. The Dunn index is a function of the ratio of the minimum cluster separation to the maximum cluster, implying that the larger the Dunn index the more compact and well separated are the clusters within the space. The Silhouette width (silwidth) measures the similarity of the SMPS spectra within a cluster [Beddows et al., 2009]. When plotted against increasing cluster number, the Dunn-Index did show high values for 7, 8, and 11 clusters, respectively (see Fig. A1 1). The choice of cluster was then made based on the competing need to have a high Dunn- Index, a high Silhouette width and a cluster number great enough to divide the data up into manageable sets of SMPS data.

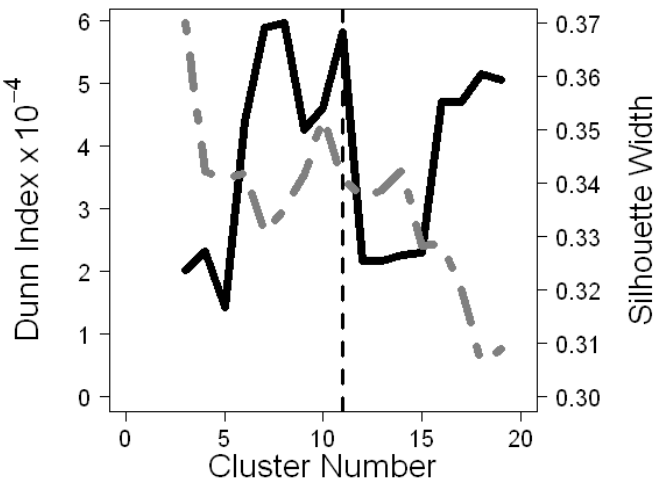

Fig. A1 1: Validation indices plotted against the cluster number for each cluster method: Dunn index (black line) and Silhouette Width (grey line) for the k-means analysis of the SMPS 2010 dataset as a function of number of cluster selected (max. limited to 20).

For the years 2010, 11 were chosen as the optimum number of clusters respectively based on a compromise between the optimum Dunn Index and Silhouette Width value, yielding Dunn Indices of 5.82 x 10^{-4} and Sihouette Width values of 0.3407 (Fig. A1 1).

The aerosol size distribution spectra and the temporal trends of each of the 11 K-means clusters obtained are reported in Fig. A1 2 and Fig. A1 3, respectively. Similar results to the one reported in Dall'Osto et al. [2011] can be seen:

- Typical ***coastal nucleation*** aerosol size distributions characterized by a clear and dominant nucleation mode at sizes less than 10 nm occurring during spring and autumn (Cluster 1 and 5). Air mass is typically maritime but can also be modified maritime in nature.
- Typical open ***ocean nucleation*** aerosol size distributions characterized by a dominant Aitken mode between 15 nm and 50 nm corresponding to the North East (NE) Atlantic high biological period (Cluster 10).The nucleation mode has grown during transit from the open ocean formation region to measurement point at Mace Head. Typical air mass is maritime.
- Typical ***anthropogenically-influenced*** size distributions generally more monomodal (accumulation), albeit with traces of bimodality occurring during autumn and winter

times (Cluster 2, 3 and 11). Typical sir mass is continential or modified marine.

- ***Background clean marine-low wind*** aerosol with a clear bimodality in the sub-micron size distribution, occurring mainly during summer times (Cluster 4, 6, 8 and 9). Maritime air mass – polar, tropical and Arctic with low contribution from primary sea-salt and more frequent in summertime.
- ***Background clean marine-high wind*** size distributions with additional mode between 300-400 nm, thought to be sea-salt. Maritime air mass – polar, tropical and Arctic with high contribution from primary sea-salt and more frequent in wintertime.

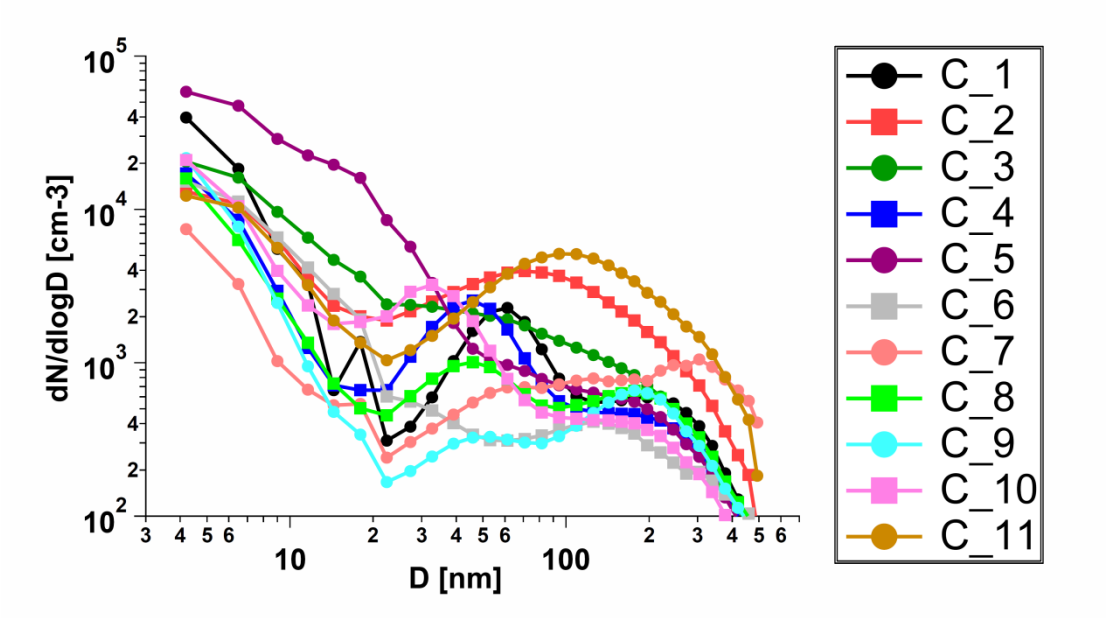

Fig A1 2: Identified K-means aerosol size distributions clusters for the 2010 dataset (11 clusters)

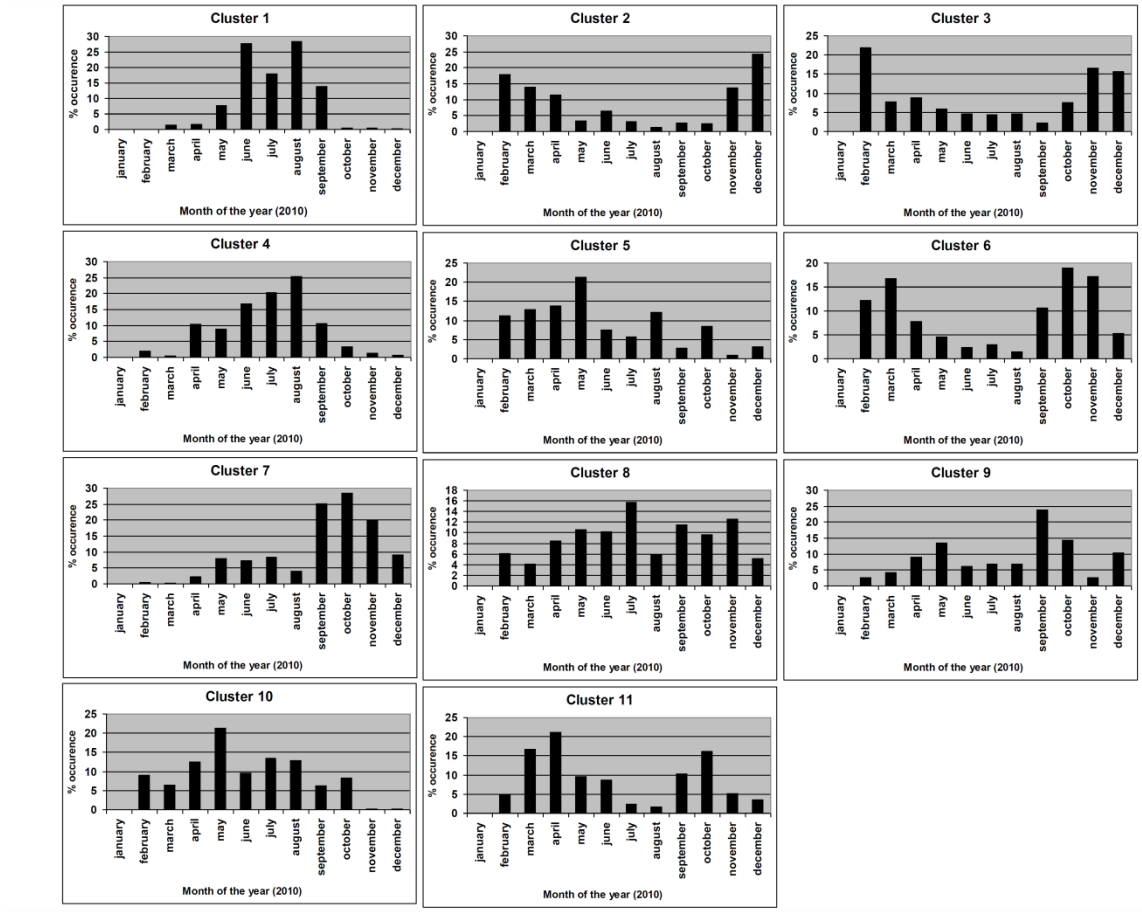

Figure A1 3: Percentage monthly occurrence of the 11 identified SMPS clusters.

The K-means clustering allows us to reduce the complex SMPS dataset into a fixed (11) types of aerosol size distributions. Following the study of Dall'Osto et al [2011], and summarised in the main manuscript text, the clusters were re-grouped into 5 more general air mass and aerosol categories, based on size distribution similarities, air mass history and meteorological parameters. Whilst the complete procedure is reported in Dall'Osto et al. [2011], we report as example values of black carbon concentrations obtained for the 11 clusters of the 2010 SMPS dataset (Fig. A1 4).

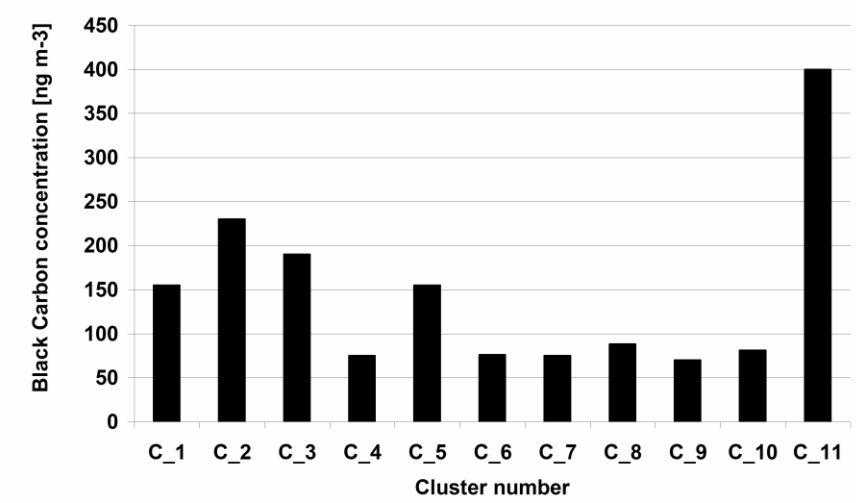

Figure A1 4: Average Black Carbon concentration for each of the 11 SMPS clusters.

In summary, the choice of using a higher number of clusters meant that the possibility of merging together two or more similar clusters could be postponed until after the automated clustering process and be left to the discretion of the operator. Visual inspection of the 2010 clusters showed that even though statistically different, they could be further reduced down to 5 chemically significantly different categories as presented in Table SI 1 (see also Dall'Osto et al. [2011]).

SMPS dataset aerosol category	**(K-means cluster number in brackets)** **% of each aerosol category**
Anthropogenically influenced	(C_2, C_3, C_11) 36%
Coastal nucleation	(C_1, C_5) 14%
Open ocean nucleation	(C_10) 7%
Low sea salt background marine	(C_4, C_6, C_8, C_9) 34%
High sea salt background marine	(C_7) 6%

Table A1 1. K-means clusters grouped according the five aerosol categories.

Appendix A2. Aerosol size distributions k-means clustering log normal fitting

The HGF-PDFs of the five aerosol categories presented in Fig. 2 were fitted with log-normal distributions to calculate the relative contribution of each of the four dominant modes to the total (normalised) number concentration. The results presented in Table 1 can visually seen in Fig. A2 1.

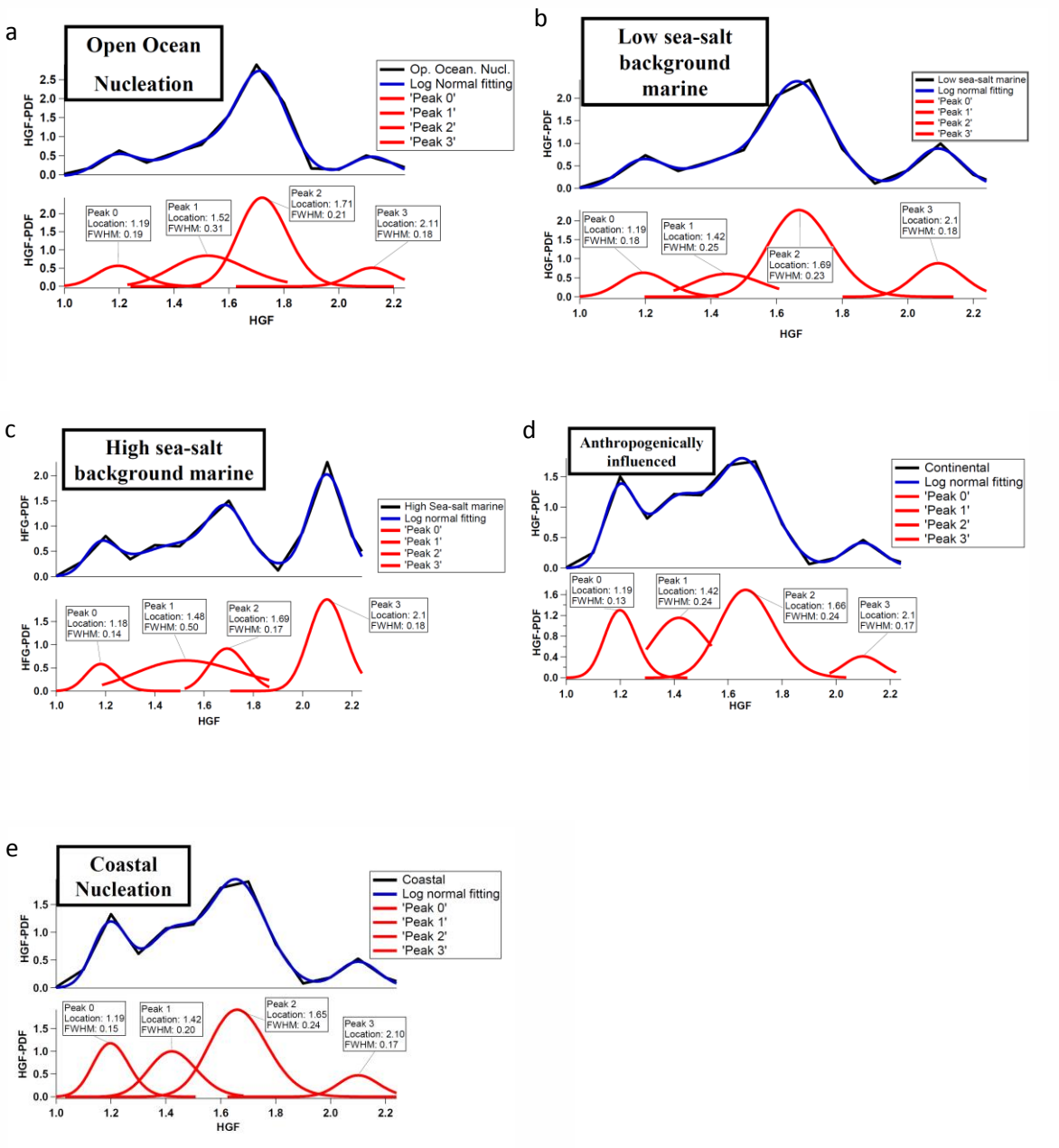

Figure A2 1 a-e: Log normal fitting of HGF-PDF reported in the Figure 2 for the five aerosol categories. Each log-normal fitting reports peak location maximum and relative full width at half maximum (FWHM).

Hygroscopic and chemical characterisation of Po Valley aerosol

J. Bialek[1], M. Dall'Osto[1], P. Vaattovaara[2], S. Decesari[3], J. Ovadnevaite[1], A. Laaksonen[4] and C. O'Dowd[1]

1School of Physics and Centre for Climate and Air Pollution Studies, National University of Ireland Galway, University Road, Galway, Ireland

[2]University of Eastern Finland, Department of Applied Physics, 70210, Kuopio, Finland

[3]Institute of Atmospheric Sciences and Climate (ISAC) of the Italian National Research Council (CNR), Via P. Gobetti 101, 40129 Bologna, Italy

[4]Finnish Meteorological Institute, Erik Palmenin aukio 1, 00560 Helsinki

Abstract

Continental summer-time aerosol in the Italian Po Valley was characterized in terms of hygroscopic properties and the influence of chemical composition therein. The campaign-average minima in hygroscopic growth factors (HGFs) occurred just before and during sunrise from 03:00–06:00, but more generally, the whole night shows very low hygroscopicity, particularly in the smaller particle sizes. The average HGFs increased from 1.18 for the smallest sized particles (35 nm) to 1.38 for the largest sizes (165 nm) for the lowest HGF period while during the day, the HGF gradually increased to achieve maximum values in the early afternoon hours from 12:00–15:00, reaching 1.32 for 35 nm particles and 1.46 for 165 nm particles. Two contrasting case scenarios were encountered during the measurement period: Case 1 was associated with westerly air flow moving at a moderate pace and Case 2 was associated with more stagnant, slower moving air from the north-easterly sector. Case 1 exhibited low diurnal temporal patterns and was associated with moderate non-refractory aerosol mass concentrations (for 50 % size cut at 1 µm) of the order of 4.5 µg m^{-3}. For Case 1, organics contributed typically to 50 % of the mass. Case 2 was characterized by > 9.5 µg m^{-3} total mass (< 1 µm) in the early morning hours (04:00), decreasing to ~ 3 µg m^{-3} by late morning (10:00) and exhibited strong diurnal changes in chemical composition, particularly in nitrate mass but also in total organic mass concentrations. Organic growth factors (OGFs) exhibited a minimum around 15:00, 1–2 h after the peak in HGF. Particles sized 165 nm exhibited moderate diurnal variability in HGF, ranging from 80 % at night to 95 % of "more hygroscopic" growth factors (i.e. GF = 1.35–1.9) around noon. The diurnal changes in HGF progressively became enhanced with decreasing particle size, decreasing from 95 % "more hygroscopic" growth factor fraction at noon to 10 % fraction at midnight, while the "less hygroscopic" growth factor fraction (1.13–1.34) increased from 5 % at noon to > 60 % and the "barely hygroscopic" growth factor fraction (1.1–1.2) increased from less than 2 % at noon to 30 % at midnight. OGFs were

generally anti-correlated to HGF and also total organic mass as measured by the aerosol mass spectrometer due to a high sulphate/organics ratio. Surprisingly, the lowest HGFs occurred for periods when nitrate mass reached peak concentrations. This may suggest formation of organonitrates and organosulphates, which significantly decreased the OGF. Coincident with the peak in nitrate was a peak in Hydrocarbon-like Organic Aerosol (HOA) and Semi-Volatile Oxygenated Organic Aerosol (SV-OOA) and analysis of the HGF probability distribution function (PDF) reveals a transformation of a predominant "More Hygroscopic" (MH) mode with HGF of 1.5 around noon, into two modes, one with a "less hygroscopic" (LH) HGF of 1.26, and another with a "barely hygroscopic" (BH) mode of 1.05. The analysis points to an internal mixture of larger size inorganic species, mainly nitrates, coated with a hydrophobic organic layer which suppresses water uptake. In addition, a new, externally mixed BH ultrafine mode appears and persists through the night.

1. Introduction

Light scattering by aerosol particles affects climate forcing through the direct backscattering of incoming solar radiation back into space. The scattering strongly depends on the aerosol's ability to absorb water (hygroscopicity), which in turn, determines the particles ambient size under a given humidity regime. Additionally, hygroscopicity can determine the particles ability to act as a cloud condensation nucleus - CCN (Hänel, 1976; Hegg et al., 1993; McFiggans et al., 2006; McInnes et al., 1998; Svenningsson et al., 1994). The aerosol's hygroscopicity may be expressed as a diameter-based hygroscopic growth factor (HGF, (Dennis, 1960)) and usually is defined as the ratio of the wet particle diameter at a given relative humidity (usually 90%) to the dry particle diameter at a given relative humidity (usually 20%). HGFs for common atmospheric inorganic salts such as ammonium sulphate and sea salt are 1.8 and 2.2, respectively, while oxidized organic aerosol possesses lower HGFs and freshly-emitted non-oxidised primary organics have a HGF close to 1.

Primary organic aerosols emitted directly into the atmosphere undergo transformation during transport due to oxidation and multi-phase chemical processes (Allan et al., 2010; Kittelson, 1998; Kupiainen & Klimont, 2007; Rogge et al., 1993) while secondary material is added both as additional, condensable, mass to existing particles, and through the modification of existing aerosol matter (Jimenez et al., 2009). The secondary formation or modification of condensed matter on pre-existing particles may dramatically change their hygroscopic behaviour (Saxena et al., 1995). Particles, previously hydrophobic, but coated with oxidized organics can start to exhibit activity as CCN and participate in cloud formation. The life-cycle of secondarily formed aerosol, however, is not well understood because of myriads of possible chemical compounds taking part in its creation. This is in contrast with the life cycle of inorganic compounds such as sulphates and nitrates whose properties and sources are well-characterized (Ansari & Pandis, 1999). Additionally, understanding the mixing state of organics and inorganics may be of great importance in describing overall impact of anthropogenic pollution on the climate.

Recent technological developments have advanced our capability to chemically-characterise atmospheric aerosols, particularly so with advances in aerosol mass spectrometry. Aerosol mass spectrometry, in conjunction with statistical analysis tools such as positive matrix factorization (PMF) has improved the capability to distinguish between secondary organic aerosol (SOA) and primary organic aerosol (POA), and, in turn, local and regional sources of OA (Lanz et al., 2007; Lee et al., 1999; Paatero & Tapper, 1994; Schauer et al., 1996; Zhang et al., 2005). There have been many laboratory studies performed on secondary organic aerosol (SOA) formation using hygroscopic tandem differential mobility analyzer (HTDMA) and aerosol mass spectrometric techniques coupled together (Baltensperger et al., 2005; Duplissy et al., 2011; Gysel et al., 2004; Massoli et al., 2011; Meyer et al., 2009; Mochida & Kawamura, 2004; Ng et al., 2006; Stratmann et al., 2010). In general, all SOA is found to be slightly hygroscopic, with water uptake less than that of typical inorganic aerosol substances. HGF values reported in the laboratory studies ranged from 1.05 (for the fresh SOA) to 1.2 (for highly oxidized SOA). The aerosol water uptake increases with time early in the experiments for the cycloalkane SOA, but decreases with time for the biogenic SOA. This behaviour could indicate competing effects between the formation of more highly oxidized

polar compounds (more hygroscopic), and formation of longer-chained oligomers (less hygroscopic). All SOA also exhibit a smooth water uptake with RH with no deliquescence or efflorescence (Varutbangkul et al., 2006). However, field applications of HTDMA and aerosol mass spectrometer (AMS) running in parallel have been rather less abundant so far (Gasparini et al., 2004; Jones et al., 2011; Jurányi et al., 2010; Mochida et al., 2008). Additionally, organic tandem differential mobility analyser (OTDMA) and aerosol mass spectrometric have been successfully used in parallel under field conditions (Jimenez et al., 2009; Raatikainen et al., 2010).

This study presents results from the deployment of an HTDMA, OTDMA and an aerosol mass spectrometer (AMS) to characterize continental aerosol properties during the 2009 EUCAARI intensive field campaign in rural region of Po Valley, as a region strongly influenced by urban and transport generated aerosol pollution.

2. Methods and Instrumentation

The HTDMA configuration used during the campaign consisted of two Hauke type differential mobility analysers (DMAs), an aerosol conditioner (heated Gore-Tex humidifier) and a condensation particles counter (CPC model 3772) with sample flow of 1 $Lmin^{-1}$. Relative humidity (RH) was controlled by a Rotronic RH probes and an Edgetech Dewmaster dew-point chilled mirror sensor. The aerosol sample was given charge equilibrium by Thermo Systems Inc. (TSI) ^{85}Kr aerosol neutralizer operating at activity of 10 mCi. The sizes measured were as follows:
35nm, 50nm, 75nm, 110nm, and 165nm. Scan length for each size was set to 180 seconds; full scan cycle was taking 15 minutes and 50 seconds.

The main principle of operation of the DMA (Knutson & Whitby, 1975; Liu et al., 1978) is to select a narrow band of an aerosol size distribution by applying high voltage to its central rod thus selecting particles with a particular electrical mobility. In this way, a monodisperse aerosol distribution is allowed to pass through the instrument. For the HTDMA, two DMA are positioned on either side of a humidification conditioner, allowing the humidification of a selected dry particle size followed by characterisation of its humidified size. Since the dry diameter of aerosol is well known (aerosol is dried by 50 tubes Nafion dryer down to 5% RH prior entering first DMA) by measuring the size of particles exiting second DMA one can calculate hygroscopic growth factor (HGF). The sizing of the wet aerosol is achieved by scanning the electrical mobility of the humidified particles and particles exiting second DMA are counted by the CPC. Sheath to aerosol flow ratio is maintained at 1:9 by use of critical orifices on both DMA's sheath flow pumps. In order to be able to dry calibrate the HTDMA, two-way valve is fitted before the dryer to bypass it as needed. Whole setup is controlled by the PC which acts as PID controller for the humidifier and a data processor and logger.

An inversion algorithm has to be applied to the measurement distribution function (MDF) of TDMA measurements to retrieve the GF-PDF's correct shape, to determine the mean GF of the sample and to provide the number fractions of particles in different GF ranges (Gysel et al., 2009). Because the TDMA's overall transfer probability depends on the GF of the particles, MDF may be smoothed and skewed. Appropriate "inversion" of the raw measurement data is therefore required in the most TDMA applications, in order to recover the actual GF-PDF of the investigated aerosol (Gysel et al., 2009). Details of the kernel calibration,

data inversion, and TDMA forward function are described (Gysel et al., 2009).

The working principle of the UFO-TDMA (ultrafine organic tandem differential mobility analyser) (Joutsensaari et al., 2001; Vaattovaara et al., 2005) is similar to the HTDMA except for ethanol being the working fluid rather than water and the particles are brought to a selected sub-saturated ethanol vapour environment where they can grow to a new size in accordance their composition and size. The ratio between the measured size in the second DMA and the size selected in the first DMA is called ethanol growth factor or organic growth factor (OGF, used in this manuscript). Depending on the chemical composition of the particles, different amounts of ethanol are consumed at a given saturation ratio by the particles. We applied the UFO-TDMA (called OTDMA in the following text) to 50 nm particles. The error estimate of the GF values is smaller than 0.01 for 50 nm particles. Uncertainties of growth factors were estimated for 50 nm particle size based on a relative growth factor change between the consecutive dry size laboratory measurements for different compounds (Vaattovaara et al. 2005). The estimation was carried out based on the 0.1 nm uncertainty in the particle diameter measurements, i.e. 0.1/50). The saturation ratio was 81±2%.

Inorganic particles such as sodium chloride and the ammonium sulphate do not grow (i.e. OGF is 1) in the sub-saturated (S = 82% - 84%) ethanol vapour while pure ammonium bisulphate or particles containing ammonium bisulphate and sulphuric acid with sulphuric acid mass fraction up to 33% grow in sub-saturated ethanol vapour when the dry particle diameter is 10 nm or smaller and S < 84% (Vaattovaara et al., 2005). Ammonium bisulphate would grow in 50 nm size to 1.02-1.03 at 81-83 % (Vaattovaara et al., 2005). However, this growth is a minor fraction compared to the total growth factor value observed in this study. More importantly, sulphuric acid or ammonium bisulphate are already neutralized to less acidic form in atmospheric 50 nm size particles and thus their OGF behave like ammonium sulphate in atmospheric conditions. On the other hand, particles composed of biogenic organics (e.g. citric acid or tartaric acid) do grow (i.e. OGF is clearly over 1). Generally, moderately oxidized organic do grow very well. It is also notable that if organic compounds are composed of non-polar compounds or if they are highly aged, they do not grow so well either. The OTDMA and the HTDMA provide complementary information about inorganics and organics affinity to ethanol and water, which can be used to indirectly probe the composition behaviour of the particle phase (Vaattovaara et al., 2009). So far, they have been successfully used in parallel to study the composition and diurnal cycles of 50-100 nm particles in different field conditions (Boy et al., 2004; Petäjä et al., 2005; Tiitta et al., 2010).

Aerosol chemical composition was measured with the Aerodyne Research Inc. high resolution, time-of- flight aerosol mass spectrometer (HR-ToF-AMS) which provides real-time size resolved composition analysis of volatile and semi-volatile particulate matter. Combination of size and chemical analysis of sub-micron aerosol mass loading with fast time resolution makes the AMS unique. The theory of operation is described in (JAYNE et al., 2000a; Jimenez et al., 2003) and (Jimenez et al., 2006). In summary, the AMS quantifies non-refractory aerosol chemical composition, covering major inorganic species such as ammonium, sulphate, nitrate, etc. plus organic species. The AMS detects composition quantitatively by combining thermal vaporization and

electron ionization. For mass concentration calculations, an empirical particle collection efficiency (CE) factor of 0.5 was used, already widely found to be representative for ambient particles in many AMS studies (Jayne et al., 2000; Canagaratna et al., 2007, Middlebrook et al., 2012) and the value of 0.5 was further validated by good inter-comparison with off-line ion mass concentration measurements obtained during the field study.

Factor analysis of AMS data enables differentiation between different OA types and determination of the oxygen content in OA. POA from fossil fuel combustion and other hydrocarbon-like OA (HOA) and biomass-burning OA (BBOA) can be distinguished as an oxygenated organic aerosol (OOA), low-volatility OOA (LV-OOA), semi-volatile OOA (SV-OOA) and cooking OA (COA). PMF (Ulbrich et al., 2009) was run on both low and high resolution AMS organic data with a focus on a 5 factor solution. The 5 factors are: OOA1 (local), OOA2 (regional), HOA, COA and SV-OOA. Although the PMF analysis was performed for the duration of the campaign for 1 to 7 factors (described in detail in supplementary document), it was found that the PMF solutions with factor numbers greater than 5 provided no new meaningful information and instead resulted in a splitting of the existing factors. The five-factor solution was thus chosen as the optimal solution following a number of considerations, including correlations between the chosen AMS PMF solution and measurements taken using the other techniques, specifically with Aerosol time of flight Mass spectrometer data (see methodology for example used in Dall´Osto et al., 2012). In this work all data are reported in the local time.

3. Measurements Location

Measurements were undertaken at San Pietro Capofiume (SPC), situated near Bologna, Emilia-Romagna, Italy (geographical coordinates: 44° 39' 0" North, 11° 38' 0" East, Figure 1). The geographical location of the SPC site makes it ideally situated for anthropogenic pollutions studies. Both rural and urban influences can be investigated and both sources of aerosol can be elucidated. SPC

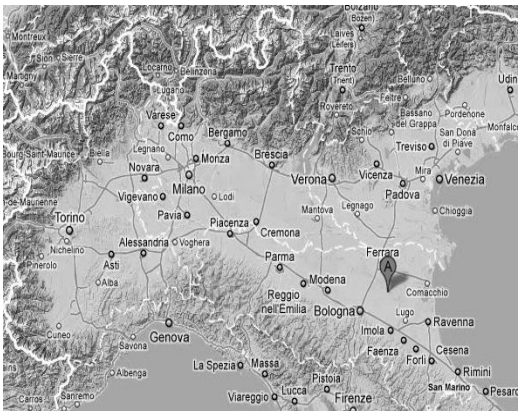

Figure 1. Po Valley is bordered by the Alps to the north and west, by the forefront of Apennines mountains to the south and the Adriatic Sea to the east. San Pietro Capofiume site (SPC) is marked with A on the map (sourced from Tele Atlas 2011).

is situated close to two major Po Valley cities: Bologna 25 km to the South, with over 300,000 inhabitants, heavy industry, and a major transportation hub; and Ferrara 20 km to the north, with 130,000 inhabitants and food and machinery industry. The site itself is surrounded by wheat and corn fields with a small food processing plant 800 m south-east from the station. During the campaign, intensive harvesting activities were performed around the site. This region of Italy is characterized by a dense network of primary and secondary roads. San Pietro Capofiume is situated close to main motorways: A14 Bologna – Rimini 22 km from the site to the South, part of motorway system connecting Milano and Adriatic coast, A13 connecting Bologna – Vanezia, 11 km from the site to the west, and motorway link from A13 to the Adriatic coast, 16 km to the north. Additionally, long range transport and aged aerosol from distant pollution sources along river Po can be investigated.

4. Meteorological Overview

Meteorological conditions in San Pietro Capofiume were characterized by weak wind speed, with prevailing E to SE wind direction for 32% of the time with ESE being the most frequent sector. The strongest wind speeds registered for this sector was 5-6 m s^{-1} but only for a fraction of time (<1%). The mean wind speed for this sector was 3.5 m s^{-1}. Highest wind speeds were recorded for W-WNW sector with maximum around 14 m s^{-1} for short duration of time (<1%). Mean wind speed for this sector was 6.3 m s^{-1}. Calm conditions (0-1m s^{-1}) amounted to 17% of total duration of campaign. The highest temperature recorded for duration of campaign was 32°C on the 3rd of July, lowest temperature recorded was 14.5°C on 11th of July.

Air mass back-trajectories were classified into 6 clusters, but essentially we discriminated between two generic types called "West", reflecting a longer range transport from western Europe and the Atlantic (two different zones, West 1 "Western Europe" and West 2 "Atlantic"), and types called "PoV", describing a weaker circulation with more regional (Po Valley) component. The analysis of shorter (24 h) back trajectories provides essentially the same results. Data for air mass classification were sourced from HYSPLIT 24h and 48h back-trajectories with a 500 m asl endpoint. Local meteorological measurements were recorded at the station. Radio-soundings at SPC are available at http://weather.uwyo.edu/upperair/sounding.html, station code: 16144. Subjective classification of synoptic weather conditions was done using the METEOSAT satellite images. Deep convective systems affected the circulation in the Po Valley sector around SPC on several days bringing strong thundery showers to the site. The circulation driven by these systems cannot be captured by the back trajectory analysis. Convective rainfalls were registered on 5th, 7th, 9th and 10th of July. The highest rainfall was registered on 9th of June with 14 mm falling in 30 minutes.

4.1 Meteorological overview for the chosen cases

4.1.1 Case 1: 07.07.2009 12:00 to 09.07.2009 12:00

In the afternoon of 7th July the air circulation was PoV WNW, captured well by the back trajectories. Showers were recorded at SPC from the precipitating systems travelling eastward over the Po Valley. In the period of 8th – 9th (until midday) July, "West1" or "West2" circulation were recorded and westerly winds captured by the ground sensors and radio soundings at all heights. Clear sky, turned to scattered clouds later in this period.

4.1.2 Case 2: 09.07.2009 12:00 to 11.07.2009 12:00

From the afternoon of 9th to 11th July lowest T_{max} of the campaign was recorded. The T_{min}, was progressively decreasing and it became more humid. Back trajectories were of types "PoV WNW", but actually the circulation was complex: westerlies persisted at the top of the boundary layer (1500 m asl), and easterly winds (from the Adriatic) intensified at ground level at the end of this period, especially on 11th July. Precipitating systems developed on the Apennines on 9th July around midday, bringing a lot of rain to Bologna and then to SPC. On 10th July, precipitating systems appeared in the eastern Po Valley with heavy rain in SPC. During these days, the boundary layer meteorology followed a typical diurnal evolution for July in the Po Valley, characterized by a

transition from a stable, shallow nocturnal surface layer to a 1500 m - thick convective mixing layer between 8:00 to 13:00 (Di Giuseppe et al., 2012).

5 Results & Discussion

HGFs for the whole duration of the campaign are displayed in Figure 2a where darker colours represent lower growth factors and black dots represent averaged HGF between all sizes per HTDMA scan. During the first part of the campaign (27.06.2009 to 05.07.2009), distinct diurnal variability and generally lower HGFs with minima during night time, reaching less than 1.2, increasing to 1.45 during daytime. The second part of campaign (5 July 2009 to 11 July 2009) shows less variability and higher general (averaged) HGF values, ranging from 1.25 to 1.4. During the last two days, the highest daytime HGF of >1.5 was achieved; but night time HGFs didn't drop below 1.25 as it was the case during the first part of the campaign.

Analysis of the aerosol hygroscopicity for the duration of the campaign allows distinguishing several periods:

- A (28 June – 2 July) correspond with the highest overall HGFs recorded along with the highest night-time HGFs.
- B (2 July – 4 July) shows the highest amplitude of diurnal variability with the lowest recorded night-time HGFs.
- C (5 – 6 July) can be described best as a transitory between two distinct periods. It was characterized by a high HGF variability.
- D (7 July – 9 July, midday) exhibited the lowest amplitude of the HGF diurnal variation for the campaign.
- E (9 July, afternoon – 11 July) was characterized again by a clear diurnal pattern of HGF with moderate amplitude between day and night.
- G (12 July) again exhibited very high day-time HGFs while night-time HGFs remained moderately high

The average diurnal variation of HGF for the duration of the campaign is shown on

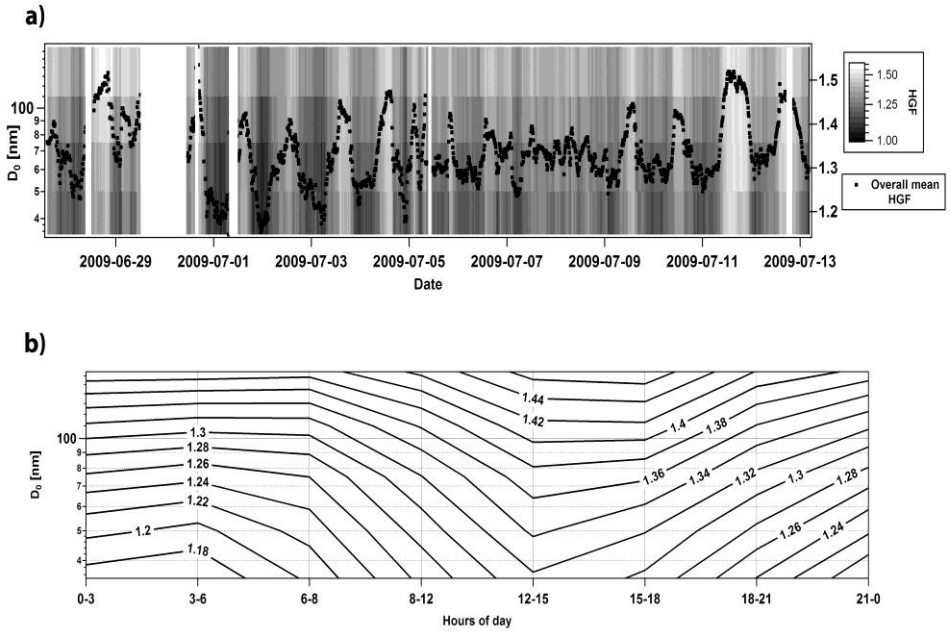

Figure 2. (a) Size resolved HGF and mean HGF for whole duration of the campaign, **(b)** Size resolved diurnal variability of HGF for whole campaign.

Figure 2b. HGF is interpolated between the five measured sizes to give overall picture of variation both in size and time. The lowest HGFs occurred in the early hours of morning (03:00-06:00), but generally, the whole night shows very low hygroscopicity, particularly in the smaller sizes. The HGF difference between the measured sizes was the biggest at night with HGF 1.18 recorded for the smallest sized particles (35 nm) and HGF 1.38 recorded for the largest sizes (165 nm). During the day, the HGF gradually increases to achieve maximum in the afternoon hours 12:00-15:00. Maximum HGFs achieved were 1.32 for 35 nm particles and 1.46 for 165 nm particles.

5.1 Diurnal Variability – Case Studies.

Two clear types of diurnal patterns were evident and are chosen for more detailed analysis. One case type was characterized by low diurnal variability while the second case was characterized by a strong diurnal pattern. The HTDMA HGF - probability distribution function (PDF) was integrated to create 4 distinctive aerosol mixing fractions (Swietlicki et al., 2008): a barely hygroscopic fraction with HGF 1-1.12 (BH); a less hygroscopic fraction with HGF 1.125 – 1.34 (LH); a more hygroscopic fraction with HGF 1.345-1.87 (MH); and sea-salt-like fraction with HGF 1.875 and above (SS, wasn't seen in this study).

5.1.1 Case 1, period D: 07.07.2009 12:00 to 09.07.2009 12:00 (Figure 3)

Temperature started to rise from 05:00 and reached maximum around of 28 ^{o}C around noon. The decrease was slowed down by the heat capacity of the ground and its long wave radiation back into the atmosphere. The minimum value of temperature, 19 ^{o}C, was recorded around 04:00. Westerly back trajectories during this period suggest advection of relatively fresher air masses (passing over the mountains). Total (AMS-derived) non-refractory aerosol mass concentrations peaked at 5 μg m^{-3} in the early afternoon, while minimum of 3 μg m^{-3} was achieved at midnight and shortly after sunrise. A diurnal pattern in the individual AMS mass components wasn't clearly visible either and very low nitrate mass level was observed (less than 0.1 μg m^{-3} through most of the day with small peak around 20:00 – 0.7 μg m^{-3}).

During 24 hours contributions of each AMS component was relatively stable with organics dominating the mass contribution, peaking at 2.5 μg m^{-3}. In terms of percentage contribution to total AMS-derived mass, organics contributed 55%, sulphate 30%, ammonium 10 % and nitrate 5%. Organic concentration had three weak maxima during the day: 2.05 μg m^{-3} around 04:00, 2.55 μg m^{-3} at 14:00 and 2.5 μg m^{-3} at 19:00. The minimum for organics was observed 1.45 μg m^{-3} around 13:00. The sulphate maximum of 2 μg m^{-3} was recorded around 13:00, while the minimum of 0.6 μg m^{-3} was recorded midnight. Ammonium followed sulphate and its maximum of 0.7 μg m^{-3} was recorded at 13:00 while a minimum of 0.3 μg m^{-3} was encountered at midnight. The AMS PMF analysis reveals a HOA contribution of 5 - 20% with peak contributions occurring at 07:00. COA contributes less than 5% while OOA2 accounts for 20-45% and OAA1 up to 40%.

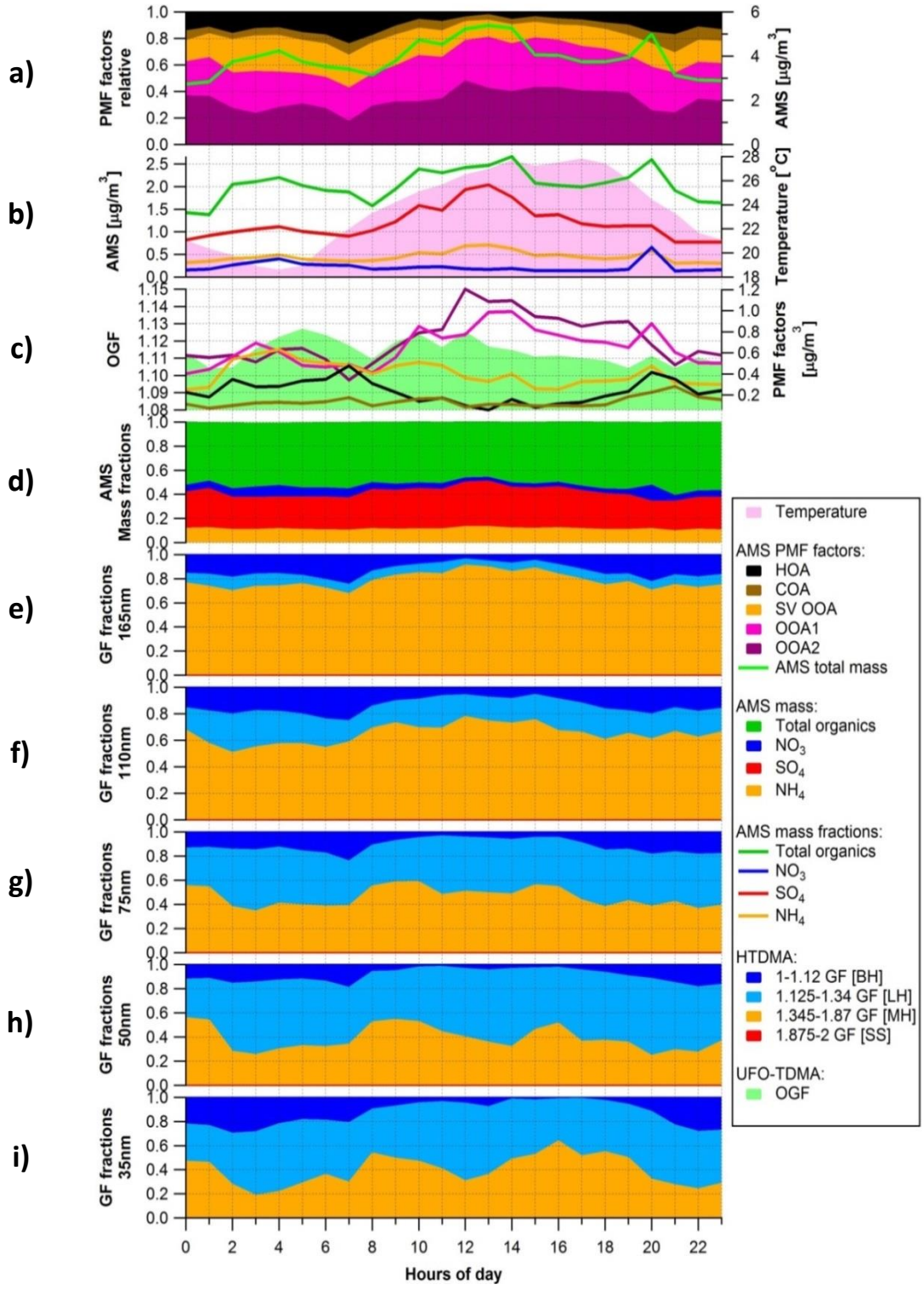

Figure 3. Diurnal pattern of relative PMF factors and AMS total mass (panel a), main chemical compounds mass variation measured by the AMS superimposed over the temperature (panel b), mass PMF factors variation superimposed over the OGF diurnal pattern (panel c), AMS mass fractions (panel d) and diurnal pattern of HGF groups (panels e to i). Note small variations of all the parameters, especially AMS mass fractions (panel d). More variation could be seen only in the mass PMF factors. Period: 07.07.2009 12:00 to 09.07.2009 12:00

In terms of HGFs, the larger sized particles (165 nm) possess the highest HGFs with 75-80% contributions from the MH GF and 5-20% from BH HGFs. As

smaller particles are considered, the MH HGF component progressively reduces to between 20-50% fraction of total particles in the 35 nm size range while the LH HGF component to fraction of 25-60%. The minimum in growth factor occurs at 03:00 – 04:00, corresponding to a relative peak in the OGF of 1.13. Second and third peaks, both of the order of 1.125, are also seen at 10:00 and 12:00. The BH fraction of HGF tracks the HOA signal the closest. OGF diurnal variation seems to follow roughly AMS organic mass load, while generally contrasted with HGF diurnal pattern, especially in BH and LH fraction. A semi-volatile fraction (SV OOA) is visible during whole day in stable concentrations with only slightly higher contributions during the night. This fraction comes from partial oxidation of organics and is represented well by diurnal variations of LH HGF group in 110 nm particle size range. It is also worth mentioning that so called "Cooking Aerosol" (COA) factor concentration is steadily increasing from around 18:00. However, the hygroscopicity and affinity to the ethanol of COA is very similar to those of HOA and SV-OOA, thus no visible changes in HGF could be observed. At the same time, OGF diurnal patter is similar to SV-OOA and OOA1. Generally, OGFs follow the total organic mass trend while the regional OOA2 concentration dominated at the measurement site. The peak of concentration for this factor was recorded around noon and slowly decreased over time maintaining its dominance till late evening. OOA1 followed closely OOA2 peaking around noon but also exhibiting a secondary peak in the evening rush hour time.

The average 50nm OGF and HGF is plotted with the total AMS organic mass and the HGF-PDF in Figure 4 where OGF increases when moderately aged, regional (OOA2) aerosol is present (Figure 3), especially when HGF reaches values around 1.2. The PDF illustrates a predominant HGF mode between 1.25 and 1.35 throughout the period, with two additional GF modes, one at 1.45 and one at 1.05, occurring at night-time. Generally, the OGFs and HGFs variations are consistent with the relative proportions of organics, sulphates and nitrates, along with changes in the oxygenated level of the organics.

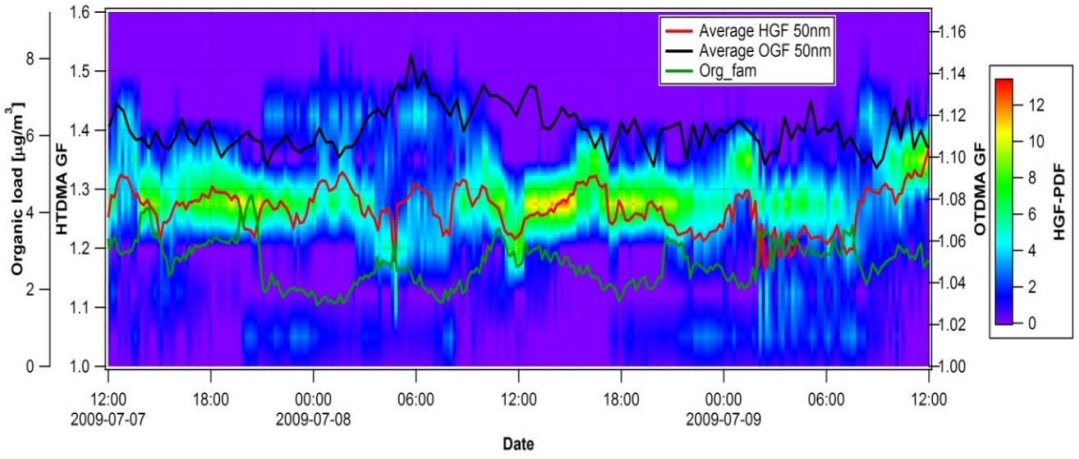

Figure 4. Organic TDMA versus HTDMA and AMS organic load (Organic families - Org_fam) for the first period. 50 nm was chosen as it was common for both instruments. Note that the OGF increases when moderately aged, regional (OOA2) aerosol is present, especially when HGF reaches values around 1.2.

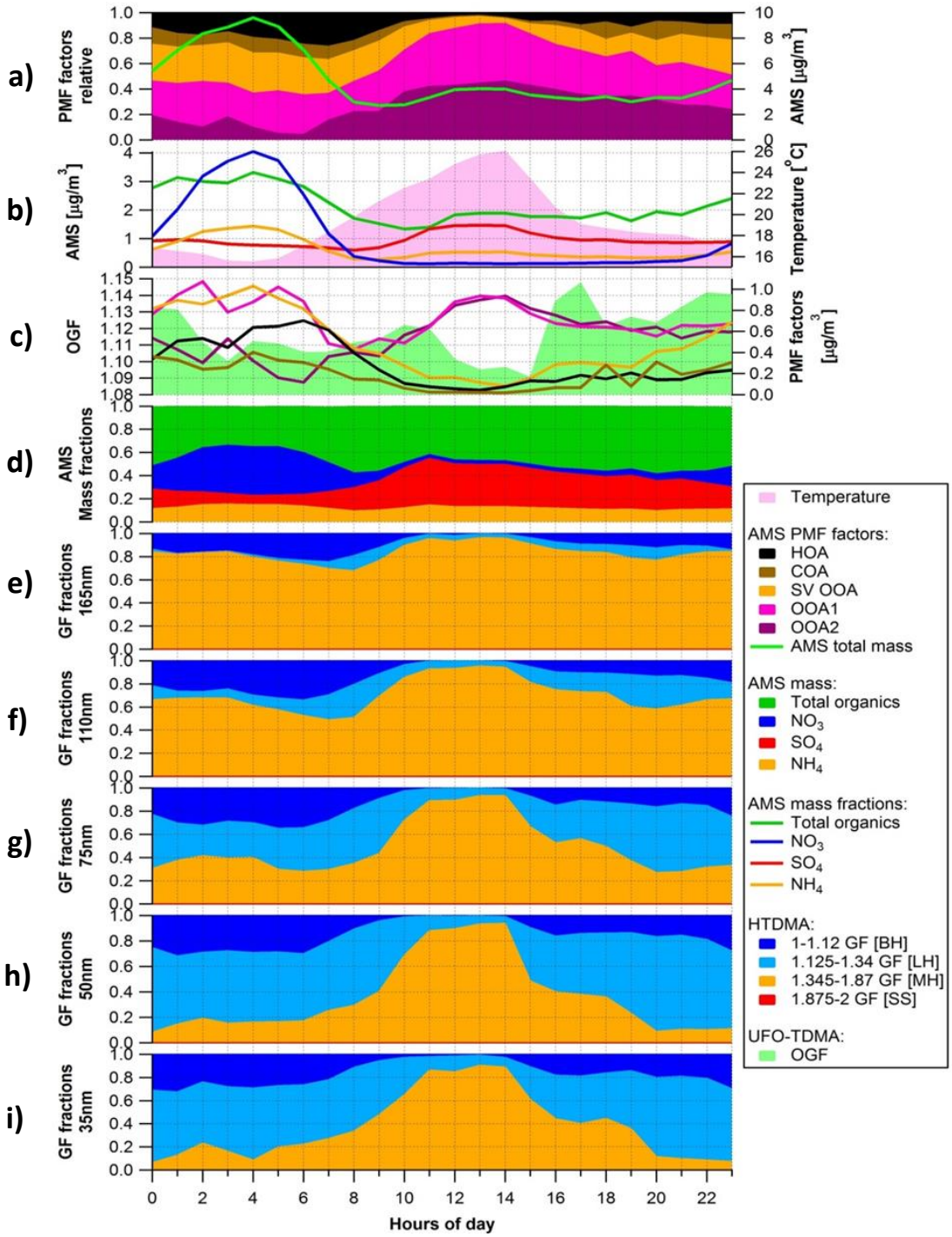

Figure 5. Diurnal pattern of relative PMF factors and AMS total mass (panel a), main chemical compounds mass variation measured by the AMS superimposed over the temperature (panel b), mass PMF factors variation superimposed over the OGF diurnal pattern (panel c), AMS mass fractions (panel d) and diurnal pattern of HGF groups (panels e to i). Note the marked variation of hygroscopic groups in sizes 35 through 75 nm and less distinct variations in the size range 110 and 165 nm. Variations follow changes in the chemical composition of the aerosol. Period: 09.07.2009 12:00 to 11.07.2009 12:00

5.1.2 Case 2, period E: 09.07.2009 12:00 to 11.07.2009 12:00 (Figure 5)

For this case, temperature was initially quite similar to *Case 1* increasing from 05:00 and peaking around noon. In the afternoon, fast development of convective

clouds cause the overcast and temperature decrease. This was further accelerated by the rain showers. Maximum of 26°C was recorded around 14:00, and a minimum of 15°C was recorded at 04:00. In contrast to *Case 1*, much higher levels of aerosol pollution was observed with peak concentrations of AMS-derived non-refractory mass exceeding 9 μg m^{-3} around 04:00, reducing to ~3 μg m^{-3} at 09:00-10:00. This reduction may be caused by deepening of boundary layer and increased mixing height, thus grater dilution of bulk aerosol may occur. A daytime peak of ~4 μg m^{-3} is seen at 13:00. The strong diurnal signal is driven by the nitrate (i.e. ammonium nitrate, based on the high HGF values in accumulation mode sizes) temporal trend, but is also notably influenced by the organic contribution. This also makes possible the formation of organonitrates during night time when nitrate and organic concentrations are high. It is worth noting that the 35 nm and 50nm HGF values (i.e. Aitken mode size particles) are low but the 110 nm and 165 nm HGF values (accumulation mode size particles) are high at night (Figure 5), thus supporting the domination of highly hygroscopic nitrates (i.e. ammonium nitrate) in the accumulation mode sizes but the "lower hygroscopicity nitrates" in the Aitken mode sizes. Possible reasons for the low hygroscopicity of particulate nitrate in the small particles are: a) coating by poorly hygroscopic organic compounds, and b) the actual chemical nature of nitrate in Aitken mode particles is organic (nitrate esters), which is consistent with the decrease of OGFs observed between midnight and ~6 AM. In fact, in previous experiments (Vaattovaara et al., 2009) it was found that OGFs of particulate organic matter decrease in high NO_x conditions and the ethanol affinity of organonitrate is apparently lower than that of the SV-OOA components forming in low-NO_x conditions. Therefore, our hypothesis of the organonitrate formation provides explanation for both the low HGFs and also the lowering of OGFs in the late night hours. Generally, the formation of organonitrates is expected to be probable, especially in the environment with a high load of NOx, NOy and organics. Typically, that kind of high load conditions are observed during night time at SPC station.

Importantly, NO_3-initiated oxidation chemistry with alkenes is able to form organonitrates at night (e.g. Atkinson et al. 2000) without sunlight. Additional data supporting the organonitrate hypothesis using the ATOFMS is included in the supplementary materials.

The highest variance was exhibited in nitrate mass which ranged from 4 μg m^{-3} at 04:00 to less than 0.1 μg m^{-3} throughout the rest of the day. Total organic concentration was the highest during night-time and its maximum also corresponds with the high concentration of nitrate, 3.2 μg m^{-3}, occurring around 04:00 (see also Figure 8). Minimum concentration of organics was recorded around 10:00 and slowly increased thereafter. Sulphate followed a different, flatter pattern, with a minimum of 0.7 μg m^{-3} around 08:00 and maximum of 1.5 μg m^{-3} around noon. Ammonium exhibited two maxima accordingly to nitrate and sulphate maxima ranging from 1.5 μg m^{-3} at 04:00 to its minimum of 0.3 μg m^{-3} at 08:00.

HOA accumulation was quite pronounced after midnight and was accelerated during the morning rush hour period. However, there is no evidence of the evening rush hour leading to HOA accumulation. This factor is also very well visible in HGF data as BH fraction which follows closely HOA's diurnal pattern in all measured sizes. COA concentration increases from around 17:00 and remains stable during

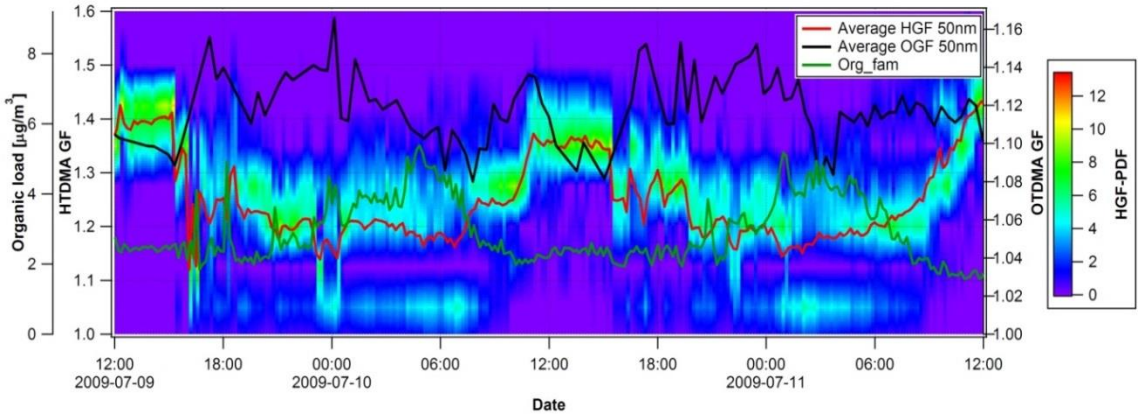

Figure 6. Organic TDMA versus HTDMA and AMS total organic load (Organic families - Org_fam) for the second period. 50 nm was chosen as it was in common for both instruments. Note that while the AMS organic mass reaches a maximum (between midnight and early morning) the OGF values decrease.

the night and seems to correspond closely to the BH fraction of HGF, adding to the HOA contribution. Similar patterns are seen for sizes in range of 35-110 nm. The SV-OOA factor concentration started to increase from around 14:00 and reached a maximum around midnight. This factor dominates the HGF LH fraction. The diurnal evolution of LH follows SV-OOA very closely in 35-75 nm size ranges.
Both OOA2 and OOA1 had equal contribution to total OOA from noon till late evening. After midnight however, local OOA1 contribution increased while regional OOA2 decreased during the night.

The MH fraction of HGFs exhibited higher diurnal variability in size range from 35nm to 75 nm than 110-165nm, with the most distinctive pattern seen in the smallest sizes. For larger particle sizes of 110nm and 165nm, a less strong diurnal pattern was seen, with an overall maximum through all sizes recorded around noon. Interestingly, two minima were also recorded in MH fraction: in late evening and again in the morning hours. A diurnal cycle was less evident in the somewhat unbalanced OGF signal during this period. However, a clear minimum of 1.09 was seen in the mid-afternoon. This minimum was related to the increase of sulphate, OOA1 and OOA2. Because OGF values decrease so strongly and HGF values increase so rapidly, the formation of organosulphates is the most probable explanation for the 50 nm OGF and HGF behaviour. This is due to a previous atmospheric observation (Vaattovaara et al. 2009) that in the case of combined sulphates and organics, OGF values decrease and HGF values increase. The minimum was followed rapidly by a peak of 1.15 at 17:00 due to local change in the air mass with less sulphate, OOA1 and OOA2, thus less organosulphates but more ethanol soluble semi-volatile OOA. This effect was enhanced by a quick temperature drop from 26 ^{o}C to 19 ^{o}C. Another OGF peak of 1.13 was just before midnight due to additional increase of SV-OOA fraction. Overall aerosol affinity to ethanol is higher during the late afternoon and night hours. The minima in the OGF seem to anti-correlate with the MH HGF fraction for sizes 35-110nm. Higher COA concentrations seem to suppress aerosol affinity to the ethanol.

Figure 6 shows that the hours of the day when the AMS organic mass reaches a maximum (between midnight and early morning) are characterized by decreasing OGF values. This behaviour seems to be partly related to a high sulphate/organics ratio. OGFs stays high as long as group of particles with mean HGF from 1.2 to 1.3

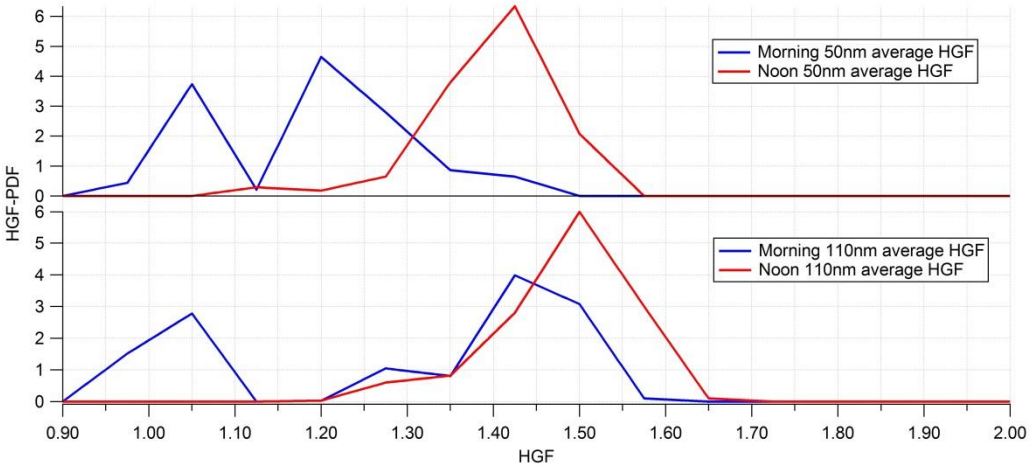

Figure 7. HGF-PDF time slices for the morning average period (04:00-05:00) and the noon average period (12:00-13:00) of average HGF for 50 nm and 110 nm sized particles. The shift toward higher HGFs during the day is more pronounced in the smaller size range.

predominates and it is lower when hydrophobic group predominates and 1.3 HGF group decreases in concentration. Occurrence of particle group with very low HGF corresponds well with AMS organic load. The OGF is generally anti-correlated to HGF exhibiting low (-0.3), but statistically significant negative correlation coefficient. The data are of different temporal resolutions which made the direct comparison more difficult to perform. Analysis of the HGF-PDF reveals a higher degree of variability in the mean HGF with the values of 1.4 through midday, reducing to 1.2 at night. During early evening through to late morning, a low HGF mode at 1.05 is also evident and persistent.

Figure 7 shows time-slice PDFs extracted for each of the HGF sizes at 04:00-05:00 (i.e. the nitrate peak, total mass peak, and HGF minimum) and at 12:00-13:00 (the OGF minimum and HGF peak) while Figure 8 shows AMS nitrates mass concentration for both morning and noon time periods. While not being quantitatively reliable, careful calculation of number concentration of particles from AMS mass concentration can give a rough idea of size regimes in which both AMS and HTDMA overlap. Analysis of nitrates number distribution in mobility equivalent diameter (Figure 9) reveals that the majority of particles are represented by 50nm-110nm size range, which overlaps both HTDMA and OTDMA measurement regime. For 50 nm particles, during the nitrate peak, two strong HGF modes are seen at 1. 04 and 1.2, with a third, less pronounced peak at 1.36. This contrasts to the noontime predominant single peak at

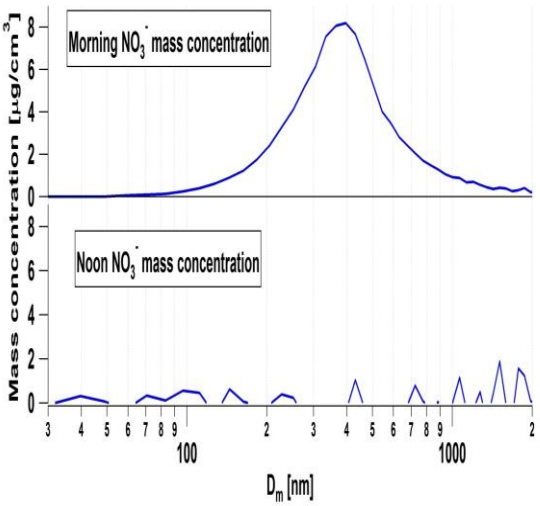

Figure 8. AMS size-segregated mass distribution of nitrates ($NO3^-$) for the morning average period (04:00-05:00) and the noon average period (12:00-13:00) of *Case 2.* During the day nitrate group disappears. The mas peak is centered around 350nm size thus easily detectable by the AMS.

1.44 and a significantly less evident HGF

mode at 1.14. For 110 nm sized particles, the HGF PDF during the nitrate peak is again tri-modal, with a primary mode at 1.4, a secondary mode at 1.04, and a third, minor, peak at 1.26. This contrasts to the noontime primary peak of 1.5 and secondary minor peak of 1.26. The general trend is twofold: (1) there is a notable reduction in the HGF associated with the MH mode, with a reduction in HGF from ~1.5 to ~1.26; and (2) there is the appearance of at least one BH mode.

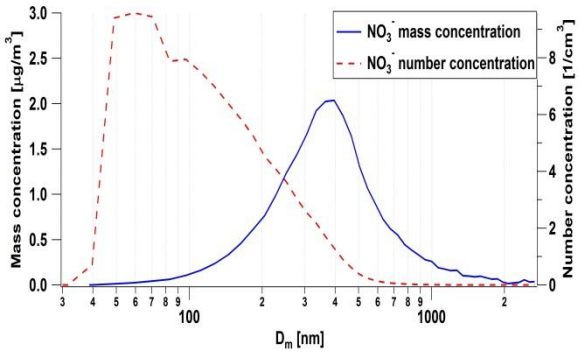

Figure 9. AMS size segregated mass and number concentration of nitrates ($NO3^-$) for *Case 2*. Note that number size concentration peaks around 50-60nm, while the mass concentration exhibits its peak around 350nm. Both AMS and HTDMA/OTDMA can reliably sample and measure relevant aerosol properties.

6 Conclusions

A HTDMA, OTDMA and AMS were deployed in the Po Valley San Pietro Capofiume research station to characterize water and ethanol uptake by the aerosol associated with the polluted continental air and how these properties are influenced by the aerosol chemical composition. The average diurnal variation of HGF for the duration of the campaign revealed the lowest HGFs occurring in early morning hours (03:00-06:00) and in the smallest sizes. The average HGFs recorded during the low HGF period were in range from 1.18 (for the smallest, 35nm particles) to 1.38 (for the largest, 165nm particles). During the day, the HGF gradually increased to achieve maximum values in the early afternoon hours from 12:00–15:00, reaching 1.32 for 35 nm particles and 1.46 for 165 nm particles. Diurnal behaviour of HGF and OGF values suggest that the Aitken mode aerosol particles can contain the organonitrates during night time and the organosulphates during day time. The 50 nm OGF shows minima and the 50 nm HGF shows maxima at noon when organosulfates are suggested to form. Additionally, the minima are seen in the 50 nm OGF and HGF values during later hours of the night when organonitrates are suggested to form.

Two cases were examined in close detail in terms of the influence of chemical composition on HGF. One case type was characterized by moderate levels of pollution and with organic matter dominating the aerosol mass. This case illustrated little diurnal variability in relative contributions of different aerosol types, HGF, or OGF. The most distinctive pattern was seen in the reduction in the MH mode from approximately 80% in 165nm sized particles to 20–40% in 35nm sized particles while the LH mode contribution increased from less than 5% to more than 30% over the same size range. For this case, organic mass contributed approximately 50% of the total non-refractory mass. OGF values positively followed the trends of the OOAs. In contrast to *Case 1*, the second selected case had more than double the aerosol mass and exhibited a strong diurnal pattern, particularly for nitrates and also for organic mass, both of which peaked in the early morning as peak mass concentration exceeded 9.5 µg m^{-3}, making also the formation of organonitrates more probable. Particularly in the smallest sized particles, a strong diurnal signal was seen in the HGFs with peak HGFs occurring around noon and minima occurring around midnight. Despite nitrate mass peaking at 4 µg m^{-3} around 04:00, the MH HGF reached its

minimum value and both the BH and LH factors reached their maximum values. OGFs were anti-correlated with HGFs, as to be expected, but were also more generally anti-correlated with total organic aerosol mass and OOAs, in particular, the OOA1 due to high and varying sulphate/organics and nitrate/organics ratios and, consequently, organosulphate and organonitrate formation. In the evening, the higher OGFs were mainly due the increase of the SV-OOA fraction. Additionally, the OGFs positively correlated with the HOA factor. Analysis of the HGF-PDF reveals a transformation of a predominant MH mode with HGF of 1.5 around noon, into two modes, one with a HGF of 1.26 (i.e. LH) and another with a HGF of 1.05 (BH). The analysis points to an internal mixture of inorganic species, mainly nitrates, coated with a hydrophobic organic layer which suppresses water uptake. In addition, a new, externally mixed BH mode appears and is persistent.

Acknowledgements
This work was supported by the FP6 EUCAARI Integrated Project, Irelands Higher Education Authority Programme for Research in Third Level Institutes (4) project Environment & Climate: Impact at Responses, and the Center of Excellence of Finnish Academy.

References.

Allan, D., Williams, P.I., Morgan, W.T., Martin, C.L., Flynn, M.J., Lee, J., Nemitz, E., Phillips, G.J., Gallagher, M.W., Coe, H. 2010. Contributions from transport, solid fuel burning and cooking to primary organic aerosols in two UK cities. Atmospheric Chemistry and Physics, 10(2), 647-668.

Ansari, A.S., Pandis, S.N. 1999. Prediction of multicomponent inorganic atmospheric aerosol behavior. Atmospheric Environment, 33(5), 745-757.

Anttila, T., Vaattovaara, P., Komppula, M., Hyvärinen, A.-P. , Lihavainen, H., Kerminen, V.-M., and Laaksonen, A. 2009. Size-dependent activation of aerosols into cloud droplets at a subarctic background site during the second Pallas Cloud Experiment (2nd PaCE): method development and data evaluation, Atmos. Chem. Phys., 9, 4841-4854.

Atkinson, R., Calvert, J.G., Kerr, J.A., Madronich, S., Moortgat, G.K., Wallington, T.J. and Yarwood. G. (2000) The mechanism of Atmospheric Oxidation of the Alkenes, Oxford Univ. Press., Oxford, UK.

Baltensperger, U., Kalberer, M., Dommen, J., Paulsen, D., Alfarra, M.R., Coe, H., Fisseha, R., Gascho, A., Gysel, M., Nyeki, S., Sax, M., Steinbacher, M., Prevot, A.S.H., Sjogren, S., Weingartner, E., Zenobi, R. 2005. Secondary organic aerosols from anthropogenic and biogenic precursors. Faraday Discussions, 130, 265-278.

Boy, M., Petäjä, T., Dal Maso, M., Rannik, Ü., Rinne, J., Aalto, P., Laaksonen, A., Vaattovaara, P., Joutsensaari, J., Hoffmann, T., Warnke, J., Apostolaki, M., Stephanou, E.G., Tsapakis, M., Kouvarakis, A., Pio, C., Carvalho, A., Römpp, A., Moortgat, G., Spirig, C., Guenther, A., Greenberg, J., Ciccioli, P., Kulmala, M. 2004. Overview of the field measurement campaign in Hyytiälä, August 2001 in the framework of the EU project OSOA. Atmospheric Chemistry and Physics, 4(3), 657-678.

Canagaratna, M. R., Jayne, J. T., Ghertner, D. A., Herndon, S., Shi, Q., Jimenez, J. L., Silva, P. J., Williams, P., Lanni, T., Drewnick, F., Demerjian, K. L., Kolb, C. E., and Worsnop, D. R. 2007. Chemical and microphysical characterization of aerosols via Aerosol Mass Spectrometry, Mass Spectrom. Rev., 26, 185–222.

Dall'Osto, M., Beddows, D.C.S., Pey, J., Rodriguez, S., Alastuey, A., Harrison, R. M., and Querol, X. 2012. Urban aerosol size distributions over the Mediterranean city of Barcelona, NE Spain, Atmos. Chem. Phys. Discuss., 12, 16457-16492, doi:10.5194/acpd-12-16457-2012.

Dennis, W.L. 1960. The growth of hygroscopic drops in a humid air stream. Discussions of the Faraday Society, 30, 78-85.

Di Giuseppe, F., A. Riccio, L. Caporaso, G. Bonafé, G. P. Gobbi and F.Angelini, 2012. "Automatic detection of atmospheric boundary layer height using ceilometer backscatter data assisted by a boundary layer model", Q. J. R. Meteorol. Soc. 138: 649–663.

Duplissy, J., De Carlo, P.F., Dommen, J., Alfarra, M.R., Metzger, A., Barmpadimos, I., Prevot, A.S.H., Weingartner, E., Tritscher, T., Gysel, M., Aiken, A.C., Jimenez, J.L., Canagaratna, M.R., Worsnop, D.R., Collins, D.R., Tomlinson, J., Baltensperger, U. 2011. Relating hygroscopicity and composition of organic aerosol particulate matter. Atmospheric Chemistry and Physics, 11(3), 1155-1165.

Gasparini, R., Li, R., Collins, D.R. 2004. Integration of size distributions and size-resolved hygroscopicity measured during the Houston Supersite for compositional categorization of the aerosol. Atmospheric Environment, 38(20), 3285-3303.

Gysel, M., McFiggans, G.B., Coe, H. 2009. Inversion of tandem differential mobility analyser (TDMA) measurements. Journal of Aerosol Science, 40(2), 134-151.

Gysel, M., Weingartner, E., Nyeki, S., Paulsen, D., Baltensperger, U., Galambos, I., Kiss, G. 2004. Hygroscopic properties of water-soluble matter and humic-like organics in atmospheric fine aerosol. Atmospheric Chemistry and Physics, 4(1), 35-50.

Hänel, G. 1976. The Properties of Atmospheric Aerosol Particles as Functions of the Relative Humidity at Thermodynamic Equilibrium with the Surrounding Moist Air, Academic Press Inc., Advances in Geophysics, Volume 19, Issue C, 1976, Pages 73-188.

Hegg, D., Larson, T., Po-Fat, Y. 1993. A theoretical study of the effect of relative humidity on light scattering by tropospheric aerosols. Journal of Geophysical Research, 98(D10), 18,435-18,439.

JAYNE, T., J., LEARD, C., D., ZHANG, X., DAVIDOVITS, P., SMITH, A., K., KOLB, E., C., WORSNOP, R., D. 2000. Development of an aerosol mass spectrometer for size and composition analysis of submicron particles. Taylor & Francis, Colchester, ROYAUME-UNI.

Jimenez, J.L., Canagaratna, M.R., Donahue, N.M., Prevot, A.S.H., Zhang, Q., Kroll, J.H., DeCarlo, P.F., Allan, J.D., Coe, H., Ng, N.L., Aiken, A.C., Docherty, K.S., Ulbrich, I.M., Grieshop, A.P., Robinson, A.L., Duplissy, J., Smith, J.D., Wilson, K.R., Lanz, V.A., Hueglin, C., Sun, Y.L., Tian, J., Laaksonen, A., Raatikainen, T., Rautiainen, J., Vaattovaara, P., Ehn, M., Kulmala, M., Tomlinson, J.M., Collins, D.R., Cubison, M.J., Dunlea, E.J., Huffman, J.A., Onasch, T.B., Alfarra, M.R., Williams, P.I., Bower, K., Kondo, Y., Schneider, J., Drewnick, F., Borrmann, S., Weimer, S., Demerjian, K., Salcedo, D., Cottrell, L., Griffin, R., Takami, A., Miyoshi, T., Hatakeyama, S., Shimono, A., Sun, J.Y., Zhang, Y.M., Dzepina, K., Kimmel, J.R., Sueper, D., Jayne, J.T., Herndon, S.C., Trimborn, A.M., Williams, L.R., Wood, E.C., Middlebrook, A.M., Kolb, C.E., Baltensperger, U., Worsnop, D.R. 2009. Evolution of organic aerosols in the atmosphere. Science, 326(5959), 1525-1529.

Jimenez, J.L., DeCarlo, P.F., Kimmel, J.R., Trimborn, A., Northway, M.J., Jayne, J.T., Aiken, A.C., Gonin, M., Fuhrer, K.,

Horvath, T., Docherty, K.S., Worsnop, D.R. 2006. Field-deployable, high-resolution, time-of-flight aerosol mass spectrometer. Analytical Chemistry, 78(24), 8281-8289.

Jimenez, J.L., Jayne, J.T., Shi, Q., Kolb, C.E., Worsnop, D.R., Yourshaw, I., Seinfeld, J.H., Flagan, R.C., Zhang, X., Smith, K.A., Morris, J.W., Davidovits, P. 2003. Ambient aerosol sampling using the Aerodyne Aerosol Mass Spectrometer. Journal of Geophysical Research D: Atmospheres Volume 108, Issue 7, 16 April 2003, Pages SOS 13-1 SOS 13-13

Jones, H.M., Crosier, J., Russell, A., Flynn, M.J., Irwin, M., Choularton, T.W., Coe, H., McFiggans, G. 2011. In situ aerosol measurements taken during the 2007 COPS field campaign at the Hornisgrinde ground site. Quarterly Journal of the Royal Meteorological Society, 137(S1), 252-266.

Joutsensaari, J., Vaattovaara, P., Vesterinen, M., Hämeri, K., Laaksonen, A. 2001. A novel tandem differential mobility analyzer with organic vapor treatment of aerosol particles. Atmospheric Chemistry and Physics, 1(1), 51-60.

Jurányi, Z., Gysel, M., Weingartner, E., Decarlo, P.F., Kammermann, L., Baltensperger, U. 2010. Measured and modelled cloud condensation nuclei number concentration at the high alpine site Jungfraujoch. Atmospheric Chemistry and Physics, 10(16), 7891-7906.

Kittelson, D.B. 1998. Engines and nanoparticles: A review. Journal of Aerosol Science, 29(5-6), 575-588.

Knutson, E.O., Whitby, K.T. 1975. Aerosol classification by electric mobility: apparatus, theory, and applications. Journal of Aerosol Science, 6(6), 443-451.

Kupiainen, K., Klimont, Z. 2007. Primary emissions of fine carbonaceous particles in Europe. Atmospheric Environment, 41(10), 2156-2170.

Lanz, V.A., Alfarra, M.R., Baltensperger, U., Buchmann, B., Hueglin, C., Prévôt, A.S.H. 2007. Source apportionment of submicron organic aerosols at an urban site by factor analytical modelling of aerosol mass spectra. Atmospheric Chemistry and Physics, 7(6), 1503-1522.

Lee, E., Chan, C.K., Paatero, P. 1999. Application of positive matrix factorization in source apportionment of particulate pollutants in Hong Kong. Atmospheric Environment, 33(19), 3201-3212.

Liu, B.Y.H., Pui, D.Y.H., Whitby, K.T. 1978. The aerosol mobility chromatograph: a new detector for sulfuric acid aerosols. Atmospheric Environment, 12(1-3), 99-104.

Massoli, P., Lambe, A.T., Ahern, A.T., Williams, L.R., Ehn, M., Mikkilä, J., Canagaratna, M.R., Brune, W.H., Onasch, T.B., Jayne, J.T., Petäjä, T., Kulmala, M., Laaksonen, A., Kolb, C.E., Davidovits, P., Worsnop, D.R. 2011. Relationship between aerosol oxidation level and hygroscopic properties of laboratory generated secondary organic aerosol (SOA) particles. Geophysical Research Letters Volume 37, Issue 24, 2010, Article number L24801, DOI: 10.1029/2010GL045258

McFiggans, G., Artaxo, P., Baltensperger, U., Coe, H., Facchini, M.C., Feingold, G., Fuzzi, S., Gysel, M., Laaksonen, A., Lohmann, U., Mentel, T.F., Murphy, D.M., O'Dowd, C.D., Snider, J.R., Weingartner, E. 2006. The effect of physical and chemical aerosol properties on warm cloud droplet activation. Atmospheric Chemistry and Physics, 6, 2593-2649.

McInnes, L., Bergin, M., Ogren, J., Schwartz, S. 1998. Apportionment of light scattering and hygroscopic growth to aerosol composition. Geophysical Research Letters, 25(4), 513-516.

Meyer, N.K., Duplissy, J., Gysel, M., Metzger, A., Dommen, J., Weingartner, E., Alfarra, M.R., Prevot, A.S.H., Fletcher, C., Good, N., McFiggans, G., Jonsson, A.M., Hallquist, M., Baltensperger, U.,

Ristovski, Z.D. 2009. Analysis of the hygroscopic and volatile properties of ammonium sulphate seeded and unseeded SOA particles. Atmospheric Chemistry and Physics, 9(2), 721-732.

Middlebrook, A.M., Bahreini, R., Jimenez, J.L., and Canagaratna, M.R. 2012. Evaluation of Composition-Dependent Collection Efficiencies for the Aerodyne Aerosol Mass Spectrometer using Field Data, Aerosol Sci. Technol., 46, 258–271, DOI:10.1080/02786826.2011.620041.

Mochida, M., Kawamura, K. 2004. Hygroscopic properties of levoglucosan and related organic compounds characteristic to biomass burning aerosol particles. Journal of Geophysical Research D: Atmospheres, 109(21), D21202 1-8.

Mochida, M., Miyakawa, T., Takegawa, N., Morino, Y., Kawamura, K., Kondo, Y. 2008. Significant alteration in the hygroscopic properties of urban aerosol particles by the secondary formation of organics. Should be: Geophysical Research Letters Volume 35, Issue 2, 28 January 2008, Article number L02804, DOI: 10.1029/2007GL031310

Ng, N.L., Kroll, J.H., Keywood, M.D., Bahreini, R., Varutbangkul, V., Flagan, R.C., Seinfeld, J.H., Lee, A., Goldstein, A.H. 2006. Contribution of first- versus second-generation products to secondary organic aerosols formed in the oxidation of biogenic hydrocarbons. Environmental Science and Technology, 40(7), 2283-2297.

Paatero, P., Tapper, U. 1994. Positive matrix factorization: a non-negative factor model with optimal utilization of error estimates of data values. Environmetrics, 5(2), 111-126.

Petäjä, T., Kerminen, V.M., Hämeri, K., Vaattovaara, P., Joutsensaari, J., Junkermann, W., Laaksonen, A., Kulmala, M. 2005. Effects of SO 2 oxidation on ambient aerosol growth in water and ethanol vapours. Atmospheric Chemistry and Physics, 5(3), 767-779.

Raatikainen, T., Vaattovaara, P., Tiitta, P., Miettinen, P., Rautiainen, J., Ehn, M., Kulmala, M., Laaksonen, A., Worsnop, D.R. 2010. Physicochemical properties and origin of organic groups detected in boreal forest using an erosol mass spectrometer. Atmospheric Chemistry and Physics, 10(4), 2063-2077.

Rogge, W.F., Hildemann, L.M., Mazurek, M.A., Cass, G.R., Simoneit, B.R.T. 1993. Sources of fine organic aerosol. 2. Noncatalyst and catalyst-equipped automobiles and heavy-duty diesel trucks. Environmental Science and Technology, 27(4), 636-651.

Saxena, P., Hildemann, L.M., McMurry, P.H., Seinfeld, J.H. 1995. Organics alter hygroscopic behavior of atmospheric particles. Journal of Geophysical Research, 100(D9), 18,755-18,770.

Schauer, J.J., Rogge, W.F., Hildemann, L.M., Mazurek, M.A., Cass, G.R., Simoneit, B.R.T. 1996. Source apportionment of airborne particulate matter using organic compounds as tracers. Atmospheric Environment, 30(22), 3837-3855.

Stratmann, F., Bilde, M., Dusek, U., Frank, G.P., Hennig, T., Henning, S., Kiendler-Scharr, A., Kiselev, A., Kristensson, A., Lieberwirth, I., Mentel, T.F., Pöschl, U., Rose, D., Schneider, J., Snider, J.R., Tillmann, R., Walter, S., Wex, H. 2010. Examination of laboratory-generated coated soot particles: An overview of the LACIS Experiment in November (LExNo) campaign. JJournal of Geophysical Research D: Atmospheres Volume 115, Issue 11, June 2010, Article number D11203, DOI: 10.1029/2009JD012628

Svenningsson, B., Hansson, H.C., Wiedensohler, A., Noone, K., Ogren, J., Hallberg, A., Colvile, R. 1994. Hygroscopic growth of aerosol particles and its influence on nucleation scavenging in cloud: Experimental results from Kleiner Feldberg. Journal of Atmospheric Chemistry, 19(1-2), 129-152.

Swietlicki, E., Hansson, H.C., Hämeri, K., Svenningsson, B., Massling, A., McFiggans, G., McMurry, P.H., Petäjä, T., Tunved, P., Gysel, M., Topping, D., Weingartner, E., Baltensperger, U., Rissler, J., Wiedensohler, A., Kulmala, M. 2008. Hygroscopic properties of submicrometer atmospheric aerosol particles measured with H-TDMA instruments in various environments - A review. Tellus, Series B: Chemical and Physical Meteorology, 60 B(3), 432-469.

Tiitta, P., Miettinen, P., Vaattovaara, P., Joutsensaari, J., Petäjä, T., Virtanen, A., Raatikainen, T., Aalto, P., Portin, H., Romakkaniemi, S., Kokkola, H., Lehtinen, K.E.J., Kulmala, M., Laaksonen, A. 2010. Roadside aerosol study using hygroscopic, organic and volatility TDMAs: Characterization and mixing state. Atmospheric Environment, 44(7), 976-986.

Ulbrich, I.M., Canagaratna, M.R., Zhang, Q., Worsnop, D.R., Jimenez, J.L. 2009. Interpretation of organic components from Positive Matrix Factorization of aerosol mass spectrometric data. Atmos. Chem. Phys., 9, 2891-2918.

Vaattovaara, P., Petäjä, T., Joutsensaari, J., Miettinen, P., Zaprudin, B., Kortelainen, A., Heijari, J., Yli-Pirilä, P., Aalto, P., Worsnop, D.R., Laaksonen, A. 2009. The evolution of nucleation- and Aitken-mode particle compositions in a boreal forest environment during clean and pollution-affected new-particle formation events. Boreal Environment Research, 14(4), 662-682.

Vaattovaara, P., Räsänen, M., Kühn, T., Joutsensaari, J., Laaksonen, A. 2005. A method for detecting the presence of organic fraction in nucleation mode sized particles. Atmospheric Chemistry and Physics, 5(12), 3277-3287.

Varutbangkul, V., Brechtel, F.J., Bahreini, R., Ng, N.L., Keywood, M.D., Kroll, J.H., Flagan, R.C., Seinfeld, J.H., Lee, A., Goldstein, A.H. 2006. Hygroscopicity of secondary organic aerosols formed by oxidation of cycloalkenes, monoterpenes, sesquiterpenes, and related compounds. Atmospheric Chemistry and Physics Discussions, 6(1), 1121-1177.

Zhang, Q., Worsnop, D.R., Canagaratna, M.R., Jimenez, J.L. 2005. Hydrocarbon-like and oxygenated organic aerosols in Pittsburgh: Insights into sources and processes of organic aerosols. Atmospheric Chemistry and Physics, 5(12), 3289-3311.

Appendix B1. Supplementary data supporting the organonitrate-driven suppression of HGF from the ATOFMS.

The ATOFMS (Aerosol Time-of-Flight Mass Spectrometry; Model 3800-100, TSI, Inc.) collects bipolar mass spectra of individual aerosol particles which are then imported into YAADA (Yet Another ATOFMS Data Analyzer) and grouped with Adaptive Resonance Theory neural network, ART-2a followed by procedure described in Dall'Osto and Harrison (2006). The ATOFMS has already proved to be a good tool to determine organonitrogen (ON) compounds (Angelino et al. 2001, Pratt et al. 2009a,b). Specifically, in the negative mass spectra, ON peaks are found at m/z -26 [CN] and m/z -42 [CNO]. Additionally, major ion peaks in the positive mass spectra at m/z 58, 59, 74, 86, and 104, 118 and 154 are all consistent with ON ATOFMS mass spectra peaks detected in previous field and laboratory studies.

During this study, the ATOFMS dataset was reduced to eight main different particle types, including sea salt, dust, organic and inorganic ones. During Case 1 and Case 2 period described in this work, four main ATOFMS particle types represented the majority of the detected single particle population: (1) EC-NIT (aged Elemental Carbon aerosol internally mixed with nitrate, average diameter by number - Av. D. about 700 nm), (2) EC-Aged (Aged Elemental carbon, Av. D. about 700 nm), (3) K-EC-NIT (Potassium, Elemental Carbon, Nitrate with Organonitrogen peaks, Av. D. 450 nm) and (4) OC-NIT-SUL (Organic Carbon, Nitrate, Sulphate with Organonitrogen peaks, Av. D. about 400 nm). The figure B1 1 shows that, whilst case 1 shows mainly ATOFMS particle types without ON compounds, the opposite scenario is seen for case 2.

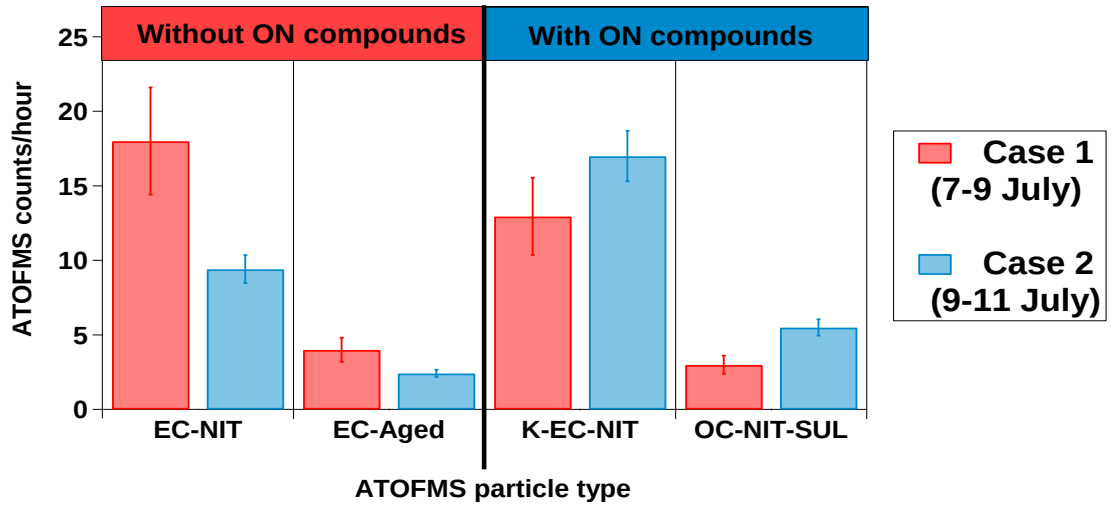

Figure B1. Four main ATOFMS particle types detected during case 1 and case 2. Please note that ATOFMS EC-NIT and ATOFMS EC-Aged (red colours) are not internally mixed with ON compounds, whereas ATOFMS K-EC-NIT and OC-NIT-SUL (blue colours) are. It is important to note the opposite trends seen for case 1 (ATOFMS red clusters) versus case 2 (ATOFMS blue clusters), supporting the ON presence in Case 2.

Primary marine organic aerosol: A dichotomy of low hygroscopicity and high CCN activity

Jurgita Ovadnevaite,[1] Darius Ceburnis,[1] Giovanni Martucci,[1] Jakub Bialek,[1] Ciaran Monahan,[1] Matteo Rinaldi,[2] Maria Cristina Facchini,[2] Harald Berresheim,[1] Douglas R. Worsnop,[3,4] and Colin O'Dowd[1]

Received 11 July 2011; revised 6 October 2011; accepted 11 October 2011; published 8 November 2011.

[1]School of Physics and Centre for Climate and Air Pollution Studies, National University of Ireland Galway, Ireland.
[2]Institute of Atmospheric Sciences and Climate,National Research Council, Bologna, Italy.
[3]Aerodyne Research, Inc., Billerica, Massachusetts, USA.
[4]Physics Department, University of Helsinki, Helsinki, Finland.

Abstract

High-time resolution measurements of primary marine organic sea-spray physico-chemical properties reveal an apparent dichotomous behaviour in terms of water uptake: specifically sea-spray aerosol enriched in organic matter possesses a low hydroscopic Growth Factor (GF∼1.25) while simultaneously having a cloud condensation nucleus/ condensation nuclei (CCN/CN) activation efficiency of between 83% at 0.25% supersaturation and 100% at 0.75%. In contrast, the activation efficiency of particles dominated by non-sea-salt (nss)-sulphate ranged between 48‐100% over supersaturation range of 0.25% ‐ 1%. Simultaneous retrieval of Cloud Droplet Number Concentration (CDNC) during primary organic aerosol plumes reveals CDNC concentrations of 350 cm^{-3} for organic mass concentrations 3‐4 μg m^{-3}. It is demonstrated that the retrieved high CDNCs under clean marine conditions can only be explained by organic sea spray and corroborates the high CCN activation efficiency associated with primary organics. It is postulated that marine hydrogels are responsible for this dichotomous behaviour.

1. Introduction

The global importance of marine aerosol particles to the CCN formation was postulated several decades ago by Charlson et al. [1987]; however, this study overlooked the existence of biogenic organic matter and cantered on the marine sulphur cycle. Later studies by O'Dowd et al. [2004] demonstrated a significant, if not dominant organic mass fraction in submicron marine aerosol, while the most recent study by Ovadnevaite et al. [2011] reported primary spray plumes enriched in organic matter with mass loadings up to 3‐4 μg m^{-3} (i.e., far greater than sulphate mass concentrations in clean marine air). Organic mass loadings of this magnitude, occurring in CCN sizes, suggest that the organic matter may contribute notably to

the CCN population. In addition, satellite observations [Meskhidze and Nenes, 2006; Sorooshian et al., 2009] indicated concurrent increases in CCN activity and/or cloud droplet concentrations in marine stratocumulus overlying chlorophyll-rich regions, pointing a possible link between organic marine aerosol and cloud droplet activation; however, it has been more difficult to determine whether this link is through secondary organic aerosol or primary (sea-spray) organic aerosol. The picture is somewhat complicated in that spray produced from biologically rich water is expected to be water insoluble [Facchini et al., 2008; Vesna et al., 2008], while that produced from secondary processes is expected to be more oxygenated and hence water soluble. Further, several recent laboratory studies [Fuentes et al., 2011; Irwin et al., 2010; Prisle et al., 2010] show a reduction of CCN activity due to hydrophobic properties of biogenic organics. Here we present comprehensive real time ambient measurements of aerosol CCN activation, hygroscopicity, chemical composition and size distributions which reveal the important role of primary marine organics in CCN activation.

2. Experiment

Continuous marine aerosol physico-chemical measurements were undertaken at the Mace Head atmospheric research station (54°19′ N, 9°54′ W), located on the west coast of Ireland [O'Connor et al., 2008]. Aerosol measurements were performed by sampling ambient particles through a community air-sampling duct 10 m above ground level. The size resolved non-refractory chemical composition of submicron aerosol particles is measured with an Aerodyne High Resolution Time of Flight Aerosol Mass Spectrometer deployed in standard mode [DeCarlo et al., 2006]. Aerosol size distributions were measured by a TSI scanning mobility particle sizer (SMPS) and a relative humidity of 40%. CCN concentrations were determined by a Droplet Measurements Technology CCN counter [Lance et al., 2006] operated at supersaturations of 0.25%, 0.5%, 0.75% and 1%. Aerosol GFs were measured using a Hygroscopic Tandem Differential Mobility Analyzer (HTDMA) and follows the EUSAAR standard installation and accuracy. GFs at 90% RH were determined for dry size particles of 35, 50, 75, 110 and 165 nm. Clean marine air is only considered in this analysis and previously described in many studies [e.g., O'Dowd et al., 2004].

3. Results

Two distinct seasons were selected from the long-term aerosol composition, size and hygroscopicity measurements to cover both primary sea-spray and secondary (sulphate dominated) aerosol production episodes. The selected periods include spray events with significant primary organic matter enrichment, typically occurring in the late summer, and secondary (predominantly sulphate) aerosol formation periods, prevalent in late spring, early summer. The dataset spanned from 11th – 28th August 2009, 14th July – 12th August 2010, and 2nd – 27th May 2009, within which the aerosol was categorized according to the AMS analysis.

CCN activation efficiency as a function of particle hygroscopicity, composition and size is presented in Figure 1 for all periods. The colour scale in Figure 1a represents the fraction of organic mass to total particle mass, while in Figure 1b, it represents the fraction of sulphate mass to total mass. The size of the circle represents weighted average particle size of the whole aerosol population for the averaging period (that is a 1-hour integration period). For example, for a bimodal size distribution with a mode at

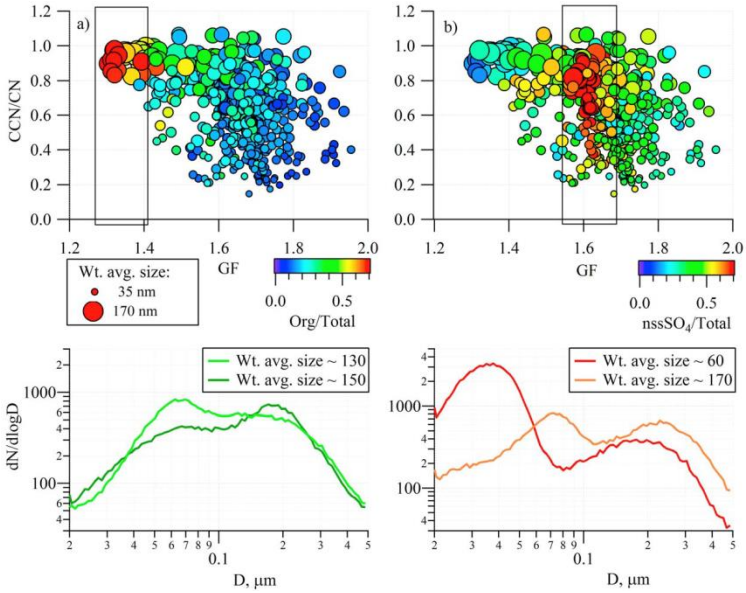

Figure 1. (a and b) CCN0.75% activity (CCN/CN) as a function of GF (at 90% RH), chemical composition (colour scale) and weighted average particle size (size of the circle). CN is the total particle number above 20 nm in diameter; the colour scale represents the dominance of a given chemical species. Measurement periods: 02nd – 27th May 2009, 11th – 28th August 2009 and 14th July – 12th August 2010. Note, the measurement periods cover periods much longer than individual plume events. In Figure 1a, the boxed region highlights particles dominated by primary organic matter while Figure 1b highlights the particles dominated by sulphate. Particles to the extreme right of both figures are dominated by sea-salt mass. (c) Two organic-dominated size distributions (on 00:00 UTC - 22:00 UTC 16th August 2009 and 13:30 UTC - 16:30 UTC 05th August 2010) and their resultant weighted diameters and (d) the same for sulphate-dominated distributions (on 21:00 UTC - 22:00 UTC 02nd August 2010 and 06:00 UTC - 10:00 UTC 09th August 2010).

65 nm and 200 nm, both with equal number concentrations, would have a weighted average particle size of 132 nm. Examples of actual organic and sulphate dominated size distributions, and their resultant weighted diameter are also shown in Figures 1c and 1d, respectively.

Aerosol dominated by organics possessed a low GF of 1.25 or less, as emphasized by the boxed area in Figure 1a, while sulphate dominance led to a GF∼1.65, as emphasized by the boxed area in Figure 1b. The points to the extreme right of each boxed area represent sea-salt dominated particles with the highest GF of >1.8. CCN activation was dependant on aerosol chemical composition, but did not follow typical hygroscopicity dependence pattern – that is, particles with the lowest GF were more readily activated than particles with the highest GF. As a result, particles clustered in the upper left corner in the graph (Figure 1), represent high organic enrichment, low GF, and high CCN activation. These particles also posses the largest mean weighted size. By contrast, particles with high sulphate or sea salt mass fractions posses a higher GF but greater ranges of mean weighted size and CCN activation efficiency. The periods during which primary marine organic matter dominated particles were associated with maritime air masses arriving from the regions of high biological activity and elevated wind speeds over the N.E. Atlantic and extended up to 30 hours in duration [Ovadnevaite et al., 2011] with organic mass concentrations approaching ∼4 µg m $^{-3}$.

The data reveal a pattern of high average weighted diameter, low solubility and high CCN activation for particles with high organic mass fraction and a broad

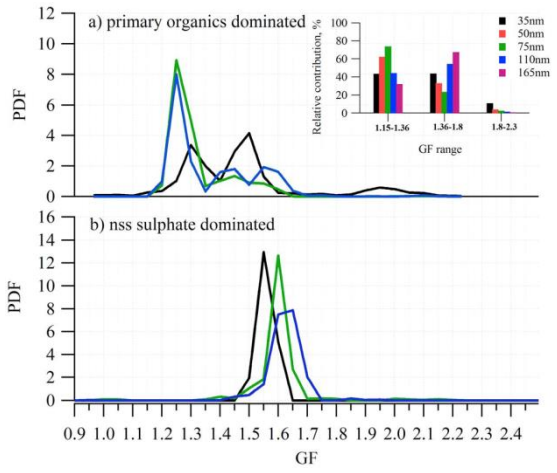

Figure 2. (a) Hygroscopic growth dependence on the particle size represented as probability density functions and average growth factor for one typical primary organic plume event on 00:00 UTC-22:00 UTC 16th August 2009 and (b) GF-PDF for typical sulphate dominated aerosol on 21:00 UTC-22:00 UTC 02nd August 2010.

range of weighted diameters, high solubility and diverse CCN activity for high inorganic mass fraction. The Probability Distribution Function (PDF) of growth factors (Figure 2) revealed an external mixture of different particle populations determined by three distinct GF modes during typical organic plume event. A less-hygroscopic mode (GF peak at 1.25) was very prominent and evident across all sizes and always contributed to at least 51% of the total particle number. However, the largest contribution to the 1.25 GF peak was from 75 nm particles (up to 75%) indicating the maximum hydrophobic organic-matter enrichment factor for that size range. A more-hygroscopic mode (GF between 1.36 and 1.8) was less prominent and subject to greater variability between particle sizes, although it contributed more to the smallest and largest measured particles (35 and 165 nm accordingly) rather than mid-sized particles. Finally, a relatively-pure sea salt mode (GF between 1.8 and 2.3) was evident (although only contributing to 10% concentration) in the smallest measured dry size (35 nm) particles. The GF-PDF for a sulphate dominated aerosol is also shown for comparison. The CCN activation efficiency for the organic dominated and sulphate dominated populations (as classified by the AMS) was examined as a function of supersaturation in Figure 3. For organic dominated particles, the activation efficiency ranged from 83% at 0.25% supersaturation to 100% at 1% supersaturation. Given that the less hygroscopic mode always contained at least 51% of the total particle number, a large fraction of particles with GF=1.25, the majority of which were ≤75 nm, must have been activated at 0.25% supersaturation. In contrast, particles dominated by sulphate mass exhibited a lower activation efficiency at 0.25% (48% activation for sulphate).

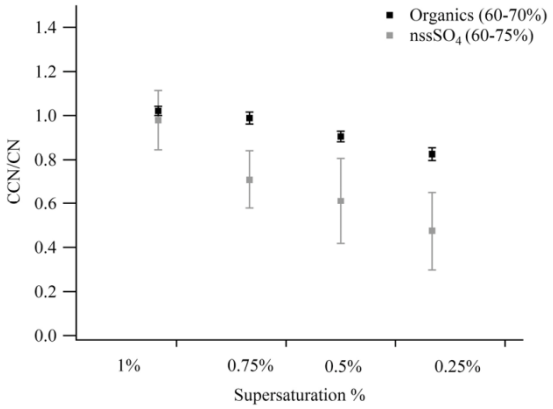

Figure 3. CCN/CN activity versus supersaturation for particles of different percentage mass composition (dominant mass percentage highlighted in brackets in figure key). Bars represent standard deviations.

Stratocumulus microphysical properties are presented for one of the primary organic plume events (4^{th}–5^{th} August 2010). CDNC derived from ground-based remote sensing measurements [Martucci and O'Dowd, 2011] ranged from 100 to 350 cm^{-3} (Figure 4). Taking the weighted average diameter from the SMPS size distribution and the AMS-derived nss sulphate and sea-spray mass concentrations, assuming both sulphate and sea-spray have the same weighted

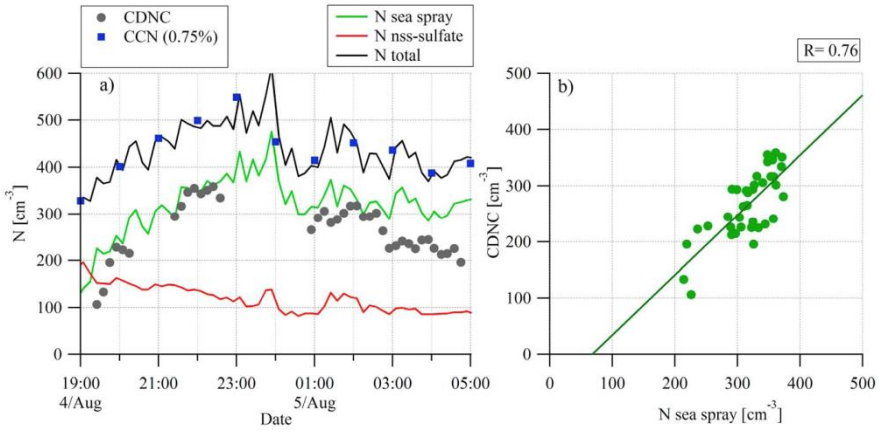

Figure 4. (a) CDNC, measured $CCN_{0.75\%}$, calculated sea-spray, sulphate and total nuclei concentration. (b) CDNC as a function of sea-spray particle concentration.

diameter but are externally mixed (where sea- spray is an internal mix of sea salt and organics), the number of nss sulphate and sea-spray potential cloud nuclei was calculated. Assumed densities were 1.4 g cm^{-3} for organics, 2.17 g cm^{-3} for sea salt, 1.83 g cm^{-3} for sulphuric acid and 1.77 g cm^{-3} for ammonium sulphate. The validity of these assumptions is reflected in the derived nuclei concentration being within 10% of the total aerosol concentration for D > 20 nm. The calculated total nuclei concentration corresponded, almost exactly, to the CCN concentration at 0.75% supersaturation. Sulphate nuclei concentration initially was of the order of 200 cm^{-3} but then fell off to ~100 cm^{-3} where it remained relatively constant. Sea-spray nuclei peaked at 450 cm^{-3}, although there was no overlapping CDNC data for these peak concentrations. For overlapping CDNC, both CDNC and sea-spray peaked at ~350 cm^{-3}, and both the absolute spray concentration and its trend matched that of CDNC with a correlation co-efficient of r = 0.76. Nss sulphate concentrations were insufficient to account for the CDNC while the latter can be almost completely accounted for by the sea-spray concentration.

4. Discussion

These results show a dichotomous behaviour for primary marine organic aerosol: that is a low hygroscopic GF but high CCN activation efficiency. Such behaviour is determined not only by particle size effects [Dusek et al., 2006], but also by chemical composition influences. Low hygroscopicity in sea-spray aerosol is determined by the specific chemical composition of organic matter transferred from the ocean surface during sea-spray production and comprising a broad spectrum of biopolymers including polysaccharides, proteins, nucleic acids, lipids and so called exopolymer substances [Facchini et al., 2008; Verdugo and Santschi, 2010]. The dichotomous behaviour may have one of a number of explanations, e.g., limited water solubility in all but the most dilute solutions and surface active properties of sea-spray organics is one possibility [Charlson et al., 2001; Facchini et al., 2008; Mircea et al., 2005; Moore et al., 2008].

Surface activity plays an important role in the Köhler equation which consists of two terms, the Raoult term and the Kelvin term - the former being more important for sub-saturated conditions, and the latter being more important for supersaturated

conditions [Irwin et al., 2010]. The balance between the two terms determines the resulting critical supersaturation needed for the particle activation. When surface tension counteracts water activity, the net effect is an enhancement of particle CCN activity. Fuentes et al. [2011] and Irwin et al. [2010] argued that a moderate reduction in surface tension at activation produced by marine organics is too low to compensate the impact on the Raoult term, but this concept also led to a disagreement between measured and modelled CCN activity when applied to the ambient environment [Irwin et al., 2010]. Moreover, surface tension measurements of aerosols containing organic matter have been limited to mainly water soluble organics. Such surface tension lowering, however, inadequately represents insoluble organics and/or colloidal material. A recent study by Ekstrom et al. [2010] indicated a much higher degree of surface tension suppression by marine organics compared to what was previously considered.

Alternatively, adsorption of water on wettable surfaces can dominate over hygroscopic uptake, leading to adsorption theory replacing Kholer Theory [Kumar et al., 2011]; however, the lack of experimental data on water vapour adsorption on wettable organic surfaces prevents a quantitative evaluation in this study. Nonetheless, the GF and activation efficiency for the organic plumes here are consistent with the activation of ~75 nm low-soluble particles at supersaturations of the order of 0.2–0.3% [Kumar et al., 2011].

The organic compounds transferred in sea-spray are potentially the same as those involved in the formation of marine gels in seawater [Chin et al., 1998; Engel et al., 2004]. The gel-forming properties of marine biopolymers may also play a role in the observed dichotomous behaviour of organics rich sea-spray particles, assuming that a three dimensional structure, similar to that of marine hydrogels, is present in these particles. At sub-saturated conditions the three-dimensional structure of the gel in sea-spray particles is expected to be more condensed and to behave like a water insoluble core, while during the particle activation the gel-like structure may be partially solubilized as an equilibrium between the gel and the truly dissolved phase is established at the higher dilution typical of this regime, as observed in sea water [Chin et al., 1998; Orellana et al., 2007]. This, together with the observed surface active properties of sea- spray organics, can contribute to reduce the particle critical supersaturation [Charlson et al., 2001; Mircea et al., 2005]. Moreover, the strong affinity of amphiphilic residues for the air-water interface, associated with rising bubbles leading to spray production, could result in surface partitioning of organic moieties which can cause a specific molecular arrangement within the gel network, with hydrophilic groups preferentially in the aerosol core and the hydrophobic groups oriented toward the air medium. A physical model describing the forces causing this specific arrangement, although simplistic with respect to the complex three-dimensional configuration of marine hydrogels, was introduced by [Ellison et al., 1999] in terms of an inverted micelle model and single particle mass spectrometry measurements lend credence to such a model [Tervahattu et al., 2002]. This specific arrangement of organic molecules as hydrogels and pseudo-inverted micelles would explain the observed CCN behaviour of primary marine aerosol and its low hygroscopicity. Additionally, such a model would allow water processing, even though the particle would have a hydrophobic surface concomitant with significant lowering of surface tension [Chakraborty and Zachariah, 2007;

Ekstrom et al., 2010; Facchini et al., 2008].

If, as assumed, marine hydrogels are transferred into the aerosol particles through bubble bursting, their peculiar physico-chemical properties may not only influence the properties of the sea-spray aerosol, but it would also affect the residual spray particle dry size. For instance, the gel network could reduce the water evaporation of spray drops, and along with the displacement of sea salt solution by larger organic molecules, could lead to a net increase in "dry" sea-spray particle size. Nonetheless, size cannot be the main factor determining activation efficiency since for some of these events, the Aitken mode dominated particle concentration over and above the accumulation mode. Given that CCN/CN activation ratio ranged from 83–100% over the 0.25–1% supersaturation range, the majority of the dominant, and organically-enriched Aitken mode (~70 nm) would have had to be activated, emphasizing the fact that chemical composition, and particularly, organic matter enrichment, particularly in the smallest potential nuclei sizes are important in the droplet activation process.

5. Conclusions

This study highlights the importance of primary marine organic aerosol to the marine CCN population. Despite being predominately hydrophobic in nature (GF~1.25), primary organic marine particles have effectively higher activation efficiency than more soluble inorganic aerosol. Sea-spray aerosol enriched in primary organic matter possessed CCN activation efficiency of between 83% (at 0.25% supersaturation) and 100% (at 0.75% and 1% supersaturation). In contrast, particles dominated by non-sea-salt (nss) sulphate ranged between 48–100% over the same supersaturation range. The CCN activity of sea-spray enriched in organic matter is corroborated by simultaneous measurements of very high CDNCs (N~350 cm−3) and where a correlation coefficient of 0.76 was calculated between CDNC and inferred sea- spray CCN concentrations. The vast majority of the CDNC could only be explained by activation of sea-spray aerosol enriched in organic matter. We suggest that this phenomenon relates to the enrichment of marine hydrogels in sea-spray aerosol.

Acknowledgments.

This work was supported by the Science Foundation Ireland (grant 08/RFP/GEO1233), HEA-PRTLI4 Environment and Climate Change: Impact and Responses programme, European Commission FP7 EUCAARI, and EPA Ireland.

The Editor thanks two anonymous reviewers for their assistance in evaluating this paper.

References

Chakraborty, P., and M. R. Zachariah (2007), "Effective" negative surface tension: A property of coated nanoaerosols relevant to the atmosphere, J. Phys. Chem. A, 111(25), 5459–5464, doi:10.1021/jp070226p.

Charlson, R. J., J. E. Lovelock, M. O. Andreae, and S. G. Warren (1987), Oceanic phytoplankton, atmospheric sulphur, cloud albedo and climate,Nature, 326(6114), 655–661, doi:10.1038/326655a0.

Charlson, R. J., J. H. Seinfeld, A. Nenes, M. Kulmala, A. Laaksonen, and M. C. Facchini (2001), Atmospheric science—Reshaping the theory of cloud formation,

Science, 292(5524), 2025–2026, doi:10.1126/science.1060096

Chin, W. C., M. V. Orellana, and P. Verdugo (1998), Spontaneous assemblyof marine dissolved organic matter into polymer gels, Nature, 391(6667), 568–572, doi:10.1038/35345.

DeCarlo, P. F., et al. (2006), Field-deployable, high-resolution, time-of-flight aerosol mass spectrometer, Anal. Chem., 78(24), 8281–8289, doi:10.1021/ac061249n.

Dusek, U., et al. (2006), Size matters more than chemistry for cloud-nucleating ability of aerosol particles, Science, 312(5778),1375–1378, doi:10.1126/science.1125261.

Ekstrom, S., B. Noziere, M. Hultberg, T. Alsberg, J. Magner, E. D. Nilsson, and P. Artaxo (2010), A possible role of ground-based microorganismson cloud formation in the atmosphere, Biogeosciences, 7(1), 387–394, doi:10.5194/bg-7-387-2010.

Ellison, G. B., A. F. Tuck, and V. Vaida (1999), Atmospheric processing of organic aer osols, J. Geo phys. R e s. , 104 (D9), 1 1 , 633 –11,6 41, doi:10.1029/1999JD900073.

Engel, A., S. Thoms, U. Riebesell, E. Rochelle-Newall, and I. Zondervan (2004), Polysaccharide aggregation as a potential sink of marine dissolved organic carbon, Nature, 428(6986), 929–932, doi:10.1038/ nature02453.

Facchini, M. C., et al. (2008), Primary submicron marine aerosol dominated by insoluble organic colloids and aggregates, Geophys. Res. Lett.,35(17), L17814, doi:10.1029/2008GL034210.

Fuentes, E., H. Coe, D. Green, and G. McFiggans (2011), On the impacts of phytoplankton-derived organic matter on the properties of the primary marine aerosol—Part 2: Composition, hygroscopicity and cloud condensation activity, Atmos. Chem. Phys., 11(6), 2585–2602, doi:10.5194/acp-11-2585-2011.

Irwin, M., N. Good, J. Crosier, T. W. Choularton, and G. McFiggans(2010), Reconciliation of measurements of hygroscopic growth and critical supersaturation of aerosol particles in central Germany, Atmos. Chem. Phys., 10(23), 11,737–11,752, doi:10.5194/acp-10-11737-2010.

Kumar, P., I. N. Sokolik, and A. Nenes (2011), Measurements of cloud condensation nuclei activity and droplet activation kinetics of fresh unprocessed regional dust samples and minerals, Atmos. Chem. Phys., 11(7), 3527–3541, doi:10.5194/acp-11-3527-2011.

Lance, S., J. Medina, J. N. Smith, and A. Nenes (2006), Mapping the operation of the DMT continuous flow CCN counter, Aerosol Sci. Technol., 40(4), 242–254, doi:10.1080/02786820500543290.

Martucci, G., and C. D. O'Dowd (2011), Ground-based retrieval of continental and marine warm cloud microphysics, Atmos. Meas. Tech. Discuss., 4(4), 4825–4865, doi:10.5194/amtd-4-4825-2011.

Meskhidze, N., and A. Nenes (2006), Phytoplankton and cloudiness in the Southern Ocean, Science, 314(5804), 1419–1423, doi:10.1126/science.1131779.

Mircea, M., et al. (2005), Importance of the organic aerosol fraction for modeling aerosol hygroscopic growth and activation: A case study in the Amazon Basin, Atmos. Chem. Phys., 5, 3111–3126, doi:10.5194/acp-5-3111-2005.

Moore, R. H., E. D. Ingall, A. Sorooshian,

and A. Nenes (2008), Molar mass, surface tension, and droplet growth kinetics of marine organics from measurements of CCN activity, Geophys. Res. Lett., 35, L07801,doi:10.1029/2008GL033350.

O'Connor, T. C., S. G. Jennings, and C. D. O'Dowd (2008), Highlights of fifty years of atmospheric aerosol research at Mace Head, Atmos. Res., 90(2–4), 338–355, doi:10.1016/j.atmosres.2008.08.014.

O'Dowd, C. D., M. C. Facchini, F. Cavalli, D. Ceburnis, M. Mircea, S. Decesari, S. Fuzzi, Y. J. Yoon, and J. P. Putaud (2004), Biogenically driven organic contribution to marine aerosol, Nature, 431(7009), 676–680, doi:10.1038/nature02959.

Orellana, M. V., T. W. Petersen, A. H. Diercks, S. Donohoe, P. Verdugo, and G. van den Engh (2007), Marine microgels: Optical and proteornic finger p rints, Mar. Ch em. , 10 5 (3 –4) , 22 9 –239, doi:10.1016/j.marchem.2007.02.002.

Ovadnevaite, J., C. O'Dowd, M. Dall'Osto, D. Ceburnis, D. R. Worsnop, and H. Berresheim (2011), Detecting high contributions of primary organic matter to marine aerosol: A case study, Geophys. Res. Lett., 38, L02807, doi:10.1029/2010GL046083.

Prisle, N. L., T. Raatikainen, A. Laaksonen, and M. Bilde (2010), Surfactants in cloud droplet activation: Mixed organic-inorganic particles, Atmos. Chem. Phys., 10(12), 5663–5683, doi:10.5194/acp-10-5663-2010.

Sorooshian, A., et al. (2009), On the link between ocean biota emissions, aerosol, and maritime clouds: Airborne, ground, and satellite measurements off the coast of California, Global Biogeochem. Cycles, 23, GB4007, doi:10.1029/2009GB003464.

Tervahattu, H., K. Hartonen, V.-M. Kerminen, K. Kupiainen, P. Aarnio, T. Koskentalo, A. F. Tuck, and V. Vaida (2002), New evidence of an organic layer on marine aerosols, J. Geophys. Res., 107(D7),4053, doi:10.1029/2000JD000282.

Verdugo, P., and P. H. Santschi (2010), Polymer dynamics of DOC networks and gel formation in seawater, Deep Sea Res., Part II, 57(16),1486–1493, doi:10.1016/j.dsr2.2010.03.002.

Vesna, O., S. Sjogren, E. Weingartner, V. Samburova, M. Kalberer, H. W. Gaggeler, and M. Ammann (2008), Changes of fatty acid aerosol hygroscopicity induced by ozonolysis under humid conditions, Atmos. Chem. Phys., 8(16),4683–4690, doi:10.5194/acp-8-4683-2008.

The Eyjafjallajökull ash plume - Part I: Physical, chemical and optical characteristics

*Colin O'Dowd [a, *], Darius Ceburnis [a], Jurgita Ovadnevaite [a], Giovanni Martucci [a], Jakub Bialek [a], Ciaran Monahan [a], Harald Berresheim [a], Aditya Vaishya [a], Tomas Grigas [a], S. Gerard Jennings [a], Philip McVeigh [a], Saji Varghese [a], Robert Flanagan [a], Damien Martin [a], Eoin Moran [b], Keith Lambkin [b], Tido Semmler [b], Cinzia Perrino [c], Ray McGrath [b]*

[a] School of Physics & Centre for Climate and Air Pollution Studies, Ryan Institute, National University of Ireland Galway, University Road, Galway, Ireland
[b] Met Éireann, Glasnevin, Glasnevin Hill, Dublin 9, Ireland
[c] Institute for Atmospheric Pollution, National Research Council, I-00015 Montelibretti, Rome, Italy

The Eyjafjallajökull ash plume was detected at the Mace Head Atmospheric Research Station numerous times from April 19th till 18th May 2010 following subsidence into, and dilution in, the boundary layer. The three strongest of these events, lasting 12-18 h, are analysed in detail in terms of physical, chemical and optical properties. The ash size distribution was bimodal with a super-micron mode of 2.5 μm diameter for the one case where it was measured. The submicron mode varied from 185 nm during the high-explosive phase to 395 nm during the low-explosive phase. Non-sea-salt (nss)-sulphate mass was 2.5 times higher during the low-explosive phase. Total particle concentrations ranged from 760 cm^{-3} to 1247 cm^{-3} and were typical of clean air in the region. Between 30% and 39% of the submicron chemical mass (i.e. exclusive of water content) was ash primarily composed of silicon dioxide while accounting for the water content, the submicron aerosol was composed of primary ash (15%), nss-sulphate (25%) and water (55%). Hygroscopic growth factors were characteristic of sulphate aerosol but revealed an internally mixed aerosol pointing to a mix of predominantly primary ash, nss-sulphate and water. For the majority of the ash plumes, all condensation nuclei (CN, diameter > 10 nm) were activated into cloud condensation nuclei (CCN) at a supersaturation of 0.25%. Aerosol absorption increased by about a factor of two in the plume, compared to background levels, while aerosol scattering coefficients increased by an order of magnitude.

1. Introduction

The Eyjafjallajökull volcano erupted explosively on the 14th April 2010, ejecting an ash plume in the atmosphere at levels between 4 km and 9 km a.m.s.l.. While the Eyjafjallajökull eruption was moderate and regarded as a mid-sized eruption (Pyle, 1999; Davies et al., 2010), it had a severe impact on aviation over Europe. The eruption occurred under north-north-westerly air flow, relative to continental Europe and under conditions of minimal precipitation resulting in rapid dispersion of the ash cloud over Central Europe, Ireland and Britain. Based on plume mass estimates from the European Volcanic Ash Advisory Centers, the European aviation authorities decided to close European airspace, impacting air traffic to 23 European countries amounting to a 75% closure of the European aerodrome network. The net effect was that more than 100,000 flights were cancelled, affecting 10 million passenger journeys between the 14th April and 20th April. Further incursions of the ash cloud over Western Europe caused additional airspace closures, sporadically, until the 18th May 2010, leading to the cancelling of about 7000 further flights. Decisions on fly or no-fly centered around an ash mass concentration of 2-4 mg m^{-3}, although no robust in-plume measurements of mass concentrations were achieved in practice. Perhaps the closest plume encounters were achieved by the DLR Falcon aircraft where plume mass concentrations of 1mg m^{-3} were briefly achieved (Schumann et al., 2011). The unexpected eruption and impact revealed several deficits in Europe's capabilities in terms of accurately detecting and predicting the ash plume mass density, thickness and vertical distribution (particularly in terms of layering effects) in near real-time. This study presents an analysis of the physico-chemical properties of volcanic plume aerosol detected at the Mace Head Supersite on the west coast of Ireland during the period from the 19th April to the 18th May 2010 and builds on recent work characterizing the properties of aerosols associated with passive Icelandic volcano emissions (Ovadnevaite et al., 2009). In particular, the relative contributions of primary ash to sulphate, the water fraction, the state of mixing, and the water uptake and cloud condensation nuclei properties are probed in detail. An overview of the eruption storeyline and emission flux is provided in this special issue by Langmann et al. (2012).

2. Experimental

Ground based in-situ and remote sensing measurements of the plume characteristics were conducted at the Mace Head Atmospheric Research Station. The Mace Head Atmospheric Research Station is located in Connemara, County Galway on the Atlantic Ocean coastline of Ireland at 53°19'30''N, 9°54'14''W and offers a clean sector from 190° through west to 300°. Meteorological records show that on average, over 60% of the air masses arrive at the station in the clean sector (Jennings et al., 2003; O'Connor et al., 2008). Air is sampled at 10 m height from a main air inlet positioned at 80-120 m from coastline (depending on tide) (http://www.macehead.org).

A Jenoptik CHM15k ceilometer was used to detect the vertical distribution of the ash plume. The ceilometer measures atmospheric target backscatter profiles over the nominal range 30m-15km with first overlap height at around 30m (full overlap at 1500m). The measuring principle is LIDAR-based with photon counting recording system and solid-state Nd:YAG laser source emitting at the 1064 nm wavelength. The operating range is 15 km where it can reliably detect lower

Table 1
Aerosol physical, chemical and optical properties associated with the three strongest plumes detected at Mace Head.

		Case		
		1	2	3
		08:05–12:35 UTC 20/04/2010	17:25 UTC 4/05/2010–02:05 UTC 5/05/2010	17:15–22:25 UTC 17/05/2010
SO_4, μg m^{-3}		2.1 ± 0.2	7.8 ± 0.3	7.2 ± 0.8
NH_4, μg m^{-3}		0.2 ± 0.04	0.18 ± 0.07	0.22 ± 0.06
NO_3, μg m^{-3}		0.04 ± 0.006	0.03 ± 0.005	0.07 ± 0.02
Org, μg m^{-3}		0.2 ± 0.05	0.45 ± 0.09	0.6 ± 0.1
PM2.5 (TEOM), μg m^{-3}		9.1 ± 1.3	10.4 ± 0.9	14.6 ± 1
PM2.5 (SMPS + APS), μg/m^3		–	–	37.7 ± 0.6 16.9 (no water[a])
PM10 (SMPS + APS), μg/m^3		–	–	46.9 ± 0.6 21.1 (no water[a])
Accumulation mode diameter, nm		185 ± 4	380 ± 2	390 ± 4
CN (CPC3010), 1 cm^{-3}		1247 ± 472	762 ± 111	993 ± 295
CN (SMPS), 1 cm^{-3}		732 ± 90	957 ± 213	1070 ± 196
CCN				
SS 0.25%	Nccn, 1 cm^{-3}	424 ± 38	684 ± 62	804 ± 88
	CCN/CNcpc	0.34	0.9	0.81
	CCN/CNsmps	0.58	0.71	0.75
SS 0.5%	Nccn, 1 cm^{-3}	496 ± 45	781 ± 64	896 ± 92
	CCN/CNcpc	0.4	1	0.9
	CCN/CNsmps	0.68	0.82	0.84
SS 0.75%	Nccn, 1 cm^{-3}	622 ± 63	852 ± 80	912 ± 109
	CCN/CNcpc	0.5	1.12	0.92
	CCN/CNsmps	0.85	0.89	0.85
Absorption, Mm^{-1}		0.36 ± 0.1	0.29 ± 0.08	0.38 ± 0.07
Scattering, Mm^{-1}				
450 nm		17.1 ± 0.5	85 ± 6	122 ± 10
550 nm		14.4 ± 0.3	61 ± 5	96 ± 7
700 nm		9.4 ± 0.2	28 ± 3	50 ± 3
Growth factor				
75 nm		1.58 ± 0.05	1.44 ± 0.14	1.58 ± 0.05
165 nm		1.7 ± 0.006	1.64 ± 0.03	1.65 ± 0.03

[a] Excluding particle bound water.

cloud layers as well as cirrus clouds. The highest vertical resolution is 15 m at which it can detect full vertical profiles of aerosol backscatter and cloud height, boundary layer height and visibility. The ceilometer is calibrated using a multi-wavelength sun photometer measuring the optical depth of the atmosphere above the ceilometer. Once the calibration is performed the signal is inverted using the Klett algorithm (Klett, 1981) assuming a LIDAR ratio of S=42 sr for λ=1064nm (Ackermann,1998). The backscatter coefficient is then determined and used to calculate the extinction coefficient through the assumed LIDAR ratio.

Aerosol absorption was measured using a Multi-Angle Absorption Photometer (MAAP). Cloud condensation nuclei (CCN) concentration was determined using a Droplet Measurements Technology CCN counter (Lance et al., 2006) operated at supersaturations of 0.25%, 0.5% and 0.75%.

On-line aerosol analyzers sampled from a 10 m height 10 cm diameter laminar flow community duct with a 50% size cut at 3.5 μm at 10 m s^{-1} (Kleefeld et al., 2002). Total particle concentrations at sizes larger than 3 and 10 nm diameter were sampled using a Thermo Systems Inc. (TSI) Condensation Particle Counter (CPC) 3025a and 3010, respectively. Size distributions were sampled using a TSI nano-Scanning Mobility Particle Sizer (SMPS) between 3 and 20 nm, scanning every 30 s, and a standard SMPS operating 10-min size distribution scans between 20 and 500 nm (Wang and Flagan, 1990).

Aerosol scattering coefficient measurements were performed by a TSI 3563 3-wavelength integrating nephelometer (Bodhaine et al., 1991). Supermicron particles were measured using a TSI Aerodynamic Particle Sizer (APS) 3321 which had 51 channel of equal logarithmic width of 0.031 within the size range of 0.54-20.0 μm. The APS was installed on May 16th, therefore, only data for the latest major plume (17th May) was available.

Hygroscopic properties of aerosol were measured using a Hygroscopic Tandem Differential Mobility Analyzer (H-TDMA), as described by Nilsson et al. (2009) and references therein. The determination of particles growth factor

(GF) is done by comparison of sizes of particles in their dry (RH ¼ 40%) and humidified state (RH ¼ 90%). An inversion algorithm is used to retrieve the GF-Probability Density Function (PDF) (Gysel et al., 2009). GFs were measured for 35, 50, 75, 110, 165 nm particle sizes.

The size resolved non-refractory chemical composition of ambient submicron aerosol particles was measured with an Aerodyne High-Resolution Time-of-Flight Aerosol Mass Spectrometer (HR-ToF-AMS). The HR-ToF-AMS focuses aerosol particles in the size range 50-600 nm quantitatively onto a hot surface (~600 ^{o}C) using an aerodynamic lens assembly (Jayne et al., 2000). The HR- ToF-AMS was deployed in the standard configuration (DeCarlo et al., 2006), taking both mass spectrum (MS) and particle time-of-flight (pToF) data. HR-ToF-AMS was routinely calibrated according to the methods described by Jimenez et al. (2003) and Allan et al. (2003).

Samples for physical and morphological investigation of volcanic ash were analyzed using SEM (Scanning Electron Microscope) with EDX (Energy Dispersive X-ray) chemical analysis method. Samples were taken during two events (19the20th April and 17the18th May) and were collected on Whatman cellulose filters. Six 2-h samples were analyzed during the April period and five 2-h samples were analyzed during the May period. The samples were placed on studs covered with conductive carbon tape and coated with gold for 3 min. All six samples were stored in clean containers to minimize contamination before or during analysis.

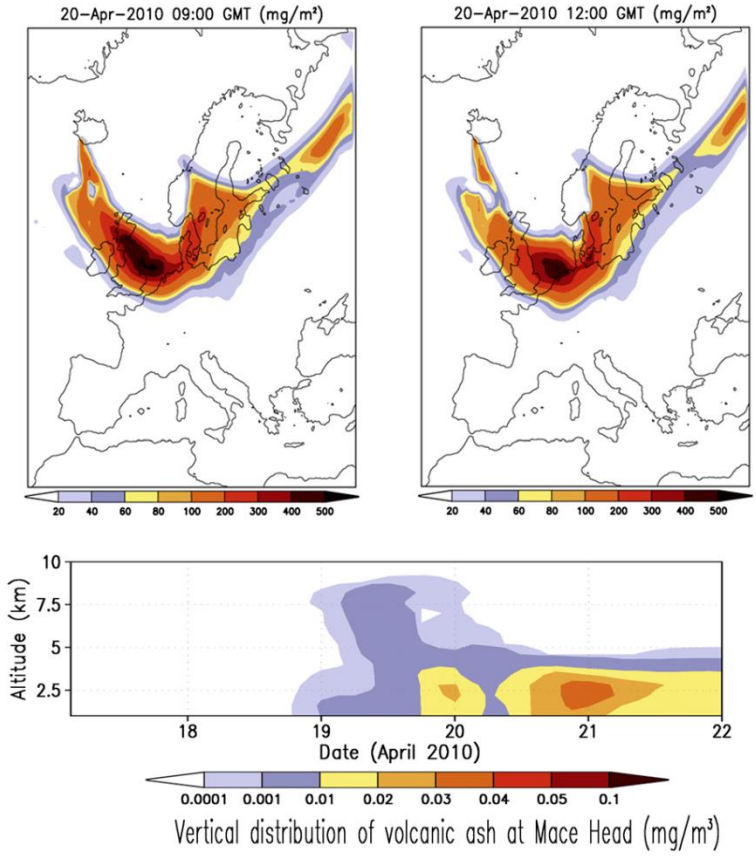

Fig. 1. (Top Left and Right) Spatial distribution of ash plume integrated column mass. (Bottom) Vertical distribution of ash plume volumetric mass concentration. Hindcasting is from the REMOTE model for 20th April 2010.

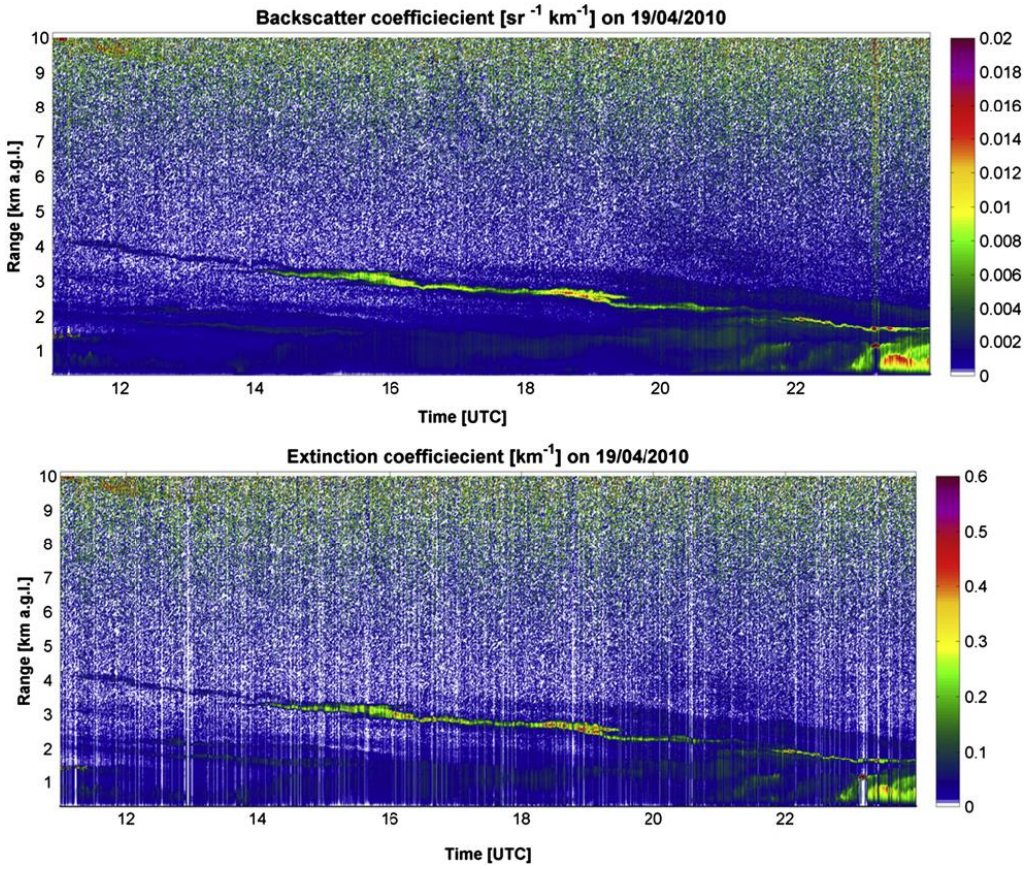

Fig. 2. Temporal evolution of volcanic plume backscatter coefficient (top) and extinction (bottom) over Mace Head on the 19th April. Data derived from the Jenoptik ceilometer.

Bulk off-line chemical analysis was conducted by the X-ray fluorescence method (XRF) designed to measure elemental composition of aerosol particles irrespective of their chemical make-up. The following elements were analyzed: Al, Ca, Cl, Cu, Cr, Fe, K, Mg, Mn, Na, Ni, Pb, Si, S, Ti, V, Zn. The analysis was done for six PM2.5 samples and four PM2.5e10 samples. PM2.5 and PM2.5e10 data from the May 17th are used in this study to reconstruct mass size distribution while other data will be published in a companion paper. In order to calculate ash content and nss-sulphate it was assumed that most of the elements were present in their main oxide forms, sulphuric was

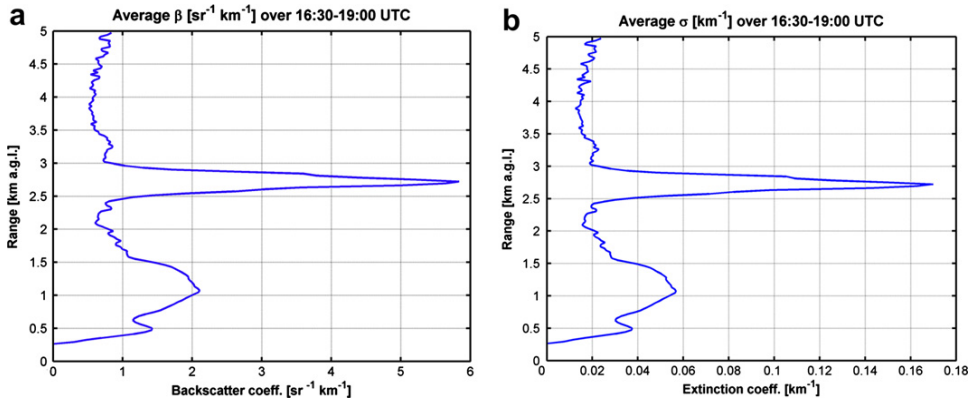

Fig. 3. (a) Vertical profile of backscatter coefficient on 19th April 2010. (b) Vertical profile of extinction coefficient on 19th April 2010.

present in the form of sulphate while sea salt was calculated as 3.2 x Na.

The 3-dimensional regional climate model, REMOTE (Langmann et al., 2008;

Varghese et al., 2011) was used to model volcanic ash dispersion from the Eyjafjallajökull volcano. First, an emission source parameterization was incorporated to include the time and height dependent emission flux from various levels above the volcano. Then, the aerosol dynamics model M7 (Vignati et al., 2004) was adapted to include the volcanic dust (primary ash) emitted at the source in terms of particle size distribution and density. The emission source parameters are from the EMEP (https://wiki.met.no/emep/emep_volcano_plume). These data are based on tephra estimates derived from preliminary thickness data obtained which was measured on the 17th April at two locations 20 and 50 km east of the volcano and agreed well with theoretical relationships derived for eruption height and volumetric flux for a number of volcanoes. Size distribution measurements of these samples allow size dependent estimates of emission rates. These derived PM10 emissions used for model parameterization during the relevant study periods ranged in value from 7 x 10^6 g s^{-1} (19th April) to 2 x 10^6 g s^{-1} (17th May).

The model was used both as a forecast as well as a hindcast tool (with re-analysis data) for research purposes. Hindcast results were compared, and found to be in good agreement, with observations and results from other dispersion models as part of the validation process which are described in detail in Part II of this paper O'Dowd et al. (2012). For all the simulations presented in the study here, global re-analysis data of 0.5° resolution obtained from ECMWF was used as boundary conditions. Ozonesondes were taken at Valentia, 150 km south of Mace Head, and in-situ at Mace Head using a Thermo Scientific model 49i UV ozone analyzer.

3. Results

The ash plume aerosol properties associated with the three strong and sustained plumes are tabulated in Table 1 and discussed per case study below.

3.1. Case 1: 19th-20th April 2010

Immediately after the eruption, the plume advected southwest from Iceland and over the north of Britain, into central Europe and then part of it advected west over Ireland in a high pressure system. The dispersion of the plume as simulated by the REMOTE regional climate model is shown in Fig. 1. The hindcast illustrated the maximum density of the plume located over the NE of England on the morning of the 20th April, advecting over the North Sea and Holland by midday of the 20th. The edge of the plume passes over Mace Head during these periods.

The plume was first detected around midday on the 19th April 2010 over Mace Head using the ceilometer (Fig. 2). A thin layer, approximately 200 m thick was detected at an altitude of 4 km and was observed to subside over the subsequent 12 h period after which it entered the boundary layer and was mixed to the surface level. The average vertical profile of backscatter coefficient and extinction from 16:50e17:00 h is shown in Fig. 3. The backscatter coefficient reached a maximum of 0.075 sr km^{-1} while extinction peaked at 1.5 km^{-1} (Fig. 3).

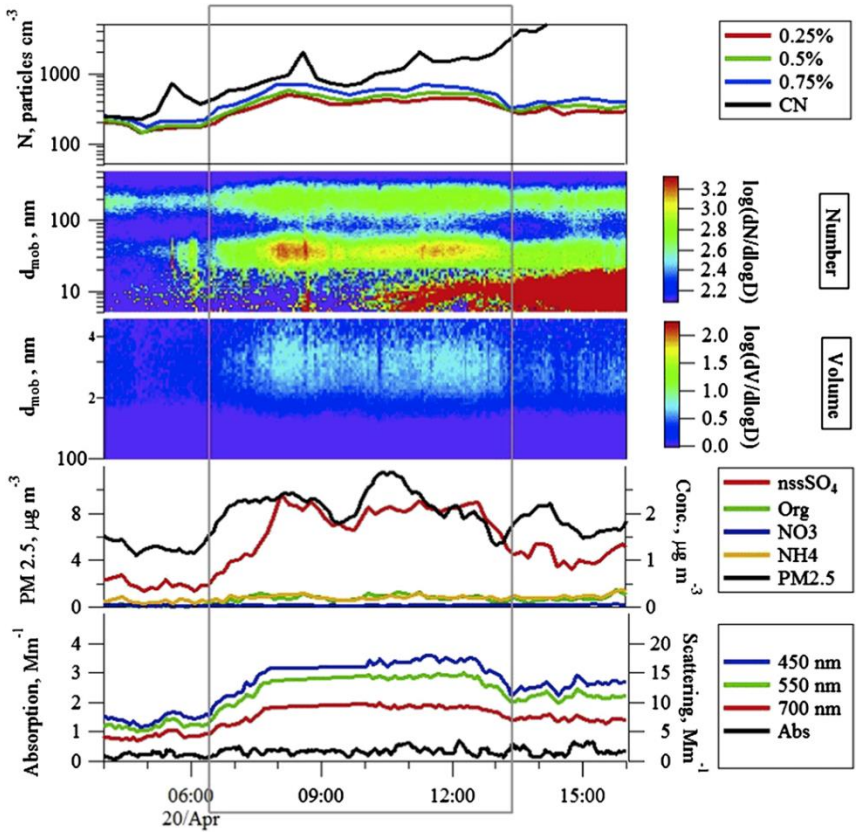

Fig. 4. (Top) Condensation Nuclei (CN) and CCN; (2nd from Top) SMPS aerosol number size distributions; (3rd from Top) SMPS particle volume distributions; (4th from Top) total particulate mass (PM2.5) AMS chemical composition; (Bottom) Aerosol scattering and absorption. The plume period (20th April 2010) is highlighted by the rectangular box.

Around midnight of the 19th/20th, as the plume subsided into the boundary layer, aerosol absorption increased from a background level of less than 0.2 Mm^{-1} to a plume average of 0.36 Mm^{-1} while the scattering coefficient, for the blue wavelength, increased from less than 10 Mm^{-1} up to ~17 Mm^{-1} (See Fig. 4). During these periods, PM2.5 increased to ~9.1 µg m^{-3}. The AMS revealed a relatively large increase in nss-sulphate mass, up to 2.1 µg m^{-3}, with no associated increase in either nitrate or organic aerosol mass. The nss-sulphate mass mode was located at 500-600 nm diameters. Aerosol average concentration for the plume duration was 1247 cm^{-3}. The plume detection revealed a strong accumulation mode with mode diameter at 185 nm, and a strong Aitken mode at 30-40 nm. Before and after the plume was detected, polluted air prevailed and both nucleation and growth events were observed. The CCN (0.75%) concentration was 622 cm^{-3} under plume conditions with a CCN/CN ratio of 0.5. It should be pointed out that an earlier detection of the plume for slightly shorter duration revealed that CCN

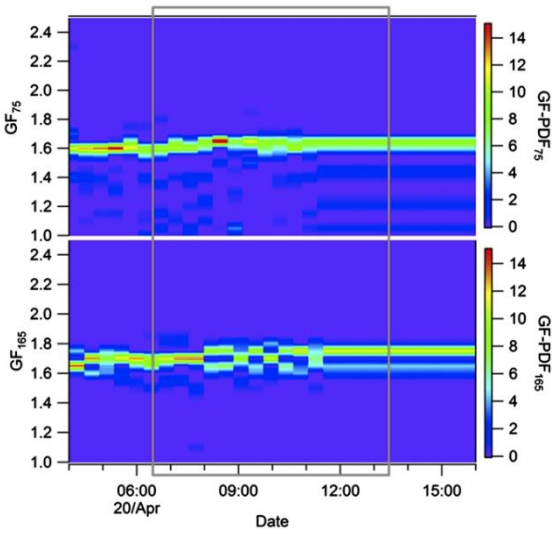

Fig. 5. Hygroscopic growth factors for 75 nm and 165 nm particle sizes.

concentrations at all supersaturations less than 0.75% were equal and the CCN/CN ratio was 1. This indicated that the volcanic aerosol were all very soluble and quite large in size such that no Kelvin effect could be detected. The higher CCN/CN ratio in the case presented appears to be due to the presence of an ultrafine aerosol typically associated with coastal particle production events. This ultrafine mode leads to elevated particle concentrations at sizes of less than 30-50 nm. The aerosol growth factor spanned from 1.58 for 75 nm sizes to 1.7 for 165 nm sizes, pointing to a strong sulphate growth factor signature (Fig. 5) and indicated an internally-mixed aerosol population. There were almost no particles with solubility less than that associated with sulphate aerosol. The high growth factors associated with the ash plume are indicative of a significant sulphate aerosol, even it is internally mixed with crustal ash and activation occurred at a low supersaturation of the order of 0.25%.

3.2. Case 2: 2nd-5th May 2010

The second major plume interaction occurred over the period from 2nd to 5th May 2010. The vertical and horizontal dispersion of the ash plume over Europe is shown in Fig. 6. The hindcast indicates almost direct connected flow between Iceland and Ireland/UK on the 4th-5th May

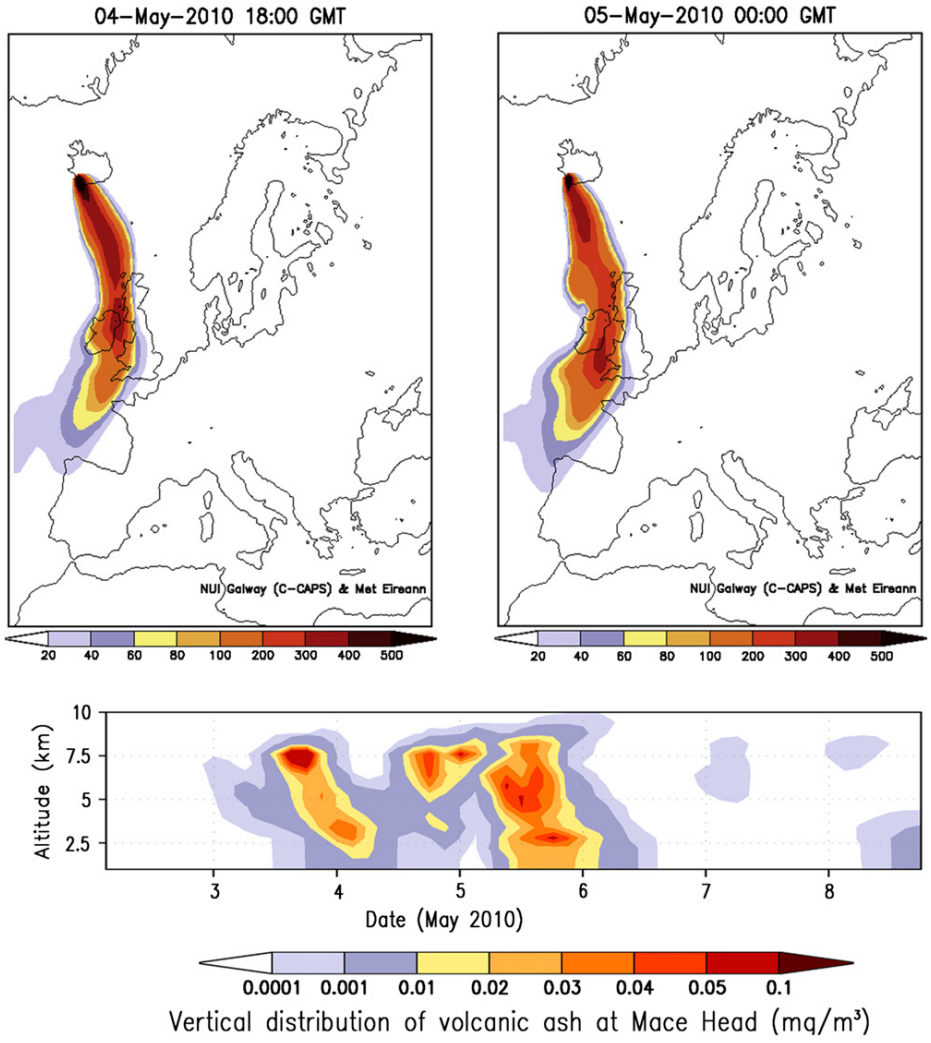

Fig. 6. (Top Left and Right) Spatial distribution of ash plume integrated column mass. (Bottom) Vertical distribution of ash plume volumetric mass concentration. 4th-5th May 2010.

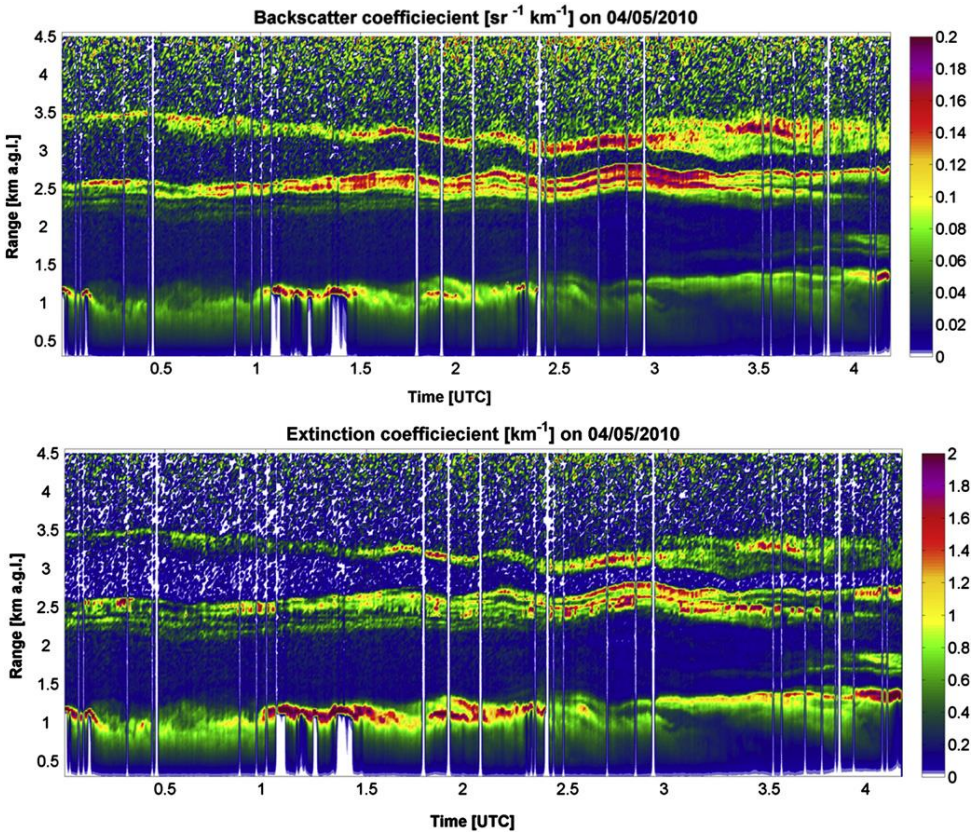

Fig. 7. Temporal evolution of volcanic plume backscatter coefficient and extinction coefficient over Mace Head on the 3rd May.

2010. This flow occurs in very clean polar air. The western edge of the ash plume flows over Mace Head with the densest part of the plume flowing over Northern Ireland and the Irish Sea.

The case on the 4th of May is selected as it is not only one of the strongest encountered; it is steady for almost 18 h in duration. The temporal and vertical structure of the plume extent over Mace Head, in terms of backscatter coefficient and extinction, is shown in Figs. 7 and 8 for the period preceding subsidence into the boundary layer on the 3rd May. Three layers of elevated backscatter and extinction coefficients are evident in the figures. At approximately 1 km, boundary layer aerosol is evident whilst two distinct and stratified volcanic plume layers are

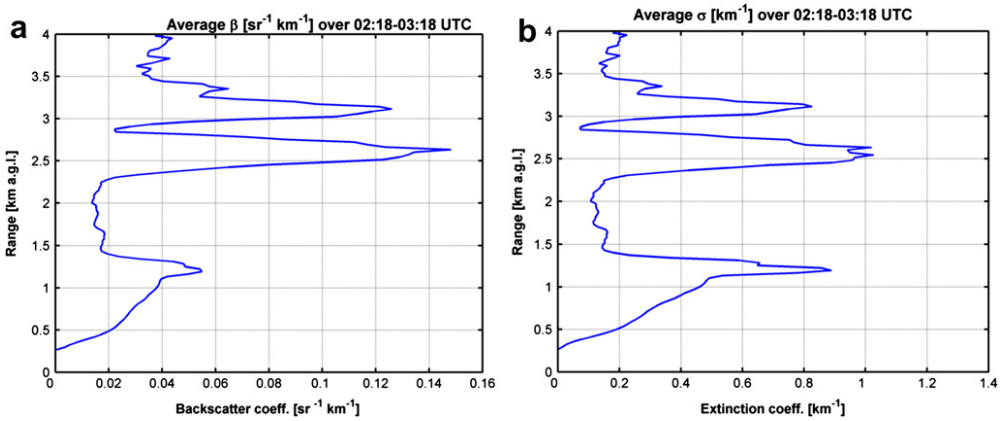

Fig. 8. (a) Vertical profile of backscatter coefficient on 3rd May 2010. (b) Vertical profile of extinction coefficient on 3rd May 2010.

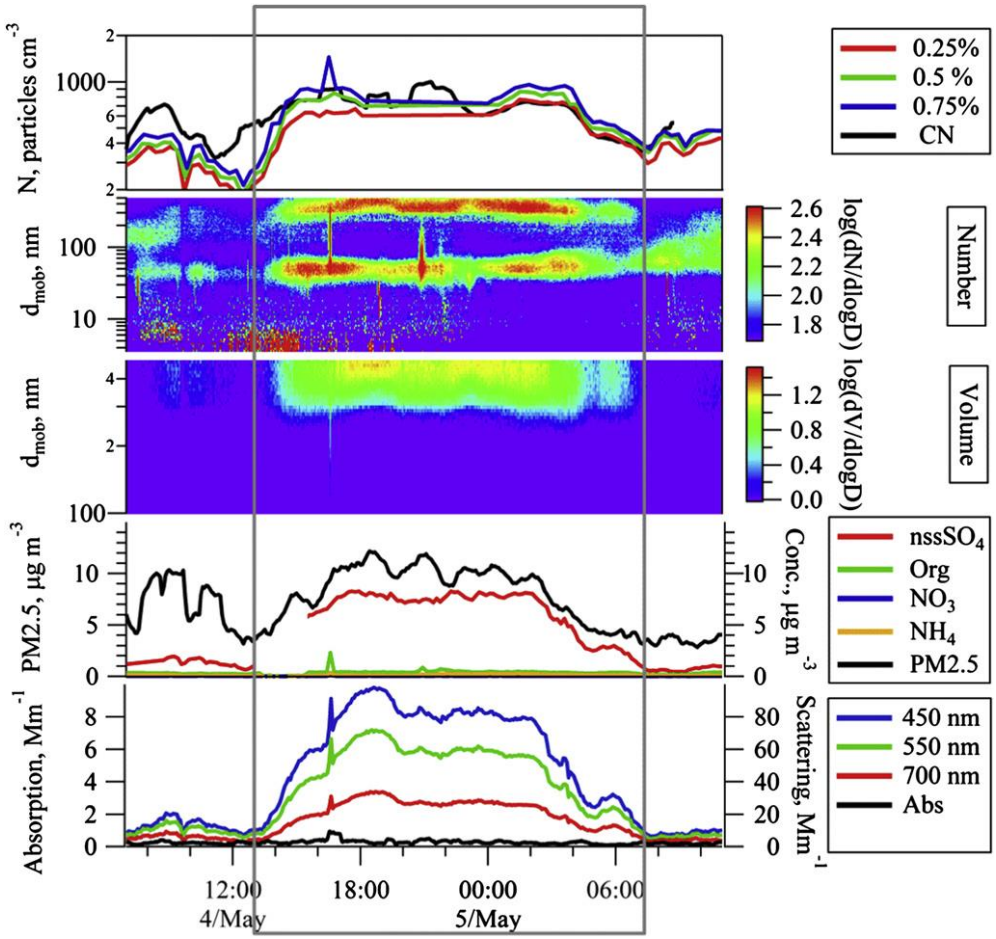

Fig. 9. (Top) Condensation Nuclei (CN) and CCN; (2nd from Top) SMPS aerosol number size distributions; (3rd from Top) SMPS particle volume distributions; (4th from Top) total particulate mass (PM2.5) AMS chemical composition; (Bottom) Aerosol scattering and absorption. The plume period (4th-5th May 2010) is highlighted by the rectangular box.

observed at 2.5 and 3.5 km altitude. Again, these layers extend 200-300m in the vertical.

The backscatter coefficient extends to 0.14 sr km^{-1} while the extinction peaks slightly above 1 km^{-1}. The backscatter coefficient in the plume layers is significantly higher than that in the boundary layer while the boundary layer extinction is nearly equivalent to the ash plume extinction in this case. Total particle concentration was less than 780 cm^{-3} and the CCN/CN ratio was approximately 1 for all supersaturations measured (Fig. 9). The almost 100% activation ratio at the lowest supersaturation of 0.25% points to a large nuclei size composed of very soluble material at the surface despite the possibility of an insoluble volcanic ash core.

The optical properties do not exhibit notable increases in absorption; however, the scattering coefficient increases from background levels of less than 10 Mm^{-1} to 28 Mm^{-1} for the red wavelength and to 85 Mm^{-1} for the blue wavelength. Concomitant with the increase in scattering, total PM2.5 increased to >10.4 µg m^{-3}, although it should be noted that this mass concentration is not unusual in either clean or polluted air at Mace Head. What is unusual, and provides the ash plume signature is the 7.8 µg m^{-3} nss-sulphate aerosol without any elevation in organic or nitrate aerosol mass. Again, the accumulation mode diameter was ~380 nm. The hygroscopic growth factor

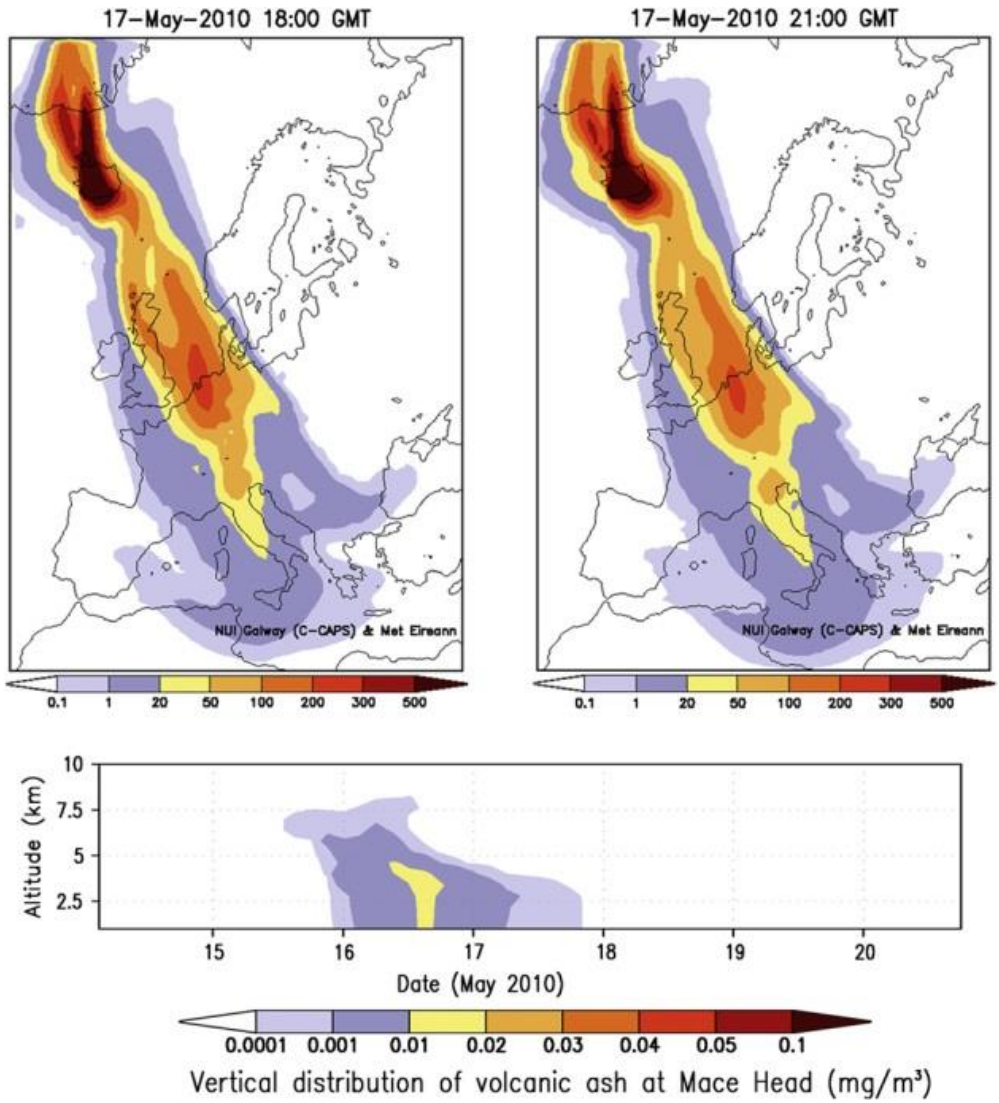

Fig. 10. (Top Left and Right) Spatial distribution of ash plume integrated column mass. (Bottom) Vertical distribution of ash plume volumetric mass concentration. 17th 18th May 2010.

probability distribution function, at all sizes, revealed almost 100% GFs of between 1.44 and 1.64, indicating a quite pure nss-sulphate composition GF, although this does not rule out sulphate-coated insoluble cores.

3.3 Case 3: May 17th-18th

The third strong event observed at Mace Head occurred on the 17th and 18th May 2010. Again, the vertical and horizontal dispersion over Europe is illustrated in Fig. 10, while Fig. 11 displays the plume descending from 4 km towards the boundary layer. The plume dispersion on the 16th and 17th of May was more concentrated over the North Sea, nevertheless, significant concentrations were still forecast over the west coast of Ireland. Also evident in Fig. 11 is boundary layer non-plume aerosol at levels below 1.5 km where stratification is also evident.

Later in the day, stratocumulus cloud forms at between 2.2 and 2.5 km altitude as is evidenced by the vertical profiles of back-scatter and extinction coefficients in Fig. 12. Above the cloud, the plume backscatter coefficient approaches 2.5km^{-1} while the extinction coefficient exceeds 0.4 km^{-1}.

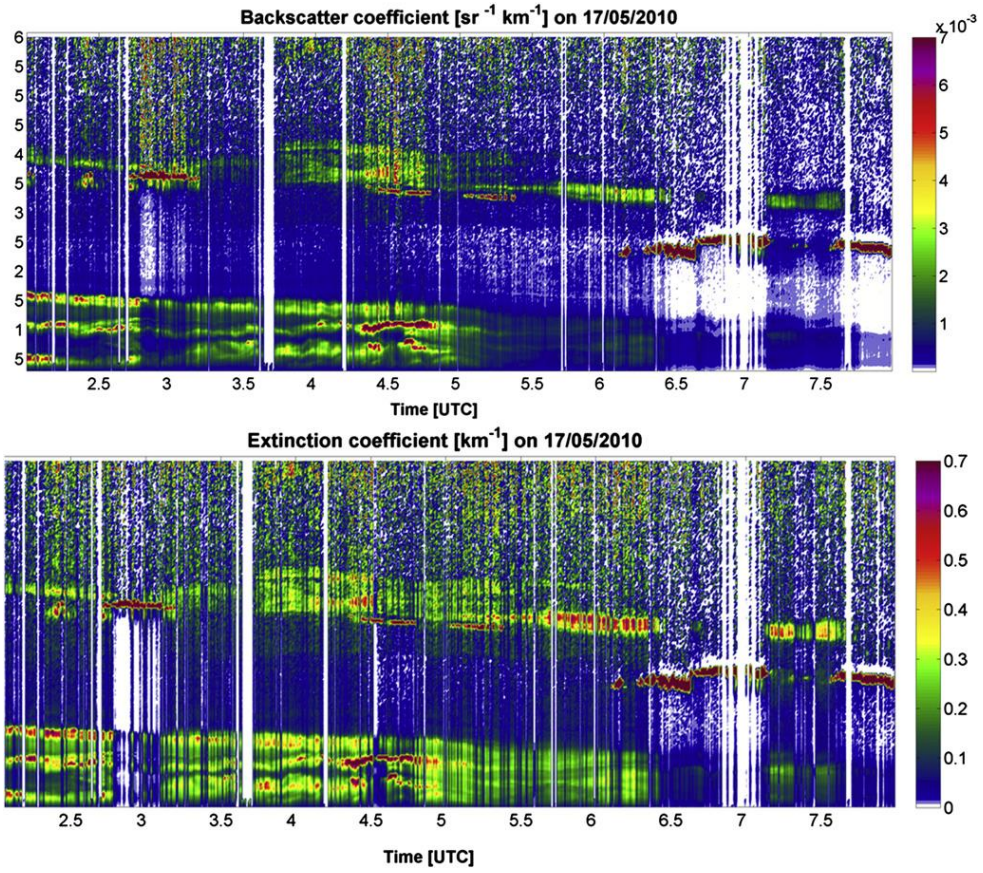

Fig. 11. Temporal evolution of volcanic plume backscatter coefficient and extinction coefficient over Mace Head on the 17th-18th May 2010.

During the plume on the 17th May, the total aerosol concentrations (Fig. 13) decreased from more than 104 cm^{-3}, associated with a nucleation and growth event, to about 890 cm^{-3} initially and then further to about 300 cm^{-3}. Again, for

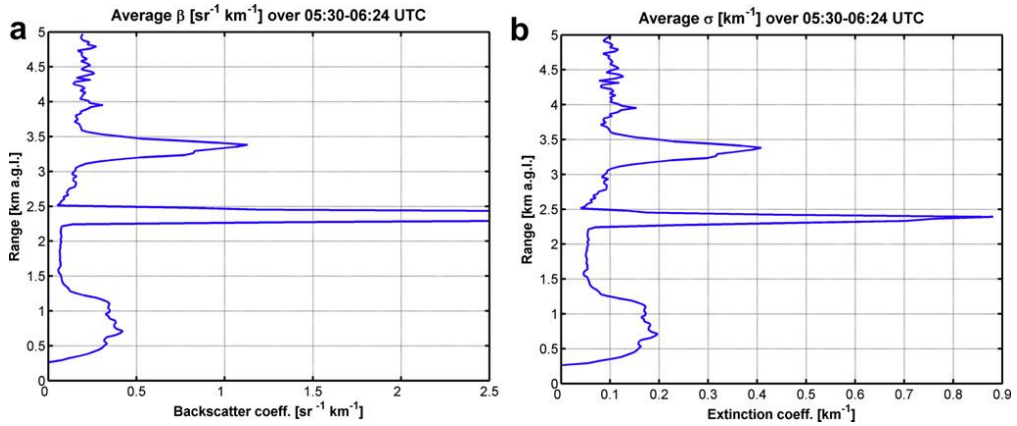

Fig. 12. (a) Vertical profile of backscatter coefficient on 17th May 2010. (b) Vertical profile of extinction coefficient on 17th May 2010.

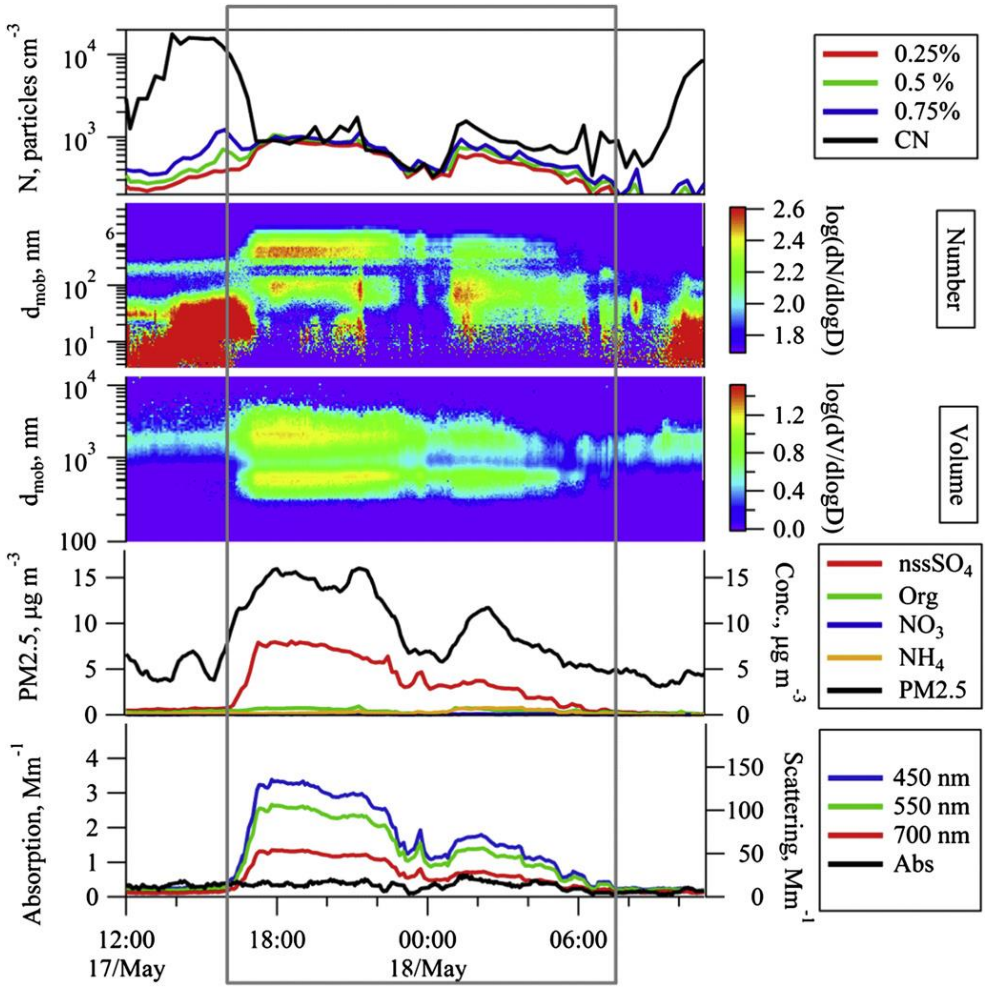

Fig. 13. (Top) Condensation Nuclei (CN) and CCN; (2nd from Top) SMPS aerosol number size distributions; (3rd from Top) SMPS particle volume distributions; (4th from Top) total particulate mass (PM2.5) AMS chemical composition; (Bottom) Aerosol scattering and absorption. The plume period (17th-18th May 2010) is highlighted by the rectangular box.

most of the duration of the plume, the CCN/CN ratio approaches 1 for all supersaturations up to 0.75% suggesting large and very soluble nuclei. The latter part of the plume had a lower CCN/CN ratio leading to a plume average of 0.81. Nss-sulphate mass for this plume averaged at 7.2 µg m^{-3} while PM2.5 mass was 14.6 µg m^{-3}. Absorption reached a plume average of 0.38 Mm^{-1}, while the red wavelength scattering was 50 Mm^{-1} and the blue wavelength scattering was 122 Mm^{-1}. Again, a very large accumulation mode, of the order of 390 nm diameter, was present compared to a typical background mode of 120-150 nm diameter (Yoon et al., 2007). For this case, the APS was deployed to measure supermicron size spectra. During the plume the combined SMPS and APS spectrometers reveal two strong mobility mass modes at 560 nm 2.6 µm. The GFs were between 1.58 and 1.65 for all sizes measured. However, examination of the derived mass size spectra exhibits striking differences between the combined APS and SMPS mass and that derived from the TEOM. This will be discussed later.

Table 2
Percentage contributions of major compound classes to particulate mass concentrations (24 h averages) during May 17th event derived from XRF analysis.

		nss SO_4, %	Ash, %	Sea-salt, %
PM10[a]	11.45 µg m^{-3}	33	39	28
PM2.5[a]	5.03 µg m^{-3}	64	30	7
PM2.5–10[a]	6.42 µg m^{-3}	10	46	44

[a] PM concentrations exclude nitrate, ammonium, organic matter and compound bound water (as in gypsum, sulphuric acid, etc.).

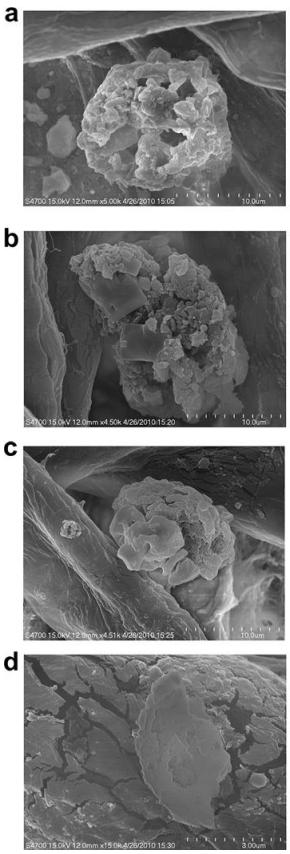

Element	Weight%	Atomic%
C	38.91	54.62
O	24.42	25.74
Si	14.86	8.92
Al	4.15	2.59
Na	2.26	1.66
S	2.96	1.55
Ca	3.60	1.51
Cl	3.13	1.49
Fe	4.28	1.29
K	1.43	0.62

Element	Weight%	Atomic%
C	46.88	59.20
O	31.58	29.94
Si	11.07	5.98
Cl	3.01	1.29
Al	2.06	1.16
Na	1.27	0.84
Mg	0.78	0.48
Fe	1.57	0.43
Ca	1.08	0.41
K	0.71	0.28

Element	Weight%	Atomic%
O	56.95	70.13
Na	8.52	7.30
Cl	11.25	6.25
Mg	6.59	5.34
Al	6.49	4.74
Si	5.66	3.97
K	2.71	1.36
Ca	1.83	0.90

Element	Weight%	Atomic%
C	37.13	47.34
O	44.13	42.24
Si	11.94	6.51
Al	3.41	1.93
Na	2.36	1.57
K	1.03	0.40

Fig. 14. SEM images of volcanic ash particles collected during the period of April 19-20. Carbon in elemental composition stems from cellulose fibres.

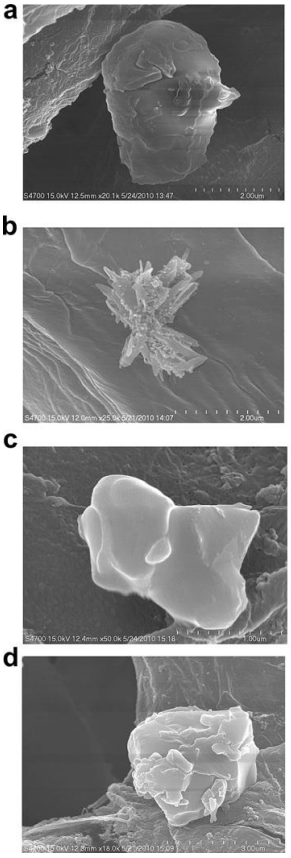

Element	Weight%	Atomic%
O K	21.60	34.50
Na K	2.51	2.79
Al K	9.92	9.39
Si K	47.58	43.28
K K	5.15	3.37
Ca K	3.42	2.18
Fe K	9.82	4.49

Element	Weight%	Atomic%
C K	54.40	63.88
O K	36.09	31.82
Na K	1.69	1.04
Mg K	0.43	0.25
Al K	0.26	0.14
S K	3.70	1.63
Cl K	0.91	0.36
Ca K	2.51	0.88

Element	Weight%	Atomic%
O K	60.49	78.76
Na K	2.08	1.89
Al K	5.71	4.41
Si K	8.45	6.27
Fe K	23.26	8.68

Element	Weight%	Atomic%
C K	15.21	22.82
O K	49.08	55.27
Na K	3.35	2.62
Al K	5.23	3.49
Si K	20.94	13.43
K K	1.40	0.65
Ca K	1.36	0.61
Fe K	3.43	1.11

Fig. 15. SEM images of the particles collected during the period of May 17-18. Carbon in elemental composition stems from cellulose fibres.

3.4 Off-line chemical analysis

The off-line PM2.5 and PM10 chemical analysis was speciated according to three main categories, namely, nss-sulphate, sea-salt and ash. The analysis is only presented for the event (24-h average) on the 17th May and results are tabulated in Table 2 where mass concentrations of the categories, exclusive of nitrate, ammonium, organic matter and compounds bound water (as in gypsum, sulphuric acid, etc.) are presented. For this event, the PM10 mass was 11.45 μm m^{-3} of which 33% was sulphate, 39% ash, and 28% sea-salt.

For PM2.5, total mass was 5.03 μm m^{-3} of which 64% was sulphate, 30% ash, and 7% sea-salt.

3.5 Scanning electron microscopy analysis

SEM samples were taken during two events: April 19the20th (the first volcanic plume reaching Mace Head after explosive eruption on April 14th) and May 17th-18th (the highest nss- sulphate loading and longest in duration event). Volcanic ash SEM analysis of the first volcanic ash plume detected on April 19th revealed a diverse morphology and composition of ash particles, but mainly consisting of silica oxide (Fig. 14a), which also was the dominant oxide in Eyjafjallajökull lava. A large number of particles contained significant amounts of sulphur, indicating secondary processes of sulphate/sulphuric acid formation from sulphur dioxide oxidation during transport in the volcanic

plume, also mixed with sea-salt (Fig. 14b) picked up during transport over oceanic regions. Volcanic glass shards (Fig. 14d) were common with the presence of Al, which oxide was the second most abundant in Eyjafjallajökull lava. Melting and re-crystallization of particles (Fig. 14c) was also evident in particles. Many of the particles were incrusted with various metals like Fe, Cr and Ti.

SEM analysis of particles collected during the period of May 17th-18th revealed less diverse composition and the particles in general and were smaller in size than during April 19th-20th period. However, more diverse glass shard particles were detected with entire glassy particles present in samples (Fig. 15b). There was a clear evidence of gypsum forming in the particles rich in calcium oxide when increasing amount of sulphuric acid became available which is evident in Fig. 16 exhibiting twinned crystal shape particle typical of growing gypsum crystal and confirmed by exclusive chemical composition of Ca, S and O.

These differences could indicate that the explosive activity of the volcano was decreasing and less of the bigger particles were ejected to significant height to be later efficiently transported over the long distances. However, melted-recrystallized-fused particles were present (Fig. 15c and d) which indicated similar particle evolution in the rising volcanic plume as during the beginning of the eruption in April.

3.6 Ozone depletion in the ash plume

On several days when the volcanic plume mixed into the boundary layer down to ground level at Mace Head the rapid increase in aerosol sulphate concentrations detected by the AMS was accompanied by a conspicuous drop in ground level ozone mixing ratios. A clear example is shown in Fig. 16 for 17th May 2010, when O_3 levels decreased by about 15 ppbv during plume arrival. Ozonesonde profiles launched at 12 GMT from the Valentia Station typically showed O_3 mixing ratios of 40-60 ppbv in the free troposphere (FT) in the absence of the plume over that region (e.g., 19th May). These observations suggested significant ozone depletion within the volcanic plume. Assuming SO_2 levels of 40-100 ppbv at plume altitudes, as observed during flight measurements north of Ireland by Schumann et al. (2011) and Heue et al. (2010), model calculations show that about 80% of the aerosol nss-sulphate concentrations can be explained by in-cloud aqueous phase oxidation dominated by ozone (Flanagan et al., 2011). Sulphate aerosol concentrations in the FT may have been on the order of 50 μg m^{-3} over Ireland in relative agreement with the airborne observations. In addition to in-cloud SO_2 oxidation, further depletion of ozone in the plume could have been caused by rapid bromine chemistry. Heue et al. (2010) measured BrO mixing ratios of 4-6 pptv in the plume on 16 May consistent with significant BrO total column densities retrieved simultaneously from GOME-2 satellite. Previous measurements (Bobrowski et al., 2007, 2003) and model simulations (von

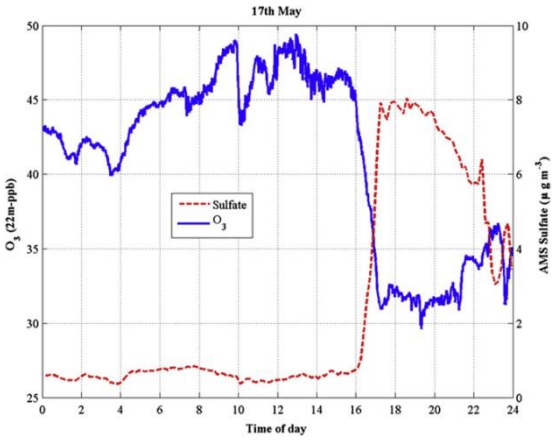

Fig. 16. Ozone and nss-sulphate concentrations as the 17th May 2010 ash plume entered the boundary layer at Mace Head.

Glasow, 2010) have shown that bromine

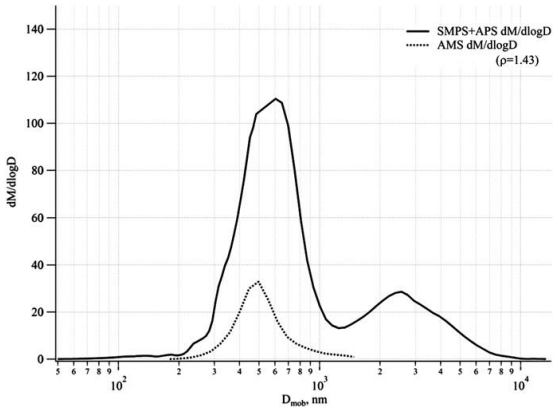

Fig. 17. Volcanic aerosol mass closure. AMS mass size distribution is of total non-refractory mass presented in mobility scale. Mass size distribution of combined SMPS and APS distributions presented in mobility scale APS aerodynamic and AMS vacuum aerodynamic sizes converted to mobility diameter assuming particle density of 1.43 g cm^{-3}. Mass discrepancy between submicron spectra is due to particle water and refractory ash components.

radical reactions in volcanic plumes can deplete ozone down to as much as 10% of its ambient background levels.

4. Discussion

The first plume period reported here represented the high- explosive part of the eruption while the latter two events represent the less-explosive period of the eruption. The high-explosive period was characterized by low SO_2 while the less-explosive period was characterized by high SO_2 emissions as determined by satellite (Evgenia Ilyinskaya, personal communication). During the high-explosive period, the ash has a smaller modal size (185 nm) concomitant with only moderate increases in nss-sulphate mass while for the less-explosive periods, the mode diameter increased to 390 nm and nss-sulphate mass amounted to 7.8 μg m^{-3}.

From the third case presented, and for when the most complete set of instruments were deployed, there were two methods to measure total particulate mass: the first, a TEOM, provided a mass measurements at PM2.5, while, second, the combination of the SMPS and APS single particle size spectrometers were used to derive a mass size distribution based on certain assumptions, including that of density. The TEOM operates on the basis of an oscillating microbalance, while the SMPS operates on particle mobility principles and the APS operates on aerodynamic time-of-flight measurements. To produce a mass distribution from the combination of the SMPS and APS, the APS diameter must be converted into a mobility diameter and a density is applied to the volume distribution to produce a mass distribution. In addition, nss-sulphate mass at PM1 was derived from the AMS and for PM2.5 and PM10 size-cuts, nss-sulphate, ash and sea-salt mass where retrieved through off-line chemical analysis.

The plume on 17th May warrants special attention as the full suite of aerosol measurements at Mace Head were deployed and revealed some intriguing differences between different measurement techniques. During this plume, the PM2.5 mass from the TEOM amounted to 14.6 μg m^{-3}, while mass from the size spectrometers, for PM2.5 mass amounted to 37.7 μg m^{-3}, and for PM10 amounted to 46.9 μg m^{-3}. For the off-line chemical analysis, only ash, sulphate and sea-salt were reported and the total amounted to 5.03 and 11.45 μg m^{-3}, respectively, for PM2.5 and PM10. The latter was averaged over a 24 h period and therefore contains significant time outside the plume, hence the lower concentrations. If one focuses on PM2.5 mass, we have a discrepancy whereby the size spectrometers report mass concentrations more than twice that of the TEOM and the nss-sulphate mass comprises ~50% of the TEOM mass and ~25% of the spectrometer mass. The

discrepancy cannot be accounted for by the ash content as the off-line chemical analysis indicated a sulphate to ash ratio of 2:1. Given that the other major chemical constituents amount to perhaps, at most, 10% of the PM2.5 mass, the most rational remaining conclusion is that the missing mass relates to the water content associated with the sulphuric acid aerosol and that this water content had not evaporated in the SMPS and APS, but had evaporated in the TEOM given its operating temperature of 50 ^{o}C. Closure between the instruments is achieved if ~55% of the PM2.5 mass is accounted for by water, and the remaining mass is nominally ~30% sulphate and ~15% ash. This results in an average density, considering primarily of nss-sulphate, ash and water, of ρ=1.43 g cm^{-3}. Fig. 17 illustrates the resulting SMPS/APS size distribution compared to the AMS non-refractory spectrum.

Particle bound water was also estimated using E-AIM (Extended Aerosol Inorganics Model) model (http://www.aim.env.uea.ac.uk/aim/aim.php) developed by the University of East Anglia (Carslaw et al., 1995; Massucci et al., 1999; Clegg and Brimblecombe, 2005; Clegg et al., 1998). Using chemical species concentrations presented in Table 2 and the range of relative humidity (50-80%) and temperatures (10-15^{o}C) estimated particle bound water content was in the range of 9.2-25.7 μg m^{-3}. Ambient relative humidity was close to 100% and unspecified drying has occurred in the community sampling duct or the instruments (SMPS and APS). However, equilibrium temperature and RH conditions possibly have not been met during the sampling time scale (~10 s) resulting in water content on a higher end of the estimation which is consistent with the indirect estimate of 20.6 μg m^{-3} of water. The resulting density of particles adding known amount of ash from Table 2 was in the range of 1.32-1.45 g cm^{-3}, consistent with an indirect estimate of 1.43 g cm^{-3}.

Despite being an internal mix of an insoluble ash fraction, the hydroscopic GF is identical to sulphate aerosol and given the large modal sizes, these particles are excellent CCN with typically 100% activation at supersaturations as low as 0.25%. The high activation efficiency of the volcanic aerosol was also reflected in ground based remotely-sensed cloud microphysics for one event where it is thought that the ash layer induced the formation of a layered cloud above the boundary layer (Martucci et al., 2012). In that study, the mean droplet concentration was ~300 cm^{-3}; however, peak concentration of ~1000 cm^{-3} were observed (i.e. similar to maximum CCN concentrations). Gassó (2008) also found major microphysical impacts on low level marine clouds from volcanic emissions on Saunders Island, South Atlantic. The Mount Michael volcano was undergoing a steady and simmering eruption and large reductions in the cloud effective radius was observed from satellite. Yuan et al. (2011) also found similar impacts on marine trade wind cumulus downwind of a gently degassing Hawaiian volcano Kilauea where increases in precipitation associated with reductions of effective radius were observed in clouds forming in-plume enriched air.

Observations of the ash plume were conducted from aircraft (Schumann et al., 2011) and also from ground based stations (e.g.,Zugspitze/Hohenpeissenberg, Flentje et al., 2010); however, direct comparison of aerosol properties is not so straight forward as few overlapping parameters. The easiest parameter to compare with is total number concentration. At Mace Head, we observed concentrations of the order of 1000 cm^{-3}, whereas, airborne measurements by Schumann et al. report concentrations in excess of 10,000 cm^{-3} and Flentje et al. only report total particle

concentrations as "enhanced or normal". Flentje et al. reported PM10 mass concentrations of the order of 40-50μgm^{-3}, similar to Mace Head, while airborne measurements by Schumann et al. report mass concentrations as high as 400 μgm^{-3}. Turbulent mixing of the 200 m thick ash plume into a boundary layer approximately 1000 m suggests that the boundary layer ash mass concentrations were likely to be diluted by a maximum factor of 5, indicating that the maximum ash cloud mass concentrations could have approached 250-300 μg m^{-3}.

5. Conclusions

The Eyjafjallajökull aerosol plume was sampled and characterized in terms of physico-chemical properties as it descended into the boundary layer. During the initial intensive explosive phase of the eruption, with low SO_2 emissions, the submicron modal diameter was of the order of 185 nm, while during the less intensive explosive phase, the modal diameter was of the order of 395 nm and the supermicron mode was of the order of 2.5 microns. The supermicron ash chemical composition was primarily silicon oxides and the submicron aerosol was composed of an internal mix of primary ash (15%), nss-sulphate (25%) and water (55%). The physical size and chemical composition result in the ash plume aerosol being very efficient CCN as evidenced by a 100% ratio efficiency for CCN/CN at supersaturations as low as 0.25%. PM10 mass concentrations compare well with other measurements from European ground based stations and are about an order of magnitude lower than that of airborne flight measurements of the plume.

Acknowledgements

The authors would like to acknowledge the following funding agencies and programmes: HEA-PRTLI4, SFI, EPA-Ireland, FP6-EUCAARI, FP6-GEOMON, FP6-EUSAAR; and the CNR-Rome for chemical analysis. Further, the Irish Centre for High End Computing is acknowledged for supercomputing resource support.

References

Ackermann, J., 1998. The extinction-to-backscatter ratio of tropospheric aerosols: a numerical study. J. Atmos. Ocean. Tech. 15, 1043-1050.

Allan, J.D., Alfarra, M.R., Bower, K.N., Williams, P.I., Gallagher, M.W., Jimenez, J.L.,McDonald, A.G., Nemitz, E., Canagaratna, M.R., Jayne, J.T., Coe, H.,Worsnop, D.R., 2003. Quantitative sampling using an aerodyne aerosol mass spectrometer: 2. Measurements of fine particulate chemical composition in two UK cities. J. Geophys. Res. 108 (D9).

Bobrowski, N., Hönninger, G., Galle, B., Platt, U., 2003. Detection of bromine monoxide in a volcanic plume. Nature 423, 273-276.

Bobrowski, N., von Glasow, R., Aiuppa, A., Inguaggiato, S., Louban, I., Ibrahim, O.W., Platt, U., 2007. Reactive halogen chemistry in volcanic plumes. J. Geophys. Res. 112, D06311. doi:10.1029/2006JD007206.

Bodhaine, B.A., Ahlquist, N.C., Schnell, R.C., 1991. 3-Wavelength nephelometers suitable for aircraft measurement of background aerosol scattering coefficient. Atmos. Environ. 25, 2267-2276.

Carslaw, K.S., Clegg, S.L., Brimblecombe, P., 1995. A thermodynamic model of the system HCl-HNO_3-$H2SO_4$-H_2O, including solubilities of HBr, from <200 K to 328 K. J. Phys. Chem. 99, 11557e11574.

Clegg, S.L., Brimblecombe, P., 2005. Comment on the "thermodynamic dissociation constant of the bisulfate ion from Raman and ion interaction modeling studies of aqueous sulfuric acid at low temperatures" by Knopf et al. J. Phys. Chem. A 109, 2703-2706.

Clegg, S.L., Brimblecombe, P., Wexler, A.S., 1998. A thermodynamic model of the system H^+-NH^{4+}-SO_4^{2-}-NO^{3-}-H_2O at tropospheric temperatures. J. Phys. Chem. A 102, 2137-2154.

Davies, S.M., et al., 2010. Widespread dispersal of Icelandic tephra: how does the Eyjafjöll eruption of 2010 compare to past Icelandic events? J. Quart. Sci. 25, 605-611.

DeCarlo, P.F., Kimmel, J.R., Trimborn, A., Northway, M.J., Jayne, J.T., Aiken, A.C., Gonin, M., Fuhrer, K., Horvath, T., Docherty, K.S., Worsnop, D.R., Jimenez, J.L., 2006. Field-deployable, high-resolution, time-of-flight aerosol mass spectrometer. Anal. Chem. 78 (24), 8281-8289.

Flanagan, R.J., Kulmala, M., O'Dowd, C.D., 2011. Factors affecting in-cloud sulphate production in the marine environment. Atmos. Environ. minor revisions.

Flentje, H., Claude, H., Elste, T., Gilge, S., Köhler, U., Plass-Dülmer, C., Steinbrecht, W., Thomas, W., Werner, A., Fricke, W., 2010. The Eyjafjallajökull eruption in April 2010-detection of volcanic plume using in-situ measurements, ozonesondes and LIDAR-ceilometer profiles. Atmos. Chem. Phys. 10, 10085-10092.

Gassó, S., 2008. The impact of weak volcanic activity on marine clouds. J. Geophys. Res. doi:10.1029/2007JD009106.

Gysel, M., McFiggans, G.B., Coe, H., 2009. Inversion of tandem differential mobility analyser (TDMA) measurements. J. Aerosol Sci. 40, 134-151.

Heue, K.-P., Brenninkmeijer, C.A.M., Baker, A.K., Rauthe-Schöch, A., Walter, D., Wagner, T., Hörmann, C., Sihler, H., Dix, B., Frieß, U., Platt, U., Martinsson, B.G., van Velthoven, P.F.J., Hermann, M., Zahn, A., Ebinghaus, R., 2010. SO2 and BrO observation in the plume of the Eyjafjallajökull volcano 2010: CARIBIC and GOME-2 retrievals. Atmos. Chem. Phys. Discuss. 10, 29631-29682.

Jayne, J.T., Leard, D.C., Zhang, X.F., Davidovits, P., Smith, K.A., Kolb, C.E., Worsnop, D.R., 2000. Development of an aerosol mass spectrometer for size and composition analysis of submicron particles. Aerosol Sci. Technol. 33 (1-2), 49-70.

Jennings, S.G., Kleefeld, C., O'Dowd, C.D., Junker, C., Spain, T. Gerard, O'Brien, P., Roddy, A.F., O'Connor, T.C., 2003. Mace Head Atmospheric Research Station - characterization of aerosol radiative parameters. Boreal Environ. Res. 8 (4), 303-314.

Jimenez, J.L., Jayne, J.T., Shi, Q., Kolb, C.E., Worsnop, D.R., Yourshaw, I., Seinfeld, J.H., Flagan, R.C., Zhang, X.F., Smith, K.A., Morris, J.W., Davidovits, P., 2003. Ambient aerosol sampling using the aerodyne aerosol mass spectrometer. J. Geophys. Res. 108 (D7) no.-8425.

Kleefeld, Ch., O'Dowd, C.D., O'Riely, S., Jennings, S.G., Aalto, P., Becker, E., Kunz, G., de Leeuw, G., 2002. The relative scattering of sub and super micron particles to aerosol light scattering in the marine boundary layer (MBL). J. Geophys. Res. 107. doi:10.1029/2000JD000262.

Klett, J.D., 1981. Stable analytical inversion solution for processing LIDAR returns. Appl. Opt. 20, 211-220.

Lance, S., Medina, J., Smith, J.N., Nenes, A., 2006. Mapping the operation of the DMT continuous flow, CCN counter. Aerosol Sci. Technol. 40, 1-13. doi:10.1080/02786820500543290.

Langmann, B., Varghese, S., Marmer, E., Vignati, E., Wilson, J., Stier, P., O'Dowd, C., 2008. Aerosol distribution over Europe: a model evaluation study with detailed aerosol microphysics. Atmos. Chem. Phys. 8, 1591-1607.

Langmann, B., Folch, A., Hensch, M., Matthias, V., 2012. Volcanic ash over Europe during the eruption of Eyjafjallajökull on Iceland, April-May 2010. Atmos. Environ. 48, 1-8.

Martucci, M., Ovadnevaite, J., Ceburnis, D., Berresheim, H., Varghese, S., Martin, D., Flanagan, R., O'Dowd, C.D., 2012. Impact of volcanic ash plume aerosol on cloud microphysics. Atmos. Environ. 48, 205-218.

Massucci, M., Clegg, S.L., Brimblecombe, P., 1999. Equilibrium partial pressures, thermodynamic properties of aqueous and solid phases, and Cl_2 production from aqueous HCl and HNO_3 and their mixtures. J. Phys. Chem. A 103, 4209-4226.

Nilsson, E., Swietlicki, E., Sjogren, S., Löndahl, J., Nyman, M., Svenningsson, B., 2009. Development of an H-TDMA for longterm unattended measurement of the hygroscopic properties of atmospheric aerosol particles. Atmos. Meas. Tech. 2, 313-318. doi:10.5194/amt-2-313-2009.

O'Connor, T.C., Jennings, S.G., O'Dowd, C.D., 2008. Highlights from 50 years of aerosol measurements at Mace Head. Atmos. Res. 90, 338-355. doi:10.1016/j.atmosres.2008.08.014.

O'Dowd, C., Varghese, S., Flanagan, R., Martin, D., Ceburnis, D., Ovadnevaite, J., Martucci, G., Bialek, J., Monahan, C., Berresheim, H., Vaishya, A., Grigas, T., Jennings, S.G., McVeigh, P., Moran, E., Lambkin, K., Semmler, T., McGrath, R., 2012. The Eyjafjallajökull ash plume e Part II: forecasting the plume dispersion. Atmos. Environ 48, 143-151.

Ovadnevaite, J., Ceburnis, D., Plauskaite-Sukiene, K., Modini, R., Dupuy, R., Rimselyte, I., Ramonet, M., Kvietkus, K., Ristovski, Z., Berresheim, H., O'Dowd, C.D., 2009. Volcanic sulphate and arctic dust plumes over the North Atlantic Ocean. Atmos. Environ. 32, 4968-4974.

Pyle, D.M., 1999. Sizes of volcanic eruptions. In: Sigurdsson, H., et al. (Eds.), Encyclopedia of Volcanology. Academic Press, pp. 263-269.

Schumann, U., et al., 2011. Airborne observations of the Eyjafjalla volcano ash cloud over Europe during air space closure in April and May 2010. Atmos. Chem. Phys. 11, 2245-2279.

Varghese, S., Langmann, B., O'Dowd, C.D., 2011. Effect of horizontal resolution on meteorology and air-quality prediction with a regional scale model. Atmos. Res. doi:10.1016/j.atmosres.2011.02.007.

Vignati, E., Wilson, J., Stier, P., 2004. M7: an efficient size-resolved aerosol microphysics module for large-scale aerosol transport models. J. Geophys. Res. 109, D22202. doi:10.1029/2003JD004485.

von Glasow, R., 2010. Atmospheric chemistry in volcanic plumes. Proc. Natl. Acad. Sci. U. S. A. 107 (15), 6594e6599.

Wang, S.C., Flagan, R.C., 1990. Scanning electrical mobility spectrometer. Aerosol Sci. Technol. 13, 230e240. doi:10.1080/02786829008959441.

Yoon, Y.J., Ceburnis, D., Cavalli, F., Jourdan, O., Putaud, J.P., Facchini, M.C., Descari, S., Fuzzi, S., Jennings, S.G., O'Dowd, C.D., 2007. Seasonal characteristics of the physico-chemical properties of North Atlantic marine atmospheric aerosols. J. Geophys. Res. doi:10.1029/2005JD007044.

Yuan, T., Remer, L.A., Yu, H., 2011. Microphysical, macrophysical and radiative signatures of volcanic aerosols in trade wind cumulus observed by the A-Train. Atmos. Chem. Phys. Discuss. 11, 6415-6455. doi:10.5194/acpd-11-6415-2011.

On the effect of wind speed on submicron sea salt mass concentrations and source fluxes

Jurgita Ovadnevaite,[1] Darius Ceburnis,[1] Manjula Canagaratna,[2] Harald Berresheim,[1] Jakub Bialek,[1] Giovanni Martucci,[1] Douglas R. Worsnop,[2,3] and Colin O'Dowd[1]

Received 22 December 2011; revised 27 June 2012; accepted 3 July 2012; published 16 August 2012.

A High Resolution Time of Flight Aerosol Mass Spectrometer (HR-ToF-AMS) was evaluated for its ability to quantify submicron sea salt mass concentrations. The evaluation included both laboratory and field studies. Quantification of the sea salt signal in the HR-ToF-AMS was achieved by taking the $^{23}Na^{35}Cl^{+}$ ion as a surrogate for sea salt and then identifying a calibration scaling factor through a comparison with mono-disperse laboratory generated sea salt aerosol. Ambient sea salt concentrations calculated using this method agreed well with those obtained by ion chromatography of filter samples, following a 1:1 regression slope and a correlation coefficient R = 0.93. A key advantage of this AMS-based method is that it allows for high time resolution measurements of sea salt (5 min) along with the speciation of other chemical compounds, including primary organics contributing to sea spray. The high-time resolution sea salt measurement capability enabled the quantification of sea salt mass in both increasing and decreasing wind speed regimes up to 26 m s^{-1}. A mass flux source function was also derived and found to have a power law wind speed dependency with an exponent of 3.1 for increasing winds and 2.3 for decreasing winds. Comparison of the mass flux relationship in this study suggests that previous schemes based on the Monahan whitecap wind speed approach significantly over-estimate the submicron mass flux. Both the whitecap wind speed component and the differential whitecap aerosol productivity component of the source flux function contribute toward the over-estimation.

1. Introduction

Sea spray aerosol is an important component of the aerosol population in the marine environment, and given that 70% of the Earth's surface is covered by oceans, sea spray contributes significantly to the global aerosol budget [Vignati et al., 2010]. In addition, sea spray plays an important role in climate, with both direct [Mulcahy et al., 2008] and indirect radiative effects [O'Dowd et al., 1999]. In order to better understand and quantify these effects, detailed information on the chemical composition, the size distribution and the abundance is required. Until recently, sea spray was generally assumed to be composed predominantly of inorganic sea salt. However, recent findings [Facchini et al., 2008; O'Dowd et al., 2004] revealed a sometimes predominant organic fraction in submicron marine aerosol mass, with organic mass fraction enrichment in the spray reaching up to 80%. These observations prompted the development of a combined organic-inorganic sea spray source function for implementation in climate and chemical transport modelling studies [Gantt et al., 2011; O'Dowd et al., 2008; Vignati et al., 2010]. Model evaluation and verification, however, benefits from long-term ambient measurements and these measurements have historically derived from filter or

impactor studies with typical sampling periods of rv1 day for bulk mass, and rv7 days, for size resolved mass distributions in marine air. Such integrated measurements are more likely to miss higher temporal structure in the data signals, and as a result of this, peak concentrations are likely to be missed. An improvement was made by deploying near real time techniques such as Particle Into Liquid Samplers (PILS), which are capable of measuring the main inorganic ions along with soluble organics at a high time resolution [Sullivan et al., 2004; Weber et al., 2003] or Aerosol Mass Spectrometry techniques for the non-refractory aerosol composition measurements. Indeed, recent deployment of high temporal resolution aerosol mass spectrometry to chemically characterize marine organic aerosol has improved our understanding of primary marine organics and has revealed primary marine organic aerosol plumes at mass concentrations far higher than previously reported [Ovadnevaite et al., 2011]. Hitherto, there has been no equivalent measurement, in terms of temporal resolution, for primary sea spray leading to a lack of high resolution information on primary sea salt mass along with associated primary organic mass enrichment factors.

The High Resolution Time of Flight Aerosol Mass Spectrometer (HR-ToF-AMS) is designed to provide high time resolution measurements of aerosol chemical composition with spectral resolution that allows for distinguishing multiple ions at the same nominal mass to charge ratio (m/z) [DeCarlo et al., 2006]. Typically the AMS is operated at a vaporizer temperature of 600^{o}C, which is optimized for quantitative detection of non-refractory ambient aerosol species such as organics, sulphate, nitrate and ammonium. Since sea salt was expected to be refractory at these temperatures, its quantification with the AMS was assumed to be only possible at higher AMS vaporizer temperatures that were less favorable for quantification of the non-refractory species [Allan et al., 2004]. However, O'Dowd and Smith [1993] demonstrated that ambient sea salt starts to evaporate at temperatures just above 600^{o}C and almost fully evaporates at 650^{o}C, suggesting that the standard HR-ToF-AMS operation temperature could be sufficient to detect sea salt.

This study evaluates the suitability of deploying theHR-ToF-AMS to undertake quantitative sea salt measurements at close to standard operating conditions and applies the technique to determine the concentration of sea salt as a function of wind speed.

2. Experimental Setup for Ambient Air Measurements

The study was undertaken at the Mace Head Atmospheric Research Station located on the west coast of Ireland facing the North East Atlantic. Station details are found in O'Connor et al. [2008]. All aerosol instruments are located in the shore laboratory about 100 m from the coastline and 5 m above mean sea level. They are connected to the laminar flow community air sampling system, which is constructed from a 100 mm diameter stainless-steel pipe with the main inlet at 10 m above ground level. The performance of this inlet is described in Kleefeld et al. [2002].

The HR-ToF-AMS [DeCarlo et al., 2006] was used for chemical composition measurements and was routinely calibrated according to the methods described by Jimenez et al. [2003] and Allan et al. [2003]. The HR-ToF-AMS was connected to the main community sampling system retaining an iso-kinetic flow. A performance of this setup was tested with 2 scanning mobility particle

sizers (SMPSs) and 2 condensation particle counters (CPCs): one of each instrument was sampling from the main inlet directly and the second in front of the HR-ToF-AMS, differences between the measurements were found to be within the instruments uncertainty range (~10%). The HR-ToF-AMS measurements were performed with a time resolution of 5 min and a vaporizer current of 1.12 A (corresponding to a vaporizer temperature of ~650^{o}C). The net overall particle transmission and detection efficiency, expressed as the collection efficiency (CE), is dependent on the particle composition. Therefore, a composition dependent CE [Middlebrook et al., 2012] was applied for the measurement periods discussed in this study. CE ranged from 0.45 to 0.97. The default CE of 0.5 was deemed appropriate for _40% of the periods of interest and dominated particularly in continental air masses. A CE of ~1 corresponded to ~60% of the measurement period and was observed for both clean marine air masses (due to very acidic aerosol) and continental polluted air masses (due to high nitrate episodes). Since sea salt concentrations were low during non-marine periods the original composition dependent CE algorithm presented in the Middlebrook et al. [2012] study was used without including the sea salt. The effect of sea salt on aerosol CE was accounted for with a calibration factor, which comprised both the CE and relative ionization efficiency (RIE) of sea salt (see Section 3 for more details).

PM2.5 (particles, or particulate matter less than 2.5 μm in size where 2.5 μm correspond to the 50% collection efficiency size) aerosol samples were taken routinely every other day using an RP 2025 Dichotomous Sampler. The Sampler was installed at the same height as the community sampling duct. The filters from the dichotomous sampler were analysed using standard Ion Chromatography (IC) methods. Aerosol size distributions were measured using an SMPS. The SMPS system comprised of a differential mobility analyser (DMA, TSI model 3071), a condensation particle counter (TSI model 3010), and an aerosol neutralizer (TSI 3077). For the sizing purpose, particles were dried below 20% relative humidity. Hygroscopic properties of aerosol were measured using a Hygroscopic Tandem Differential Mobility Analyzer (HT-DMA), as described in Rader and McMurry [1986] and followed the European Supersite for Atmospheric Aerosol Research (EUSAAR) network standard configuration and deployment as summarized by Nilsson et al. [2009]. An aerosol particle growth factor (GF) at 90% relative humidity (RH), defined as the ratio of the particle diameter at RH = 90% to that at RH = 20%, was determined for dry size particles of 35, 50, 75, 110 and 165 nm.

The wind speed and direction was measured on the 10m tower by a Vector Instruments wind monitor (model W200P/ A100L). The coastal measurements have been extensively compared with the offshore wind data revealing a very good agreement [Gantt et al., 2011].

3. Experimental Setup for Laboratory and Sea Salt calibration

The HR-ToF-AMS was calibrated using sea salt aerosol generated from artificial seawater using SIGMA sea salt dissolved in deionized water. The solution was nebulized with a TSI atomizer (model 3076), and a DMA configured to generate a 300 nm monodisperse particle size distribution flow from the nebulized polydisperse flow, fed directly into the AMS inlet. Relative humidity in the sample line was maintained at about 65%.

The high resolution mass spectrum was measured and analysed using the standard high resolution AMS data analysis tool (PIKA v1.10h) [DeCarlo et al., 2006]. 36 high resolution ions contributed to the sea salt fragmentation pattern, but only 7 ions had a significant influence on the derived aerosol mass, namely $^{23}Na^{+}$, $^{35}Cl^{+}$, $^{35}Cl^{+}$, $^{23}Na^{35}Cl^{+}$ and isotopes $^{37}Cl^{+}$, $H^{37}Cl^{+}$, $^{23}Na^{37}Cl^{+}$. Two approaches were chosen to obtain the sea salt mass from the AMS measurements: approach (1) centered on adding up all sea salt ions to obtain a new high resolution sea salt "family", or ensemble, of ions using the data analysis tool and approach (2) centered on using only the $^{23}Na^{35}Cl^{+}$ ion fragment as the signature of sea salt. Inter-comparisons between these two different approaches to derive AMS sea salt mass with the known sea salt mass concentrations in the laboratory generated calibration particles were used to derive the scaling factors needed to obtain the quantitative AMS-derived sea salt concentrations. For the first approach, a scaling factor of 2.5 was found to be appropriate for this calibration. The scaling factor for the second approach was much larger, at 51, as only one ion was scaled. The scaling factors derived in these calibrations reflect a combined AMS detection efficiency for sea salt, which encapsulates the AMS collection efficiency and the relative ionization efficiency.

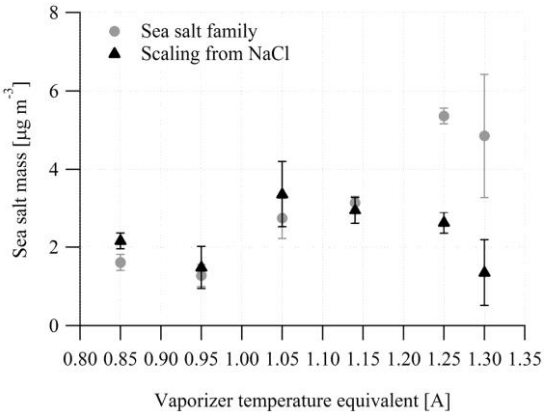

Figure 1. Sea salt detection dependence on the vaporizer temperature obtained for the nebulized artificial seawater. In this graph the temperature is presented as a vaporizer current in order to avoid discrepancies between the real heater temperature and one measured by a thermocouple. Error bars represent standard deviations.

Further investigation into the selected approaches revealed a high Na^{+} ion sensitivity to the instrument tuning. A significant proportion of sodium can become ionized thermally rather than by electron ionization. This "surface ionization" is undesirable because it produces positive ions in very large numbers and does not easily yield quantitative data [Allan et al., 2004]. However, by tuning the instrument's heater bias voltage (that is increasing it by 0.1–0.2 V above the normally used maximum value, until the area under the m/z 23 signal rapidly drops, but maintaining optimal signatures for other m/z signals) it is possible to prevent the thermally ionized ions from reaching the detector. Nevertheless, considering that Na^{+} has a significant contribution to the sea salt family, the surface ionization could affect a total sea salt quantification if the instrument tuning is not adjusted for the sea salt measurements.

HR-ToF-AMS mass concentrations were obtained by subtracting the general

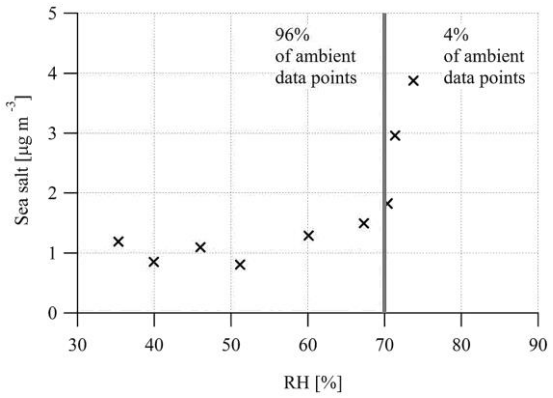

Figure 2. Sea salt detection dependence on the aerosol flow relative humidity obtained for the nebulized artificial seawater. For the comparison, grey zone represents 96% of relative humidity variations in the inlet during ambient measurements.

background mass spectrum (i.e., spectrum from aerosol-free carrier gas flow) from the total measured spectra (i.e., from the combined aerosol and gas flow). Although the majority of the gas was removed by differential pumping, providing vacuum down to 10^{-8} Torr, the carrier gas and a slow vaporization from the heater had to be accounted for. Thus, the aerosol beam was alternatively modulated every ~3 s to allow the measurement of both the combined carrier gas and particle mass spectra and the carrier gas-only mass spectra [DeCarlo et al., 2006]. Slowly evaporating compounds lead to high background mass spectra [Salcedo et al., 2010], which can, depending on the particular species be comparable to, or even higher than, the measurement signal, resulting in a low signal-to-noise ratio. In these studies, the sodium ion had a high background signal, even exceeding the measurement signal up to a factor of 10, concomitant with a large delay time. The sodium background signal evaporated completely only 12 h after aerosol flow termination, while Cl^+ and HCl^+ had shorter, but still significant, evaporation times of ~2 h. The slow timescale for evaporation of the Cl^+, HCl^+ and Na^+ ion signals suggests that these ions are most likely produced by the slow decomposition process associated with the oven surface. In contrast, the $^{23}Na^{35}Cl^+$ background signal was ~10 times lower than the measurement signal, and the evaporation delay time was less than 5 min (i.e., less than the selected averaging time-base of the instrument), indicating the efficient vaporization from the heater.

The test of the instrument's sea salt detection efficiency dependence on vaporizer temperature revealed that the exact fragmentation pattern could be slightly dependent on the heater temperature. For this study, the temperature is presented as a vaporizer current in order to avoid discrepancies between the real heater temperature and one measured by a thermocouple. The vaporizer currents used ranged from 0.85 A (~500^{o}C) to 1.3 A (~800^{o}C). The temperature effect on $^{23}Na^{35}Cl^+$ ion was different from what was anticipated: specifically, a high vaporizer current of 1.3 A negatively affected $^{23}Na^{35}Cl^+$ ion detection, as the signal intensity decreased (Figure 1). This could be explained by two processes: (1) an increase in the fragmentation of $NaCl^+$ ions due to the higher heater temperature, resulting in lower ion concentration and (2) an increase in an ion thermal velocity, which would result in a shorter time that ions spend in the detection region compared to the cooler temperatures associated with lower currents, thus, a decrease in detection [Allan et al., 2004]. In contrast, sodium ion intensity increased with increasing temperature, indicating that higher fragmentation of $NaCl^+$ ion and, partially, surface ionization [Allan et al., 2004] led to a higher Na^+ concentration (Figure 1).

The dependence of AMS sea salt detection efficiency on particle phase (or water content) was evaluated by sampling the highest purity sea salt as possible since even the smallest amount of organic matter internally mixed with sea salt may potentially affect particle behavior under

different relative humidities. Sea salt dissolved in deionized water was again nebulized, but in this experiment, the resulting aerosol flow was filtered to select only particles with a GF = 2.2 (i.e., the GF of pure sea salt particles). A nafion dryer (Perma Pure PD-200T) was then introduced between the HTDMA output and the HR-ToF-AMS inlet in order to regulate RH while concurrently measuring relative humidity of the flow and sea salt concentration at the same constant aerosol supply (in terms of size and number). This experiment revealed that the HR-ToF-AMS quantification depends on the particle phase for RH higher than 70% (Figure 2). The effect of humidity on AMS quantification of sea salt is similar to that previously reported for laboratory $(NH_4)_2SO_4$ particles [Middlebrook et al., 2012]. Previous studies [Matthew et al., 2008; Middlebrook et al., 2012] have shown that the AMS collection efficiency (CE) is dependent on particle phase such that dry particles bounce off the AMS vaporizer while wet particles are collected with unit efficiency. The phase dependent CE of $(NH_4)_2SO_4$, for example, changes sharply from 0.35 at RH < 80% to a CE of 1 at RH > 80%. If we assume the similar behavior for sea salt, the CE of sea salt is likely 1 at >75% RH, and 0.25 at RH < 70% (Figure 2). Accordingly, the sea salt relative ionization efficiency (RIE) can be determined from the scaling factor, which combines the CE (the net overall particle transmission and detection efficiency) and the RIE (the relative ionization efficiency of the species in interest relative to nitrate [Alfarra et al., 2004]) and is equal to (1/CE)*(1/RIE). Considering that CE = 0.25 at RH < 70%, RIE should be ~1.6. Whereas, NaCl+ RIE, could be determined using the $NaCl^+$ fraction in the total sea salt family (~4%), which would result in RIE ~2. Typically, the AMS ionization efficiency (IE) reflects vaporization, ionization, and detection efficiencies. However, vaporization and detection is similar across the m/z range, thus different RIE classes for inorganic and organic compounds arise from the differences in ionization. Yet these assumptions might not be applicable for the sea salt aerosol, as each of the sea salt ions could be affected to different extents by the vaporization and ionization and these effects can even offset each other. Taking all this into account, RIE numbers presented above should be taken more as guidance, but not the strict values. Moreover, calibration factors may be valid only for this particular instrument (with its particular tuning), thus, every instrument should be calibrated individually in order to derive its own sea salt quantification, or conversion, factor.

It should also be noted that the HR-ToF-AMS measurements at Mace Head are always accompanied by RH measurements within the inlet, immediately up stream of the instrument, and analysis of these data show that 96% of the aerosol entering the AMS were sampled at RH < 70%, suggesting that the Mace Head measurements of AMS-derived sea salt mass are, to a larger degree, free from humidity-driven artifacts.

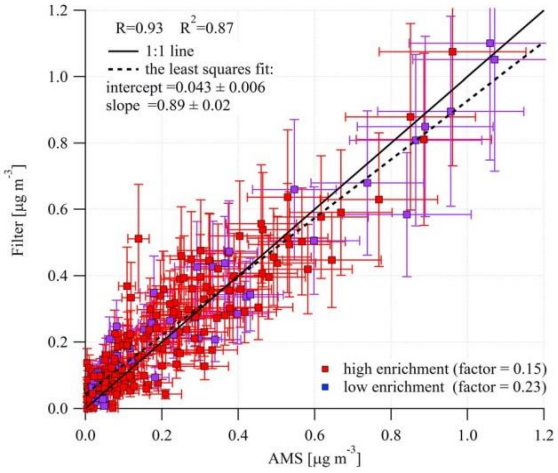

Figure 3. The comparison between the HR-ToF AMS and Ion chromatography sea salt measurements. Colors represent different factors applied for the periods of low and high organic enrichment, when deriving PM1 sea salt concentration from PM2.5 filter measurements. Error bars represent the IC and HR-ToF AMS measurement uncertainties.

The above mentioned laboratory tests suggest that second approach of scaling sea salt concentration using the single $^{23}Na^{35}Cl^+$ ion is more robust than the sea salt family approach. Moreover, exploring ambient origins of separate ions included in the possible sea salt ion family indicated that Na^+ and $NaCl^+$ seen by the HR-ToF-AMS come only from sea salt, while Cl^+ and HCl^+ also had significant sources in pollution aerosol as well as marine sources. This is consistent with previous studies [Chang and Allen, 2006; Salcedo et al., 2006], which reported that anthropogenic emissions of molecular chlorine during daylight hours readily photolyze and that the resulting atomic chlorine rapidly abstracts hydrogen from hydrocarbons, producing HCl, which in turn reacts with ammonia (NH_3), ultimately producing NH_4Cl. The latter can accumulate in fine particles and be fragmented in the HR-ToF-AMS as Cl^+ ion. Although the contribution from Cl^+ would be lower than that from HCl^+, it would still have an effect in polluted air masses. These implications pointed to an unavoidable need of assigning Cl^+ proportions arising from different sources to some ions without any other source than sea salt. Consequently, the best candidate seemed to be the $NaCl^+$ ion, having a single sea salt origin as well as the largest signal-to-noise ratio. Therefore, constraining the majority of the sea salt ions from the $NaCl^+$ ion would not have any advantage over the second method. Moreover, the latter is much easier to apply and gives consistent measurements. It should be noted; however, that in a marine air influenced by pollution, sea salt can undergo significant processing in terms of Cl displacement by nitric or sulfuric acid, then the sea salt mass derived using the aforementioned approach would not include the processed sea salt component. An extension of the approach could be developed, in principle, to quantify this processed component of sea salt; however, given that we only focus here on pristine marine air masses in N.E. Atlantic air, such an extension is beyond the scope of this work.

4. Comparison of Online and Off-Line Sea Salt Concentrations

Sea salt concentrations derived from the HR-ToF-AMS were compared with concentrations derived from the off-line filter analysis using standard ion chromatography methods. But because the HR-ToF-AMS measures PM1 particles (particles of 1 μm or less in size, where 1 μm corresponds to the 50% sampling efficiency cut-off size) and the routine filter measurements at Mace Head are performed on the PM2.5 particles, differences between absolute measured concentrations were expected, and indeed, found. Moreover, long-term observations at Mace Head indicated a varying ratio between PM1 and PM2.5 mass depending on the season, or more specifically, the enrichment of organics in sea spray. The PM1/PM2.5 percentage ratio ranges from 10 to 25% [Cavalli et al., 2004]. Therefore, different scaling factors were

applied for the periods of low and high organic enrichment, 0.23 and 0.15, respectively, when deriving PM1 sea salt concentration from the PM2.5 filter measurements. Scaling uncertainties were on the order of 25% and propagated into the total IC measurement uncertainties resulting ~32% overall uncertainty. A comparison between the AMS sea salt measurements, derived from $NaCl^+$ ion, and the PM1 filter sea salt concentration derived from the PM2.5 measurements is presented in Figure 3. The overall HR-ToF-AMS sea salt measurement uncertainty was found to be ~20% and encapsulated the following uncertainties: IE determination uncertainty (~10%); flow uncertainty (~0.5%); lens transmission together with NaCl evaporation from the heater uncertainty (~15%); and scaling uncertainty (~5%). The first two uncertainties were documented in the study of Bahreini et al. [2009] and are common for all species measured by the AMS, while the lens transmission, evaporation and scaling uncertainties were evaluated from the sea salt laboratory experiments presented in this study.

Good agreement between the off-line chemical analysis and the AMS sea salt measurements in the field samples supported the results from the laboratory calibrations. The majority (>70%) of the inter-comparison data-points agreed within 20% and the correlation coefficient, R, was equal to 0.93 and R^2 was 0.87. The scatter in the comparison may have arisen from both the AMS collection efficiency and the PM1 scaling factor selected as a function of season. In addition, ion chromatography results also depend on the signal strength and a low signal-to-noise ratio could lead to an overestimation of sea salt mass under low-concentrations conditions [Elbergali and Brereton, 1994].

On the other hand, the scaling factors derived in the laboratory calibrations would depend on the lens transmission of the particular instrument as there is some variation between specific aerodynamic lenses in different instruments [Bahreini et al., 2008; Liu et al., 2007; Zhang et al., 2004].

The expected isotope ratio between $^{23}Na^{35}Cl$ and $^{23}Na^{37}Cl$ is equal to 3.13 [de Laeter et al., 2003]. This ratio was, indeed, maintained in the AMS measurements for the comparison period presented above, providing further confidence in the correct sea salt detection.

5. Sea Salt Mass Dependency on Wind Speed

Two cases of elevated concentration sea salt plumes over North East Atlantic waters are presented in Figure 4, one occurring on the 8th November 2010 and the other on the 11th November 2010. The plumes were detected as the wind direction backed northerly into the clean sector at Mace Head (between 190^o–300^o) and the wind speed increased to a peak value of 20 m s^{-1} during the first plume and 26 m s^{-1} during the second plume.

Sea salt plumes registered by the AMS coincided with an increase in aerosol hygroscopicity from a typical sulfate GF of 1.6 to a GF of 2.2, which is characteristic of pure sea salt particles. As the measurements were undertaken during the low biological activity period, all other chemical compounds approached very low background "winter" concentrations (e.g., sulfate mass <190 ng m^{-3}; organic mass <60 ng m^{-3}; black carbon mass <10 ng m^{-3}; nitrate mass <17 ng m^{-3} and ammonium mass below the detection limit of 38 ng m^{-3}).

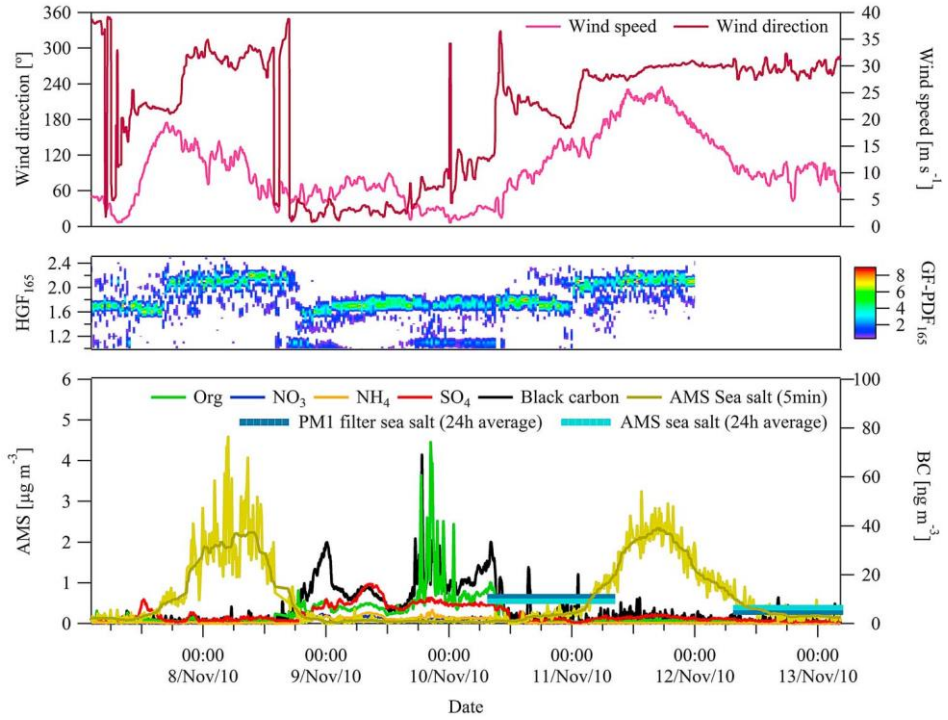

Figure 4. (top) Wind speed, wind direction observed for two sea salt plumes on 8th November 2009 and 11th November 2009. (middle) Hygroscopic growth factor for the corresponding period. (bottom) Five- minute and 24-h resolution sea salt mass derived from the HR-ToF-AMS and 24-h salt mass from the ion chromatography. Also shown are sulfate, nitrate, and organic masses from the AMS and black carbon mass from the Multi-Angle Absorption Photometer.

The AMS-derived sea salt mass increased and decreased with wind speed as expected. Although the maximum 5-min mass concentration exceeded 4.5 mg m^{-3}, in the first plume, the running mean peaked at about 2.2 mg m^{-3} while the running mean in the second plume peaked at about 2.4 mg m^{-3}.

Both plumes lasted ~30 h. The routine 24 h filter samples missed the plumes due to the sampling strategy employed at Mace Head (i.e., generally every second 24-h period); however, the off-line measurements still would not have captured the fine structure of the sea salt plumes, or the peak concentrations observed by the online AMS if they were run every 24 h period. The two off-line filter samples overlapped with the start and the end of the plume and are in close agreement with the 24 h AMS sea salt averages (Figure 4, bottom). The sea salt plume structure and peak concentrations are quite similar to the structure and concentrations found in the primary organic sea spray plumes observed during periods of high biological activity [Ovadnevaite et al., 2011].

The high time resolution measurements of sea salt mass enabled the quantification of sea salt mass as a function of increasing and decreasing wind speed as illustrated in Figure 5. Only the second sea salt plume was selected for further analysis due to its greater range of wind speed (i.e., up to 26 m s^{-1}); a higher degree of symmetry in the increasing and decreasing wind speed slopes; and a more stable clean-sector wind direction. Furthermore, this period was practically cloud and precipitation free with only sparse small, fair weather, cumulus cells with intermittent low levels of drizzle.

At the lowest wind speed encountered (i.e., <4 m s^{-1}) both relationships (for increasing and decreasing wind speed) converge on a background submicron sea salt mass concentration of 0.09 µg m^{-3}, and as wind speed increases, they follow a

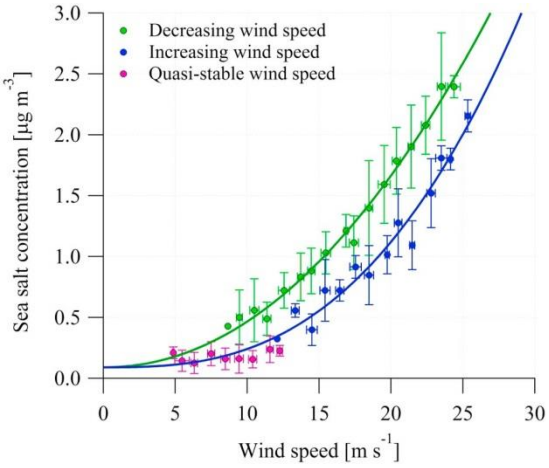

Figure 5. Sea salt wind speed–concentration relationships for increasing and decreasing wind speed history regimes: increasing is in dark blue; decreasing is in green. Purple represents quasi-stable wind speed conditions just after the decreasing wind speed regime (12:00 UTC 12th November– 12:00 UTC 13th November 2010). Five-minute data points are binned to the wind speed intervals equal to 1 m s^{-1}.

power law mass-concentration versus 10-m wind speed (U10) dependency, albeit with different exponents. For increasing wind speed, the power law exponent was higher (U2.8) than the decreasing wind speed power law exponent (U2.1). The net result indicates that mass concentrations measured during reducing wind speeds are significantly higher than those measured under increasing wind speeds.

The difference between concentration-wind speed relationships for increasing and decreasing wind speed histories is consistent with the observed whitecap coverage dependency on wave history: whitecap coverage increases with wave age under the same wind speed conditions [Callaghan et al., 2008; Sugihara et al., 2007], suggesting that an increase in the sea salt production flux due to a higher whitecap coverage under decreasing wind fields compared to increasing wind fields.

Submicron aerosol particles are expected to be uniformly mixed in the marine boundary layer [Lewis and Schwartz, 2004], thus an effective sea spray aerosol (SSA) production flux, F_{eff}, was estimated from the sea spray concentration (C) divided by a filling time (τ) and multiplied by the marine boundary layer height (H_{MBL}):

$$F_{eff} = \frac{C \times H_{MBL}}{\tau} \quad (1)$$

The atmospheric boundary layer height, derived from the ground-based LIDAR measurements using the Temporal Height Tracking (THT) algorithm [Haeffelin et al., 2012; Milroy et al., 2012], was found to be within the range of 720–1290 m above the ground level over the plume duration period, while τ was assumed to be the filling time (approximately 1.5–2 days). This method is known as the Statistical Wet Deposition Method for estimation production flux and is critically discussed in Lewis and Schwartz [2004] who conclude that this approach cannot provide any information on the wind speed dependence of the sea salt production flux since the sea salt particles measured are likely to be produced far away under conditions different from local conditions at the time of measurement. However, we contend that in this particular case, we can apply the approach to determine a production flux for the following reasons: the deep low-pressure system associated with this plume event formed over the North East Atlantic approximately 1.5–2 days before arriving at Mace Head and we take t, the filling time, not as the time since the last precipitation event as considered in Lewis and Schwartz [2004], but the time between the cyclone formation and subsequent arrival, in terms of connected flow, at Mace Head. Further, the local wind speed was representative of the upwind wind fields as obtained from NOAA Air Resources Laboratory for the 12:00 UTC 11 November 2010 (Figure 6).

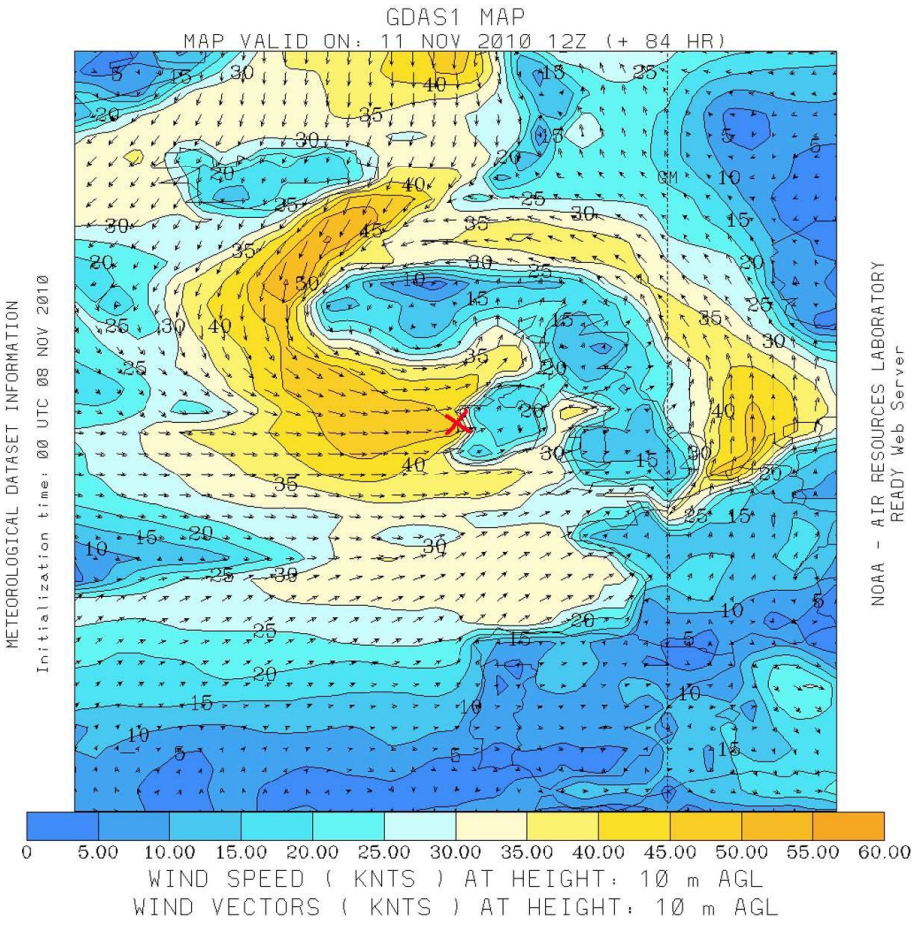

Figure 6. Wind speed field (in knots) for the 12:00 UTC 11 November 2010 obtained from the NOAA Air Resources Laboratory. Accordingly, the local wind speed measured at Mace Head was equal to 24.1 m s^{-1} (46.8 knots). It is in the rage of upwind wind speeds presented by NOAA (45–50 knots). Mace Head is marked in red.

Although dry deposition is assumed to be negligible for the submicron particles [Hoppel et al., 2002], it was taken into account and contributed 2–4% compared to the production flux. As mentioned, this period was practically cloud and precipitation free, which suggests that the wet-deposition and coalescence removal processes contributed to a similarly negligible removal flux. The resulting production flux is represented in Figure 7.

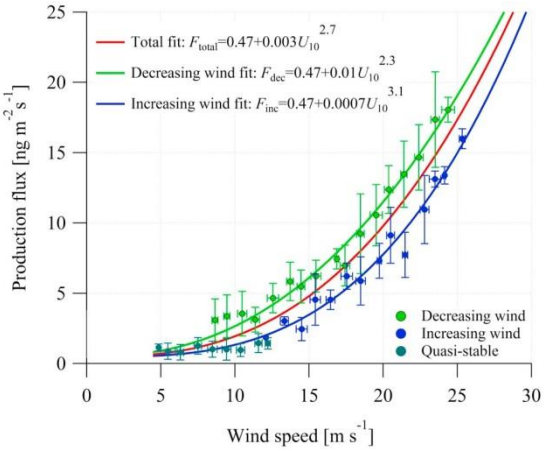

Figure 7. Sea spray production flux for increasing and decreasing wind speed history regimes. The intercept in the power function represents the starting aerosol flux at the onset of the whitecap, with the flux being 0 before the whitecap onset and making a step transition into minimum value after the onset.

Without differentiating between increasing and decreasing wind speed regimes, and taking all the data into a single function relationship, the wind speed dependence converges to $F = 0.47 + 0.003U_{10}^{2.7}$, which is closely in line with the refitted sea spray production flux formulation from the Geever et al. [2005] ambient measurements [O'Dowd et al., 2008]. Though, only the power exponent can be directly compared, as the

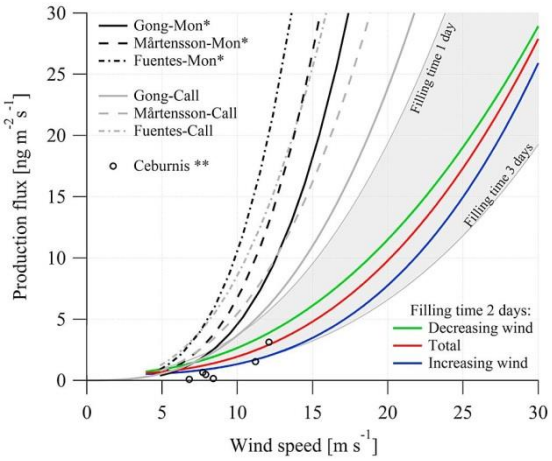

Figure 8. Production flux dependence on the wind speed. Colour lines represent the flux derivations from the AMS sea salt measurements at different wind speed regimes. Grey area represents the measured flux uncertainty due to the different time of filling. Black lines illustrate the fluxes based on Monahan and Muircheartaigh [1980] whitecap–wind speed relationship and derived from Gong [2003], Mårtenssonet al. [2003] and Fuentes et al. [2010] parameterizations. Grey lines represent the same parameterizations with the Callaghan et al. [2008] whitecap–wind speed relationship. One asterisk indicates that number flux presented in the original work was recalculated to the mass flux; two asterisks indicate sea salt fluxes calculated using data from Ceburnis et al. [2008].

coefficients would differ for a number flux (presented in Geever et al. [2005]) and a mass flux (presented in this study). Differentiating between increasing and decreasing wind speeds, the mass flux parameterizations are $F = 0.47 + 0.01U_{10}^{2.3}$ and $F = 0.47 + 0.0007U_{10}^{3.1}$, respectively. The intercept in the power function represents the starting aerosol flux at the onset of the whitecap, with the flux being 0 before the whitecap onset and making a step transition into minimum value after the onset. Assuming that the minimum wind speed needed for the onset of detectable white capping is approximately 3.7 m s^{-1} [Callaghan et al., 2008], the minimum aerosol flux would be ~0.68 ng $m^{-2}s^{-1}$. Taking this into account, the flux equation should be expressed as follows:

$$F(U_{10}) = \begin{cases} 0 & \text{if } U_{10} < 3.7\,\mathrm{m\,s^{-1}} \\ 0.47 + 0.003U_{10}^{2.7}, & \text{if } U_{10} \geq 3.7\,\mathrm{m\,s^{-1}} \end{cases} \quad (2)$$

A more detailed comparison with existing source functions derived from the whitecap method is presented in Figure 8. Unfortunately, the original function from Monahan et al. [1986] is mainly valid for the particles larger than those measured by the HR-ToF-AMS, thus a comparison of the above scheme focuses on submicron flux parameterizations of Gong [2003] and Mårtensson et al. [2003], both of which are based on Monahan's whitecap–wind speed relationship. These particular parameterizations are extensively used in large-scale models. The corresponding number flux was simulated for a particle size range directly comparable to the AMS measurement size range (D_p = 0.03–0.58 μm or vacuum aerodynamic diameter, as measured in the HR-ToF- AMS, $D_{va} \cong$ 0.05–1 μm) and converted the integrated number flux over this size range into a corresponding mass flux as a function of wind speed. This comparison revealed a significantly more sensitive mass flux prediction as a function of wind speed for the Gong [2003] and Mårtensson et al. [2003] functions compared to the function presented from this study. This suggests that these source functions over-predict the sea salt flux as a function of wind speed - an apparent over prediction supported the critical discussions in the recent de Leeuw et al. [2011] review paper, which suggests existing submicron number flux parameterizations appear to over predict boundary layer number concentrations compared to what is actually measured. Even, the most-recent whitecap - aerosol productivity scheme, derived by Fuentes et al. [2010], also tends to over-predict boundary layer mass concentrations (Figure 8) relative to the current study. It should be noted that the current study is the only study of the four

Table 1. Mass Concentrations at Two Wind Speeds (10 and 25 m s^{-1}) Derived From Different Parameterizations[a]

	Mass Concentration ($\mu g\ m^{-3}$)						
		Monahan's Whitecap–Wind Speed Relationship			Callaghan's Whitecap–Wind Speed Relationship		
Wind Speed	This Study (AMS)	Gong	Mårtensson et al.	Fuentes et al.	Gong	Mårtensson et al.	Fuentes et al.
10 m s^{-1}	0.3	0.8	1.1	1.7	0.6	0.9	1.3
25 m s^{-1}	2.6	15.9	23.4	37	6.6	9.8	15.4

[a]*Gong* [2003], *Mårtensson et al.* [2003], and *Fuentes et al.* [2010] aerosol production parameterizations applied with either *Monahan and Muircheartaigh* [1980] or *Callaghan et al.* [2008] whitecap–wind speed parameterization. Concentrations derived from the relationship presented in this study (equation (2)) are also shown. The boundary layer height of 1200 m and the filling time of 2 days were assumed for all calculations here.

presented here which is based on field measurements.

The mass flux calculations from the sea salt mass concentration involved the use of a filling time parameter τ, which determination from the air mass back trajectories could have had propagated some uncertainties into these calculations. Therefore, the grey area in Figure 8 represents the range of possible variations due to differences in τ. The largest reasonable filling time was assumed to be ~3 days (the typical lifetime of a submicron sea salt particle against precipitation scavenging [Hoppel et al., 2002]) and the shortest was equal to 1 day. The filling time, which could have led to a fair agreement with the parameterization by Gong [2003], was estimated to be less than 10 h, which is regarded as unrealistically short, particularly given the lack of precipitation and cloud processes to contribute to removal mechanisms.

There may be several reasons for the mass flux overestimation by the whitecap method: one relates is the whitecap area-to-wind speed parameterization; and another relates to the parameterization of aerosol number (or mass) productivity-to-whitecap area. The former parameterization has recently been improved on through analysis using digital image processing of sea-state photographs and removing the subjectivity in determining the intensity threshold that distinguishes whitecap from the surrounding water, along with the increased number of the averaging points [de Leeuw et al., 2011]. Results of this new parameterization were presented in the study by Callaghan et al. [2008] and with a power law fitting of the same data set reported by Goddijn-Murphy et al. [2011].

Taking into account an improved whitecap–wind speed relationship, we replaced the Monahan component with the Callaghan et al. [2008] whitecap scheme and found a reduced flux-to-wind speed dependency. The modified Gong-Callaghan, Mårtensson-Callaghan and Fuentes- Callaghan parameterizations, while leading to a much better agreement with our source function, still reside outside the range presented based on 1–2 days filling time (Figure 8).

PM1 mass flux was also evaluated in the gradient study by Ceburnis et al. [2008], while they didn't provide the separate sea salt mass flux in the original paper, it is presented in Figure 8. The data points fell into grey area encompassing the range of uncertainty of the wet deposition statistical method, but the power law fitting is limited to a small number of data points and a restricted wind speed range of 12 m s^{-1}.

In addition, the variation in the HR-ToF-AMS aerodynamic lens cut-off could have had an effect on the mass concentrations measured by the HR-ToF-AMS. Since the real lens transmission efficiency was not evaluated for this particular instrument, the sensitivity of the production flux to different assumed vacuum aerodynamic cut-offs applied for the modelled mass size distributions was tested. The typical HR-ToF-AMS aerodynamic lens cut-off of 1 μm (50% transmission efficiency for the particle vacuum aerodynamic

diameter, D_{va}, of 1 μm or mobility diameter, D_m, of 0.58 μm) is applied to the Gong-Callaghan parameterization and presented as the upper limit of the modelled flux (Figure 9), whereas a cut-off of 0.6 μm (D_m of 0.35 μm) reflects the lower limit. The range in between these limits represents intermediate cut-off sizes. Reducing the cut-off size brings the modelled flux closer to the one measured by the HR-ToF- AMS, but only the extreme case of 0.6 μm cut-off partially overlaps with the uncertainty range of the HR-ToF-AMS measurements; however, it still remains far from the most probable measured flux suggested by this study (solid red curve in Figure 9). Considering that originally the Gong- Callaghan parameterization was the closest to the measurements in this study, the case of the Gong-Callaghan parameterization with 0.6 μm cut-off reflects the lowest possible limit for the modelled fluxes. All other parameterizations based on the Monahan and Muircheartaigh [1980] whitecap parameterization would, therefore, be significantly above the uncertainty range of the measurements.

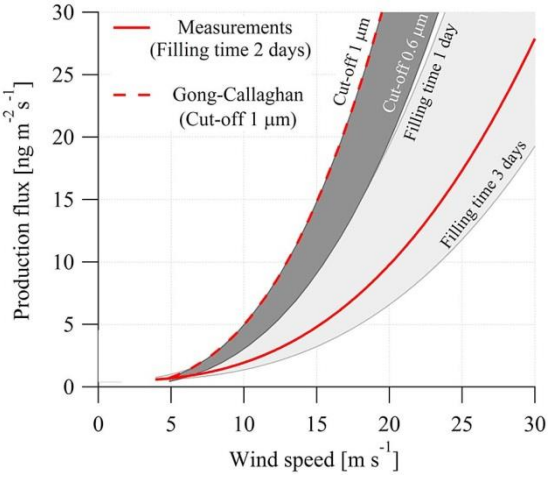

Figure 9. Production flux dependence on different vacuum aerodynamic size cut-offs assumed for the Gong-Callaghan parameterization. The dark grey area represents the uncertainty due to different cut-offs applied on the modelled mass flux distributions and the light grey area is the uncertainty of the production flux measured by the AMS (the same as in Figure 8). The most probable dependencies are presented in red.

Ultimately, the source flux must be able to explain observed concentrations; however, using the Gong [2003], Mårtensson et al. [2003] or Fuentes et al. [2010] scheme leads to peak concentrations of 15.9 μg m^{-3}, 23.4 μg m^{-3} and 37 μg m^{-3} respectively for the maximum wind speed of 25 m s^{-1} (Table 1). These mass concentrations are simply too high for submicron sea salt mass concentrations at the reported wind speed, having never been observed. The overestimation is between a factor of 3–10 depending which source function is used. A good level of confidence in the sea salt mass concentrations derived from the AMS has been demonstrated both for the overall AMS-IC intercomparison (Figure 3) and for this particular plume (Figure 4), thus the remaining differences could be explained by drawbacks in either whitecap–wind speed relationship or aerosol productivity versus whitecap parameterization. Some improvement is seen in the use of a more recent whitecap–wind speed relationship (Figure 9 and Table 1), leaving more improvement required in the aerosol productivity versus whitecap parameterization. It should be noted that while there are some differences between the AMS-derived mass and filter-derived mass measurements, they are far from a factor of 3, and even farther from a factor of 10.

6. Conclusions

A HR-ToF-AMS was tuned and calibrated to enable the quantification of submicron sea salt mass, which has not been achieved previously. The quantification was achieved by taking the $^{23}Na^{35}Cl^+$ ion as a surrogate for sea salt, corroborated by confirming a $^{37}Cl^+$ and $^{35}Cl^+$ isotope ratio of 3.13, and then identifying a calibration scaling factor through comparison with mono-disperse laboratory-generated

synthetic sea salt aerosol. The HR-ToF-AMS was deployed to make ambient sea salt measurements in clean air at Mace Head and the results from two notable sea salt plumes are reported. Peak sea salt mass concentrations exceeding 4 μg m^{-3} were encountered although running mean concentrations were of the order of 2.4 μg m^{-3} (corresponding to a wind speed of ~26 m s^{-1}). The mass concentration as a function of wind speed was found to follow a power law dependency on U_{10}; however, different exponents were observed for increasing and decreasing wind fields. Increasing winds led to a $U_{10}^{2.8}$ dependency while decreasing winds led to a $U_{10}^{2.1}$ relationship. One of the plumes was deemed suitable for extracting a mass flux source function. For the submicron aerosol mass flux–wind speed dependency, an exponent of 3.1 was found for increasing wind speeds and an exponent of 2.3 was found for decreasing wind speeds. Comparison to other source functions based on the Monahan wind speed–whitecap coverage suggested that existing source functions [e.g., Gong, 2003; Mårtensson et al., 2003; Fuentes et al., 2010] significantly over-estimate the source flux at all wind speeds below 25 m s^{-1}. Replacing the Monahan component of the source flux with the more recent Callaghan et al. [2008] whitecap–wind speed relationship brings the previous source functions closer to that presented in this study and based on the AMS measurements at Mace Head. However, we also conclude that the aerosol number, or mass, production parameterization as a function of whitecap coverage is also over-estimated.

Acknowledgments. This work was supported by the Science Foundation Ireland (grant 08/RFP/GEO1233), HEA-PRTLI4 Environment and Climate: Impact and Responses program, European Commission IP EUCAARI, EPA-Ireland, and the European Space Agency (Support To Science Element: Oceanflux Sea Spray Aerosol). We would also like to thank Adrian Callaghan (NUI Galway and Scripps Institution of Oceanography, UCSD), Jose-Luis Jimenez (University of Colorado at Boulder) and Damien Martin (NUI Galway) for the valuable comments and discussions.

References

Alfarra, M. R., et al. (2004), Characterization of urban and rural organic particulate in the lower Fraser valley using two aerodyne aerosol mass spectrometers, Atmos. Environ., 38(34), 5745–5758, doi:10.1016/j.atmosenv.2004.01.054.

Allan, J. D., J. L. Jimenez, P. I. Williams, M. R. Alfarra, K. N. Bower, J. T. Jayne, H. Coe, and D. R. Worsnop (2003), Quantitative sampling using an Aerodyne aerosol mass spectrometer - 1. Techniques of data interpretation and error analysis, J. Geophys. Res., 108(D3), 4090, doi:10.1029/2002JD002358.

Allan, J. D., et al. (2004), Submicron aerosol composition at Trinidad Head, California, during ITCT 2K2: Its relationship with gas phase volatile organic carbon and assessment of instrument performance, J. Geophys. Res., 109, D23S24, doi:10.1029/2003JD004208.

Bahreini, R., E. J. Dunlea, B. M. Matthew, C. Simons, K. S. Docherty, P. F. DeCarlo, J. L. Jimenez, C. A. Brock, and A. M. Middlebrook (2008), Design and operation of a pressure-controlled inlet for airborne sampling with an aerodynamic aerosol lens, Aerosol Sci. Technol., 42(6), 465–471, doi:10.1080/02786820802178514.

Bahreini, R., et al. (2009), Organic aerosol formation in urban and industrial plumes near Houston and Dallas, Texas, J. Geophys. Res., 114, D00F16, doi:10.1029/2008JD011493.

Callaghan, A., G. de Leeuw, L. Cohen, and C. D. O'Dowd (2008), Relationship of oceanic whitecap coverage to wind speed and wind history, Geophys. Res. Lett., 35, L23609, doi:10.1029/2008GL036165.

Cavalli, F., et al. (2004), Advances in characterization of size-resolved organic matter in marine aerosol over the North Atlantic, J. Geophys. Res., 109, D24215, doi:10.1029/2004JD005137.

Ceburnis, D., C. D. O'Dowd, G. S. Jennings, M. C. Facchini, L. Emblico, S. Decesari, S. Fuzzi, and J. Sakalys (2008), Marine aerosol chemistry gradients: Elucidating primary and secondary processes and fluxes, Geophys. Res. Lett., 35, L07804, doi:10.1029/2008GL033462.

Chang, S. Y., and D. T. Allen (2006), Chlorine chemistry in urban atmospheres: Aerosol formation associated with anthropogenic chlorine emissions in southeast Texas, Atmos. Environ., 40, suppl. 2, 512–523, doi:10.1016/j.atmosenv.2006.04.070.

DeCarlo, P. F., et al. (2006), Field-deployable, high-resolution, time-of-flight aerosol mass spectrometer, Anal. Chem., 78(24), 8281–8289, doi:10.1021/ac061249n.

de Laeter, J. R., J. K. Bohlke, P. De Bievre, H. Hidaka, H. S. Peiser, K. J. R. Rosman, and P. D. P. Taylor (2003), Atomic weights of the elements: Review 2000 - (IUPAC technical report), Pure Appl. Chem., 75(6), 683–800, doi:10.1351/pac200375060683.

de Leeuw, G., E. L. Andreas, M. D. Anguelova, C. W. Fairall, E. R. Lewis, C. O'Dowd, M. Schulz, and S. E. Schwartz (2011), Production flux of sea spray aerosol, Rev. Geophys., 49, RG2001, doi:10.1029/2010RG000349.

Elbergali, A. K., and R. G. Brereton (1994), Influence of noise, peak position and spectral similarities on resolvability of diode-array high- performance liquid-chromatography by evolutionary factor-analysis, Chemom. Intell. Lab. Syst., 23(1), 97–106, doi:10.1016/0169-7439(93) E0068-F.

Facchini, M. C., et al. (2008), Important source of marine secondary organic aerosol from biogenic amines, Environ. Sci. Technol., 42(24), 9116–9121, doi:10.1021/es8018385.

Fuentes, E., H. Coe, D. Green, G. de Leeuw, and G. McFiggans (2010), On the impacts of phytoplankton-derived organic matter on the properties of the primary marine aerosol–Part 1: Source fluxes, Atmos. Chem. Phys., 10(19), 9295–9317, doi:10.5194/acp-10-9295-2010.

Gantt, B., N. Meskhidze, M. C. Facchini, M. Rinaldi, D. Ceburnis, and C. D. O'Dowd (2011), Wind speed dependent size-resolved parameterization for the organic mass fraction of sea spray aerosol, Atmos. Chem. Phys., 11(16), 8777–8790, doi:10.5194/acp-11-8777-2011.

Geever, M., C. D. O'Dowd, S. van Ekeren, R. Flanagan, E. D. Nilsson, G. de Leeuw, and U. Rannik (2005), Submicron sea spray fluxes, Geophys. Res. Lett.,

32, L15810, doi:10.1029/2005GL023081.

Goddijn-Murphy, L., D. K. Woolf, and A. H. Callaghan (2011), Parameterizations and algorithms for oceanic whitecap coverage, J. Phys. Oceanogr., 41(4), 742–756, doi:10.1175/2010JPO4533.1.

Gong, S. L. (2003), A parameterization of sea-salt aerosol source function for sub- and super-micron particles, Global Biogeochem. Cycles, 17(4),1097, doi:10.1029/2003GB002079.

Haeffelin, M., et al. (2012), Evaluation of mixing-height retrievals from automatic profiling lidars and ceilometers in view of future integrated networks in Europe, Boundary Layer Meteorol., 143(1), 49–75, doi:10.1007/s10546-011-9643-z.

Hoppel, W. A., G. M. Frick, and J. W. Fitzgerald (2002), Surface source function for sea-salt aerosol and aerosol dry deposition to the ocean surface, J. Geophys. Res., 107(D19), 4382, doi:10.1029/2001JD002014.

Jimenez, J. L., et al. (2003), Ambient aerosol sampling using the Aerodyne Aerosol Mass Spectrometer, J. Geophys. Res., 108(D7), 8425, doi:10.1029/2001JD001213.

Kleefeld, C., C. D. O'Dowd, S. O'Reilly, S. G. Jennings, P. Aalto, E. Becker, G. Kunz, and G. de Leeuw (2002), Relative contribution of submicron and supermicron particles to aerosol light scattering in the marine boundary layer, J. Geophys. Res., 107(D19), 8103, doi:10.1029/2000JD000262.

Lewis, E. R., and S. E. Schwartz (2004), Sea Salt Aerosol Production: Mechanisms, Methods, Measurements and Models—A Critical Review, Geophys. Monogr. Ser., vol. 152, 413 pp., AGU, Washington, D. C., doi:10.1029/GM152.

Liu, P. S. K., R. Deng, K. A. Smith, L. R. Williams, J. T. Jayne, M. R. Canagaratna, K. Moore, T. B. Onasch, D. R. Worsnop, and T. Deshler (2007), Transmission efficiency of an aerodynamic focusing lens system: Comparison of model calculations and laboratory measurements for the Aerodyne Aerosol Mass Spectrometer, Aerosol Sci. Technol., 41(8), 721–733, doi:10.1080/02786820701422278.

Mårtensson, E. M., E. D. Nilsson, G. de Leeuw, L. H. Cohen, and H. C. Hansson (2003), Laboratory simulations and parameterization of the primary marine aerosol production, J. Geophys. Res., 108(D9), 4297, doi:10.1029/2002JD002263.

Matthew, B. M., A. M. Middlebrook, and T. B. Onasch (2008), Collection efficiencies in an Aerodyne Aerosol Mass Spectrometer as a function of particle phase for laboratory generated aerosols, Aerosol Sci. Technol., 42(11), 884–898, doi:10.1080/02786820802356797.

Middlebrook, A. M., R. Bahreini, J. L. Jimenez, and M. R. Canagaratna (2012), Evaluation of composition-dependent collection efficiencies for the aerodyne aerosol mass spectrometer using field data, Aerosol Sci. Technol., 46, 258–271, doi:10.1080/02786826.2011.620041.

Milroy, C., et al. (2012), An assessment of pseudo-operational ground- based light detection and ranging sensors to determine the boundary-layer structure in the coastal atmosphere, Adv. Meteorol., 18,

929080, doi:10.1155/2012/929080.

Monahan, E. C., and I. O. Muircheartaigh (1980), Optimal power-law description of oceanic whitecap coverage dependence on wind-speed, J. Phys. Oceanogr., 10(12), 2094–2099, doi:10.1175/1520-0485(1980)010<2094:OPLDOO>2.0.CO;2.

Monahan, E. C., D. E. Spiel, and K. L. Davidson (1986), A model of marine aerosol generation via whitecaps and wave disruption, in Oceanic White- caps and Their Role in Air-Sea Exchange Processes, edited by E. C. Monahan and G. MacNiocaill, pp. 167–174, D. Reidel, Dordrecht, Netherlands.

Mulcahy, J. P., C. D. O'Dowd, S. G. Jennings, and D. Ceburnis (2008), Significant enhancement of aerosol optical depth in marine air under high wind conditions, Geophys. Res. Lett., 35, L16810, doi:10.1029/2008GL034303.

Nilsson, E., E. Swietlicki, S. Sjogren, J. Londahl, M. Nyman, and B. Svenningsson (2009), Development of an H-TDMA for long-term unattended measurement of the hygroscopic properties of atmospheric aerosol particles, Atmos. Meas. Tech., 2(1), 313–318, doi:10.5194/amt-2-313-2009.

O'Connor, T. C., S. G. Jennings, and C. D. O'Dowd (2008), Highlights of fifty years of atmospheric aerosol research at Mace Head, Atmos. Res., 90(2–4), 338–355, doi:10.1016/j.atmosres.2008.08.014.

O'Dowd, C. D., and M. H. Smith (1993), Physicochemical properties of aerosols over the Northeast Atlantic: Evidence for wind-speed related submicron sea-salt aerosol production, J. Geophys. Res., 98(D1), 1137–1149, doi:10.1029/92JD02302.

O'Dowd, C. D., J. A. Lowe, M. H. Smith, and A. D. Kaye (1999), The relative importance of non-sea-salt sulphate and sea-salt aerosol to the marine cloud condensation nuclei population: An improved multi-component aerosol-cloud droplet parametrization, Q. J. R. Meteorol. Soc., 125(556), 1295–1313, doi:10.1002/qj.1999.49712555610

O'Dowd, C. D., M. C. Facchini, F. Cavalli, D. Ceburnis, M. Mircea, S. Decesari, S. Fuzzi, Y. J. Yoon, and J. P. Putaud (2004), Biogenically driven organic contribution to marine aerosol, Nature, 431(7009), 676–680, doi:10.1038/nature02959.

O'Dowd, C. D., B. Langmann, S. Varghese, C. Scannell, D. Ceburnis, and M. C. Facchini (2008), A combined organic-inorganic sea-spray source function, Geophys. Res. Lett., 35, L01801, doi:10.1029/2007GL030331.

Ovadnevaite, J., C. O'Dowd, M. Dall'Osto, D. Ceburnis, D. R. Worsnop, and H. Berresheim (2011), Detecting high contributions of primary organic matter to marine aerosol: A case study, Geophys. Res. Lett., 38, L02807, doi:10.1029/2010GL046083.

Rader, D. J., and P. H. McMurry (1986), Application of the tandem differential mobility analyzer to studies of droplet growth or evaporation, J. Aerosol Sci., 17(5), 771–787, doi:10.1016/0021-8502(86)90031-5.

Salcedo, D., et al. (2006), Characterization of ambient aerosols in Mexico City during the MCMA-2003 campaign with Aerosol Mass Spectrometry:

Results from the CENICA Supersite, Atmos. Chem. Phys., 6, 925–946, doi:10.5194/acp-6-925-2006.

Salcedo, D., T. B. Onasch, A. C. Aiken, L. R. Williams, B. de Foy, M. J. Cubison, D. R. Worsnop, L. T. Molina, and J. L. Jimenez (2010), Determination of particulate lead using aerosol mass spectrometry: MILAGRO/ MCMA-2006 observations, Atmos. Chem. Phys., 10(12), 5371–5389, doi:10.5194/acp-10-5371-2010.

Sugihara, Y., H. Tsumori, T. Ohga, H. Yoshioka, and S. Serizawa (2007), Variation of whitecap coverage with wave-field conditions, J. Mar. Syst., 66(1–4), 47–60, doi:10.1016/j.jmarsys.2006.01.014

Sullivan, A. P., R. J. Weber, A. L. Clements, J. R. Turner, M. S. Bae, and J. J. Schauer (2004), A method for on-line measurement of water-soluble organic carbon in ambient aerosol particles: Results from an urban site, Geophys. Res. Lett., 31, L13105, doi:10.1029/2004GL019681.

Vignati, E., M. C. Facchini, M. Rinaldi, C. Scannell, D. Ceburnis, J. Sciare, M. Kanakidou, S. Myriokefalitakis, F. Dentener, and C. D. O'Dowd (2010), Global scale emission and distribution of sea-spray aerosol: Sea-salt and organic enrichment, Atmos. Environ., 44(5), 670–677, doi:10.1016/j.atmosenv.2009.11.013.

Weber, R., et al. (2003), Intercomparison of near real time monitors of PM2.5 nitrate and sulfate at the U.S. Environmental Protection Agency Atlanta Supersite, J. Geophys. Res., 108(D7), 8421, doi:10.1029/ 2001JD001220.

Zhang, X., K. A. Smith, D. R. Worsnop, J. L. Jimenez, J. T. Jayne, C. E. Kolb, J. Morris, and P. Davidovits (2004), Numerical characterization of particle beam collimation: Part II integrated aerodynamic-lens–nozzle system, Aerosol Sci. Technol., 38(6), 619–638, doi:10.1080/02786820490479833.

Nitrogenated and Aliphatic Organic Vapours as Possible Drivers for Marine Secondary Organic Aerosol Growth

Manuel Dall'Osto[1,5], Darius Ceburnis[1], Ciaran Monahan[1], Douglas R. Worsnop[2,3], Jakub Bialek[1], Markku Kulmala[2], Theo Kurtén[2], Mikael Ehn[2], John Wenger[4], John Sodeau[4], Robert Healy[4] and Colin O'Dowd[1].

[1] *School of Physics and Centre for Climate and Air Pollution Studies, Ryan Institute, National University of Ireland Galway, University Road, Galway, Ireland*

[2]*Department of Physics, FI-00014 University of Helsinki, Finland.*

[3]*Aerodyne Inc., Massachusetts, Boston, USA.*

[4] *Department of Chemistry and Environmental Research Institute, , University College Cork, Ireland.*

[5]*now at: Institute of Environmental Assessment and Water Research, Consejo Superior de Investigaciones Científicas (CSIC), C/ LLuis Solé i Sabarís S/N 08028 Barcelona, Spain (manuel.dallosto@gmail.com)*

Abstract

Measurements of marine aerosol chemistry, using state-of-the-art mass spectrometry, as well as aerosol microphysics, hygroscopicity and cloud condensation nuclei (CCN) activity where undertaken during new particle growth events. The events were detected in air advecting over North East (NE) Atlantic waters during the EUCAARI Intensive Observation Period in June 2008 at Mace Head, Ireland. During these growth events, the aerosol mass spectrometers illustrated increases in accumulation mode aerosol phase nitrogenated and aliphatic compounds thought to condense from the gas phase. Since the composition changes observed in the accumulation mode occurred simultaneously to the growth of the accumulation, Aitken and nucleation modes, the growth of both the nucleation mode and the Aitken mode is attributed to the condensation of these species. Nitrogenated compounds like amines are also plausible candidates in the nucleation process, as suggested by quantum mechanics calculations. It is also plausible that amides and organic nitrites, also identified by the mass spectromemters, are possible candidate chemical compounds, suggesting that multiple types of chemical species may be contributing. Given that these open ocean aerosol formation and growth events occur in very clean polar marine air masses, we suggest that the organic compounds responsible for particle formation and growth are mainly of biogenic origin. Despite increasing the particle number concentration, the initial effect is to suppress hygroscopicity and CCN activity.

1. Introduction

Nucleation is a significant source of new aerosol particles; and their subsequent particle production and growth can increase the cloud condensation nuclei (CCN) population in the global atmosphere [e.g., *Kulmala et al.,* 2004; *Spracklen et al.,* 2008]. However, its importance in marine air has not been clearly established. New particle production has been most extensively studied in North East Atlantic marine air masses arriving at the Mace Head Atmospheric Research Station. Those events studied in the clean marine air have been almost exclusively coastal, or tidal-driven events produced as macro algae are exposed to the atmosphere. Iodo-compound emissions have been related to these coastal nucleation events [*O'Dowd et al.,* 1998, 2002]. By contrast, this study focuses on the occurrence of open ocean events as opposed to coastal events. In remote marine environments new particle formation events have only occasionally been observed [*Koponen et al.,* 2002; *Heintzenberg et al.,* 2004, *Ehn et al.* 2010]. The aforementioned studies point to marine boundary layer particle production while one event reported by *Covert et al.,* [1996] was attributed to entrainment of free tropospheric air. By analyzing 7 years of continuous SMPS measurements taken at the Mace Head coastal station, recently *O'Dowd et al.* [2010] found that open ocean new particle production and growth events occur more frequently than previously thought during periods of high oceanic productivity in NE Atlantic waters. For the first time, events were identified during which a recently formed nucleation mode (about 10-15 nm diameter) was observed to grow into an Aitken mode (about 50 nm diameter) over periods of up to 48 hours [O'Dowd et al., 2010]. Ehn et al. [2010] reported the first off-shore observations of four purely open ocean new particle formation events detected in the North

Atlantic region, consistent with the studies obtained by the analysis of the data from the Mace Head station [*Dall'Osto et al.* 2010, *O'Dowd et al.* 2010] and ruling out any coastal influence.

Despite extensive research focused on an intriguing climate–marine ecosystem feedback system the chemical species forming and growing new marine aerosol particles have remained elusive. Initial theories [*Charlson et al.* 1987] suggested dimethylsulphide (DMS)-derived sulphuric acid, and to a lesser degree, methane sulphonic acid (MSA), could be responsible for the formation and growth of new particles in marine air.

While MSA has been successfully measured in accumulation mode of the marine aerosol [*Andreae et al.*, 1990, *Barnes et al.*, 2006, *Zorn et al.* 2008], this has yet to be corroborated in terms of the critical growth stages of cluster to nucleation and Aitken mode sizes. Inorganic species such as sulphuric acid (SA) and iodine oxides can typically explain the nucleation of stable clusters of the order of 1 – 1.5 nm in size; however, condensable organic vapours are required to grow clusters into aerosol particles and CCN for the marine boundary layer [*Vuollekoski et al.* 2008].

Thus, there is a missing source of secondary organic aerosol which accounts for the stabilisation of clusters and their subsequent growth into aerosol particles. One of the most important questions to address is what organic species drives the growth of nucleated clusters into nucleation mode (5-20 nm) particles and ultimately into Aitken (30-100 nm) and accumulation (100-250 nm) mode particles where they potentially contribute to the marine CCN population. Modelling studies have postulated that SOA resulting from oceanic isoprene emissions explains the growth of new particles into CCN sizes [*Meskhidze et al.* 2006]; however, this source of SOA has been ruled out based on unrealistically-high isoprene emission fluxes in the initial study [*Arnold et al.* 2009].

Clarke et al. [1998] linked a nucleation event on the Pacific Ocean after precipitation to naturally produced DMS but the measurements, combined with dynamic modeling, showed additional unknown gases were posited to have induced a nucleation process.

More recently, relevant concentrations of dimethyl- and diethylammonium salts (DMA^+ and DEA^+) were measured in submicrometer marine aerosol collected over the ocean during periods of high biological activity in clean air masses [Facchini et al. 2008, Sorooshian et al. 2009] and were attributed to SOA formation processes. These salts comprised 11% of the water-soluble SOA mass fraction and 35% of the water soluble organic nitrogen fraction – no information was attained on water insoluble nitrogen species. MSA was, however, found to represent the largest mass fraction of water soluble SOA.

In summary, while sulphate, MSA, and various organic species, have been quantified in the accumulation mode, this does not elucidate which species are involved in the early-stage growth since, particularly for organics, many organics are thermodynamically unstable in 10 nm sized particles but stable in 100 nm particles. This study follows the investigation of nucleation mode growth events in the NE Atlantic marine boundary layer presented by O'Dowd et al. [2010]. We present detailed physical and chemical properties of the marine aerosols during such events. The experiment was part of the EUCAARI Intensive Observing Period, a 4-week campaign to measure aerosol physical, chemical and optical properties, atmospheric structure, and cloud

microphysics was conducted from mid-May to mid-June, 2008 [Dall'Osto et al. 2010].

2. Methods

2.1 Location

The Mace Head Atmospheric Research Station is located in Connemara, County Galway on the Atlantic Ocean coastline of Ireland at 53° 19'36"N, 9° 54'14"W and offers a clean oceanic sector from 190° through west to 300°. Air is sampled at 10 m height from a main tower community sampling duct positioned at 80-120 m from coast line depending on tide. More information about the station can be found in O'Connor et al., [2008]. Meteorological records show that on average, over 60% of the air masses arrive at the station in the clean sector [Jennings et al., 2003]. Air mass classification is achieved first by wind sector at Mace Head with only wind direction within 200° to 290° being regarded as clean marine in origin. Secondly, soot carbon mass is used as an air mass tracer with only periods with mass loadings less than 50 ng m^{-3} being accepted as clean marine levels. If there is any ambiguity over particular cases, a range of gas phase tracers such as CO and H-CFCs can be utilized [Cavalli et al. 2004]. Finally, and once the marine air periods are filtered, the air mass is categorized according to standard meteorological air mass classifications and in terms of air mass type arriving at Mace Head using NOAA HYSPLIT air mass 5-day back trajectories. Figure 1 illustrates a polar marine (*mP*) air mass arriving at Mace Head. Polar marine air 5 days prior to arrival at Mace Head typically is located 60°-70°N (between Greenland and Canada) and 45°-60°W prior to advection south-east over the North Atlantic. This is representative of the typical air masses in which these events are detected. Figure 1 also shows Chlorophyll-A concentrations taken from the NASA MODIS satellite platform during the month of measurements. The open ocean production and growth events described here were all associated with *mP* air masses. The measurements are interpreted in conjunction with quantum chemistry simulations of evaporation rates of possible nucleating species.

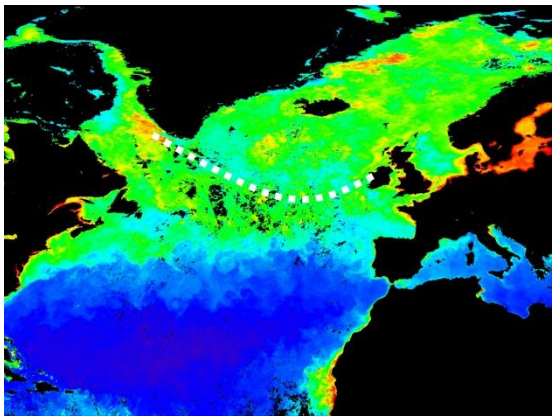

Figure 1. Air mass back trajectories for polar marine air (ending at 12 UTC 5th June 2008, time period concomitant with the nucleation event reported in Figure 2a) imposed on MODIS chlorophyll-a sea-water concentration map for 15th May – 15th June 2008.

2.2 Instrumentation

2.2.1 Real-time physical instrumentation

Aerosol size distributions were measured with a TSI nano-Scanning Mobility Particle Sizer covering dry particle sizes from 3.5 nm to 20 nm and a TSI Scanning Mobility Particle Sizer covering dry particle sizes from 15 nm to 550 nm. More information on the different types of aerosol size distributions encountered during the May-June EUCAARI intensive field study can be found elsewhere [Dall'Osto et al. 2010, Dall'Osto et al. 2011a]. Total particle concentrations at sizes larger than 3 and 10 nm diameter were sampled using a TSI Condensation Particle Counter (CPC) 3025A and 3010, respectively. Hygroscopic properties of aerosol were

measured using a Hygroscopic Tandem Differential Mobility Analyzer (H-TDMA), as described in Nilsson et al., [2009]. Growth factors (GFs) were quantified at relative humidities between 40% and 90%. GFs are determined for dry size particles of 35, 50, 75, 110 and 165 nm [Dall'Osto et al. 2010]. Cloud condensation nuclei (CCN) concentration was determined using a Droplet Measurements Technology CCN counter [Lance et al., 2006] operated at supersatuations of 0.1%, 0.25%, 0.5% and 1%. Basic meteorological parameters such as wind speed, direction, relative humidity, atmospheric pressure, precipitation, global radiation, UV-radiation are measured at the 10 m height level, with some duplication at 22 m.

2.2.2 Real-time chemical instrumentation

Two on-line aerosol mass spectrometers were operated at the measurement site, an ATOFMS (Model 3800-100, TSI, Inc.) and a HR-ToF-AMS (Aerodyne Research, Inc.). The ATOFMS collects bipolar mass spectra of individual aerosol particles between 200 nm and 3 μm in vacuum aerodynamic diameter size [Su et al. 2004]. The ATOFMS collected about 600,000 single particle positive and negative mass spectra during the EUCAARI intensive field study [Dall'Osto et al. 2010]. The TSI ATOFMS dataset was imported into YAADA (Yet Another ATOFMS Data Analyzer) and single particle mass spectra were grouped with Adaptive Resonance Theory neural network, ART-2a [Song et al. 1999]. Twenty ATOFMS clusters were obtained, some of which described natural (sea salt, dust) and anthropogenic aerosols [Dall'Osto et al. 2010]. A unique ART-2a ATOFMS cluster (cluster Org-N) describing a number of open ocean nucleation events was composed of about 1,800 single particle mass spectra (0.7% of the total sampled) and it is presented for the first time in this study.

The HR-ToF-AMS [DeCarlo et al., 2006] focuses aerosol particles in the size range 50-600 nm quantitatively onto a hot surface (~600 °C) using an aerodynamic lens assembly [Jayne et al., 2000, Canagaratna et al. 2007]. Non-refractory particle components flash-evaporate on the hot surface; the evolving vapour is electron impact (70 eV) ionized and the ions are transported into an orthogonal extraction ToF-MS for high-resolution mass analysis. The instrument provides quantitative mass loading information on non-refractory components using a well characterised series of calibrations and error estimations. The HR-ToF-AMS [DeCarlo et al., 2006] was deployed in the standard configuration, taking both mass spectrum (MS) and particle time of flight (pToF) data. The MS mode was run in "V-mode" with a mass resolution of up to 3000 m/Δm alternatively with a "W-mode" by using a second reflectron, which increases resolution to 6000 m/Δm but decreases sensitivity by approximately one order of magnitude. The instruments were calibrated and data obtained here were validated by comparing with other aerosol measurements [Dall'Osto et al. 2010].

Black carbon mass was measured using both a McGee Scientific Aethalometer AE-16 and a Multi-Angle Absorption Photometer (MAAP).

2.3 Quantum Chemistry Simulations

Recent experimental studies of nucleations occurring in continental areas have observed an enhancement in the ternary nucleation rate in the presence of amines [Berndt et al., 2010; Erupe et al., 2010]. Amines have also been shown to contribute to particle growth [Wang et al., 2010a, b]. Computational studies predict particulate amine levels may be enhanced relative to ammonia, despite the much lower atmospheric concentrations of

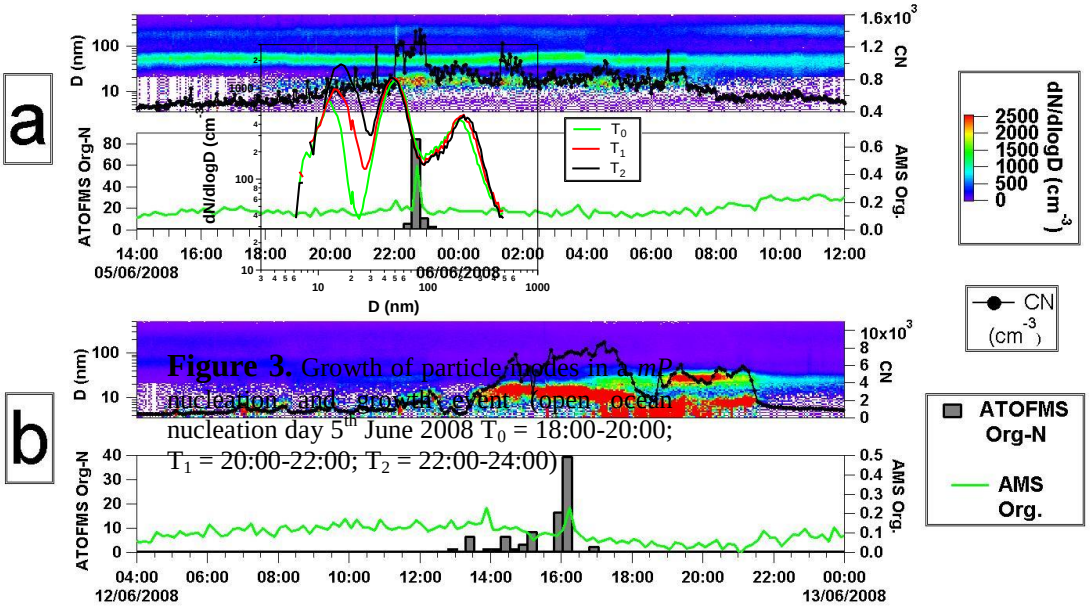

Figure 3. Growth of particle modes in a *mP* nucleation and growth event (open ocean nucleation day 5th June 2008 T_0 = 18:00-20:00; T_1 = 20:00-22:00; T_2 = 22:00-24:00)

Figure 2. Aerosol size distributions contour plots for two open ocean growth events. A recently formed 10-20 nm nucleation mode is detected at Mace Head at 22:00 hours for the first case (a) and 14:00 for the second case (b). Shown also is the total condensation nuclei particle concentration. Below each size distribution plot is the temporal trends of ATOFMS cluster Org-N particle counts and AMS Org. mass concentrations (micrograms m^{-3}) concentrations coinciding with the appearance of the growing nucleation mode (see Section 3.2).

amines [Barsanti et al., 2009; Kurten et al., 2008].

Aliphatic amines and MSA are important emissions in the marine environment [Facchini et al. 2008, Sorooshian et al. 2009]. Bzdek et al. [2011] reported that dimethylaminium methanesulfonate salts are preferred over ammonium methanesulfonate salts. The presence of alkyl amines and MSA could potentially promote open ocean nucleation and growth through a reduction of vapor evaporation rates.

In order to test this, quantum mechanics calculations were carried out. Briefly, all calculations were performed using the Turbomole program suite and the RI-MP2 method with the frozen-core approximation. Evaporation rates of different clusters to each other, rather than in computing quantitatively reliable absolute evaporation rates, were compared. For calculating the collision rate, pure-liquid densities were used for sulfuric acid, MSA and DMA monomers and the pure sulfuric acid and MSA dimmers. Simulating SA, DMA and MSA vapours, the concentration of SA+DMA+MSA clusters was calculated for different formation pathways.

3. Results

3.1 Detection of open ocean nucleation events

During the field study [Dall'Osto et al. 2010] we detected four open ocean particle production events in polar marine air masses (*mP*), lasting about 3-12 hours. As an example, the two events with the highest particle number concentrations are reported in Figure 2 as contour plot of the aerosol size distributions measured during the selected events. A significant nucleation mode is observed at sizes between 10 and 20 nm, indicative of a recent open ocean new particle formation event [O'Dowd et al. 2010]. In addition, this nucleation mode is observed to grow over time scales of several hours. In fact, size distributions extracted (Figure 3) at the beginning of the plume, mid-plume and end of the plume period illustrate that

the nucleation, Aitken, and Accumulation mode are all under-going growth with the largest modal-growth observed in the nucleation mode as it grows at a rate of 3.5 nm per hour from 11 nm to 20 nm. During this particular event (Figure 2a, Figure 3), the total number concentration (D>10 nm) increased from about 500 cm^{-3} to about 1500 cm^{-3}, accounting for an increase of ~200% in the total aerosol population. Further analysis of the Mace Head data set reveals regular occurrence of these events extending even as long as 48 hours and possessing a seasonality trend with peak frequency of occurrence in May and minimum in November to February [O'Dowd et al. 2010]. Cluster analysis of 6,578 hourly aerosol size distributions over the year 2008 (75% data coverage) identified three size distributions representative of different stages of open ocean production and growth events and revealed such events occurring 32.6% of the time in NE Atlantic air [Dall'Osto et al. 2011a]. This relatively high frequency of event occurrence confirms that these events are an important source of secondary aerosol particles in clean marine air, at least over the NE Atlantic. It is important to note that one nucleation event of this type was detected with the ATOFMS also during open ocean measurements taken on board of the research vessel Celtic Explorer [Dall'Osto et al. 2011b], although only in this study full chemical and physical properties are presented.

3.2 Aerosol chemical characterisation during open ocean formation and growth events

The ATOFMS measurements revealed unique organic nitrogen features in its mass spectra of individual particles coincident with the appearance of the open-ocean nucleation mode. The average positive and negative ion mass spectra of this particle type, labeled as Org-N are shown in Figure 4a and exhibit peaks due to hydrocarbon organic fragments at m/z 12 (C), m/z 27 (C_2H_3), m/z 36 (C_3), m/z 39 (C_3H_3) as well as oxidized organic species (C_2H_3O at m/z 43). Inorganic species can be found at m/z 23 (Na), m/z 39 (K) and m/z -95 (CH_3SO_3), m/z -97 (HSO_4). Specific organic nitrogen peaks

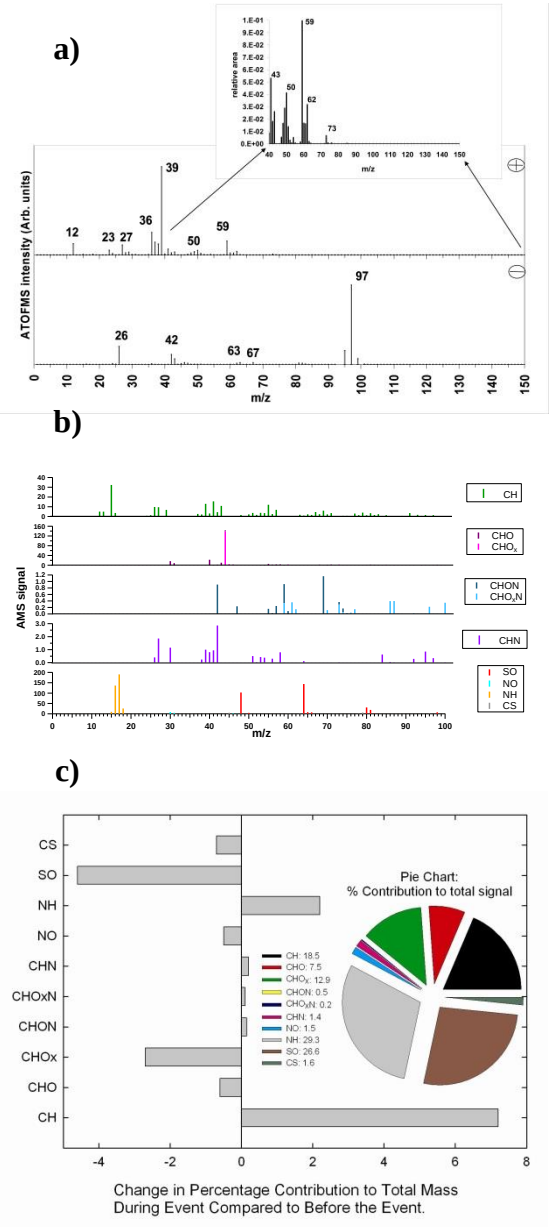

Figure 4. (a) ATOFMS and (b) AMS Aerosol Mass Spectra during the periods of nucleation mode detection; (c) Change in species percentage contribution to total mass during the event compared to before the event and percentage contribution of species to total AMS signal during the event.

at m/z -26 (CN) and -42 (CNO), as well as m/z 59 and m/z 73 [Angelino et al. 2001], are key features of this ATOFMS particle type which dominates the average mass spectra collected during nucleation events. As indicated in Figure 2a-b, the Org-N particle type is clearly coincident with the appearance of the nucleation mode and its subsequent growth.

The ATOFMS mass spectrum is qualitative in that the intensities of the mass spectral peaks are not directly proportional to the component mass but are dependent on the particle matrix, the coupling between the laser and the particle and the shot-to-shot variability of the laser [Dall'Osto et al. 2006]. However, the ATOFMS can provide quantitative information on particle number as a function of composition providing a measure of all particle components and can be used to assess mixing state. The ATOFMS provides information on the abundance of different types of aerosol particles as a function of particle size with high time resolution. Three other ATOFMS ART-2a particle types were classified before and during the events, named NaCl cluster (showing mainly NaCl peaks), K-Sulphate cluster (Potassium and Sulphate) and OC-K-Sulphate (Organic carbon, Potassium and Sulphate) [Dall'Osto et al. 2010]. Whilst clusters NaCl and K-Sulphate decreased during the open ocean nucleation event (from 15% to 8%; from 63% to 59%, respectively), cluster OC-K-Sulphate was found to increase (from 22% to 24%). These findings support an additional source of organic material condensing on the existing aerosols.

Without treating the ATOFMS data with ART-2a analysis, the same conclusion can be drawn by averaging all the raw positive and raw negative single particles ATOFMS mass spectra detected before (about 1,800) and during (about 1,800) the event. Figure 5 shows positive and negative ATOFMS spectral differences for periods during event minus period before event. Peaks above the horizontal line represent components more abundant in during the open ocean nucleation; below the line are those with greater abundance before the event. During the open ocean nucleation event, higher peak areas for m/z 27, m/z 37, m/z 39, m/z 50 (all organic peaks mainly due to CH families) and m/z 59 and m/z 73 (organic nitrogen peaks) can be seen. In the negative mass spectra, higher values for m/z -26 (CN) and m/z -42 (CNO) dominates. Instead, higher peak areas for other compounds (NaCl, MSA and Sulphate) can be seen below the horizontal line. Higher values for peak areas generally associated with elemental carbon (EC, m/z -36 (C_3), m/z 12 (C), m/z 36(C_3)) were also found.

a)

The V-mode HR-ToF-AMS data were analyzed using a separate high-resolution spectra toolbox known as PIKA to determine the chemical formulas contributing to distinct m/z ratios [De Carlo et al. 2006]. Quantitative analysis of the aerosol chemical composition using the HR-ToF-AMS shows (Figure 4b) a dominant fraction of hydrocarbon-like organic aerosol at m/z 39 (C_3H_3), m/z 41 (C_3H_5), m/z 43 (C_3H_7), m/z 55 (C_4H_7) representing 18.5% (Figure 4c) of the total signal (equating to 46% of the organic signal). Increased signals can also be seen for NH, and amine families (CHN with peaks at m/z 58 C_3H_8N, m/z 84 $C_5H_{10}N$ and m/z 95 C_6H_9N) as well as other organo-nitrogen (CHO_xN with m/z 59 C_2H_5NO, m/z 69 C_3H_3NO and m/z 86 $C_3H_4NO_2$) ones [Farmer et al. 2010, Figure SI 4].

Table 1 shows that whilst there is a total AMS signal increase of 36.7%, this is not reflected in all the species but only in hydrocarbon and nitrogen containing organic aerosols, as well as nitrogen peaks (NH). By taking the difference in

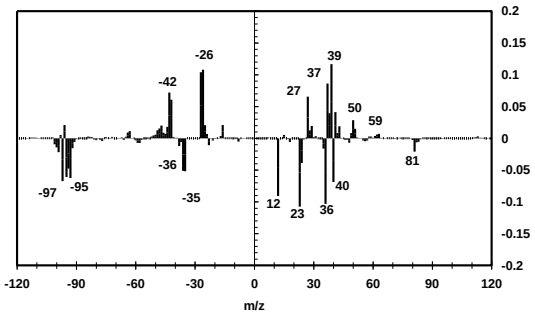

Figure 5. Plot illustrating the differences observed for the average positive and negative ion ATOFMS spectra detected before and during the nucleation period. The peaks above the horizontal line represent components more abundant during the open ocean nucleation; below the line are those with greater abundance before the event.

individual species percentage contribution to the total AMS signal, during the event compared to before the event, (Table 1 and Figure 4c), increased contributions were identified for CH (7.2%) and NH (2.3%) as well as for organo-nitrogen classes; whilst decreased contributions are identified for SO (-4.6%) and oxidised OA (-0.6% and -2.7% for CHO and CHO_x respectively). The dominance of the hydrocarbon-like contribution to SOA enhancement is seen readily in Figure 4c. For example, the percentage contribution of CH to the total signal increases from 11.3% before the event to 18.5% during the event, representing a 64% increase in the relative contribution of CH to the total signal during the event.

Amide compounds detected with ATOFMS were recently suggested to be formed through the following dehydration reaction between carboxylic acids and amines [Pratt et al. 2009]. Nitroalkanes and amides were generated by mechanisms of progressive oxidation of primary aliphatic amines [Vehkamäki et al. 2006]. Whilst amine compounds have been previously linked with aerosol formation and growth in continental sites, ATOFMS and AMS data herein presented shows also amide compounds cannot be excluded in the marine aerosol growth process although we do not have yet a proposed mechanism for its formation.

In summary, the indirect evidence for the participation of marine nitrogen-containing organic gases in the growth of nucleation mode (5-20 nm) particles is the direct presence of nitrogen-containing and hydrocarbon-like organics in larger submicron particles simultaneously detected with the ATOFMS and the AMS. The deployment of such instruments to measure the chemical composition of growing ultrafine particles has been measured previously, although in different environments. Using an AMS, Zhang et al. [2004] were able to show that the composition of the growing particles (33-60 nm in a vacuum aerodynamic diameter or about 18-33 nm in physical diameter) was predominantly sulphuric acid during the earliest observable stages of formation events in the urban area of Pittsburgh. Also using an AMS in Hyytiala, a forested site in southern Finland, Allan et al. [2006] were also able to distinguish with an AMS the grown particles in the <100 nm regime several hours after an event, confirming that the particles were principally organic in composition. By using an ATOFMS, Creamean et al. [2011] measured the aerosol chemistry during new particle formation events at a remote rural Sierra Nevada mountain site, showing an enrichment of amines in the particle phase.

However, to our knowledge this is the first study where simultaneous AMS and ATOFMS measurements have been taken to study particle formation events. Whilst the ATOFMS measures coarse particles with aerodynamic diameter > 100 nm, the AMS can detect particles with lower diameter (down to 50 nm), although with lower efficiency [Su et al. 2004, Canagaratna et al. 2007]. In this study, it is likely that the composition of coarse particles is affected by product of condensation and coagulation processes occurring during open ocean nucleation events, hence providing indirect evidence. Finally it is worth to mention that direct

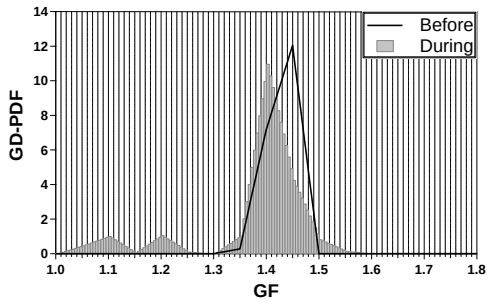

Figure 6. Change in aerosol hygroscopic aerosol growth for 75 nm particles, measured by the TDMA before and during the growth event.

measurement of the role of aminium salt formation in atmospheric nanoparticle growth are also currently possible by using the Thermal Desorption Chemical Ionization Mass Spectrometer (TDCIMS) and Ultrafine Hygroscopicity Tandem Differential Mobility Analyzers [Smith et al., 2010].

3.3 Aerosol hygroscopicity and CCN properties during open ocean formation and growth events

The nitrogenated and aliphatic vapors would be expected to be non-water soluble leading to a negative impact on water uptake by the growing particles and their resultant CCN activity. Hygroscopic growth, or water uptake factor, measured as an increase in equilibrium diameter between 30% and 90% relative humidity (determined by a HTDMA) and their cloud nucleating ability as determined by the CCN counter operating a supersaturations of 0.1%, 0.25%, 0.5% and 1% were evaluated prior to and during the growth events. Average lognormal fitting of open ocean nucleation event aerosol size distribution (Figure 3)

Table 1. Difference in AMS mass spectra signal contributions from different species before and after the growth events.

Species	Total signal Before event (% in bracket)	Total signal During event (% in bracket)	Diff signal (in %)	diff % of total signal
CH	103 (11.4)	229 (18.5)	121.4	7.2
CHO	73.8 (8.1)	92.7 (7.5)	25.6	-0.6
CHO_x	141.5 (15.6)	158.3 (12.9)	12.1	-2.7
CHON	3.5 (0.4)	6.6 (0.5)	90.8	0.15
CHO_xN	1.3 (0.1)	2.8 (0.2)	113.3	0.1
CHN	11.1 (1.2)	17.4 (1.4)	56.8	0.2
NO	18.3 (2.0)	18.6 (1.5)	1.8	-0.5
NH	245 (27.0)	360.5 (29.3)	0.1	2.2
SO	283.3 (31.2)	327.7 (26.6)	15.7	-4.6
CS	19.9 (2.2)	18.2 (1.5)	-8.8	-0.7
TOTAL	900.7 (100)	1231.2 (100)	36.7	0

showed a nucleation mode at 16.1±25nm (other two modes at 47±20nm and 208±18nm, respectively). The growth-factor of the pre-existing aerosol (at sizes of 75 nm) decreased from 1.45 to 1.40 accompanied by the appearance of two low-solubility externally-mixed aerosol types with growth-factors between 1.15 and 1.20 (Figure 6). Whilst a similar pattern was seen at smaller (35 nm) and larger sizes (165 nm), the more evident shift towards lower GF was seen for particle size bins at 50, 75 and 110nm. This trend is consistent with the organic vapour condensing on the existing, and larger, soluble aerosol thereby reducing its solubility (lower GF). A similar but more extreme change was observed in the CCN activity, where notable reductions in CCN concentrations are observed during the event, despite an increase in total particle concentration from ~900 cm^{-3} to ~5,000 cm^{-3} (Figure 2b). Specifically, there is a 55% decrease in CCN at 1% supersaturation from 321 cm^{-3} to 176 cm^{-3}, extending to a 60% decrease at 0.1% from 169 cm^{-3} to 102 cm^{-3}. However, not only the increase in particulate hydrocarbons but also the reduction of the sulphate mass fraction (Figure 4c) could be linked to the reduction in CCN activity.

4. Discussion and conclusion

This study focuses on open ocean new-particle formation events detected during the intensive EUCAARI field study conducted at Mace Head in May-June 2008. Real time chemical composition data of marine aerosols were acquired with state-of-the-art techniques, including HR-ToF-AMS and ATOFMS. The chemical composition of the accumulation mode particles during such events was found to show an enhanced fraction of nitrogenated and aliphatic compounds. Since the two particle mass spectrometer do not measure particles in the range 5-20nm, we can only state that the accumulation mode chemical species detected in increased concentrations during the growth were also likely to be involved in the growth process of the nucleation mode, and perhaps even initial nucleation. The basis for this is that it is reasonable to assume the chemical composition changes observed in the growing accumulation mode particles results from condensation since all modes are growing simultaneously, and further, the condensing species is likely to be the same across all modes. In essence, the results indicate that N-containing organic species appear to be a key component in the formation and/or growth of marine aerosol particles. The ATOFMS shows specific markers such as m/z 59 and m/z 73 and other carbonaceous ion associated with amines [Angelino et al. 2001, Pratt et al. 2009]. The AMS also shows an enhancement of ion categories of NH, CH, CHN, CHO_xN and CHON. Given that the AMS mass spectra results from major molecular fragmentation, it is not known at this stage if NH and CH originates from ammonium and/or aliphatic compounds or nitrogenated organic compounds. However, the simultaneous detection of the other AMS ion categories (CHN, CHO_xN) supports the suggestion that nitrogenated organic ion families are detected with the ATOFMS. A role of amines in the initial stages of nucleation is also compatible with the reported quantum mechanic calculations. Amine-containing clusters were extremely strongly bounded and unlikely to evaporate, in line with the study of Loukonen et al. [2010] and Bzdek et al. [2011]. Sulphur compounds were not found to increase; supporting quantum chemical simulation showing particle formation via sulphur species is unlikely [Pirjola et al. 2000; Pirjola and Kulmala, 2001]. With regards the organic nitrogen species involved in the open ocean events, the AMS mass spectra show some peaks with at least one oxygen atom in each fragment. Thus amines are not the

only possible chemical compounds, as amides and organic nitrites are also consistent with the AMS observations. It is interesting that the ATOFMS spectra suggest amines and/or aliphatic nitrogen. The two particle mass spectrometers are not necessarily inconsistent, and suggest that multiple types of chemical species are present.

Despite increasing the particle number concentration, the initial effect is to suppress hygroscopicity and CCN activity. Those open ocean nucleation events originated in the clean marine sector, therefore it is likely that the organic compounds responsible for particle formation and growth are mainly of biogenic origin. These particle production and extended growth events occur predominantly in maritime polar and maritime Arctic air masses.

Future work should aim to evaluate more carefully the molecular-level composition of candidate chemical compounds involved in the open ocean nucleation events.

Acknowledgements

This work was funded by the European Commission Framework Programme 6 EUCAARI Integrated Project, Ireland Higher Education Authority Programme for Research in Third Level Institutes - Cycle 4, Science Foundation Ireland,and the Irish Environmental Protection Agency.

References

Allan, J. D., Alfarra, M. R., Bower, K. N., Coe, H., Jayne, J. T., Worsnop, D. R., Aalto, P. P., Kulmala, M., Hyötyläinen, T., Cavalli, F., and Laaksonen, A.: Size and composition measurements of background aerosol and new particle growth in a Finnish forest during QUEST 2 using an Aerodyne Aerosol Mass Spectrometer, Atmos. Chem. Phys., 6, 315-327, doi:10.5194/acp-6-315-2006, 2006

Andreae, M.O. (1990), Ocean-atmosphere interactions in the global biogeochemical sulfur cycle, Mar. Chem., 30 (1-3), 1-29.

Angelino, S.; Suess, D. T.; Prather, K. A. Formation of aerosol particles from reactions of secondary and tertiary alkylamines: Characterization by aerosol time-of-flight mass spectrometry. Environ. Sci. Technol. 2001, 35 (15), 3130–3138.

Arnold, S. R., Spracklen, D. V., Williams, J., Yassaa, N., Sciare, J., Bonsang, B., Gros, V., Peeken, I., Lewis, A. C., Alvain, S., and Moulin, C.: Evaluation of the global oceanic isoprene source and its impacts on marine organic carbon aerosol, Atmos. Chem. Phys., 9, 1253-1262, doi:10.5194/acp-9-1253-2009, 2009

Barnes, I., J. Hjorth, and N. Mihalopoulos (2006), Dimethyl sulfide and dimethyl sulfoxide and their oxidation in the atmosphere, Chem. Rev., 106 (3), 940-975.

Barsanti, K. C., McMurry, P. H., and Smith, J. N.: The potential contribution of organic salts to new particle growth, Atmos. Chem. Phys., 9, 2949-2957, doi:10.5194/acp-9-2949-2009, 2009

Berndt, T., Stratmann, F., Sipila, M., Vanhanen, J., Petaja, T., Mikkil a, J., Gruner, A., Spindler, G., Lee Mauldin III, R., Curtius, J., Kulmala, M., and Heintzenberg, J.: Laboratory study on new particle formation from the reaction OH + SO2: influence of experimental conditions, H2O vapour, NH3 and the amine tert-butylamine on the overall process, Atmos. Chem. Phys., 10, 7101–7116, doi:10.5194/acp-10-7101-2010, 2010.

Bzdek, B. R., Ridge, D. P., and Johnston, M. V.: Amine exchange into ammonium bisulfate and ammonium nitrate nuclei, Atmos. Chem. Phys., 10, 3495-3503, doi:10.5194/acp-10-3495-2010, 2010

Bzdek, B. R., Ridge, D. P., and Johnston, M. V.: Reactivity of methanesulfonicacid salt clusters relevant to marine air, J. Geophys. Res.-Atmos., 116, D03301,doi:10.01029/02010JD015217, 2011.

Canagaratna, M. R., Jayne, J. T., Jimenez, J. L., Allan, J. D., Alfarra, M. R., Zhang, Q., Onasc, T. B., Drewnick, F., Coe, H., Middlebrook, A., Delia, A., Williams, L. R., Trimborn, A. M., Northway, M. J., DeCarlo, P. F., Kolb, C. E., Davidovits, P. and Worsnop D. R.: Chemical and microphysical characterization of ambient aerosols with the aerodyne aerosol mass spectrometer, Mass Spectrom. Reviews, 26, 185-222, 2007.

Cavalli,F., M.C. Facchini, S. Decesari, M. Mircea, L. Emblico, S. Fuzzi, D. Ceburnis, Y.J. Yoon and C.D. O'Dowd, J.-P. Putaud and A. Dell'Acqua, Advances in characterization of size resolved organic matter in marine aerosol over the North Atlantic, J. Geophys. Res, doi:10.1029/2004JD0051377, 2004.

Charlson, R.J., J.E. Lovelock, M.O. Andreae and S.G. Warren, Oceanic phytoplankton, atmospheric sulphur, cloud albedo and climate, Nature 326, 655-661, 1987.

Clarke, A. D., Davis, D., Kapustin, V. N., Eisele, F., Chen, G., Paluch, I., Lenschow, D.,

Bandy, A. R., Thornton, D., Moore, K., Mauldin, L., Tanner, D., Litchy, M., Carroll, M.

A., Collins, J., and Albercook, G.: Particle Nucleation in the Tropical Boundary Layer and Its Coupling to Marine Sulfur Sources, Science, 282, 89-92,10.1126/science.282.5386.89, 1998.

Covert, D. S., V. N. Kapustin, P. K. Quinn, and T. S. Bates (1996), Physical properties of marine boundary layer aerosol particles of the mid Pacific in relation to sources and meteorological transport, J. Geophys. Res., 101, 6919–6930, doi:10.1029/95JD03068

Creamean JM, Ault AP, Ten Hoeve JE, Jacobson MZ, Roberts GC, Prather KA. Measurements of Aerosol Chemistry during New Particle Formation Events at a Remote Rural Mountain Site. Environ Sci Technol. 2011 Oct 1;45(19):8208-16.

Dall'Osto, M., R. M. Harrison, D. C. S. Beddows, E. J. Freney, M. R. Heal and R. J. Donovan (2006). "Single-particle detection efficiencies of aerosol time-of-flight mass spectrometry during the North Atlantic marine boundary layer experiment." Environmental Science & Technology 40(16): 5029-5035.

Dall'Osto, D. Ceburnis, G. Martucci, J. Bialek, R. Dupuy, S. G. Jennings, H. Berresheim, J. C. Wenger, J. R. Sodeau, R. M. Healy, M. C. Facchini, M. Rinaldi, L. Giulianelli, E. Finessi, D. Worsnop, and C. D. O'Dowd, Aerosol properties associated with air masses arriving into the North East Atlantic during the 2008 Mace Head EUCAARI intensive observing period: an overview Atmos. Chem. Phys., 10, 1–23, 2010, doi:10.5194/acp-10-1-2010

Dall'Osto, M., Monahan, C., Greaney, R., Beddows, D. C. S., Harrison, R. M., Ceburnis, D., and O'Dowd, C. D.: A statistical analysis of North East Atlantic (submicron) aerosol size distributions, Atmos. Chem. Phys., 11, 12567-12578, doi:10.5194/acp-11-12567-2011, 2011a.

Dall'Osto, M., J. D. Allan, P. I. Williams, J. Crosier, H. Coe, G. Mc. Figgans, S. Decesari, R.M. Harrison and C. O'Dowd. Open ocean mass spectrometry characterization of Natural and Anthropogenic Aerosols over the North East Atlantic –JGR-Atmosphere, under revision, 2011b

DeCarlo, P. F., J. R. Kimmel, A. Trimborn, M. J. Northway, J. T. Jayne, A. C. Aiken, M. Gonin, K. Fuhrer,T. Horvath, K. S. Docherty, D. R. Worsnop and J. L. Jimenez. "Field-deployable, high-resolution, time-of-flight aerosol mass spectrometer." Analytical Chemistry 78(24): 8281-8289. 2006

Ehn, M., Vuollekoski, H., Pet ¨ aj ¨ a, T., Kerminen, V.-M., Vana, M., Aalto, P. P., de Leeuw, G., Ceburnis, D., Dupuy, R., ODowd, C. D., and Kulmala, M.: Growth rates during coastal and marine new particle formation in western Ireland, J. Geophys. Res., 115, D18 218, doi:10.1029/2010JD014292, 2010

Erupe, M. E., Viggiano, A. A., and Lee, S.-H.: The effect of trimethylamine on atmospheric nucleation involving H2SO4, Atmos. Chem. Phys. Discuss., 10, 27673–27693, 10 doi:10.5194/acpd-10-27673-2010, 2010.

Facchini, M.C., Decesari, S., Rinaldi, M., Carbone, C., Finessi, E., Mircea, M., Fuzzi, S., Moretti, F., Tagliavini, E., Ceburnis, D., O'Dowd, C.. Important source of marine secondary organic aerosol from biogenic amines. Environ. Sci. Technol. 42 (24), 9116–9121. doi:10.1021/es8018385. 2008

Farmer, D.K., A. Matsunaga, K.S. Docherty, J.D. Surratt, J.H. Seinfeld, P.J. Ziemann, and J.L. Jimenez. Response of the Aerosol Mass Spectrometer to organonitrates and organosulfates and implications for field studies. Proceedings of the National Academy of Sciences of the USA, 107, 6670-6675, 2010 DOI: 10.1073/pnas.0912340107

Heintzenberg, J., W. Birmili, A. Wiedensohler, A. Nowak, and T. Tuch (2004), Structure, variability and persistence of the submicrometre marine aerosol, Tellus, Ser. B., 56, 357-367.

Jennings, S. G., Kleefeld, C., O'Dowd, C. D., Junker, C., Gerard Spain, T., O'Brien, P., Roddy, A. F., and O'Connor, T. C.: Mace Head Atmospheric Research Station-characterization of

aerosol radiative parameters, Boreal Environ. Res., 8(4), 303–314, 2003.

Koponen, I., A. Virkkula, R. Hillamo, V.-M. Kerminen, and M. Kulmala (2002), Number size distributions and concentrations of marine aerosols: Observations during a cruise between the English Channel and the coast of Antarctica, J. Geophys. Res., 107, 4753, doi:10.1029/2002JD002533.

Kulmala, M., Vehkamaki, H., Petaja, T., Dal Maso, M., Lauri, A., Kerminen, V. M., Birmili, W., and McMurry, P. H. () Formation and growth rates of ultrafine atmospheric particles: a review of observations, J. Aerosol Sci., 35, 143–176, 2004.

Kulmala, M., K. E. J. Lehtinen, and A. Laaksonen, Cluster activation theory as an explanation of the linear dependence between formation rate of 3nm particles and sulphuric acid concentration, Atmos. Chem. Phys., 6, 787-793, 2006

Kulmala, M., Asmi, A., Lappalainen, H. K., Carslaw, K. S., Pöschl, U., Baltensperger, U., Hov, Ø., Brenquier, J.-L., Pandis, S. N., Facchini, M. C., Hansson, H.-C., Wiedensohler, A., and O'Dowd, C. D.: Introduction: European Integrated Project on Aerosol Cloud Climate and Air Quality interactions (EUCAARI) – integrating aerosol research from nano to global scales, Atmos. Chem. Phys., 9, 2825-2841, doi:10.5194/acp-9-2825-2009, 2009.

Kurtén, T., Loukonen, V., Vehkamäki, H. and Kulmala, M.: Amines are likely to enhance neutral and ion-induced sulfuric acid-water nucleation in the atmosphere more effectively than ammonia, Atmos. Chem. Phys., 8, 4095-4103, 2008.

Lance, S., Medina, J., Smith, J. N., and Nenes, A.: Mapping the operation of the DMT Continuous Flow, CCN Counter, Aerosol Sci. Technol., 40, 1–13, doi:10.1080/02786820500543290, 2006.

Meskhidze, N. and Nenes, A. Phytoplankton and Cloudiness in the Southern Ocean, Science, 314 , 1419-1423, 2006

Nilsson, E., Swietlicki, E., Sjogren, S., L¨ondahl, J., Nyman, M., and Svenningsson, B.: Development of an H-TDMA for longterm unattended measurement of the hygroscopic properties of atmospheric aerosol particles, Atmos. Meas. Tech., 2, 313–318,doi:10.5194/amt-2-313-2009, 2009.

O'Connor, T. C., Jennings, S. G., and O'Dowd, C. D.: Highlights from 50 years of Aerosol Measurements at Mace Head, Atmos.Res., 90, 338–355, doi:10.1016/j.atmosres.2008.08.014, 2008.

O'Dowd, C. D., M. Geever, M. K. Hill, M. H. Smith, and S. G. Jennings (1998), New particle formation: Nucleation rates and spatial scales in the clean marine coastal environment, Geophys. Res. Lett., 25, 1661–1664, doi:10.1029/98GL01005.

O'Dowd, C. D., et al. (2002), A dedicated study of New Particle Formation and Fate in the Coastal Environment (PARFORCE): Overview of objectives and achievements, J. Geophys. Res., 107(D19), 8108, doi:10.1029/ 2001JD000555.

O'Dowd, C., C. Monahan, and M. Dall'Osto (2010), On the occurrence of open ocean particle production and growth events, Geophys. Res. Lett., 37, L19805, doi:10.1029/2010GL044679.

Pirjola, L., C. D. O'Dowd, I. M. Brooks, and M. Kulmala (2000), Can new particle formation occur in the clean marine boundary layer?, *J. Geophys. Res.*, 105(D21), 26,531–26,546, doi:10.1029/2000JD900310.

Pirjola, L., Kulmala, M., 2001. Development of particle size and composition distribution with a novel aerosol dynamics model. Tellus 53B, 491–509

Portmann, S.: MOLEKEL, Version 4.3.win32. Swiss Center for Scientific Computing (CSCS)/ETHZ, Switzerland, 2002.

Pratt, K.A., L.E. Hatch, and K.A. Prather, Seasonal Volatility Dependence of Ambient Particle Phase Amines. Environ. Sci. Technol., 2009. 43: p. 5276-5281.

Smith, J.N., Barsanti, K.C., Friedli, H., Ehn, M., Kulmala, M., Collins, D.R., Scheckman, J.H., Williams, B.J., McMurry, P.H. 2010: Observations of aminium salts in atmospheric nanoparticles and possible climatic implications. Proceedings of the National Academy of Sciences (PNAS), 107, 6634-6639, 10.1073/pnas.0912127107.

Song, X. H., Hopke, P. K., Fergenson, D. P., and Prather, K. A.: Classification of single particles analyzed by ATOFMS using an artificial neural network, ART-2A, Anal. Chem., 71(4), 860–865, 1999.

Sorooshian A., Padrò L.T., Nenes A., Feingold G., McComiskey A., Hersey S.P., Gates

H., Jonsson H.H., Miller S.D., Stephens G.L., Flagan R.C. and Seinfeld J.H., 2009, On the link between ocean biota emissions, aerosol, and maritime clouds: Airborne, ground, and satellite measurements off the coast of California. Global Biogeochemical Cycles, 23, GB4007, doi:10.1029/2009GB003464.

Spracklen, D. V., Carslaw, K. S., Kulmala, M., Kerminen, V.-M., Sihto, S.-L., Riipinen, I., Merikanto, J., Mann, G.W., Chipperfield, M. P., Wiedensohler, A., Birmili,W., and Lihavainen, H.: Contribution of particle formation to global condensation nuclei concentrations, Geophys. Res. Lett., 35, L06808, doi:10.1029/2007GL033038, 2008

Su, Y. X., Sipin, M. F., Furutani, H., and Prather, K. A. (2004). Development and Characterization of an Aerosol Time-of-Flight Mass Spectrometer With Increased Detection Efficiency, Anal. Chem. 76(3):712–719.

Vuollekoski, H., V.-M. Kerminen, T. Anttila, S.-L. Sihto, M. Vana, M. Ehn, H. Korhonen, G. McFiggans, C. D. O'Dowd and M. Kulmala,, Iodine dioxide nucleation simulations in coastal and remote marine environments, J. Geophys. Res., 114, D02206, doi:10.1029/2008JD010713, 2008.

Wang, L., Khalizov, A. F., Zheng, J., Xu, W., Ma, Y., Lal, V., and Zhang, R.: Atmospheric nanoparticles formed from heterogeneous reactions of organics, Nat. Geosci., 3, 238–242, doi:10.1038/ngeo778, 2010a.

Wang, L., Lal, V., Khalizov, A. F., and Zhang, R.: Heterogeneous chemistry of alkylamines with sulfuric acid: Implications for atmospheric formation of alkylaminium sulfates, Environ. Sci. Technol., 44, 2461–2465, doi:10.1021/es9036868, 2010b.

Yang, X.-H., M. I. Scranton and C. Lee (1994) Seasonal variations in concentration and microbial uptake of methylamines in estuarine waters. Mar. Ecol. Progr. Ser., 108: 303-312.

Yoon, Y.J., D. Ceburnis, F. Cavalli, O. Jourdan, J.P. Putaud, M.C. Facchini, S. Descari, S. Fuzzi, , S.G. Jennings, C.D. O'Dowd. Seasonal characteristics of the physico-chemical properties of North Atlantic marine atmospheric aerosols J. Geophys. Res., doi:10.1029/2005JD007044, 2007.

Zahardis, J., Geddes, S., and Petrucci, G. A.: The ozonolysis of primary aliphatic amines in fine particles, Atmos. Chem. Phys., 8, 1181-1194, doi:10.5194/acp-8-1181-2008, 2008

Zhang, Qi, Stanier, C., Canagaratna, M., Jayne, J., Worsnop, D., Pandis, S. and Jimenez, J. (2004), Insights into Nucleation Burst and Particle Growth in Pittsburgh Based on Aerosol Mass Spectrometry. Environmental Science & Technology 38(18), 4797-4809

Zorn, S. R., Drewnick, F., Schott, M., Hoffmann, T., and Borrmann, S.: Characterization of the South Atlantic marine boundary layer aerosol using an Aerodyne Aerosol Mass Spectrometer, Atmos. Chem. Phys. Discuss., 8, 4831-4876, doi:10.5194/acpd-8-4831-2008, 2008

5 Conclusions and Future Outlook

This work focuses on the characterization of North East Atlantic aerosol, under both clean marine air conditions as well as anthropogenic polluted conditions. The utilized techniques enabled to, in the first instance, characterize water uptake properties (i.e. hygroscopicity), in the second instance, indirectly characterize the chemical composition and in the third instance, elucidate the state of mixing of the aerosol population. In addition to measurements of air arriving into and out of the North East Atlantic, characterization of aerosol properties was undertaken in perhaps one of Europe's most polluted regions, namely, the Po Valley (in between Milan and Bologna, Italy).

The deployment of the H-TDMA hygroscopicity measurement system at Mace Head and in the Po Valley provided invaluable insight into properties of primary and secondary aerosol produced in both marine and suburban environments. Long term HGF measurements enabled synergetic use of complementary measurements to elucidate key aerosol properties, which were supplemented by the CCN measurements and HR-Tof-AMS chemical compositional measurements, as well as by aerosol microphysical and the optical properties.

Marine air aerosol hygroscopicity and CCN activity analysis revealed surprising results in terms of the effect of primary organic compounds on the activation efficiency of biogenically-enriched aerosol particles. Specifically, the analysis revealed a dichotomy in terms of water uptake. In the sub-saturated humidity fields, primary enrichment of organics in sea spray aerosol leads to lower water uptake as a function of increasing relative humidity. In the super-saturated water vapour fields, the organically-enriched sea-spray activates with 100% efficiency, and, under certain plume conditions, organic sea spray can lead to ~ 400 cm^{-3} cloud droplet number concentrations – rivalling those associated with polluted clouds. These results point to significant impact on both direct and indirect radiative forcing, albeit in contrasting manners. While the indirect effect quantification is beyond the scope of this work, this work has allowed the quantification of the impact of primary organic enrichment on the direct radiative effect of sea spray.

In terms of long-term statistics, cluster data analysis from a two-year measurement period revealed 5 distinct classifications of combined microphysical size distributions and HGFs:

- *High Sea-Salt Marine*,
- *Low Sea-Salt Marine*,
- *Open Ocean Nucleation*,
- *Coastal Nucleation*
- *Continental*

with the following modes contributing HGF values to the above 5 categories:

- NH (nearly hydrophobic): 1-1.19,
- LH (low hygroscopicity): 1.2-1.52,
- MH (mainly hygroscopic): 1.65-1.7,
- SS (sea salt): 2.2

Overall, the contribution to number concentration by organic aerosol to the total particle concentration, based on hygroscopicity measurements, was estimated to vary from 25-35% during low and high sea salt under clean, marine air conditions, 35% during marine open ocean nucleation events and up to 60% during anthropogenic polluted episodes. This estimation, along with other studies presented in this thesis, has several major implications:

1) Even under the cleanest marine air conditions, during strong primary aerosol production events, one-third of submicron aerosol particles contain predominantly-organic matter with a possible suppression of the hygroscopic growth effect,

2) Secondary marine aerosol carries slightly higher amount of organics than primary marine aerosol, but secondary organic matter is also more oxygenated, hence the higher HGF than in case of primary organic aerosol,

3) Anthropogenic aerosol is in 60% dominated by organic matter, and may have a drastically decreased CCN activity and hygroscopicity.

As the measurements at Mace Head station continue, future long-term studies of aerosol hygroscopicity and the CCN activation efficiency should be performed using the bigger datasets. This will enable to reach higher precisions in the statistical analysis and also can add additional events (such as organic plumes during biogenically active periods) to the clustered variables. Additionally, by including back trajectory clusters, the analysis would improve in the scope of the aerosol origins.

Coastal episodes of new particles formation are believed to be influenced by iodine compounds released by species of macro algae *Laminaria digitata*. Low oxygen iodine polymers are less hygroscopic than more oxygenated compounds, and thus exhibit lower HGF (around 1.2). Previous studies revealing low HGFs associated with the nucleation mode during the coastal nucleation events were corroborated by this study. However, more detailed study focusing on the nucleation mode of the aerosol in the marine environment should be conducted using new HTDMA setups, allowing for investigation of particles in the size range of 3-10nm. Such precision can be achieved by employing DMAs with much higher sample – to – sheath ratios and different geometrical dimensions. Using HTDMA as a highly efficient particle sieve could enable the investigation of pure substances (assuming a bi-modal HGF-PDF mixing state) by spectrometer, or other kind of particle analyser/counter connected in parallel. By changing the working fluid of the TDMA, one could be able to investigate particular chemical groups of particles which exhibit specific affinity to a given solvent.

A detailed case study of open ocean nucleation plumes, for two cases, revealed that amongst potential gaseous precursors, nitrogenated compounds such as amines can stabilize clusters from evaporating, effectively increasing the nucleation and growth process thus promoting open ocean new particle production. This suggests that amides and organic nitrate may also play a key role in nucleation and growth processes. Future studies in this field using the modified HTDMA/AMS couple could help to narrow the groups of potential precursors and greatly reduce amount of work needed for chemical identification of organic/inorganic compounds in the aerosol particles.

Studies into ash particles emitted during eruption of the Eyjafjallajökull volcano revealed that this source of natural primary and secondary aerosol can significantly influence not only optical properties of air masses, but can also cause changes in clouds cover and albedo by effectively seeding them with CCN. In the investigation of the ash cloud it was concluded that the supermicron ash chemical composition was primarily silicon oxides and the submicron aerosol was composed of an internal mix of primary ash (15%), nss-sulphate (25%) and water (55%). The physical size and chemical composition resulted in the ash plume aerosol being very efficient CCN as evidenced by a 100% ratio efficiency for CCN/CN at supersaturations as low as 0.25%. Additionally, this study confirmed good agreement between ground measurements from several European sites (including Mace Head) and output of the REMOTE regional climate model used to predict ash cloud dispersion. Future studies should involve placement of the size segregated CCNc in various zones around an active volcano. Data obtained from such experiment, supplemented by HTDMA/AMS tandem, would greatly broaden the knowledge about the chemico-physical properties of emitted ash and secondary aerosol resulting from transformation of the gaseous precursors into a particulate matter. Such studies are needed to elucidate the fate of the volcanic aerosol and, as a result, to improve current dispersion models used by aviation authorities for emergency response to ash threat. This is important not only from the aviation safety perspective, but can also improve funding possibilities if such studies prove useful to the decision makers.

Studies into Po Valley regional production and long range aerosol transport show, that large urban centres and extensive agricultural areas are contributing greatly to secondary aerosol production, especially in the fine mode which typically has low HGF properties. In particular, there was strong suppression of hygroscopicity of particles in the size range 35-75 nm even in high nitrate concentration cases. Large diurnal variations in chemical composition were observed with massive peaks in nitrates, albeit without an increase in HGF, but also coherent with an increase in the hydrocarbon-like AMS family. This suggests a hydrophilic coating around the inorganic nitrate, thus suppressing water uptake. Other possible explanation of this phenomenon may be production of the organo-nirates which, despite causing a strong nitrate signal in the AMS, exhibit lower HGF in comparison with the pure ammonium nitrate. Future studies in this aspect will help to better understand the impact of big industrial/rural centres on the global aerosol population and, ultimately, on the global climate.

This study represents one of the first synergetic combinations of aerosol mass spectrometer chemical composition information with the HGF information resulting in very good success in the quantification of, specifically, marine aerosol influences on the direct radiative effect. Future work could probe the synergy between HGF and more specific mass spectral chemical fingerprints for reducing uncertainty associated with the direct effect and to begin to elucidate the indirect effect. In any event, this work has produced a parameterization for the impact of organic enrichment on sea spray water uptake which is currently being implemented in the ECHAM global climate general circulation model to assess the feedback between future climate change, oceanic productivity and contributions to the global radiative budget. Improvements in the global climate models are of a great importance for future climate change mitigation scenarios. It can also lead to better understanding of complex interactions between gas and particulate domains, ultimately enabling their users to better forecast long-term implications of possible climate engineering programs, deployed to counteract changing climate.

Acknowledgments

Atmospheric science is like the atmosphere itself: vast and boundless. Traversing it alone would be an impossible task. Luckily, I had a lot of help!

First and foremost, I'd like to thank my supervisor Professor Colin O'Dowd for a God-like patience and superb mentoring during my cruise through the PhD. His often acute and painful but very to-the-point remarks helped me to adjust my often crazy ideas to scientific standards. I want to thank Dr. Darius Ceburnis for help in experiments and for the scientific quarrels during long trips to Mace Head (and for fruitful lessons of proper commercial vehicle driving style!). I thank Dr. Jurgita Ovadnevaite for her precious time she has spent with me explaining the basics of marine environment atmospheric physics. Thanks go also to Dr. Regis Dupuy who introduced me to the Mace Head instrumentation. I thank folks from the Room 201 for excellent ambient, lunches together and a lot of laugh (especially Crazy Cat Lady). I'd like to thank Professor Gerard Jennings for lightning-fast proof reading of my crippled grammar thesis. I thank Dr. Tom O'Connor who basically founded the Mace Head station and made this work possible at all. Brendan Kelly, thank you for your technical support and all the clerical work needed for Mace Head to operate properly. Finally, I thank my wife for excellent support and keeping me sane through all those years spent together in Ireland while working on my PhD. You have been the light in all the murky days and a shadow in the heat of summer. Thank you.

References

Aitken, J., A. 1897. On some nuclei of cloudy condensation. *Tran. R. Soc. Edin.*, **XXXIX**.

Allan, D., Williams, P.I., Morgan, W.T., Martin, C.L., Flynn, M.J., Lee, J., Nemitz, E., Phillips, G.J., Gallagher, M.W., Coe, H. 2010. Contributions from transport, solid fuel burning and cooking to primary organic aerosols in two UK cities. *Atmospheric Chemistry and Physics*, **10**(2), 647-668.

Allen, M.D., Raabe, O.G. 1985. Slip Correction Measurements of Spherical Solid Aerosol Particles in an Improved Millikan Apparatus. *Aerosol Science and Technology*, **4**(3), 269-286.

Andreae, M.O., Charlson, R.J., Bruynseels, F., Storms, H., Van Grieken, R., Maenhaut, W. 1986. Internal mixture of sea salt, silicates, and excess sulfate in marine aerosols. *Science*, **232**(4758), 1620-1623.

Andreae, M.O., Elbert, W., Demora, S.J. 1995. Biogenic Sulfur Emissions and Aerosols over the Tropical South-Atlantic .3. Atmospheric Dimethylsulfide, Aerosols and Cloud Condensation Nuclei. *Journal of Geophysical Research-Atmospheres*, **100**(D6), 11335-11356.

Ansari, A.S., Pandis, S.N. 1999. Prediction of multicomponent inorganic atmospheric aerosol behavior. *Atmospheric Environment*, **33**(5), 745-757.

Ashu-Ayem, E.R., Nitschke, U., Monahan, C., Chen, J., Darby, S.B., Smith, P.D., O'Dowd, C.D., Stengel, D.B., Venables, D.S. 2012. Coastal Iodine Emissions. 1. Release of I2 by Laminaria digitata in Chamber Experiments. *Environmental Science & Technology*, **46**(19), 10413-10421.

Asmi, E., Frey, A., Virkkula, A., Ehn, M., Manninen, H.E., Timonen, H., Tolonen-Kiviṁaki, O., Aurela, M., Hillamo, R., Kulmala, M. 2010. Hygroscopicity and chemical composition of antarctic sub-micrometre aerosol particles and observations of new particle formation. *Atmospheric Chemistry and Physics*, **10**(9), 4253-4271.

Ayers, G.P., Gras, J.L. 1991. Seasonal relationship between cloud condensation nuclei and aerosol methanesulphonate in marine air. *Nature*, **353**(6347), 834-835.

Baltensperger, U., Kalberer, M., Dommen, J., Paulsen, D., Alfarra, M.R., Coe, H., Fisseha, R., Gascho, A., Gysel, M., Nyeki, S., Sax, M., Steinbacher, M., Prevot, A.S.H., Sjogren, S., Weingartner, E., Zenobi, R. 2005. Secondary organic aerosols from anthropogenic and biogenic precursors. *Faraday Discussions*, **130**, 265-278.

Berg, O.H., Swietlicki, E., Krejci, R. 1998. Hygroscopic growth of aerosol particles in the marine boundary layer over the Pacific and Southern Oceans during the First Aerosol Characterization Experiment (ACE 1). *Journal of Geophysical Research B: Solid Earth*, **103**(D13), 16535-16545.

Berresheim, H., Elste, T., Tremmel, H.G., Allen, A.G., Hansson, H.C., Rosman, K., Dal Maso, M., Makela, J.M., Kulmala, M., O'Dowd, C.D. 2002. Gas-aerosol relationships of H2SO4, MSA, and OH: Observations in the coastal marine boundary layer at Mace Head, Ireland. *Journal of Geophysical Research-Atmospheres*, **107**(D19), -.

Bigg, E.K. 2007. Sources, nature and influence on climate of marine airborne particles. *Environmental Chemistry*, **4**(3), 155-161.

Bigg, E.K., Leck, C. 2008. The composition of fragments of bubbles bursting at the ocean surface. *Journal of Geophysical Research D: Atmospheres*, **113**(11).

Boy, M., Petäjä, T., Dal Maso, M., Rannik, Ü., Rinne, J., Aalto, P., Laaksonen, A., Vaattovaara, P., Joutsensaari, J., Hoffmann, T., Warnke, J., Apostolaki, M., Stephanou, E.G., Tsapakis, M., Kouvarakis, A., Pio, C., Carvalho, A., Römpp, A., Moortgat, G., Spirig, C., Guenther, A., Greenberg, J., Ciccioli, P., Kulmala, M. 2004. Overview of the field measurement campaign in Hyytiälä, August 2001 in the framework of the EU project OSOA. *Atmospheric Chemistry and Physics*, **4**(3), 657-678.

Burkholder, J.B., Curtius, J., Ravishankara, A.R., Lovejoy, E.R. 2003. Laboratory studies of the homogeneous nucleation of iodine oxides. *Atmos. Chem. Phys. Discuss.*, **3**(5), 4943-4988.

Busch, B., Kandler, K., Schutz, L., Neususs, C. 2002. Hygroscopic properties and water-soluble volume fraction of atmospheric particles in the diameter range from 50 nm to 3.8 mu m during LACE 98. *Journal of Geophysical Research-Atmospheres*, **107**(D21), -.

Cainey, J.M., Keywood, M., Bigg, E.K., Grose, M.R., Gillett, R.W., Meyer, M. 2007a. Flux chamber study of particle formation from Durvillaea potatorum. *Environmental Chemistry*, **4**(3), 151-154.

Cainey, J.M., Keywood, M., Grose, M.R., Krummel, P., Galbally, I.E., Johnston, P., Gillett, R.W., Meyer, M., Fraser, P., Steele, P., Harvey, M., Kreher, K., Stein, T., Ibrahim, O., Ristovski, Z.D., Johnson, G., Fletcher, C.A., Bigg, E.K., Gras, J.L. 2007b. Precursors to Particles (P2P) at Cape Grim 2006: campaign overview. *Environmental Chemistry*, **4**(3), 143-150.

Cavalli, F., Facchini, M.C., Decesari, S., Emblico, L., Mircea, M., Jensen, N.R., Fuzzi, S. 2006. Size-segregated aerosol chemical composition at a boreal site in southern Finland, during the QUEST project. *Atmospheric Chemistry and Physics*, **6**(4), 993-1002.

Chance, R., Baker, A.R., Kuepper, F.C., Hughes, C., Kloareg, B., Malin, G. 2009. Release and transformations of inorganic iodine by marine macroalgae. *Estuarine Coastal and Shelf Science*, **82**(3), 406-414.

Charlson, R.J., Lovelock, J.E., Andreae, M.O., Warren, S.G. 1987. Oceanic phytoplankton, atmospheric sulphur, cloud albedo and climate. *Nature*, **326**(6114), 655-661.

Crahan, K.K., Hegg, D.A., Covert, D.S., Santarpia, J.L., Jonsson, H., Buzorius, G., Collins, D. 2006. Organics in the Northeastern Pacific and their impacts on aerosol hygroscopicity in the subsaturated and supersaturated regimes. *Atmospheric Chemistry and Physics Discussions*, **6**(3), 4213-4249.

Cropp, R.A., Gabric, A.J., McTainsh, G.H., Braddock, R.D., Tindale, N. 2005. Coupling between ocean biota and atmospheric aerosols: Dust, dimethylsulphide, or artifact? *Global Biogeochemical Cycles*, **19**(4).

Cubison, M.J., Coe, H., Gysel, M. 2005. A modified hygroscopic tandem DMA and a data retrieval method based on optimal estimation. *Journal of Aerosol Science*, **36**(7), 846-865.

Dall'Osto, M., Harrison, R.M. 2011. Urban organic aerosols measured by single particle mass spectrometry in the megacity of London. *Atmos. Chem. Phys. Discuss.*, **11**(2), 5043-5078.

Dennis, W.L. 1960. The growth of hygroscopic drops in a humid air stream. *Discussions of the Faraday Society*, **30**, 78-85.

Duplissy, J., De Carlo, P.F., Dommen, J., Alfarra, M.R., Metzger, A., Barmpadimos, I., Prevot, A.S.H., Weingartner, E., Tritscher, T., Gysel, M., Aiken, A.C., Jimenez, J.L., Canagaratna, M.R., Worsnop, D.R., Collins, D.R., Tomlinson, J., Baltensperger, U. 2011. Relating hygroscopicity and composition of organic aerosol particulate matter. *Atmospheric Chemistry and Physics*, **11**(3), 1155-1165.

Duplissy, J., Gysel, M., Sjogren, S., Meyer, N., Good, N., Kammer-Mann, L., Michaud, V., Weigel, R., Martins Dos Santos, S., Gru-Ening, C., Villani, P., Laj, P., Sellegri, K., Metzger, A., McFig-Gans, G.B., Wehrle, G., Richter, R., Dommen, J., Ristovski, Z., Baltensperger, U., Weingartner, E. 2009. Intercomparison study of six HTDMAs: Results and recommendations. *Atmos. Meas. Tech.*, **2**, 363-378.

Dusek, U., Frank, G.P., Hildebrandt, L., Curtius, J., Schneider, J., Walter, S., Chand, D., Drewnick, F., Hings, S., Jung, D., Borrmann, S., Andreae, M.O. 2006. Size matters more than chemistry for cloud-nucleating ability of aerosol particles. *Science*, **312**(5778), 1375-1378.

Ehn, M., Petaja, T., Aufmhoff, H., Aalto, P., Hameri, K., Arnold, F., Laaksonen, A., Kulmala, M. 2007. Hygroscopic properties of ultrafine aerosol particles in the boreal forest: diurnal variation, solubility and the influence of sulfuric acid. *Atmospheric Chemistry and Physics*, **7**, 211-222.

Flanner, M.G., Zender, C.S., Randerson, J.T., Rasch, P.J. 2007. Present-day climate forcing and response from black carbon in snow. *Journal of Geophysical Research D: Atmospheres*, **112**(11).

Fuentes, E., Coe, H., Green, D., McFiggans, G. 2011. On the impacts of phytoplankton-derived organic matter on the properties of the primary marine aerosol - Part 2: Composition, hygroscopicity and cloud condensation activity. *Atmospheric Chemistry and Physics*, **11**(6), 2585-2602.

Gasparini, R., Li, R., Collins, D.R. 2004. Integration of size distributions and size-resolved hygroscopicity measured during the Houston Supersite for compositional categorization of the aerosol. *Atmospheric Environment*, **38**(20), 3285-3303.

Gasparini, R., Li, R., Collins, D.R., Ferrare, R.A., Brackett, V.G. 2006. Application of aerosol hygroscopicity measured at the Atmospheric Radiation Measurement Program's Southern Great Plains site to examine composition and evolution. *Journal of Geophysical Research D: Atmospheres*, **111**(5).

Grose, M., Sakurai, H., Savstrom, J., Stolzenburg, M.R., Watts Jr, W.F., Morgan, C.G., Murray, I.P., Twigg, M.V., Kittelson, D.B., McMurry, P.H. 2006. Chemical and physical properties of ultrafine diesel exhaust particles sampled downstream of a catalytic trap. *Environmental Science and Technology*, **40**(17), 5502-5507.

Gysel, M., McFiggans, G.B., Coe, H. 2009. Inversion of tandem differential mobility analyser (TDMA) measurements. *Journal of Aerosol Science*, **40**(2), 134-151.

Gysel, M., Weingartner, E., Nyeki, S., Paulsen, D., Baltensperger, U., Galambos, I., Kiss, G. 2004. Hygroscopic properties of water-soluble matter and humic-like organics in atmospheric fine aerosol. *Atmospheric Chemistry and Physics*, **4**(1), 35-50.

Hameri, K., Vakeva, M., Aalto, P.P., Kulmala, M., Swietlicki, E., Zhou, J., Seidl, W., Becker, E., O'Dowd, C.D. 2001. Hygroscopic and CCN properties of aerosol particles in boreal forests. *Tellus Series B-Chemical and Physical Meteorology*, **53**(4), 359-379.

Hämeri, K., Väkevä, M., Aalto, P.P., Kulmala, M., Swietlicki, E., Zhou, J., Seidl, W., Becker, E., O'Dowd, C.D. 2001. Hygroscopic and CCN properties of aerosol particles in boreal forests. *Tellus, Series B: Chemical and Physical Meteorology*, **53**(4), 359-379.

Hänel, G. 1976. The Properties of Atmospheric Aerosol Particles as Functions of the Relative Humidity at Thermodynamic Equilibrium with the Surrounding Moist Air, Vol. 19, pp. 73-188.

Hansen, J., Sato, M., Lacis, A., Ruedy, R. 1997. The missing climate forcing. *Philosophical Transactions of the Royal Society B: Biological Sciences*, **352**(1350), 231-240.

Hegg, D., Larson, T., Po-Fat, Y. 1993. A theoretical study of the effect of relative humidity on light scattering by tropospheric aerosols. *Journal of Geophysical Research*, **98**(D10), 18,435-18,439.

Hennigan, C.J., Westervelt, D.M., Riipinen, I., Engelhart, G.J., Lee, T., Collett, J.L., Jr., Pandis, S.N., Adams, P.J., Robinson, A.L. 2012. New particle formation and growth in biomass burning plumes: An important source of cloud condensation nuclei. *Geophys. Res. Lett.*, **39**(9), L09805.

Hinds, W. 1999. *Aerosol Technology: Properties, Behavior, and Measurement of Airborne Particles (Wiley-Interscience)*. Wiley-Interscience.

JAYNE, T., J., LEARD, C., D., ZHANG, X., DAVIDOVITS, P., SMITH, A., K., KOLB, E., C., WORSNOP, R., D. 2000a. *Development of an aerosol mass spectrometer for size and composition analysis of submicron particles*. Taylor & Francis, Colchester, ROYAUME-UNI.

Jayne, J.T., Leard, D.C., Zhang, X., Davidovits, P., Smith, K.A., Kolb, C.E., Worsnop, D.R. 2000b. Development of an aerosol mass spectrometer for size and composition analysis of submicron particles. *Aerosol Science and Technology*, **33**(1-2), 49-70.

Jimenez, J.L., Canagaratna, M.R., Donahue, N.M., Prevot, A.S.H., Zhang, Q., Kroll, J.H., DeCarlo, P.F., Allan, J.D., Coe, H., Ng, N.L., Aiken, A.C., Docherty, K.S., Ulbrich, I.M., Grieshop, A.P., Robinson, A.L., Duplissy, J., Smith, J.D., Wilson, K.R., Lanz, V.A., Hueglin, C., Sun, Y.L., Tian, J., Laaksonen, A., Raatikainen, T., Rautiainen, J., Vaattovaara, P., Ehn, M., Kulmala, M., Tomlinson, J.M., Collins, D.R., Cubison, M.J., Dunlea, E.J., Huffman, J.A., Onasch, T.B., Alfarra, M.R., Williams, P.I., Bower, K., Kondo, Y., Schneider, J., Drewnick, F., Borrmann, S., Weimer, S., Demerjian, K., Salcedo, D., Cottrell, L., Griffin, R., Takami, A., Miyoshi, T., Hatakeyama, S., Shimono, A., Sun, J.Y., Zhang, Y.M., Dzepina, K., Kimmel, J.R., Sueper, D., Jayne, J.T., Herndon, S.C., Trimborn, A.M., Williams, L.R., Wood, E.C., Middlebrook, A.M., Kolb, C.E., Baltensperger, U., Worsnop, D.R. 2009. Evolution of organic aerosols in the atmosphere. *Science*, **326**(5959), 1525-1529.

Jimenez, J.L., DeCarlo, P.F., Kimmel, J.R., Trimborn, A., Northway, M.J., Jayne, J.T., Aiken, A.C., Gonin, M., Fuhrer, K., Horvath, T., Docherty, K.S., Worsnop, D.R. 2006. Field-deployable, high-resolution, time-of-flight aerosol mass spectrometer. *Analytical Chemistry*, **78**(24), 8281-8289.

Jimenez, J.L., Jayne, J.T., Shi, Q., Kolb, C.E., Worsnop, D.R., Yourshaw, I., Seinfeld, J.H., Flagan, R.C., Zhang, X., Smith, K.A., Morris, J.W., Davidovits, P. 2003. Ambient aerosol sampling using the Aerodyne Aerosol Mass Spectrometer. *J. Geophys. Res.*, **108**(D7), 8425.

Jones, H.M., Crosier, J., Russell, A., Flynn, M.J., Irwin, M., Choularton, T.W., Coe, H., McFiggans, G. 2011. In situ aerosol measurements taken during the 2007 COPS

field campaign at the Hornisgrinde ground site. *Quarterly Journal of the Royal Meteorological Society*, **137**(S1), 252-266.

Jones, M., Walker, S. 1994. Private indentures for life service in peace and war, 1278-1476. *Camden Miscellany*, **32**(3), 15.

Joutsensaari, J., Vaattovaara, P., Vesterinen, M., Hämeri, K., Laaksonen, A. 2001. A novel tandem differential mobility analyzer with organic vapor treatment of aerosol particles. *Atmospheric Chemistry and Physics*, **1**(1), 51-60.

Jurányi, Z., Gysel, M., Weingartner, E., Decarlo, P.F., Kammermann, L., Baltensperger, U. 2010. Measured and modelled cloud condensation nuclei number concentration at the high alpine site Jungfraujoch. *Atmospheric Chemistry and Physics*, **10**(16), 7891-7906.

Kaku, K.C., Hegg, D.A., Covert, D.S., Santarpia, J.L., Jonsson, H., Buzorius, G., Collins, D.R. 2006. Organics in the northeastern pacific and their impacts on aerosol hygroscopicity in the subsaturated and supersaturated regimes. *Atmospheric Chemistry and Physics*, **6**(12), 4101-4115.

Kittelson, D.B. 1998. Engines and nanoparticles: A review. *Journal of Aerosol Science*, **29**(5-6), 575-588.

Knutson, E.O., Whitby, K.T. 1975. Aerosol classification by electric mobility: apparatus, theory, and applications. *Journal of Aerosol Science*, **6**(6), 443-451.

Koch, D., Del Genio, A.D. 2010. Black carbon semi-direct effects on cloud cover: Review and synthesis. *Atmospheric Chemistry and Physics*, **10**(16), 7685-7696.

Kohler, H. 1936. The nucleus in and the growth of hygroscopic droplets. *Transactions of the Faraday Society*, **32**, 1152-1161.

Kreidenweis, S.M., Koehler, K., DeMott, P.J., Prenni, A.J., Carrico, C., Ervens, B. 2005. Water activity and activation diameters from hygroscopicity data - Part I: Theory and application to inorganic salts. *Atmospheric Chemistry and Physics*, **5**(5), 1357-1370.

Kulmala, M., Kerminen, V.M. 2008. On the formation and growth of atmospheric nanoparticles. *Atmospheric Research*, **90**(2-4), 132-150.

Kulmala, M., Pirjola, L., Makela, J.M. 2000. Stable sulphate clusters as a source of new atmospheric particles. *Nature*, **404**(6773), 66-69.

Kulmala, M., Vehkamäki, H., Petäjä, T., Dal Maso, M., Lauri, A., Kerminen, V.M., Birmili, W., McMurry, P.H. 2004. Formation and growth rates of ultrafine atmospheric particles: A review of observations. *Journal of Aerosol Science*, **35**(2), 143-176.

Kupiainen, K., Klimont, Z. 2007. Primary emissions of fine carbonaceous particles in Europe. *Atmospheric Environment*, **41**(10), 2156-2170.

Kupper, F.C., Carpenter, L.J., McFiggans, G.B., Palmer, C.J., Waite, T.J., Boneberg, E.M., Woitsch, S., Weiller, M., Abela, R., Grolimund, D., Potin, P., Butler, A., Luther, G.W., Kroneck, P.M.H., Meyer-Klaucke, W., Feiters, M.C. 2008. Iodide accumulation provides kelp with an inorganic antioxidant impacting atmospheric chemistry. *Proceedings of the National Academy of Sciences of the United States of America*, **105**(19), 6954-6958.

Küpper, F.C., Schweigert, N., Ar Gall, E., Legendre, J.M., Vilter, H., Kloareg, B. 1998. Iodine uptake in Laminariales involves extracellular, haloperoxidase-mediated oxidation of iodide. *Planta*, **207**(2), 163-171.

Lanz, V.A., Alfarra, M.R., Baltensperger, U., Buchmann, B., Hueglin, C., Prévôt, A.S.H. 2007. Source apportionment of submicron organic aerosols at an urban site by factor analytical modelling of aerosol mass spectra. *Atmospheric Chemistry and Physics*, **7**(6), 1503-1522.

Lee, E., Chan, C.K., Paatero, P. 1999. Application of positive matrix factorization in source apportionment of particulate pollutants in Hong Kong. *Atmospheric Environment*, **33**(19), 3201-3212.

Lewis, E.R., Schwartz, S.E. 2004. Sea Salt Aerosol Production: Mechanisms, Methods, Measurements, and Models: A Critical Review

American Geophysical Union, **152**.

Li, C.S., Lin, W.H., Jenq, F.T. 1993. Characterization of outdoor submicron particles and selected combustion sources of indoor particles. *Atmospheric Environment. Part B, Urban Atmosphere*, **27**(4), 413-424.

Liu, B.Y.H., Pui, D.Y.H., Whitby, K.T. 1978. The aerosol mobility chromatograph: a new detector for sulfuric acid aerosols. *Atmospheric Environment*, **12**(1-3), 99-104.

Lohmann, U., Feichter, J. 2005. Global indirect aerosol effects: A review. *Atmospheric Chemistry and Physics*, **5**(3), 715-737.

Lovelock, J.E. 1979. Gaia: a new look at life on Earth. *Gaia: a new look at life on Earth.*

Mårtensson, E.M., Nilsson, E.D., de Leeuw, G., Cohen, L.H., Hansson, H.C. 2003. Laboratory simulations and parameterization of the primary marine aerosol production. *Journal of Geophysical Research D: Atmospheres*, **108**(9), AAC 15-1 AAC 15-12.

Massling, A., Leinert, S., Wiedensohler, A., Covert, D. 2006. Hygroscopic growth of sub-micrometer and one-micrometer aerosol particles measured during ACE-Asia. *Atmospheric Chemistry and Physics Discussions*, **6**(6), 12267-12300.

Massling, A., Wiedensohler, A., Busch, B., Neususs, C., Quinn, P., Bates, T., Covert, D. 2003. Hygroscopic properties of different aerosol types over the Atlantic and Indian Oceans. *Atmospheric Chemistry and Physics*, **3**, 1377-1397.

Massoli, P., Lambe, A.T., Ahern, A.T., Williams, L.R., Ehn, M., Mikkilä, J., Canagaratna, M.R., Brune, W.H., Onasch, T.B., Jayne, J.T., Petäjä, T., Kulmala, M., Laaksonen, A., Kolb, C.E., Davidovits, P., Worsnop, D.R. 2011. Relationship between aerosol oxidation level and hygroscopic properties of laboratory generated secondary organic aerosol (SOA) particles&#8221. *Geophys. Res. Lett.*, **38**(3), L03805.

McFiggans, G., Artaxo, P., Baltensperger, U., Coe, H., Facchini, M.C., Feingold, G., Fuzzi, S., Gysel, M., Laaksonen, A., Lohmann, U., Mentel, T.F., Murphy, D.M., O'Dowd, C.D., Snider, J.R., Weingartner, E. 2006. The effect of physical and chemical aerosol properties on warm cloud droplet activation. *Atmospheric Chemistry and Physics*, **6**, 2593-2649.

McFiggans, G., Bale, C.S.E., Ball, S.M., Beames, J.M., Bloss, W.J., Carpenter, L.J., Dorsey, J., Dunk, R., Flynn, M.J., Furneaux, K.L., Gallagher, M.W., Heard, D.E., Hollingsworth, A.M., Hornsby, K., Ingham, T., Jones, C.E., Jones, R.L., Kramer, L.J., Langridge, J.M., Leblanc, C., LeCrane, J.P., Lee, J.D., Leigh, R.J., Longley, I., Mahajan, A.S., Monks, P.S., Oetjen, H., Orr-Ewing, A.J., Plane, J.M.C., Potin, P., Shillings, A.J.L., Thomas, F., Von Glasow, R., Wada, R., Whalley, L.K., Whitehead, J.D. 2010. Iodine-mediated coastal particle formation: An overview of the Reactive Halogens in the Marine boundary layer (RHaMBLe) Roscoff coastal study. *Atmospheric Chemistry and Physics*, **10**(6), 2975-2999.

McFiggans, G., Coe, H., Burgess, R., Allan, J., Cubison, M., Alfarra, M.R., Saunders, R., Saiz-Lopez, A., Plane, J.M.C., Wevill, D., Carpenter, L., Rickard, A.R., Monks, P.S. 2004. Direct evidence for coastal iodine particles from Laminaria

macroalgae – linkage to emissions of molecular iodine. *Atmos. Chem. Phys.*, **4**(3), 701-713.

McInnes, L., Bergin, M., Ogren, J., Schwartz, S. 1998. Apportionment of light scattering and hygroscopic growth to aerosol composition. *Geophysical Research Letters*, **25**(4), 513-516.

Meyer, N.K., Duplissy, J., Gysel, M., Metzger, A., Dommen, J., Weingartner, E., Alfarra, M.R., Prevot, A.S.H., Fletcher, C., Good, N., McFiggans, G., Jonsson, A.M., Hallquist, M., Baltensperger, U., Ristovski, Z.D. 2009. Analysis of the hygroscopic and volatile properties of ammonium sulphate seeded and unseeded SOA particles. *Atmospheric Chemistry and Physics*, **9**(2), 721-732.

Mie, G. 1907. Die optischen Eigenschaften kolloider Goldlösungen. *Zeitschrift für Chemie und Industrie der Kolloide*, **2**(5), 129-133.

Mihele, C.M., Wiebe, H.A., Lane, D.A. 2002. Particle formation and gas/particle partition measurements of the products of the naphthalene-OH radical reaction in a smog chamber. *Polycyclic Aromatic Compounds*, **22**(3-4), 729-736.

Mircea, M., Facchini, M.C., Decesari, S., Cavalli, F., Emblico, L., Fuzzi, S., Vestin, A., Rissler, J., Swietlicki, E., Frank, G., Andreae, M.O., Maenhaut, W., Rudich, Y., Artaxo, P. 2005. Importance of the organic aerosol fraction for modeling aerosol hygroscopic growth and activation: A case study in the Amazon Basin. *Atmospheric Chemistry and Physics*, **5**(11), 3111-3126.

Mochida, M., Kawamura, K. 2004. Hygroscopic properties of levoglucosan and related organic compounds characteristic to biomass burning aerosol particles. *Journal of Geophysical Research D: Atmospheres*, **109**(21), D21202 1-8.

Mochida, M., Miyakawa, T., Takegawa, N., Morino, Y., Kawamura, K., Kondo, Y. 2008. Significant alteration in the hygroscopic properties of urban aerosol particles by the secondary formation of organics. *Geophys. Res. Lett.*, **35**(2), L02804.

Mochida, M., Nishita-Hara, C., Furutani, H., Miyazaki, Y., Jung, J., Kawamura, K., Uematsu, M. 2011. Hygroscopicity and cloud condensation nucleus activity of marine aerosol particles over the western North Pacific. *Journal of Geophysical Research D: Atmospheres*, **116**(6).

Monahan, C., Vuollekoski , H., Kulmala, M., Dowd, C. 2010. Simulating Marine New Particle Formation and Growth Using the M7 Modal Aerosol Dynamics Modal. *Advances in Meteorology*, **2010**.

Murphy, D.M., Anderson, J.R., Qulnn, P.K., McLnnes, L.M., Brechtel, F.J., Kreidenwels, S.M., Middlebrook, A.M., Pósfai, M., Thomson, D.S., Buseck, P.R. 1998. Influence of sea-salt on aerosol radiative properties in the Southern Ocean marine boundary layer. *Nature*, **392**(6671), 62-65.

Ng, N.L., Kroll, J.H., Keywood, M.D., Bahreini, R., Varutbangkul, V., Flagan, R.C., Seinfeld, J.H., Lee, A., Goldstein, A.H. 2006. Contribution of first- versus second-generation products to secondary organic aerosols formed in the oxidation of biogenic hydrocarbons. *Environmental Science and Technology*, **40**(7), 2283-2297.

O'Dowd, C., Ceburnis, D., Ovadnevaite, J., Martucci, G., Bialek, J., Monahan, C., Berresheim, H., Vaishya, A., Grigas, T., Jennings, S.G., McVeigh, P., Varghese, S., Flanagan, R., Martin, D., Moran, E., Lambkin, K., Semmler, T., Perrino, C., McGrath, R. 2012. The Eyjafjallajökull ash plume - Part I: Physical, chemical and optical characteristics. *Atmospheric Environment*, **48**, 129-142.

O'Dowd, C., McFiggans, G., Creasey, D.J., Pirjola, L., Hoell, C., Smith, M.H., Allan, B.J., Plane, J.M.C., Heard, D.E., Lee, J.D., Pilling, M.J., Kulmala, M. 1999. On

the photochemical production of new particles in the coastal boundary layer. *Geophysical Research Letters*, **26**(12), 1707-1710.

O'Dowd, C., Monahan, C., Dall'Osto, M. 2010. On the occurrence of open ocean particle production and growth events. *Geophysical Research Letters*, **37**.

O'Dowd, C.D., Aalto, P., Hameri, K., Kulmala, M., Hoffmann, T. 2002a. Aerosol formation - Atmospheric particles from organic vapours. *Nature*, **416**(6880), 497-498.

O'Dowd, C.D., Aalto, P., Hämeri, K., Kulmala, M., Hoffmann, T. 2002b. Atmospheric particles from organic vapours. *Nature*, **416**(6880), 497-498.

O'Dowd, C.D., Becker, E., Kulmala, M. 2001. Mid-latitude North-Atlantic aerosol characteristics in clean and polluted air. *Atmospheric Research*, **58**(3), 167-185.

O'Dowd, C.D., de Leeuw, G. 2007. Marine aerosol production: a review of the current knowledge. *Philosophical Transactions of the Royal Society A: Mathematical, Physical and Engineering Sciences*, **365**(1856), 1753-1774.

O'Dowd, C.D., Facchini, M.C., Cavalli, F., Ceburnis, D., Mircea, M., Decesari, S., Fuzzi, S., Yoon, Y.J., Putaud, J.P. 2004. Biogenically driven organic contribution to marine aerosol. *Nature*, **431**(7009), 676-680.

O'Dowd, C.D., Hameri, K., Makela, J.M., Pirjola, L., Kulmala, M., Jennings, S.G., Berresheim, H., Hansson, H.C., de Leeuw, G., Kunz, G.J., Allen, A.G., Hewitt, C.N., Jackson, A., Viisanen, Y., Hoffmann, T. 2002c. A dedicated study of New Particle Formation and Fate in the Coastal Environment (PARFORCE): Overview of objectives and achievements. *Journal of Geophysical Research-Atmospheres*, **107**(D19), -.

O'Dowd, C.D., Hämeri, K., Mäkelä, J.M., Pirjola, L., Kulmala, M., Jennings, S.G., Berresheim, H., Hansson, H.C., De Leeuw, G., Kunz, G.J., Allen, A.G., Hewitt, C.N., Jackson, A., Viisanen, Y., Hoffmann, T. 2002d. A dedicated study of New Particle Formation and Fate in the Coastal Environment (PARFORCE): Overview of objectives and achievements. *Journal of Geophysical Research D: Atmospheres*, **107**(19).

O'Dowd, C.D., Jimenez, J.L., Bahreini, R., Flagan, R.C., Seinfeld, J.H., Hameri, K., Pirjola, L., Kulmala, M., Jennings, S.G., Hoffmann, T. 2002e. Marine aerosol formation from biogenic iodine emissions. *Nature*, **417**(6889), 632-636.

O'Dowd, C.D., Langmann, B., Varghese, S., Scannell, C., Ceburnis, D., Facchini, M.C. 2008. A combined organic-inorganic sea-spray source function. *Geophysical Research Letters*, **35**(1).

Orellana, M.V., Matrai, P.A., Leck, C., Rauschenberg, C.D., Lee, A.M., Coz, E. 2011. Marine microgels as a source of cloud condensation nuclei in the high Arctic. *Proc Natl Acad Sci U S A*, **108**(33), 13612-13617.

Ovadnevaite, J., Ceburnis, D., Martucci, G., Bialek, J., Monahan, C., Rinaldi, M., Facchini, M.C., Berresheim, H., Worsnop, D.R., O'Dowd, C. 2011a. Primary marine organic aerosol: A dichotomy of low hygroscopicity and high CCN activity. *Geophysical Research Letters*, **38**(21).

Ovadnevaite, J., O'Dowd, C., Dall'Osto, M., Ceburnis, D., Worsnop, D.R., Berresheim, H. 2011b. Detecting high contributions of primary organic matter to marine aerosol: A case study. *Geophysical Research Letters*, **38**(2).

Paatero, P., Tapper, U. 1994. Positive matrix factorization: a non-negative factor model with optimal utilization of error estimates of data values. *Environmetrics*, **5**(2), 111-126.

Palmer, C.J., Anders, T.L., Carpenter, L.J., Kupper, F.C., McFiggans, G.B. 2005. Iodine and halocarbon response of Laminaria digitata to oxidative stress and links to atmospheric new particle production. *Environmental Chemistry*, **2**(4), 282-290.

Petäjä, T., Kerminen, V.M., Hämeri, K., Vaattovaara, P., Joutsensaari, J., Junkermann, W., Laaksonen, A., Kulmala, M. 2005. Effects of SO 2 oxidation on ambient aerosol growth in water and ethanol vapours. *Atmospheric Chemistry and Physics*, **5**(3), 767-779.

Quinn, P.K., Bates, T.S. 2011. The case against climate regulation via oceanic phytoplankton sulphur emissions. *Nature*, **480**(7375), 51-56.

Quinn, P.K., Bates, T.S. 2005. Regional aerosol properties: Comparisons of boundary layer measurements from ACE 1, ACE 2, Aerosols99, INDOEX, ACE Asia, TARFOX, and NEAQS. *Journal of Geophysical Research D: Atmospheres*, **110**(14), 1-24.

Quinn, P.K., Charlson, R.J., Bates, T.S. 1988. Simultaneous observations of ammonia in the atmosphere and ocean. *Nature*, **335**(6188), 336-338.

Raatikainen, T., Vaattovaara, P., Tiitta, P., Miettinen, P., Rautiainen, J., Ehn, M., Kulmala, M., Laaksonen, A., Worsnop, D.R. 2010. Physicochemical properties and origin of organic groups detected in boreal forest using an erosol mass spectrometer. *Atmospheric Chemistry and Physics*, **10**(4), 2063-2077.

Rissler, J., Pagels, J., Swietlicki, E., Wierzbicka, A., Strand, M., Lillieblad, L., Sanati, M., Bohgard, M. 2005. Hygroscopic behavior of aerosol particles emitted from biomass fired grate boilers. *Aerosol Science and Technology*, **39**(10), 919-930.

Rogge, W.F., Hildemann, L.M., Mazurek, M.A., Cass, G.R., Simoneit, B.R.T. 1993. Sources of fine organic aerosol. 2. Noncatalyst and catalyst-equipped automobiles and heavy-duty diesel trucks. *Environmental Science and Technology*, **27**(4), 636-651.

Rosenfeld, D. 2006. Aerosol-Cloud Interactions Control of Earth Radiation and Latent Heat Release Budgets. *Space Science Reviews*, **125**(1), 149-157.

Saxena, P., Hildemann, L.M., McMurry, P.H., Seinfeld, J.H. 1995. Organics alter hygroscopic behavior of atmospheric particles. *Journal of Geophysical Research*, **100**(D9), 18,755-18,770.

Schauer, J.J., Kleeman, M.J., Cass, G.R., Simoneit, B.R.T. 1999. Measurement of emissions from air pollution sources. 2. C 1 through C 30 organic compounds from medium duty diesel trucks. *Environmental Science and Technology*, **33**(10), 1578-1587.

Schauer, J.J., Kleeman, M.J., Cass, G.R., Simoneit, B.R.T. 2001. Measurement of emissions from air pollution sources. 3. C1-C29 organic compounds from fireplace combustion of wood. *Environmental Science and Technology*, **35**(9), 1716-1728.

Schauer, J.J., Rogge, W.F., Hildemann, L.M., Mazurek, M.A., Cass, G.R., Simoneit, B.R.T. 1996. Source apportionment of airborne particulate matter using organic compounds as tracers. *Atmospheric Environment*, **30**(22), 3837-3855.

Seinfeld, J., Pandis, S. 2006. *Atmospheric Chemistry and Physics: From Air Pollution to Climate Change*. Wiley-Interscience, Textbook.

Seinfeld, J.H., Pandis, S.N. 1998. *Atmospheric Chemistry and Physics*.

Sellegri, K., O'Dowd, C.D., Yoon, Y.J., Jennings, S.G., de Leeuw, G. 2006. Surfactants and submicron sea spray generation. *Journal of Geophysical Research-Atmospheres*, **111**(D22).

Shaw, G.E., Benner, R.L., Cantrell, W., Clarke, A.D. 1998. On the regulation of climate: A sulfate particle feedback loop involving deep convection. *Climatic Change*, **39**(1), 23-33.

Solomon, S., Qin, D., Manning, M., Chen, Z., Marquis, M., Averyt, K.B., Tignor, M., Miller, H.L. 2007. *Climate Change 2007 - The Physical Science Basis: Working Group I Contribution to the Fourth Assessment Report of the IPCC*. Cambridge University Press.

Stratmann, F., Bilde, M., Dusek, U., Frank, G.P., Hennig, T., Henning, S., Kiendler-Scharr, A., Kiselev, A., Kristensson, A., Lieberwirth, I., Mentel, T.F., Pöschl, U., Rose, D., Schneider, J., Snider, J.R., Tillmann, R., Walter, S., Wex, H. 2010. Examination of laboratory-generated coated soot particles: An overview of the LACIS Experiment in November (LExNo) campaign. *Journal of Geophysical Research D: Atmospheres*, **115**(11).

Svenningsson, B., Bilde, M., Rissler, J., Swietlicki, E. 2007. What about water uptake by mixtures of four of the most important atmospheric aerosol ions: NH4+, Na+, SO4 2-, and Cl-? *European Aerosol Conference*.

Svenningsson, B., Hansson, H.C., Wiedensohler, A., Noone, K., Ogren, J., Hallberg, A., Colvile, R. 1994. Hygroscopic growth of aerosol particles and its influence on nucleation scavenging in cloud: Experimental results from Kleiner Feldberg. *Journal of Atmospheric Chemistry*, **19**(1-2), 129-152.

Svenningsson, I.B., Hansson, H.C., Wiedensohler, A., Hallberg, A., Ogren, J.A., Noone, K.J. 1992. Hygroscopic growth of aerosol particles in the Po Valley. *Tellus, Series B*, **44 B**(5), 556-569.

Swietlicki, E., Hansson, H.C., Hämeri, K., Svenningsson, B., Massling, A., McFiggans, G., McMurry, P.H., Petäjä, T., Tunved, P., Gysel, M., Topping, D., Weingartner, E., Baltensperger, U., Rissler, J., Wiedensohler, A., Kulmala, M. 2008. Hygroscopic properties of submicrometer atmospheric aerosol particles measured with H-TDMA instruments in various environments - A review. *Tellus, Series B: Chemical and Physical Meteorology*, **60 B**(3), 432-469.

Swietlicki, E., Zhou, J., Covert, D.S., Hämeri, K., Busch, B., Väkeva, M., Dusek, U., Berg, O.H., Wiedensohler, A., Aalto, P., Mäkelä, J., Martinsson, B.G., Papaspiropoulos, G., Mentes, B., Frank, G., Stratmann, F. 2000. Hygroscopic properties of aerosol particles in the northeastern Atlantic during ACE-2. *Tellus, Series B: Chemical and Physical Meteorology*, **52**(2), 201-227.

Tiitta, P., Miettinen, P., Vaattovaara, P., Joutsensaari, J., Petäjä, T., Virtanen, A., Raatikainen, T., Aalto, P., Portin, H., Romakkaniemi, S., Kokkola, H., Lehtinen, K.E.J., Kulmala, M., Laaksonen, A. 2010. Roadside aerosol study using hygroscopic, organic and volatility TDMAs: Characterization and mixing state. *Atmospheric Environment*, **44**(7), 976-986.

Tomlinson, J.M., Li, R., Collins, D.R. 2007. Physical and chemical properties of the aerosol within the southeastern Pacific marine boundary layer. *Journal of Geophysical Research D: Atmospheres*, **112**(12).

Topping, D.O., McFiggans, G.B., Coe, H. 2005. A curved multi-component aerosol hygroscopicity model framework: Part 1 - Inorganic compounds. *Atmospheric Chemistry and Physics*, **5**(5), 1205-1222.

Trebs, I., Bohn, B., Ammann, C., Rummel, U., Blumthaler, M., Königstedt, R., Meixner, F.X., Fan, S., Andreae, M.O. 2009. Relationship between the NO2 photolysis frequency and the solar global irradiance. *Atmos. Meas. Tech.*, **2**(2), 725-739.

Tunved, P., Hansson, H.C., Kerminen, V.M., Ström, J., Dal Maso, M., Lihavainen, H., Viisanen, Y., Aalto, P.P., Komppula, M., Kulmala, M. 2006a. High natural aerosol loading over boreal forests. *Science*, **312**(5771), 261-263.

Tunved, P., Korhonen, H., Ström, J., Hansson, H.C., Lehtinen, K.E.J., Kulmala, M. 2006b. Is nucleation capable of explaining observed aerosol integral number increase during southerly transport over Scandinavia? *Tellus, Series B: Chemical and Physical Meteorology*, **58**(2), 129-140.

Twomey, S. 1977a. The influence of pollution on the shortwave albedo of clouds. *Journal of the Atmospheric Sciences*, **34**, 1149-1152.

Twomey, S. 1977b. The Influence of Pollution on the Shortwave Albedo of Clouds. *Journal of the Atmospheric Sciences*, **34**(7), 1149-1152.

Twomey, S. 1974. Pollution and the planetary albedo. *Atmospheric Environment (1967)*, **8**(12), 1251-1256.

Ulbrich, I.M., Canagaratna, M.R., Zhang, Q., Worsnop, D.R., Jimenez, J.L. 2009. Interpretation of organic components from Positive Matrix Factorization of aerosol mass spectrometric data. *Atmos. Chem. Phys.*, **9**, 2891-2918.

Vaattovaara, P., Huttunen, P.E., Yoon, Y.J., Joutsensaari, J., Lehtinen, K.E.J., O'Dowd, C.D., Laaksonen, A. 2006. The composition of nucleation and Aitken modes particles during coastal nucleation events: Evidence for marine secondary organic contribution. *Atmospheric Chemistry and Physics Discussions*, **6**(2), 3337-3379.

Vaattovaara, P., Petäjä, T., Joutsensaari, J., Miettinen, P., Zaprudin, B., Kortelainen, A., Heijari, J., Yli-Pirilä, P., Aalto, P., Worsnop, D.R., Laaksonen, A. 2009. The evolution of nucleation- and Aitken-mode particle compositions in a boreal forest environment during clean and pollution-affected new-particle formation events. *Boreal Environment Research*, **14**(4), 662-682.

Vaattovaara, P., Räsänen, M., Kühn, T., Joutsensaari, J., Laaksonen, A. 2005. A method for detecting the presence of organic fraction in nucleation mode sized particles. *Atmospheric Chemistry and Physics*, **5**(12), 3277-3287.

Vakeva, M., Hameri, K., Aalto, P.P. 2002a. Hygroscopic properties of nucleation mode and Aitken mode particles during nucleation bursts and in background air. *Journal of Geophysical Research-Atmospheres*, **107**(D19), -.

Vakeva, M., Kulmala, M., Stratmann, F., Hameri, K. 2002b. Field measurements of hygroscopic properties and state of mixing of nucleation mode particles. *Atmospheric Chemistry and Physics*, **2**, 55-66.

Vallina, S.M., Simó, R., Gassó, S., de Boyer-Montégut, C., del Río, E., Jurado, E., Dachs, J. 2007. Analysis of a potential "solar radiation dose-dimethylsulfide-cloud condensation nuclei" link from globally mapped seasonal correlations. *Global Biogeochemical Cycles*, **21**(2).

Van Dingenen, R., Putaud, J.P., Martins-Dos Santos, S., Raes, F. 2005. Physical aerosol properties and their relation to air mass origin at Monte Cimone (Italy) during the first MINATROC campaign. *Atmospheric Chemistry and Physics*, **5**(8), 2203-2226.

Varutbangkul, V., Brechtel, F.J., Bahreini, R., Ng, N.L., Keywood, M.D., Kroll, J.H., Flagan, R.C., Seinfeld, J.H., Lee, A., Goldstein, A.H. 2006. Hygroscopicity of secondary organic aerosols formed by oxidation of cycloalkenes, monoterpenes, sesquiterpenes, and related compounds. *Atmospheric Chemistry and Physics Discussions*, **6**(1), 1121-1177.

Vignati, E., Wilson, J., Stier, P. 2004. M7: An efficient size-resolved aerosol microphysics module for large-scale aerosol transport models. *Journal of Geophysical Research: Atmospheres*, **109**(D22), D22202.

Virkkula, A., Van Dingenen, R., Raes, F., Hjorth, J. 1999. Hygroscopic properties of aerosol formed by oxidation of limonene, alpha-pinene, and beta-pinene. *Journal of Geophysical Research-Atmospheres*, **104**(D3), 3569-3579.

Weber, R.J., Marti, J.J., McMurry, P.H., Eisele, F.L., Tanner, D.J., Jefferson, A. 1996. Measured atmospheric new particle formation rates: Implications for nucleation mechanisms. *Chemical Engineering Communications*, **151**, 53-64.

Weber, R.J., McMurry, P.H., Tanner, D.J., Eisele, F.L.E., Fred L., Kreidenweis, S.M., Schillawski, R.D., Baumgardner, D. 1998. A study of new particle formation and growth involving biogenic and trace gas species measured during ACE 1. *Journal Name: Journal of Geophysical Research; Journal Volume: 103; Journal Issue: D13; Other Information: PBD: Jul 1998*, Medium: X; Size: pp. 16385-16396.

Weingartner, E., Burtscher, H., Baltensperger, U. 1997. Hygroscopic properties of carbon and diesel soot particles. *Atmospheric Environment*, **31**(15), 2311-2327.

Weingartner, E., Gysel, M., Baltensperger, U. 2002. Hygroscopicity of aerosol particles at low temperatures. 1. New low-temperature H-TDMA instrument: Setup and first applications. *Environmental Science and Technology*, **36**(1), 55-62.

Zhang, Q., Worsnop, D.R., Canagaratna, M.R., Jimenez, J.L. 2005. Hydrocarbon-like and oxygenated organic aerosols in Pittsburgh: Insights into sources and processes of organic aerosols. *Atmospheric Chemistry and Physics*, **5**(12), 3289-3311.

Zhou, J., Swietlicki, E., Berg, O.H., Aalto, P.P., Hämeri, K., Nilsson, E.D., Leck, C. 2001a. Hygroscopic properties of aerosol particles over the central Arctic Ocean during summer. *Journal of Geophysical Research D: Atmospheres*, **106**(D23), 32111-32123.

Zhou, J.C., Swietlicki, E., Berg, O.H., Aalto, P.P., Hameri, K., Nilsson, E.D., Leck, C. 2001b. Hygroscopic properties of aerosol particles over the central Arctic Ocean during summer. *Journal of Geophysical Research-Atmospheres*, **106**(D23), 32111-32123.

List of all publications

Bialek, J.; Dall'Osto, M.; Ovadnevaite, J.; Vaattovaara, P.; Decesari, S.; Laaksonen, A. and O'Dowd, C.; Hygroscopic and Chemical Characterisation of Po Valley Aerosol, 2013, ACPD

Bialek, J.; Dall'Osto, M.; Monahan, C.; Beddows, D.; O'Dowd, C.; On the contribution of organics to the North East Atlantic aerosol number concentration, Environmental Research Letters,7,4,044013,2012, IOP Publishing

Ovadnevaite, J.; Ceburnis, D.; Canagaratna, M.; Berresheim, H.; Bialek, J.; Martucci, G.; Worsnop, D.R.; O'Dowd, C.; On the effect of wind speed on submicron sea salt mass concentrations and source fluxes, Journal of Geophysical Research,117,D16,D16201,2012,American Geophysical Union

Dall'Osto, M.; Ceburnis, D.; Monahan, C.; Worsnop, D.R.; Bialek, J.; Kulmala, M.; Kurtén, T.; Ehn, M.; Wenger, J.; Sodeau, J.; Nitrogenated and aliphatic organic vapors as possible drivers for marine secondary organic aerosol growth, Journal of Geophysical Research,117,D12,D12311,2012,American Geophysical Union

O'Dowd, C.; Ceburnis, D.; Ovadnevaite, J.; Martucci, G.; Bialek, J.; Monahan, C.; Berresheim, H.; Vaishya, A.; Grigas, T.; Jennings, S.G.; The Eyjafjallajökull ash plume–Part I: Physical, chemical and optical characteristics, Atmospheric Environment, 48, 129-142, 2012, Elsevier

Ceburnis, D.; Ovadnevaite, J.; Martucci, G.; Bialek, J.; Monahan, C.; Rinaldi, M.; Facchini, C.; Berresheim, H.; Worsnop, DR; O'Dowd, C.; A dichotomy in primary marine organic aerosol-cloud-climate system, AGU Fall Meeting Abstracts, 1, 02, 2011,

Ovadnevaite, J.; Ceburnis, D.; Martucci, G.; Bialek, J.; Monahan, C.; Rinaldi, M.; Facchini, M.C.; Berresheim, H.; Worsnop, D.R.; O'Dowd, C.; Primary marine organic aerosol: A dichotomy of low hygroscopicity and high CCN activity, Geophysical Research Letters,38,21,L21806,2011,American Geophysical Union

O'Dowd, C.; Varghese, S.; Martin, D.; Flanagan, R.; Ceburnis, D.; Ovadnevaite, J.; Martucci, G.; Bialek, J.; Monahan, C.; Berresheim, H.; The Eyjafjallajökull ash plume–Part 2: Simulating ash cloud dispersion with REMOTE, Atmospheric Environment, 2011, Elsevier

Fierz-Schmidhauser, R.; Zieger, P.; Vaishya, A.; Monahan, C.; Bialek, J.; O'Dowd, CD; Jennings, SG; Baltensperger, U.; Weingartner, E.; Light scattering enhancement factors in the marine boundary layer (Mace Head, Ireland), Journal of Geophysical Research, 115,D20,D20204, 2010, American Geophysical Union

Dall'Osto, M.; Ceburnis, D.; Martucci, G.; Bialek, J.; Dupuy, R.; Jennings, SG; Berresheim, H.; Wenger, JC; Healy, RM; Facchini, MC; Corrigendum to, Atmospheric Chemistry & Physics,10,,8549-8549,2010

Dall'Osto, M.; Ceburnis, D.; Martucci, G.; Bialek, J.; Dupuy, R.; Jennings, SG; Berresheim, H.; Wenger, J.; Healy, R.; Facchini, MC; Aerosol properties associated with air masses arriving into the North East Atlantic during the 2008 Mace Head EUCAARI intensive observing period: an overview, Atmospheric Chemistry & Physics,10, 8413-8435, 2010

Dall'Osto, M.; Ceburnis, D.; Martucci, G.; Bialek, J.; Dupuy, R.; Jennings, SG; Berresheim, H.; Wenger, JC; Sodeau, JR; Healy, RM; Aerosol properties associated with air masses arriving into the North East Atlantic during the 2008 Mace Head EUCAARI intensive observing period: an overview, Atmospheric Chemistry & Physics Discussions, 9, 26265-26328, 2009

Decesari, S.; Carbone, C.; Finessi, E.; Giulianelli, L.; Rinaldi, M.; Gobbi, G.P.; Angelini, F.; Caporaso, L.; Fuzzi, S.; Dall'Osto, M.; Bialek, J.; O'Dowd, C.; Secondary aerosol formation at a European pollution hot spot: Results from the summer 2009 Po Valley experiment, 2009, American Association for Aerosol Research, Hyatt Regency Minneapolis, Minneapolis, Minnesota, USA http://aaarabstracts. com/AAAR/

Dall'Osto, M.; Bialek, J.; Dupuy, J.; Ceburnis, D.; Worsnop, D.; O'Dowd, C.; ",Case study: elevated methanesulfonic acids (MSA) concentrations in an ultrafine particle events originated in the tropical Atlantic Ocean, 2009, American Association for Aerosol Research, Hyatt Regency Minneapolis, Minneapolis, Minnesota, USA http://aaarabstracts.com/AAAR/